MOLECULAR EVOLUTION OF HUMAN H3N2 INFLUENZA A VIRUSES DURING ADAPTATION TO THE SWINE HOST

by

MATIAS IGNACIO CARDENAS PEREZ

(Under the Direction of Daniela S. Rajao)

ABSTRACT

Influenza A viruses (FLUAV) have a wide host range. While its natural hosts are aquatic birds of the genus *Anseriformes* and *Charadriiformes*, including ducks, geese, gulls, and swans, among others, FLUAV can infect various animals, including bats, dogs, horses, chickens, and pigs. Pigs are considered a "mixing vessel" host because they can be infected with FLUAV from multiple species, which can promote the emergence of novel FLUAVs with zoonotic and pandemic potential as occurred with the swine-origin 2009 pandemic H1N1 virus. Nonetheless, human-to-swine transmission events are more common than zoonotic infections. Despite some of these human-origin viruses becoming established in swine and contributing to the diversity of viruses circulating in pigs globally, little is known about the biological processes driving the adaptation of FLUAV following human-to-swine transmission.

The studies presented here aimed to evaluate the molecular evolution of human-origin H3N2 viruses to the swine host using an *in vivo* sustained transmission model. Samples collected during the study were sequenced using next-generation sequencing and viral variants that emerged were characterized *in vivo* and *in vitro*.

The results presented in this dissertation highlight the critical role of infection of the lower respiratory tract and alveolar macrophages for onward transmission of human-like viruses during adaptation to swine, mainly mediated by changes in the HA protein such as the A138S amino acid change. We also found an important role of calcium limiting infection of human viruses in pigs, suggesting a novel role of calcium in the host range of FLUAV. This process was shown to be modulated by the neuraminidase low-affinity calcium-binding pocket which is structurally different in human and swine H3N2 viruses, leading to enhanced stability of the NA tetramer of swine viruses under calcium-depleted conditions. Additionally, we found that previous immunity leads to a different viral evolutionary pathway compared to non-immunized animals, resulting in selection of HA variants such a V186G and F193Y. These changes in the HA resulted in a reduction of glycans supporting binding of FLUAV which seems to be compensated by increased affinity for sialic acid.

The data presented here provides insights into host barriers limiting human FLUAV adaptation to pigs and the complexities associated with the host immune response that influenza A viruses must overcome to become established in the new host populations.

INDEX WORDS: Influenza A virus, Human-origin, Adaptation, Swine, Alveolar macrophages, Calcium, Previous immunity, Evolution

MOLECULAR EVOLUTION OF HUMAN H3N2 INFLUENZA A VIRUSES DURING ADAPTATION TO THE SWINE HOST

by

MATIAS IGNACIO CARDENAS PEREZ

B.Sc., Universidad de Santiago de Chile, Chile, 2020

A Dissertation Summitted to the Graduate Faculty of The University of Georgia in Partial Fulfilment of the Requirements for the Degree

DOCTOR OF PHILOSOPHY

Athens, Georgia

2024

MOLECULAR EVOLUTION OF HUMAN H3N2 INFLUENZA A VIRUSES DURING ADAPTATION TO THE SWINE HOST

by

MATIAS IGNACIO CARDENAS PEREZ

Major Professor:	Daniela S. Rajao
Committee:	Daniel R. Perez
	Silvia Carnaccini
	Tavis Anderson

Electronic Version Approved:

Ron Walcott
Dean of the Graduate School
The University of Georgia
December 2024

DEDICATION

This dissertation is dedicated to my mom and my aunt for their unconditional support throughout these years.

ACKNOWLEDGEMENTS

I would like to acknowledge my PhD advisor Dr. Daniela S. Rajao for allowing me to pursue my different interests in FLUAV and for believing in me and my ideas. I would also like to recognize Dr. Daniel Perez for his help and advice that made this research possible. On this line, I would like to thank my committee members Dr. Tavis Anderson and Dr. Silvia Carnaccini for their guidance and advice designing my experiments.

I would also like to acknowledge all the previous and current members of the Rajao and the Perez lab, including Brittany, Brianna, Joaquin, Flavio, Claire, and Sasha for all their help with the never-ending experiments and most importantly, their friendship. Their constant support in and out of the lab made this journey a lot easier.

I would like to thank my family, especially my mom and my aunt for their endless love and support. Finally, I would like to recognize all my friends back home, including Camila, Gabi, Tiare, Victor, Pablo, Jacque, Cata, and Isi for their unconditional friendship, and always waiting for me to go back home so we could keep up to date.

TABLE OF CONTENTS

LIST OF TABLES

LIST OF FIGURES

Supplementary

CHAPTER 1

INTRODUCTION

Influenza A viruses (FLUAV) are enveloped viruses with a genome composed of 8 single-stranded, negative-sensed RNA segments [1]. The virus has two major surface glycoproteins: the hemagglutinin (HA) and the neuraminidase (NA) [1], and to date, 19 HA and 11 NA subtypes have been described [2, 3]. These proteins are the major antigenic components of the virus envelope and elicit neutralizing antibodies [4]. Among the subtypes, H1N1 and H3N2 viruses are currently circulating in humans [5], and H3N2 viruses accounted for 70% of the total reported FLUAV cases of the 2022-2023 influenza season in North America [6]. One of the major challenges controlling FLUAV is the virus's rapid evolution due to two main mechanisms: antigenic shift and antigenic drift [7]. Antigenic shift is the exchange of the HA (and sometimes NA) genes between two strains infecting the same host, with the potential to generate new strains to which the population does not have immunity [8]. Genetic drift is the slow accumulation of mutations in the surface proteins (mainly HA) that randomly appear during FLUAV replication due to the lack of a proofreading mechanism of the viral RNA-dependent RNA polymerase [9]. Some of these mutations that arise provide a fitness benefit to the virus through antibody escape, and this may lead to a process known as antigenic drift. Similarly, the viral RNA polymerase can also introduce mutations in the colloquially named "internal genes," which have been associated with interspecies transmission and adaptation [10].

The natural hosts of FLUAV are aquatic birds, mainly of the genus *Anseriformes* and *Charadriiformes*, including ducks, geese, gulls, and swans, among others [11]. However, numerous reports have shown that FLUAV can infect various animals, including bats, dogs, horses, chickens, and pigs [12]. Pigs are considered a "mixing vessel" host because they can be infected with avian, human, and swine FLUAV [13-15], which can promote the emergence of novel FLUAV with zoonotic and pandemic potential, as occurred with the pandemic H1N1 virus in 2009 [16]. Nonetheless, human-to-swine transmission events are more common than zoonotic infections [17, 18]. Despite some of these human-origin viruses becoming established in swine and contributing to the diversity of viruses circulating in pigs globally, little is known about the biological processes driving human-to-swine adaptation of FLUAV.

Hemagglutinin has been considered one of the most important factors driving interspecies transmission of FLUAV [19]. This glycoprotein is found as a homotrimer on the virus surface, and each monomer possesses a receptor-binding site (RBS) [20]. HA recognizes specific glycans that share the main feature of having a terminal galactose bound to sialic acid (SA) [20], except H17, H18, and H19 subtypes that recognize the major histocompatibility complex (MHC) class II instead [21, 22]. Generally, FLUAV recognizes N-acetylneuraminic acid (Neu5Ac) linked to galactose by α2,3 or α2,6 linkages [23]. The SA linkage is a critical host determinant since avian FLUAV preferentially binds to α2,3-linked SA, whereas mammalian isolates bind to α2,6-linked receptors [24]. Humans and swine have a similar distribution of SA in the respiratory tract [18], showing predominantly α2,6-SA in the upper respiratory tract, and α2,3-linked SA receptors increase in quantity towards the lower respiratory tract [25]. Several point

mutations in the HA RBS have been described to modulate the receptor preference of the virus [26]. Recently, the A138S (H3 numbering) mutation near the RBS was associated with increased binding and viral replication in swine tracheal cells *in vitro* of a human-origin virus [27], supporting the role of the HA as a key factor modulating infection of pigs with human FLUAV.

More attention has recently been given to the fact that the SA glycosidic linkage may not be the only factor restricting the FLUAV binding [28]. SA is commonly present as complex carbohydrate molecules bound to proteins or lipids on the cell surface, and glycome studies have described that Neu5Ac can be linked to glycans of different lengths on the plasma membrane. Interestingly, avian FLUAV seems to have a higher affinity for short carbohydrate chains when compared to human FLUAV [29], suggesting that the molecule to which the SA is linked also contributes to FLUAV host specificity. Similarly, the glycan topology also plays a role in the FLUAV host range. The α2,3-linked SA adopts a cone-like structure, while α2,6-linked SA is found in a cone-like and an umbrella-like structure. These structural differences require the interaction of different amino acids in the HA RBS with the sialic acid molecule, and this differential interaction has been proposed as an explanation of the preference shift between α2,3/α2,6 induced by the E190 and Q226 mutations in the RBS [28].

NA is the second most abundant surface protein in the FLUAV viral particle [30]. This enzyme antagonizes HA and plays a critical role during the FLUAV replication cycle by cleaving SA from the cell surface to allow the new viral progeny to be released [30]. Because of their opposite but complementary roles, a functional balance between HA avidity and NA activity is required for a successful infection [31, 32]. The HA/NA

balance has been shown to be important in interspecies transmission of FLUAV. For example, the pandemic H1N1 virus from 2009 that jumped to humans from swine had low HA avidity and NA hydrolase activity, contrasting the swine precursor that exhibited high HA avidity and low NA activity [33]. More generally, low NA activity seems to be common in swine H1N1 FLUAV. Previous studies reported that viruses exhibiting almost undetectable NA activity are not inhibited by swine mucus but by human mucus and are not transmissible in ferrets [34], which supports the role of NA in the host range of FLUAV. Recently, a study demonstrated that calcium plays a critical role in NA evolution and adaptation since mutations in the low-affinity calcium-binding pocket of the NA modify the calcium requirements for optimal replication, viral particle release, and NA activity of the pandemic 2009 H1N1 virus (pH1N1) [35]. This is particularly important since this study also pointed out that NA could form heterotetramers with subunits carrying stabilizing and destabilizing mutations, which provides an additional mechanism to regulate NA activity and modify the HA/NA balance [35].

Besides the surface proteins, the polymerase complex is also a key determinant of FLUAV host specificity [36]. This complex is a heterotrimer formed by PB2, PB1, and PA that acts as an RNA-dependent RNA polymerase [37]. PB1 is the most conserved subunit and displays RNA-dependent RNA polymerase activity [38]. The PB2 subunit recognizes the cap structure of cellular mRNAs that will be further used in viral mRNAs in a process known as cap-snatching [39], and PA exhibits endonuclease activity, which is responsible for the cap cleavage from cellular mRNAs [40]. Temperature has been shown to modulate FLUAV replication by impacting different steps of the virus' replication cycle. The polymerase complex shows no activity at high temperatures, most likely due

to the inability of the complex to bind the promoter, and this effect has been linked to host range restriction [41]. Avian FLUAV usually infects the respiratory and gastrointestinal (GI) tract of birds [42]. The temperature of the lower respiratory tract and the GI tract of birds is approximately 41°C [43], which contrasts with the human upper respiratory tract in which the temperature is 33°C and increases to 37°C in the lower respiratory tract [44]. This temperature difference between humans and birds is a host barrier that viruses must overcome for interspecies transmission. To overcome this barrier, the polymerase complex must acquire adaptative mutations in key residues, such as residue 627 in the PB2 protein. Residue 627 of avian viruses is usually glutamic acid (Glu, E) [45], and the introduction of lysin (Lys, L) at position 627 allows replication and transmission in mammals due to enhanced polymerase activity at lower temperatures [46]. Similarly, introducing PB2 R714 and PA R615 in an avian FLUAV enhances polymerase activity and pathogenicity in mice and ferrets [47, 48]. Pigs have a slightly higher temperature than humans in the lower respiratory tract (39°C) [18], and this seems to allow viruses carrying the avian signature E627 in the PB2 to replicate in pigs. However, other compensatory mutations might also be required for optimal virus replication and transmission in pigs [49, 50].

Upon FLUAV infection, several viral components not found in host cells, termed pathogen-associated molecular patterns (PAMPs), trigger an immune response aiming to clear the infection [51]. The innate immune response is the first line of defense and is characterized by being rapid and nonspecific [52]. Once FLUAV enters a cell, the pattern-recognition receptors (PRRs), including the retinoic acid-inducible gene-I protein (RIG-I) and some Toll-like receptors (TLR), recognize PAMPS such as the FLUAV genome [53]

and induce an antiviral state in the infected cell. This response is characterized by the activation of different interferon regulatory factors (IRFs) and NF-kB [51], ultimately leading to multiple immune-related genes' expression. To overcome the host antiviral response, FLUAV has developed several mechanisms to prevent the expression of antiviral proteins. The non-structural protein 1 (NS1) is a small protein with multiple domains and functions and has been described to interact with more than 252 different cellular proteins [54]. Noteworthy, NS1 can block interferon (IFN) production by multiple mechanisms, such as by sequestering double-stranded RNA and inhibiting the protein kinase R (PKR), which is crucial in the RIG-I signaling pathway [55], and therefore preventing RIG-I recognition [56] and the export of mature cellular mRNAs from the nucleus [57]. Some of these mechanisms have been shown to be host-specific and might restrict the FLUAV host range [58]. For example, avian-origin but not human-origin NS1 can bind through a C-terminal PDZ-binding domain to different host's PDZ-containing proteins [59]. By binding to PDZ-containing proteins, the virus prevents apoptosis of the infected cell [60] and enhances virus replication. Ultimately, all the signaling pathways activated after FLUAV recognition in the infected cell will lead to the transcription of various pro-inflammatory cytokines and interferon-stimulated genes. The secretion of these cytokines will recruit different immune cells to the site of infection, such as dendritic cells, neutrophils, and alveolar macrophages [61, 62].

Alveolar macrophages (AMs) are the most abundant immune cells in the lungs and account for up to 98% of cells in bronchoalveolar lavage fluid in pigs [63]. AMs contribute to the first line of defense against respiratory pathogens and are essential in developing innate and adaptative immune responses during FLUAV infection. Previous

reports showed that they play a critical role in controlling FLUAV infection via producing type I interferons and other pro-inflammatory cytokines such as TNF-a, IL-6, and IL-10, together with their intrinsic phagocytic activity [64, 65]. Moreover, AMs play a significant role in building antibody-mediated protection against FLUAV and inducing and regulating the primary anti-FLUAV cytotoxic T-cell response [66, 67]. AM-depleted mice infected with FLUAV have higher lung replication, overexpression of pro-inflammatory cytokines, increased tissue damage, and higher mortality, underscoring that AMs are imperative for combatting FLUAV infection [68-70]. While AMs are essential for the anti-influenza immune response, they have been previously reported to be susceptible to FLUAV infection with contradictory results [71, 72]. Numerous FLUAV HA subtypes show limited virus replication within these cells except for a subset of highly pathogenic and low pathogenic H5 viruses that efficiently replicate in swine, mice, and human AMs [72-75]. Nonetheless, H3 and H1 viruses have also been described to infect mice AMs [76]. Previous literature suggests that FLUAV infection of AMs induces death by apoptosis [21] and impairs the immune activity of AMs via PPARg repression [77, 78]. This transcription factor regulates AMs activity and is activated after GM-CSF stimulation [79, 80]. GM-CSF and PPARg have also been described as the main factors promoting monocyte differentiation into AMs and their proliferation [81, 82]. However, the effect, if any, of FLUAV infection of AMs on virus tropism and host range is still unknown [83].

One of the most established strategies to control FLUAV viruses is vaccination. Vaccination is a common practice in swine herds, mainly focused on sows and piglets, and it has been shown to reduce clinical signs and spread of the virus [84]. Inactivated

vaccines are the most commonly used vaccines in pigs and stimulate IgG production against HA and, to a lesser extent, against NA [85]; however, unless the field strain is an exact match of the vaccine strain, they do not offer sterilizing protection, and the virus is still able to replicate at reduced levels in the infected animal. This replication window may allow the virus to evolve with some mutations in the surface proteins that allow escape from the antibodies induced by the vaccine [86]. These viruses, referred to as "escape mutants," can transmit among the population even in vaccinated individuals. This process seems to be stochastic, and previous literature suggests that when pigs are infected with either swine H1N1 or H3N2 strains, the virus is under positive selection in vaccinated animals and that the majority of the changes occur in the RBS, the stalk domain, and the fusion peptide of the HA [87, 88]. Conversely, the NA seems to only accumulate mutations in the head domain [87]. Nonetheless, it is still unknown if previous non or low cross-reactive immunity can affect the adaptation of human viruses to the swine host.

Research objectives and aims.

The goal of this project is to understand the host and viral factors limiting FLUAV interspecies transmission between humans and pigs. This project is based on a sustained transmission model in swine of a human-origin H3N2 virus carrying the A138S mutation since it shows enhanced affinity for swine cells *in vitro*. Using this model, viruses will be passaged *in vivo* in multiple transmission events to allow evolution. Any detected viral mutations will be characterized *in vivo* and *in vitro* to understand the impact of any fixed mutations in the viral proteins that might be required for successful infection and to

define potential adaptation mechanisms. This includes the host's immune response, receptor specificity, and the HA/NA balance.

Specific Aim 1: *To analyze the effect of the A138S mutation in the HA gene of a human-origin H3N2 in the adaptation to the swine host in vivo.*

I. Compare virus distribution in the lower respiratory tract of hVIC/11-, hVIC/11^{A138S}-, and sOH/04-infected pigs.

II. Evaluate the immune response triggered by each virus in different lung anatomical sections.

III. Compare the abundance of immune cell populations recruited to different lung anatomical sections of hVIC/11-, hVIC/11^{A138S}-, and sOH/04-infected pigs.

Specific Aim 2: *To understand the HA and NA evolutionary constraints limiting human FLUAV infection and transmission in pigs.*

I. Set up an *in vivo* sustained transmission model of FLUAV in pigs.

II. Evaluate the molecular evolution of hVIC/11^{A138S} and sOH/04 *in vivo* during four rounds of transmission by sequencing of the HA and NA segments from nasal swabs and BALF samples using the MiSeq platform.

III. Characterize the viral variants identified using *in vitro* assays.

Specific Aim 3: *To analyze the effect of previous immunity on virus evolution and adaptation of a human-origin H3N2 virus in a sustained transmission model in pigs.*

I. Characterize hVIC/11^{A138S} evolution after infection of previously vaccinated pigs in a sustained transmission model by sequencing nasal swabs and BALF samples using the MiSeq platform.

II. Evaluate the antigenicity and replication, and other viral properties of the variants identified in the previous objective.

CHAPTER 2

LITERATURE REVIEW

Influenza viruses.

Influenza viruses belong to the *Orthomyxoviridae* family, which consist of nine genera including *Alphainfluenzavirus, Betainfluenzavirus, Gammainfluenzavirus, Deltainfluenzavirus,* and *Isavirus* among others. These are classified serologically according to their reactivity against the nucleoprotein and the matrix protein [89]. Influenza A, B, and C have been reported to infect humans [90-92] while Influenza D have only been reported in cattle and pigs [93]. Contrary to influenza B, C, and D, which show restricted host range, influenza A viruses (FLUAV) have a wide host range and can infect different animals, including chickens, dogs, horses, whales, bats, pigs, and humans [12]. The FLUAV natural host is considered to be aquatic birds of the genus *Anseriformes* and *Charadriiformes,* which includes ducks, geese, gulls, and swans [11, 94], and other animals are considered secondary hosts. FLUAV can be further classified based on the cross-reactivity of the surface proteins hemagglutinin (HA) and neuraminidase (NA), and to date 19 different HA and 11 NA subtypes have been described [2]. Among these, H3N2 and H1N1 subtypes currently circulate in humans [95, 96] with varied prevalence depending on the season: e.g., H3N2 was the most prevalent subtype reported during the 2022-2023 flu season in North America [97, 98]. FLUAV is the only influenza subtype known to cause pandemics such as the 1918 H1N1, 1957 H2N2, 1968 H3N2, and the 2009 H1N1 (pH1N1) [99] because of its intrinsic ability to mutate and escape immunity which favors transmission.

Virus structure.

FLUAV viral particles are enveloped and pleomorphic, with both spherical and filamentous particles being described [100]. Spherical virions normally are 100 nm in diameter while filamentous are up to 5 mm in length [101]. Filamentous particles seem to be selected *in vivo* as they are frequently found in human clinical samples [102] and some reports have suggested a role of the host in the selection of a particular shape [103]. However, it is widely accepted that point mutations in the matrix gene affect the virion structure but it is still unclear how this process takes place [104].

FLUAV has a segmented genome, comprising 8 single-stranded, negative-sensed, RNA segments that encode at least 11 proteins **(Table 2.1)** [105]. Segments 1, 2, and 3 encode the viral RNA-dependent RNA polymerase (RdRp) subunits polymerase basic 2 (PB2), polymerase basic 1 (PB1), and polymerase acidic (PA), respectively [106, 107]. PB1 possesses the conserved viral RNA-dependent RNA polymerases motifs such as pre-A motif and motifs A to E which can be further divided in the subdomains known as the palm, thumbs, and fingers together with a magnesium-binding pocket that modulates nucleotide addition to the nascent viral RNA (vRNA) [108]. Additionally, the PB1 segment also encodes a short protein PB1-F2. This protein has been shown to enhance FLUAV pathogenicity by promoting polymerase activity and inducing apoptosis [109]. Additionally, a third protein named PB1-N40 has been found to be encoded in the PB1 segment [110]. Although the function of this protein remains to be elucidated, it has been proposed that it might act in conjunction with PB1-F2 [111]. PB2 possess a cap-binding domain [112] that participates in the synthesis of viral mRNA by binding the cap of cellular RNAs that are further cleaved by PA and added to the new viral mRNA [40].

Moreover, PB2 has been shown to interfere with the JAK/STAT signaling thus preventing interferon expression and suppressing the cellular immune response [113]. In addition to PB2, a small peptide denominated PB2-S1 was described to be encoded in a novel spliced mRNA [114]. This peptide was shown to interfere with RIG-I signaling; therefore, preventing interferon expression [115]. Similarly, a frame shift during translation of the PA segment allows the synthesis of the PA-X peptide which has been shown to repress the host's immune response by preventing expression of critical anti-FLUAV genes [116]. The polymerase complex (PB1, PB2, and PA) in association with each vRNA wrapped around with multiple copies of the viral nucleoprotein (NP) encoded in segment 5 [117], form the viral ribonucleoprotein complex (vRNP), which are considered the minimal infectious unit of FLUAV [118]. Segment 4 encodes the viral hemagglutinin (HA) which together with the neuraminidase (NA) protein encoded in segment 6 are the two surface glycoproteins of the viral particle [119] and trigger the majority of the antibody response against the virus [120]. The HA main function is to recognize the cellular receptor sialic acid [121] or the Major Histocompatibility II complex (MHCII) [22, 122] on the cell surface to promote entry into the target cell. Additionally, a fusion peptide in the HA is exposed under low pH in endosomes to promote release of the viral genome into the cytoplasm [123]. NA is the second most abundant surface glycoprotein [124] and hydrolases sialic acid to promote budding of the viral progeny [125]. Furthermore, NA activity has been associated with the ability of the virus to move through the respiratory mucus by degrading and therefore preventing binding to decoy receptors [126]. Development of new techniques such as surface plasmon resonance and biolayer interferometry have demonstrated that a functional

balance between HA avidity and NA activity is critical for successful infection by preserving virus motility [127].

Table 2.1 FLUAV segments, proteins encoded, and function.

Segment	Size	Protein encoded	Function
1	2341	PB2	Cap-binding IFN suppression
		PB2-S1	IFN suppression
2	2341	PB1	Viral polymerase
		PB1-F2	Apoptosis modulation
		PB1-N40	Unknown
3	2233	PA	Endonuclease
		PA-X	Host gene expression shutoff
4	1778-1728	HA	Sialic acid and/or MHCII binding Membrane fusion
5	1565	NP	vRNA binding protein
6	1470-1453	NA	Sialic acid hydrolysis
7	1027	M1	Capsid protein
		M2	Proton channel
8	890	NS1	Interferon antagonist
		NS2	vRNA nuclear export

Segment 7 encodes two structural proteins: M1 and M2 [128]. M1 is the capsid protein and coats the inner part of the viral particle enclosing the viral genome [129]. Similarly, M2 can be found in the viral capsid and acts a proton channel that allows acidification of the viral particle in the endosomes during the early stages of infection [130]. Lastly, segment 8 codes for two proteins: the non-structural protein 1 (NS1) and the non-structural protein 2 (NS2) [131]. NS1 is a small peptide that has been shown to be critical for FLUAV successful infection as it is a potent interferon repressor [132]; therefore, it downregulates and suppresses the host's immune response during infection

[133]. NS2, also named nuclear export protein (NEP), promotes the export of newly synthetized vRNPs from the nucleus to the cytoplasm to be packed in new viral particles [134]

Replication cycle.

The replication cycle begins when the HA recognizes sialic acid on the surface of the target cells [135]. This process induces endocytosis to allow entry of FLUAV into the cell [136]. Sialic acid itself is not able to induce endocytosis, therefore it has been proposed that it acts as a primary anchor for the virus to then activate a secondary receptor with the ability to induce the required endocytic pathways [137]. This hypothesis has been supported by the discovery that the epidermal growth factor receptor (EGFR) and some calcium-dependent voltage channels interact directly with FLUAV in a sialic-acid dependent fashion during the early stages of infection to promote uptake of the virus [138, 139].

FLUAV induces two main mechanisms for entry: clathrin-mediated endocytosis (CME) and macropinocytosis [140]. These two mechanisms are triggered simultaneously by the virus. It is believed that since CME induces the formation of small endosomes (»150 nm in diameter) [141], which allows the entry of spherical viral particles (»120 nm in diameter), macropinocytosis is mainly exploited by filamentous particles [140], as macropinosomes can vary in size from 200 nm to 5 mm in length [142]. Both routes participate in the endosome maturation process and lead to the formation of a late endosome [143]. The lower pH of late endosomes induces a conformational change in the M2 proton channels that allows an influx of protons inside the viral particle [144].

Further acidification of the viral particle destabilizes the M1 matrix and frees the vRNPs from its interaction with M1 [145]. Simultaneously the HA undergoes a conformational change that culminates with the exposure of the fusion peptide that promotes the fusion of the viral and the endosome membranes [146]. At the end of this process, the vRNPs are released to the cytoplasm and trafficked into the nucleus due to nuclear localization sequences found in NP [147].

In the nucleus, the viral polymerase begins the transcription of the viral genome [148]. FLUAV mRNAs presents structural similarities to cellular mRNAs and are capped and polyadenylated [149], although these modifications are not introduced using the regular cellular machinery. As the viral polymerase cannot cap the viral mRNAs in a traditional manner, this process takes place via “cap snatching” [40]. The PB2 subunit recognizes the cap structure of cellular mRNAs [150], which are cleaved by PA at 10-13 nt downstream the recognition site of PB2 [151]. These fragments are further used as a primer for the transcription of viral mRNA [152]; therefore, generating capped mRNAs. The viral mRNA polyadenylation occurs by introducing copies of the conserved U-stretch found in the 5’ end of the vRNA template [153]. Mature viral mRNAs are then exported to the cytoplasm by the cellular machinery through the nuclear pore complex [154]. In the cytoplasm, most of the viral mRNAs are translated by cytosolic ribosomes except for the membrane-associated proteins of the virus (HA, NA, and M2), which are translated by reticulum-associated ribosomes [155]. Newly synthetized proteins in the reticulum are transported to the Golgi apparatus by anterograde transport in COPII-coated vesicles, where they are glycosylated and then trafficked to the plasma membrane [156]. The viral polymerase subunits and nucleoproteins return to the nucleus to assemble

new vRNPs [157] that are then exported, in a process mediated by NS2 [158], and packed into new viral particles.

FLUAV viral particle release process is still widely unknown and numerous knowledge gaps are still to be filled. It is accepted that this process takes place in lipid rafts domains which are characterized by a high cholesterol and sphingolipids content [159, 160]. The HA and NA proteins are intrinsically associated in lipid rafts [161] and mutations in the HA transmembrane domain that direct lipid raft association have been shown to attenuate FLUAV replication [162]. Contrary to HA and NA, M1 does not have a transmembrane domain that direct the protein to the plasma membrane, instead it has been hypothesized that M1 is recruited to the budding site by recognizing the cytoplasmatic tail of either HA or NA [163] combined with a strong interaction with M2 [164]. Once in the membrane, M1 interacts with the vRNPs via NP [165] to pack the viral genome into new viral particle. Therefore, a scaffold protein that provides support to the nascent virion and recruits the vRNPs. Although the genome packaging mechanism remains largely unknown it is widely accepted that a set of unique packaging signals in each segment allow the recognition of individual segments to be packed via a complex network of RNA-RNA interactions [166]. Finally, the nascent virion buds most likely by the action of M2, which has been reported to be able to curve the plasma membrane at the budding site upon recognition of cholesterol in the lipid raft by two cholesterol-recognition sites in its cytoplasmatic tail [167]. Although this process is not well-understood, evidence supports that recruitment of M2 to the site of budding by M1 starts the process [101].. Finally, the nascent virion buds most likely by the action of M2, which has been reported to be able to curve the plasma membrane at the budding site

upon recognition of cholesterol in the lipid raft by two cholesterol-recognition sites in its cytoplasmatic tail [167]. Although this process is not well-understood, evidence supports that recruitment of M2 to the site of budding by M1 starts the process [101].

The surface glycoproteins

The HA protein is a homotrimer in which each monomer is present as two subunits, HA1 and HA2, a result of the proteolytic processing of the HA0 precursor **(Figure 2.1)** [168, 169]. The sialic acid receptor binding site (RBS) can be found in the HA1 domain [20]. Four residues located within this pocket are conserved among all sialic acid-binding HAs H1-H16 subtypes: Y98, W153, H183, and Y195 (H3 numbering) [20]. These residues contribute to sialic acid binding by directly stabilizing the SA moiety of the glycan in the pocket [19]. Additional structural elements known as the 130-loop, 150-loop, 190-helix, and 220-loop contribute to the structural integrity of the HA RBS and participate in sialic acid binding [170]. Mammalian-adapted HAs normally bind to a2,6-linked sialic acid while avian-origin HAs preferred a2,3-linked sialic acid. This binding preference has been shown to be determined by a few amino acids in or near the RBS. For instance, avian H1 exhibit a dual binding for a2,6- and a2,3-linked sialic acid, while human-origin H1 can only bind a2,6-linked sialic acid [171, 172]. This difference was demonstrated to be caused by two amino acid substitutions: while E190 and G225 are present in avian H1s, human isolates tend to have D190 and D225 [173].

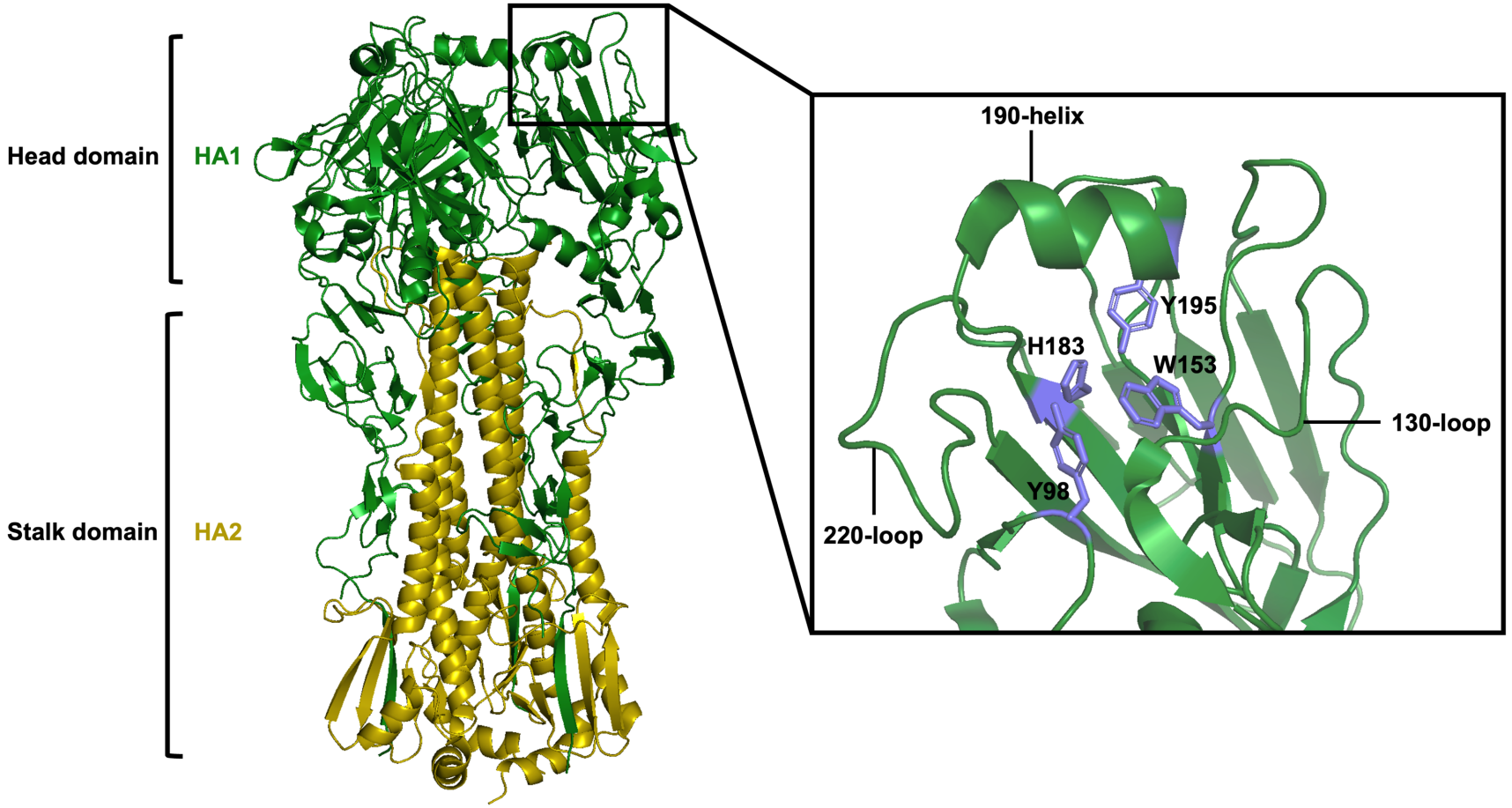
Head domain
HA1
Stalk domain
HA2
190-helix
Y195
H183
W153
130-loop
Y98
220-loop

Figure 2.1 FLUAV HA trimer structure. Crystal structure of the A/Victoria/361/2011 HA trimer (PDB: 4O5N [174]) showing the HA1 (green) and HA2 (gold) subunits. The sialic acid binding pocket can be found in the globular portion of the HA1. Residues Y98, W153, Y183, and Y195 (purple) are highly conserved among all sialic acid-binding HA subtypes (H1-H16). The sialic acid binding pocket is also formed by secondary structures such as the 130-loop, 190-helix, and 220-loop that provide structural stability.

Upon interaction with sialic acid, the virus is internalized via endocytosis or macropinocytosis [140, 175, 176], and the endosome is subsequently acidified which favors a conformational change in the HA protein [177]. This change exposes the positively charged fusion peptide found in the HA2 in order to fuse the virus and the endosomal membrane and release the FLUAV genome into the cytoplasm. This is a multistep process than can be generally divided into three main steps. First, due to the lower pH, the HA1 domain is protonated which lead to loss of intra and inter subunit interactions that allow water molecules to interact with the B-loop of the HA2 N-terminus [178]. Secondly, interaction of water with the B-loop of the HA2 triggers a loop-to-helix conformational change that forms a superhelix with the three monomers [179]. Lastly, the superhelix intermediate collapses and exposes the fusion peptide towards the endosomal membrane for a subsequent refolding of the helix comprised between residues 106-112 into a loop that juxtaposes the membranes allowing the formation of the fusion pore [180].

The viral NA helps during the budding stage, favoring release of the viral progeny from the infected cell, and also favors movement through the respiratory mucus by preventing binding to decoy receptors along with allowing the virus to roll on the surface of the target cell [32]. The NA is a homotetrameric type II transmembrane protein, consisting of a catalytic head, a stalk, a transmembrane region and a cytoplasmic tail domain [181]. Each NA monomer exhibits a catalytic pocket, but maximum catalytic efficiency is only observed in its tetrameric form [182]. The catalytic site consists of an inner shell formed by R118, D151, R152, R224, E276, R292, R372, and Y406 [183].

These residues directly interact with sialic acid and are highly conserved across multiple NA subtypes except for bat-derived NAs which seem to lack any enzymatic activity [184, 185]. Additionally, 10 other amino acids (E119, R156, W178, S179, D198, I222, E227, E277, N294, and E425) form an outer shell which does not directly interact with sialic acid during the catalytic process [186], instead, they are believed to be important to maintain the catalytic site structure [187]. The exact catalytic mechanism employed by FLUAV NA remains to be elucidated as it seems to differ from reactions previously described for NAs from other microorganisms. Nonetheless, studies have pointed out that FLUAV NA-mediated SA hydrolysis occurs via a nucleophilic mechanism mediated by Y406 to produce a planar, oxocarbonium ion intermediate [30].

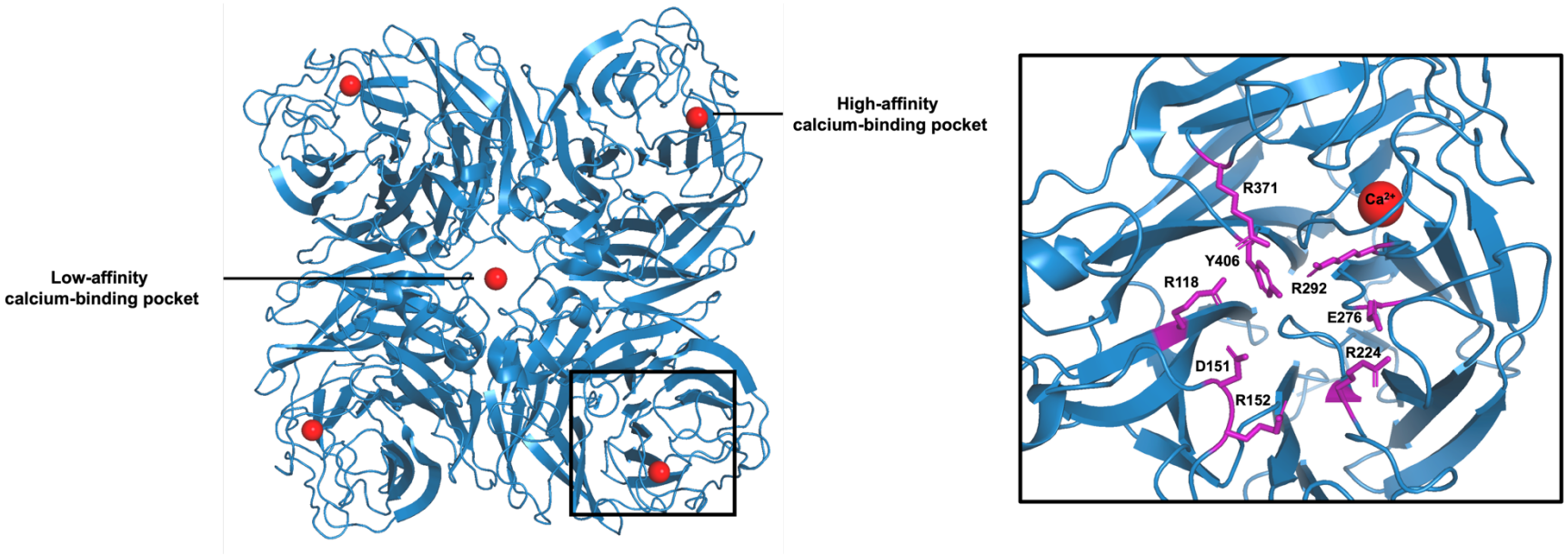

Figure 2.2 FLUAV NA tetramer structure. Crystal structure of the A/Tanzania/205/2010 NA tetramer (PDB: 4GZO [188]). Most NA subtypes possess at least a high-affinity calcium-binding pocket located in the catalytic site of each monomer. Some subtypes, including N1s and N2s can also bind a second calcium ion (red) in the symmetry axis of the tetramer known as the low-affinity calcium-binding pocket. Each monomer has a catalytic site and the catalytic residues (R118, D151, R152, R224, E276, R292, R372, and Y406) are highly conserved among all NA subtypes.

Calcium is a cofactor in the NA-mediated SA hydrolysis and most NA subtypes have a high-affinity calcium-binding pocket [189]. This pocket is formed by D293, G297, G345, D324, and N347 located within the catalytic site [190] and calcium binding here is believed to reposition the catalytic residues to allow proper SA binding [191]. The catalytic residues are highly conserved among different subtypes highlighting that FLUAV does not seem to accrue mutations in the catalytic pocket that modify the NA activity [30]. Additionally, some subtypes possess a low-affinity calcium-binding pocket in the fourfold symmetry axis of the tetramer [192]. Crystal structure analysis of the pH1N1 N1 revealed that the low-affinity calcium-binding pocket is formed by K111, D113, and most importantly Y170 [35]. Coordination of calcium in the symmetry axis of N1s has been demonstrated to stabilize the tetramer and promote thermal stability and indirectly enhances NA enzymatic activity since it is highly dependent on the tetramer stability [193]. This evidence suggests that mechanisms such as modulation of calcium binding in the NA calcium-binding pocket might serve as strategies used by FLUAV to regulate NA activity and restore the HA/NA balance whenever disrupted.

Factors limiting interspecies transmission of FLUAV.

FLUAV exhibits a wide host range including humans, poultry, cattle, equine, seals, bats, among others [194], however, FLUAV natural host are considered to be aquatic birds [195]. FLUAV interspecies transmission is frequent but subsequent persistence in the new host requires successful adaptation of the virus, which frequently involves changes in the receptor specificity of the virus [196]. N-acetylneuraminic acid linked with a a2,3 conformation to a terminal galactose molecule (Galβ(1,4)Glc/ GlcNAc,

Neu5Ac) are abundant in the gastrointestinal and respiratory tracts of birds and, therefore, avian-adapted viruses have a preference for these types of receptors [197]. Conversely, mammalian-adapted viruses mostly bind a2,6 SA [198] since these glycans are more abundant in the upper respiratory tract of mammals. However, it has been recently shown that N-acetylneuraminic acid is not the only glycoside recognized by FLUAV. Studies with highly pathogenic H5 viruses have demonstrated that H5s can bind to N-acetylgalactosamine in the form of sialilated or non-sialilated Galb(1,3)GalNac instead of sialilated Galβ(1,4)Glc/GlcNAc [199]. Additionally equine-adapted H7N7 and H3N8 viruses preferably bind N-glycolylneuraminic acid (Neu5Gc) instead of Neu5Ac [200] suggesting that viruses must recognize host-specific glycans in order to transmit in a new host. Therefore, mutations affecting the binding preference of the HA to different sialic acids can modulate the host range of the viruses [24]. The ability of FLUAV to infect a new host does not only rely on the ability to bind to certain sialic acid conformations, but also on the pH stability of the HA trimer. This has been experimentally demonstrated in multiple reports, especially in the adaptation process of avian-origin FLUAV to pigs. Residues 205 and 72 have been shown to play a pivotal role in the HA trimer stability as they form intermonomer interactions [201], and mutation of either amino acid results in changes in the pH stability of the HA; therefore modulating the pH threshold required to induce fusion [202]. Moreover, the HA acid stability has been linked with the pandemic potential of the pH1N1 virus [203]. The swine precursor exhibited relatively high pH of activation (5.5-6.0) that steadily decreased until 2009 (5.5) [12, 203, 204], and kept decreasing in the human population to finally stabilize at a pH of 5.2 [203]. This suggests that even though similar, adaptation of swine-origin viruses to humans might require

changes in the acid stability of the HA. In addition to the HA, the NA protein also plays a role during adaptation; however, its role has been understudied. The FLUAV NA is an enzyme that exhibits sialidase activity and its main role during infection is to allow virus movement throughout the respiratory mucus and assist newly synthetized viral particles release after budding [126, 205]. Because of its opposite role to HA, a functional balance between HA avidity and NA activity must be maintained in order to produce a successful infection [31], and, hence, its role in affecting host range may be associated with the maintaining the HA balance.

Besides the sialic acid preference of the viruses, the polymerase complex (PB1, PB2, and PA) also seems to play a major role during adaptation to a new host [36]. Humans have a temperature of 33°C in the upper respiratory tract and 37°C in the lower respiratory tract [206]; therefore, human-adapted viruses must be able to replicate and transcribe their genome at those temperatures. Conversely, FLUAV normally replicates in the GI tract of birds in which the temperature is slightly higher than in humans (41°C) [207]. This temperature difference can limit the replication of human viruses in birds and vice versa. This occurs because the polymerase complex of different FLUAVs display different temperatures at which the polymerase activity is optimal (normally 37°C for mammalian viruses and 41°C for avian viruses), which limits the hosts that a particular virus can infect [208]. This seems to be the consequence of alteration in the interaction between the polymerase complex with the vRNA, which ultimately inhibits both replication and transcription of the viral genome [41]. Additionally, the vRNA can adopt different secondary and tertiary structures depending on the temperature, which is mainly

modulated by the nucleotide composition of each individual segment. These vRNA structures can also inhibit the viral polymerase activity [209, 210].

In order to limit viral infections, organisms have developed multiple strategies to prevent replication of the invading pathogen. For example, Toll-like receptors (TLR) in the cytoplasm can sense the presence of different pathogen associated molecular patters (PAMPs), such as double-stranded RNA, which is not found in healthy cells [211]. Recognition of the FLUAV genome by TLRs triggers the innate response, which is mainly driven by interferon type I, II, and III (IFN) production [212, 213]. Studies have shown that IFN-g exerts a potent anti-FLUAV activity [214]. The protection mediated by IFN-g is achieved when the cell enters an "antiviral state" characterized by the activation of multiple interferon-stimulated genes (ISGs) [215]. For example, ISG15 has been shown to be covalently attached to NS1 [216]; therefore, preventing the innate immune response shutdown mediated by this protein. Another well-studied ISG is the Mx protein, which inhibits FLUAV replication by selectively preventing FLUAV vRNPs trafficking into the nucleus by binding to NP [217, 218]. Because the specificity of Mx for FLUAV is determined by only a few amino acids, the effectiveness of Mx-mediated FLUAV inhibition can vary among species [219]. Acquisition of mutations in the NP gene can help FLUAV to escape the Mx barrier; however, this significantly affects FLUAV growth in both avian and human cells [220]. Besides ISGs induction, IFN-g can also prevent FLUAV entry into surrounding cells *in vitro* by reducing the a2,3 and a2,6 SA clusters sizes on the plasma membrane without affecting the sialic acid density [221].

To prevent cells entering an antiviral state, FLUAV has developed several strategies through evolutionary time. NS1 is the main viral protein repressing the host's

immune response [222]. This protein has been shown to repress IFN at the pre- and post-transcriptional level. NS1 can directly bind to the retinoic acid-inducible gene-I (RIG-I), which is normally found in the cytoplasm, and upon activation induces the expression of IFN-b [223]. By sequestering RIG-I, NS1 not only prevents IFN expression but also prevents recognition of the viral genome. Alternatively, the C-terminal domain of the NS1 protein has been shown to interact with some nuclear proteins that participate in the mRNA maturation process, such as the cleavage and polyadenylation specific factor (CPSF) and the poly(A)-binding protein II (PABII) [224]. By targeting these factors, FLUAV blocks the export of mature cellular mRNAs and, therefore, prevents IFN expression at the post-transcriptional level [225]. Interestingly, some of these processes seem to be host specific as NS1 can interact with cellular factors through a PDZ-binding motif [226]. This interaction leads the cell to an anti-apoptotic state, which ultimately favors FLUAV replication. Nonetheless, this has only been observed in avian isolates [60, 227]. In addition to NS1, NS2/NEP can also directly interact with PB1 and PB2, which enhances the polymerase activity [228]. This has been demonstrated to be critical for efficient replication of H5N1viruses in mammalian cells without the need of any mammalian-adaptative mutations in the polymerase complex [229]. It is believed that the polymerase enhancement is the result of a stabilization of the cRNA molecules that indirectly favor the synthesis of new vRNA copies [229].

The human-swine interface.

Human FLUAV has been introduced to pigs multiple times giving rise to distinct phylogenetic lineages **(Figure 2.3)**. FLUAV was first detected in pigs in 1918 and

retrospective studies confirmed that it was most likely the result of an introduction of the human pandemic 1918 H1N1 virus [230]. This virus became established in the swine population in the United States generating the classical H1N1 lineage (cH1N1) that was the most important lineage in circulation until the 1990s [230]. Similarly, in 1970 in Taiwan was first detected a human H3N2 in pigs, similar to A/Hong Kong/1/1968 and named as A/Hong Kong/01/1968-like [231]. Nonetheless, H3N2 viruses showed a low prevalence (1.1%) in North America compared to H1N1 (51%) and were sporadically detected in the United States without causing illness [232]. However, in 1998 a rare FLUAV outbreak in North Carolina and followed by outbreaks in Minnesota, Iowa, and Texas occurred [233]. Sequencing of the outbreak isolates revealed it was a triple reassortant (TRIG) H3N2 virus carrying segments from the cH1N1 lineage (NS, NP, and M), human-seasonal H3N2 (PB1, HA, and NA), and avian-origin (PB2 and PA) [234]. These H3N2 TRIG viruses became endemic in the swine population, generating distinct phylogenetic clades that were initially divied into four groups (C-I to C-III) [235]. Cluster C-III was the most frequently detected and has continued to be detected at high levels in swine. In the following years the TRIG constellation was also detected in H1N1 viruses and became predominant in swine [236], as data suggested that these gene combinations resulted in a virus that transmitted efficiently [27]. TRIG viruses were occasionally detected in humans, but there were fewer than 30 zoonotic infections described between 1998-2010 [237], but limited to no human-to-human transmission was observed [238]. In April 2009 an unusual H1N1 (pH1N1) outbreak in humans was reported in Mexico [239] and rapidly spread to North America and the rest of the world. Due to high human-to

human transmission [240, 241] this swine-origin H1N1 was declared the first pandemic of the 21st century .

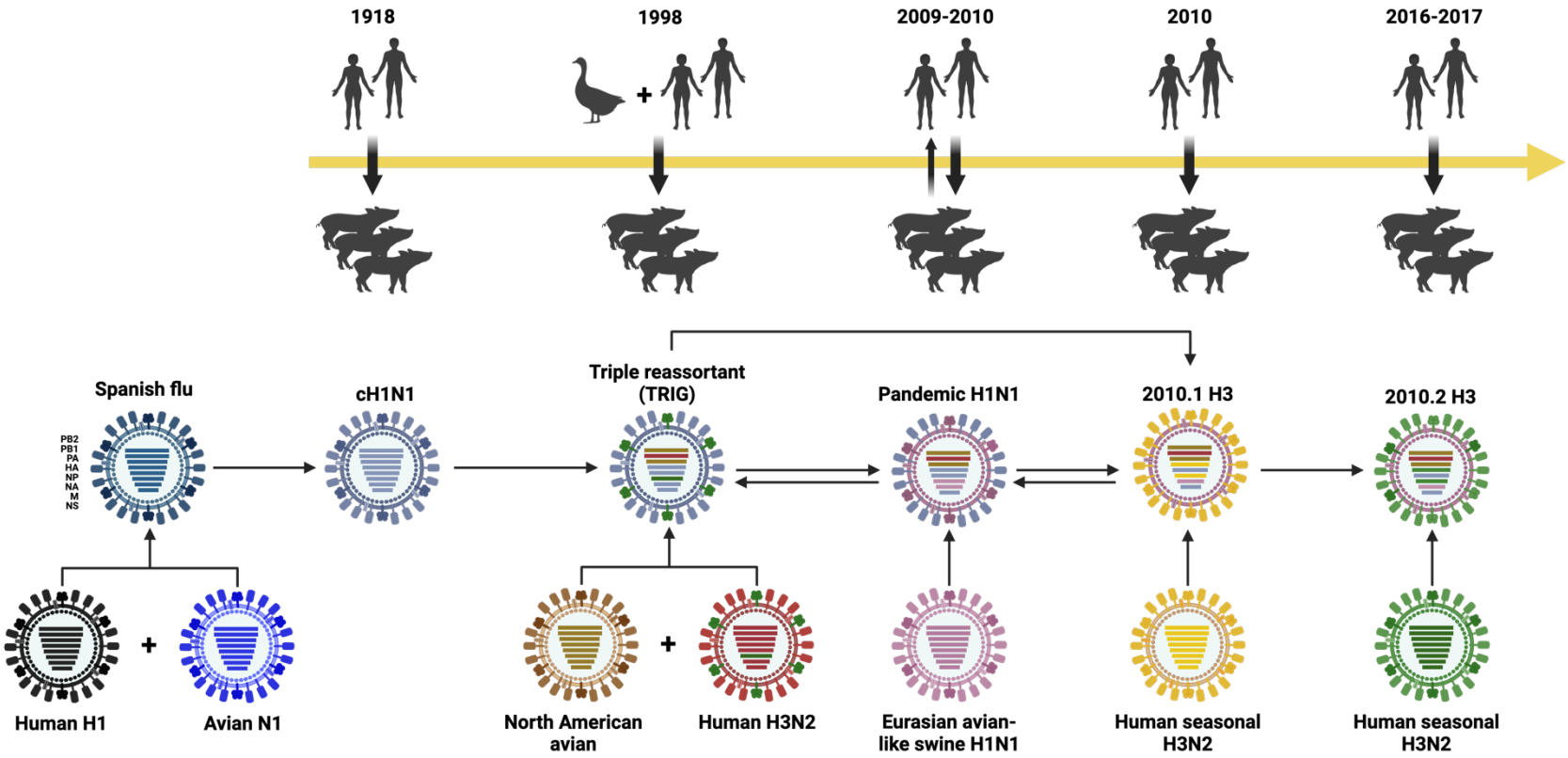
1918
1998
2009-2010
2010
2016-2017
Spanish flu
cH1N1
Triple reassortant (TRIG)
Pandemic H1N1
2010.1 H3
2010.2 H3
PB2
PB1
PA
HA
NP
NA
M
NS
Human H1
Avian N1
North American avian
Human H3N2
Eurasian avian-like swine H1N1
Human seasonal H3N2
Human seasonal H3N2

Figure 2.3 Evolution of FLUAV in the swine population. Introduction of the Spanish flu (H1N1) gave rise to the classical H1N1 lineage. This lineage circulated in pigs for nearly 70 years until in 1998 it reassorted with a North American avian and a human seasonal H3N2, which resulted in the triple reassortant backbone (TRIG). Further reassortment of an Eurasian avian-like swine H1N1 with the TRIG backbone originated the pandemic H1N1 virus in 2009. This pH1N1 was reintroduced to pigs becoming endemic. Eventually the virus reassorted and gained TRIG genes and replaced the TRIG M segment. Subsequently In the early 2010s a human seasonal H3N2 virus crossed to pigs and initially reassorted with the pandemic H1N1-derived backbone. This H3 became endemic in swine herds in North America and originated a new lineage known as 2010.1. Eventually, the virus also gained TRIG internal genes. Similarly, during the 2016-2017 FLUAV season, another human-to-swine spillover occurred. This virus became endemic in pigs and generated a new H3 lineage known as 2010.2.

Further sequencing efforts showed the virus originated in pigs and was the result of several reassortment events occurring in different swine FLUAV lineages for at least 10 years previous to the outbreak [16]. The pH1N1 was reintroduced multiple times back to pigs due to human-to-swine spillovers in different countries [242]. Reintroduction of pH1N1 allowed reassortment with endemic swine strains, and the virus appears to cause mild illness in swine [243]. Eventually, this virus became established in the swine population as a new lineage known as the H1N1-pandemic lineage, greatly increasing the genetic diversity of FLUAV circulating in swine [242]. Notably, in 2012 a reassortant H3N2 virus was reported circulating in swine heard in North America [244]. This virus possessed human-origin H3 and N2 segments and internal genes from the pH1N1 virus [245] which favored transmissibility among pigs and resulted in the establishment of a new H3 HA lineage known as the 2010.1 lineage. In 2017, another human-to-swine spillover resulted in another lineage that is now referred to as the 2010.2 H3 lineage; this virus was found to have human-origin surface genes, internal genes derived from the TRIG backbone, and the pandemic M segment [246]. Human H3N2 detection in swine are frequently reported, being the most recent during the 2022-2023 FLUAV season [247]. However, this virus was shown to cause mild disease and no transmission to contact animals from experimentally inoculated pigs was observed [247]. These reports highlight the relationship between human and swine FLUAV, and demonstrate that human-to-swine spillovers are frequent. Transmission of human viruses to pigs has contributed to the antigenic diversity of FLUAV in swine herds. Nonetheless, not all of the introductions lead to the establishment of the virus in pigs, denoting that human seasonal viruses are not efficient at transmitting in pigs, and there must be changes in the

genome of the virus that support efficient infection and transmission in the new host. Although major efforts have been performed to understand the barriers human viruses must overcome to become adapted to pigs, important knowledge gaps remain to be filled.

Host barriers limiting human-origin FLUAV infection of swine.

Pigs have been considered a "mixing vessel" host as they can be infected by avian-, human-, and swine-adapted FLUAV due to the presence of both a2,3 and a2,6 SA in their respiratory tract [25]. Coinfection of pigs with multiple subtypes can result in reassortment, with the potential to generate novel FLUAVs with the ability to infect and transmit among humans, as occurred with the pH1N1 virus in 2009 that quickly spread worldwide [16, 248]. Nonetheless, zoonotic infections are rare and swine-origin viruses normally do not persist in the human population [235, 249]. Contrary, reverse zoonotic infections are more frequent and human viruses are commonly detected in swine herds [246]. The introduction of human viruses to pigs has contributed to increasing the genetic diversity of FLUAV circulating in pigs [250]. However, wholly human viruses replicate and transmit poorly in swine [247] and the few that persist normally reassort shortly after introduction and acquire swine-adapted internal genes [17, 251], allowing the continued circulation of human-origin HA and NA segments, although with mutations, in swine to continue the adaptation process. This was demonstrated with a human-seasonal H3N2 virus, in which the wholly human virus failed to infect and transmit in pigs, but the virus carrying the same HA and NA in a swine-adapted backbone (PB2, PB1, PA, NP, NS, and M) led to transmission and acquisition of HA mutations (A138S, V186G, and F193Y) that increased affinity for swine cells *in vitro* [27]. Hence, initial reassortment with

circulating swine-adapted FLUAV seems to be a first critical step in the adaptation of human viruses to pigs, which then promotes acquisition of adaptative mutations in the surface glycoproteins.

The molecular basis of the adaptation of human viruses to pigs are poorly understood. The HA protein is the main determinant of the host range of FLUAV, and generally, interspecies transmission involves a switch in the receptor preference of the virus, e.g.: recognition of a2,6 SA by avian viruses allows them to infect mammals [252]. However, both human and swine express mostly a2,6 SA in their upper respiratory tract and similar receptor distribution overall [18]. Nonetheless, human FLUAV seems to not bind efficiently to swine cells [27], suggesting that there are swine-specific a2,6 SA conformations that are utilized by swine but not human viruses. Further, unlike other mammals, humans cannot synthetize Neu5Gc due to a mutation in the gene coding for the CMP N-acetyl neuraminic acid hydroxylase that inactivates the enzyme [253]. This difference has been postulated as one of the determinants limiting human FLUAV infection of pigs [254], a species that expresses Neu5Gc. However, while some studies found that swine viruses recognize both Neu5Gc and Neu5Ac and human FLUAV fail to bind to Neu5Gc [254, 255], others have not found significant differences in the binding preference for Neu5Ac or Neu5Gc of swine and human viruses [256, 257]. Moreover, swine H3N2 viruses were shown to recognize a2,6 SA with a higher affinity than human H3N2, and affinity for this type of receptor seemed to increase with the level of adaptation to pigs, suggesting that the strength of the interaction with a2,6 Neu5Ac could also play a role in this process [258]. Nonetheless, although SA distribution in the respiratory tract of humans and pigs is overall similar, the abundance of each Neu5Ac

diverges. Swine have a higher density of a2,6 SA in the upper respiratory tract (nose and trachea) and a2,3 abundance gradually increases towards the lower respiratory tract [25]. In contrast, humans mainly express a2,6 SA throughout the respiratory tract, and a2,3 SA seems to be restricted to bronchi, and alveolar epithelial cells, and goblet cells to a lesser extent [259]. This difference could potentially affect infection of human viruses through the respiratory tract of pigs, restricting replication to specific sites such as the upper respiratory tract.

Since human-origin HA seems to rapidly acquire mutations in the swine host, the NA activity is likely to also be modified to maintain the HA/NA balance. However, it is unclear if all mutation have a functional balance. Studies have shown that early isolates of the pH1N1 virus detected in humans exhibited increased NA activity compared to a swine-adapted precursor, but similar levels of a2,6 binding, suggesting the HA/NA balance was disrupted upon jump to humans [33]. Interestingly, by restoring the HA/NA balance, higher levels of droplet transmission were seen in ferrets, suggesting that a functional balance does not only facilitate infection of a new host but can also affect transmission of the virus [260]. Similar findings were observed in studies where successful infection of pigs with human-adapted HA- and NA-bearing viruses results in limited to no transmission in the swine host [258]. Despite the relevance of the HA/NA balance, little is known about the molecular mechanisms employed by FLUAV to modulate NA activity.

The temperature of the lower respiratory tract of pigs is slightly higher than that of humans (39°C vs 37°C). Because of this difference, viruses jumping to pigs experience a different local environment and different selective pressures; viruses that persist likely

acquire mutations in the polymerase genes that facilitate proper replication and transcription of the viral genome [261]. An alternate approach for a novel virus to persist is via reassortment whereby human seasonal viruses, during coinfection with endemic swine viruses, acquire swine-adapted polymerase genes [18]. There is evidence that the majority of novel interspecies transmission events that result in persistent transmission in the new hosts have acquired one or more genes through reassortment. Not only the polymerase genes, but the NP segment seems to also play a role in adaptation to swine. Recent surveillance in the United States has shown an increase for the detection of the NP gene from the pandemic H1N1 lineage since 2019 [262], replacing the TRIG NP that circulated in pigs for over 20 years [263]. This change was shown to increase transmission among pigs, although this effect seems to be dependent on the HA gene [263]. Similarly, the pH1N1 M segment demonstrated a "selective sweep" and replaced the previously dominant TRIG M gene that was established in the swine population [264]. This change was demonstrated to enhance be associated with virus morbidity and mortality in mice by enhancing replication in the lungs and the lesions causes by FLUAV [264]. Introduction of the pandemic M segment into a 7+1 human H3N2 virus resulted in enhanced shedding in pigs but no transmission, contrasting a wholly human virus which failed to infect pigs [27], suggesting that the pandemic M gene confers a fitness advantage in pigs.

Molecular evolution of human-origin HA and NA in the swine host

By the time most human-origin viruses are detected in swine, many mutations have been acquired, particularly on the surface proteins, making these viruses quite

different from precursor strains. However, the HA1 portions of the human-origin H3 HA continue to evolve antigenically away from the seeding human seasonal lineages, with recent phylogenetic analyses showing rapid evolution particularly after the pH1N1 reintroduction in swine [242]. For the strains in the 1990.4 lineage, this shift has been linked to changes at positions 145, 155, 156, 158, 159, and 189 [265]. Mutations in at least one of these positions were shown to decrease cross-reactivity and therefore could have favored immune escape of FLUAV in pigs due to a reduced antibody recognition [266]. Position 145 seemed to have a particular role in the antigenic evolution of these viruses [266]. All these mutations fall within the HA RBS proximity, but little is known about their impact on receptor binding. Interestingly, N145K was later shown to not directly reduce antibody recognition [267]. Instead, acquisition of this mutation increased receptor binding avidity which increased binding to red blood cells, consequently leading to reduction of hemagglutinin inhibition (HI) titers [267, 268]. Further, residues 156 and 158 were associated with the replication phenotype of swine H3N2 viruses [269]. Particularly, K156 and G158 were identified in viruses exhibiting reduced antibody recognition and greater replication capacity in MDCK cells than viruses carrying E156 and E158 [269]. Although no studies were performed regarding the sialic acid affinity of the different mutants, it was hypothesized that they increased affinity for host-specific sialic acid structures [269]. Substitution T159N in addition to T155V and E190D were shown to favor adaptation of avian-origin H3 to the swine host [24]. Viruses carrying these adaptative mutations and swine-adapted internal genes showed efficient replication in swine *in vivo* coupled with enhanced pig-to-pig and pig-to-ferret transmission [270].

Two separate human-origin N2 introductions have been reported in U.S swine herds in 1998 and 2002 [271]. These introductions gave rise to two different phylogenetic clades of N2s currently circulating in swine which are antigenically distinct from human N2s, although they were originated from a human precursor [271]. Specifically, changes in positions 263, 265, 331, 332, 367, 369, 400, 401, 402, and 435 have been found to account for these antigenic differences [271], none of which participate in the catalytic process. However, temporal evolution of H3 and N2 genes in US swine population show similar rates of evolution between the two proteins [272], suggesting that changes in one protein imposes an evolutionary pressure in the other to evolve, possibly to maintain the HA/NA balance. FLUAV NAs exhibit an overall higher substrate affinity for a2,3 SA over a2,6 SA [273, 274], suggesting that adaptation of avian-origin viruses may involve a switch in the NA substrate preference to enhance catalysis in presence of a2,6 SA [273]. However, mammalian viruses always retain the ability to degrade a2,3 SA in addition to a2,6 SA. Nonetheless, since the NA catalytic site is not affected, it remains unclear how FLUAV modulates NA activity to restore the balance, as most changes observed in human-origin N2s detected in swine seem to favor antigenic escape rather than modulate NA enzymatic activity.

Effect of previous immunity on the evolutionary trajectory of FLUAV

Vaccination is the most effective measure against FLUAV in swine herds [275]. Although several vaccines are approved for use in swine, they do not offer sterilizing protection and suboptimal protection against heterosubtypic infections has been reported [276]. Contrary to the selection of human vaccine strains organized by the World Health

Organization (WHO), there is not an established protocol in place to select FLUAV strains to use in swine vaccines [275]. In the United States around 70% of the swine population is vaccinated and the only licensed vaccines are inactivated and multivalent (H1N1, H3N2, and/or H1N1) [277]. In recent years a new vaccine against H3N2 based on non-replicative alphavirus particle was approve for animal use [278]. Nonetheless, in North America, close to 50% of all vaccines used are inactivated, autogenous against herd-specific viruses [277].

Whole inactivated vaccines (WIV) normally induce a strong antibody response against the vaccine antigen. In the FLUAV context, they mainly target the HA, NA, M, and NP proteins [279]. Nonetheless, the majority of the neutralizing antibodies target the HA surface protein [280]. By binding to the HA, the antibodies prevent attachment to the cellular receptor and thus preventing infection [281, 282]. Antibodies targeting NA cannot prevent infection, but they can reduce the efficiency of new viral particles release by inhibiting the sialidase activity of the NA [283]; however, anti-NA antibodies remain largely understudied. As mentioned above, for the antibodies to work the best, the vaccine strain must closely related match to the challenge virus. Since the H3s of human- and swine-adapted viruses are antigenically distinct [244, 266], reports have shown that vaccination of pigs can reduce but not prevent swine-to-human spillovers [284]. Similarly, studies have shown that ferret sera raised against swine H3N2 exhibit little to no cross-reactivity with contemporary human vaccine strains or candidate vaccine viruses [285] thus suggesting that human viruses could easily jump to pigs even if they were vaccinated. This is further supported by a study presented by Zeller, et al. [285] in which human-like H3N2 viruses detected in swine during the 2022-2023 FLUAV season were

antigenically distinct from circulating swine strains. This study highlights that human viruses could have crossed to swine regardless of the vaccination status of the animal. However, no studies have evaluated the effect of vaccination on the evolution trajectory of human H3N2 viruses in immunized pigs.

Vaccination was shown to affect the evolutionary trajectory of swine H1N1 and H3N2 viruses in pigs in previous studies. Since most changes were detected in the surface proteins HA and NA, antibody escape seems to drive evolution of these viruses in vaccinated animals [87]. The HA was shown to accumulate mutations in the head and the stalk domains, while the NA exhibited most changes in the head domain [87]. However, although these amino acid changes were hypothesized to prevented antibody recognition, their real biological significance was not evaluated. Another study evaluated the evolution of the Eurasian avian-like swine FLUAV in vaccinated and non-vaccinated pigs, showing that the Eurasian viruses seem to acquire mutations more rapidly in vaccinated compared to non-vaccinated animals [286]. Interestingly, the transmission bottleneck was loose regardless of the vaccination status of the animals, most likely due to the antigenic mismatch between the vaccine strain and the challenge virus used [286]. Although these previous findings suggest that vaccination increases the substitution rate of FLUAV in the swine host, these studies were performed using endemic pig viruses. Hence, the impact of vaccination in the inter- and intra-host evolutionary trajectory of human viruses following spillover to pigs remains unknown.

CHAPTER 3

AMINO ACID 138 IN THE HA OF A H3N2 SUBTYPE INLFUENZA A VIRUS INCREASES AFFINITY FOR THE LOWER RESPIRATORY TRACT AND ALVEOLAR MACROPHAGES IN PIGS

Matias Cardenas, Brittany Seibert, Brianna Cowan, Ana Luiza S. Fraiha, Silvia Carnaccini, L. Claire Gay, Flavio Cargnin Faccin, C. Joaquin Caceres, Tavis K. Anderson, Amy L. Vincent Baker, Daniel R. Perez and Daniela S. Rajao. (2024). PLoS Pathogens 20(2). Reprinted here with permission of the publisher.

Abstract

Influenza A virus (FLUAV) infects a wide range of hosts and human-to-swine spillover events are frequently reported. However, only a few of these human viruses have become established in pigs and the host barriers and molecular mechanisms driving adaptation to the swine host remain poorly understood. We previously found that infection of pigs with a 2:6 reassortant virus (hVIC/11) containing the hemagglutinin (HA) and neuraminidase (NA) gene segments from the human strain A/Victoria/361/2011 (H3N2) and internal gene segments of an endemic swine strain (sOH/04) resulted in a fixed amino acid substitution in the HA (A138S, mature H3 HA numbering). Further analysis revealed that 138S has become predominant among swine H3N2 viruses, contrasting with human isolates where A138 is prevalent. To understand the role of the HA A138S substitution in the adaptation of a human-origin FLUAV HA to swine, we infected pigs with the hVIC/11^{A138S} mutant and analyzed pathogenesis and transmission compared to hVIC/11 and sOH/04. Our results showed that the hVIC/11^{A138S} virus had an intermediary pathogenesis between hVIC/11 and sOH/04. The hVIC/11^{A138S} infected the upper respiratory tract, right caudal, and both cranial lobes while hVIC/11 was only detected in nose and trachea samples. Viruses induced a distinct expression pattern of various pro-inflammatory cytokines such as IL-8, TNF-a, and IFN-b. Flow cytometric analysis of lung samples revealed a significant reduction of porcine alveolar macrophages (PAMs) in hVIC/11^{A138S}-infected pigs compared to sOH/04 while a MHCII^{low}CD163^{neg} population was increased. The hVIC/11^{A138S} showed a higher affinity for PAMs than hVIC/11, noted as an increase of infected PAMs in bronchoalveolar lavage fluid (BALF), and showed no differences in the percentage of HA-positive PAMs compared to sOH/04. This increased infection of PAMs led to an overexpression of granulocyte-monocyte

colony-stimulating factor (GM-CSF) stimulation but a reduced expression of peroxisome proliferator-activated receptor gamma (PPARg) in the sOH/04-infected group. Analysis using the PAM cell line 3D4/21 revealed that the A138S substitution improved replication and apoptosis induction in this cell type compared to hVIC/11 but at lower levels than sOH/04. Overall, our study indicates that adaptation of human viruses to the swine host involves an increased affinity for the lower respiratory tract and alveolar macrophages.

Introduction

Influenza A viruses infect various animals, including birds, pigs, and humans [287]. While some strains have a restricted host range, it is well-documented that some viruses can jump between species [288]. A clear example is the emergence of the 2009 swine-origin H1N1 pandemic virus that rapidly spread worldwide in humans [16]. However, human-to-swine transmissions of FLUAV are more frequent than zoonotic events [17, 18]. Although human-origin H1N1 and H3N2 FLUAV infections in pigs are frequent, H3N2 infections are generally self-limiting, and a reduced number of viruses evolve enough to become prevalent in the swine population [235]. One of the most recent examples is the spillover of a human-origin H3N2 during the 2010/2011 season that became established as a new H3N2 swine FLUAV lineage in North America (known as the 2010.1 lineage) [244]. Despite many of these human-origin viruses becoming established in swine and contributing to the diversity of viruses circulating in pigs globally, little is known about the biological processes driving human-to-swine adaptation. Previous reports showed that acquiring swine-origin FLUAV internal genes is critical [244, 289]. Since the temperature of the lower respiratory tract of pigs is slightly higher than that of humans [18], the polymerase complex must be adapted to higher temperatures to overcome this host barrier, potentially through reassortment or gain of adaptative mutations [290, 291]. It has also been shown that the HA gene can adapt to the new host via introduction of changes increasing receptor-binding affinity of the HA protein [29, 292]. As a consequence, alterations of the NA gene are essential to maintain the balance between HA avidity and NA activity [33]. In addition, the ability of the virus

to suppress or evade host-specific immune responses can also drive FLUAV evolution aiding in the establishment of viral infections during cross-species transmission.

Alveolar macrophages (AMs) are the most abundant immune cells in the lungs and account for up to 98% of cells in bronchoalveolar lavage fluid in pigs [63]. AMs contribute to the first line of defense against respiratory pathogens and are essential in developing innate and adaptative immune responses during FLUAV infection. Previous reports showed that they play a critical role in controlling FLUAV infection via the production of type I interferons and other pro- and anti-inflammatory cytokines such as TNF-a, IL-6, and IL-10 together with their intrinsic phagocytic activity [64, 65]. Moreover, AMs play a significant role in building antibody-mediated protection against FLUAV, inducing and regulating the primary anti-FLUAV cytotoxic T-cell response [66, 67]. AM-depleted animals infected with FLUAV have higher lung replication, overexpression of pro-inflammatory cytokines, increased tissue damage and higher mortality, underscoring that AMs are imperative for combatting FLUAV infection [68-70]. While AMs are essential for the anti-influenza immune response, they have been previously reported to be susceptible to FLUAV infection [71, 72]. However, numerous FLUAV HA subtypes show limited virus replication within these cells except for a subset of both highly pathogenic and low pathogenic H5 viruses that efficiently replicate in swine, mice, and human AMs [72-75]. Nonetheless, both H3 and H1 viruses have also been described to infect mice AMs [76]. Previous literature suggests that FLUAV infection of AMs not only induces death by apoptosis [21], but also impairs the immune activity of AMs via peroxisome proliferator-activated receptor gamma (PPARg) repression [77, 78]. This transcription factor regulates AMs activity and is activated after

granulocyte-monocyte colony-stimulating factor (GM-CSF) stimulation [79, 80]. GM-CSF and PPARg have also been described as main factors promoting monocyte differentiation into AMs and their proliferation [81, 82]. However, the effect, if any, of FLUAV infection of AMs on virus tropism and host range is still unknown [83].

To assess the adaptation of human-derived HA to pigs and its implications on the swine immune response, we generated an H3N2 reassortant virus (hVIC/11) containing the HA and NA segments of a human seasonal A/Victoria/361/2011 (H3N2) virus and the remaining genes forming an internal gene constellation highly adapted to pigs. This internal gene constellation is formed by a combination of the triple reassortant internal gene (TRIG) cassette and the 2009 pandemic matrix (M) gene which was the most prevalent constellation circulating from 2014-2019 in North American swine herds. When pigs were inoculated with the hVIC/11 virus, a point mutation near the receptor-binding site of the HA protein (A138S) became fixed in contact pigs [27]. This mutation improved binding and replication in swine tracheal cells *in vitro* [27]. To further understand the impact of this mutation on pathogenesis and transmission, pigs were inoculated with a hVIC/11 virus carrying the A138S amino acid change (hVIC/11^{A138S}) and compared to the original hVIC/11 and a swine-origin H3N2 virus A/turkey/Ohio/313053/2004 (sOH/04). We found that hVIC/11^{A138S} infected the upper and lower respiratory tract, while hVIC/11 was only detected in the upper respiratory tract by 5 days post infection (dpi). PAMs in bronchoalveolar lavage (BALF) samples were significantly decreased in sOH/04- and hVIC/11^{A138S}-infected pigs but not in hVIC/11-infected animals. This reduction of PAMs was accompanied by an increased number of FLUAV-infected PAMs; however, only sOH/04 suppressed PPARg

expression. Upon further analysis using the porcine alveolar macrophage cell line 3D4/21, we found that the A138S mutation increases the virus' ability to replicate and induce apoptosis in PAMs compared to hVIC/11 but at lower levels than sOH/04, suggesting that the decreased number of PAMs observed *in vivo* could be due to FLUAV-induced apoptosis.

Materials and Methods

Ethics statement

Animal studies were reviewed and approved by the Institutional Animal Care and Use Committee (IACUC) at the University of Georgia (protocol A2019 03-031-Y3-A9). Studies were conducted under biosafety level 2 containment and following the Guide for the Care and Use of Agricultural Animals in Research and Teaching.

Cells and viruses

Madin-Darby canine kidney (MDCK) cells were maintained in Dulbecco's Modified Eagles Medium (DMEM, Sigma-Aldrich, St Louis, MO) supplemented with 10% fetal bovine serum (FBS, Sigma-Aldrich, St Louis, MO), 2mM L-glutamine (Sigma-Aldrich, St Louis, MO), and 1% antibiotic/antimycotic (Sigma-Aldrich, St Louis, MO). 3D4/21 cells were maintained in Roswell Park Memorial Institute media (RPMI-1640, Sigma-Aldrich, St Louis, MO) supplemented with 10% FBS, 2mM L-glutamine, 1% antibiotic/antimycotic, 1 mM non-essential amino acids (Sigma-Aldrich, St Louis, MO), and 1 mM sodium pyruvate (ThermoFisher Scientific, Waltham, MA). All cell lines were cultured at 37°C under 5% CO_2. Viruses used in this study were: a reassortant carrying seven genes from A/turkey/Ohio/313053/2004 and the pandemic H1N1pdm09 (A/California/04/09) matrix gene (sOH/04); a reassortant carrying the HA and NA genes from A/Victoria/361/2011 and internal genes from sOH/04 (hVIC/11); and hVIC/11^{A138S} which only differs from hVIC/11 by an A to S amino acid substitution at position 138 in the HA gene (H3 nomenclature). Notably, the PB2, PB1, PA, NP, M, and NS genes were

the same for all viruses. These viruses have been previously reported by our group [27]. Viral titers were determined by $TCID_{50}$ using the Reed and Muench method [293].

Electron Microscopy

Viruses were adsorbed for 5 minutes in formvar-carbon-coated copper grids (ThermoFisher Scientific, Waltham, MA). After adsorption, samples were fixed with 0.7% glutaraldehyde (Sigma-Aldrich, St Louis, MO) for 5 minutes at room temperature. After, samples were negatively stained with 3% phosphotungstic acid pH 7.0 (Sigma-Aldrich, St Louis, MO) for 60 seconds. Finally, the excess stain was drained, and the grids were dried on filter papers. Viruses were imaged using a JEOL JEM1011 transmission electron microscope (JEOL USA, Peabody, MA) at 80 kV.

In vitro growth kinetics

MDCK cells were seeded in Opti-MEM (Life Technologies, Carlsbad, CA, USA) and incubated overnight or until a 70-80% confluency was reached. Cells were infected at a multiplicity of infection (MOI) of 0.01 for 1 hour at 37°C or 39°C. Immediately after, plates were washed three times with phosphate-buffered saline (PBS) and fresh Opti-MEM containing 1 mg/ml of tosylsulfonyl phenylalanyl chloromethyl ketone (TPCK)-treated trypsin (Worthington Biochemicals, Lakewood, NJ) was added. Timepoints were collected at 0, 12, 24, 48, and 72 hours post-infection (hpi). Viral RNA was extracted using the MagMax-96 AI/ND viral RNA isolation kit (ThermoFisher Scientific, Waltham, MA) according to the manufacturer's instructions. A one-step real-time quantitative PCR (RT-qPCR) using the Quantabio qScript XLT One-Step RT-qPCR ToughMix kit

(Quantabio, Beverly MA) targeting the M segment was used to determinate viral titers. The reaction master mix was prepared by mixing 1X Quantabio master mix, 0.5 mM of each primer, 0.3 mM TaqMan probe and 5 mL of RNA. Finally, viral titers were calculated according to a standard curve of an exact match of virus stock of known titer based on a $TCID_{50}$ equivalent ($TCID_{50}$eq/mL) standard curve.

Growth kinetics in 3D4/21 cells were performed by infecting cells at MOI of 0.01 for 1 hour at 37°C. After infection, cells were washed three times with PBS and supplemented with fresh infection media (RMPI-1640, 0.3% BSA, 2 mM L-glutamine, 1% antibiotic/antimycotic, 1 mM non-essential amino, 1 mM sodium pyruvate, and 250 ng/mL TPCK-treated trypsin).

Plaque assay

MDCK cells were seeded in 6-well plates at 10^6 cells/well and were incubated overnight at 37°C or until a 100% confluency before use. The next day cells were infected with 10-fold serial dilution of the viral stock for 1 hour at 37°C. After infection, cells were washed three times with PBS and overlayed with Opti-MEM containing 0.8% Avicel. Plates were incubated for 72 hours at 37°C or 39°C. Finally, cells were fixed for 1 hour with 37% formaldehyde (Sigma-Aldrich, St Louis, MO), rinsed twice with PBS, and stained for 15 minutes with 0.5% crystal violet in 20% methanol.

Thermal stability

The thermal stability of the viruses was assessed by normalizing them to 32 HAU in PBS. Then, samples were incubated for 1 hour at the indicated temperatures.

Afterward, samples were immediately placed in ice, and HA titers were measured using 0.5% turkey red blood cells.

NA enzymatic activity

NA sialidase activity was measured as previously described by Marathe, Leveque [294]. Briefly, viruses were diluted, and the dilution of choice was the one that met the following parameters: within the linear range and a saturated 2′-(4-Methylumbelliferyl)-α-D-N-acetylneuraminic acid sodium salt hydrate (MUNANA, Sigma-Aldrich, St Louis, MO) concentration. The chosen dilution was then used to calculate NA kinetic constants by performing kinetics for 60 minutes at 37°C at 1000, 500, 250, 125, 62.5, 31.25, 16.63, 7.81, 3.91, and 1.95 mM MUNANA. Fluorescence was measured every 60 seconds at excitation and emission wavelengths of 360 nm and 460 nm, respectively, using a Synergy HTX Multi-Mode Microplate Reader (Agilent BioTek, Santa Clara, CA).
The inner filter effect was corrected by measuring MUNANA absorbance at 4-Methylumbelliferone (4-MU) emission wavelength at different concentrations. Using the corrected fluorescence, 4-MU production over time was calculated using a standard curve and data was fitted to the Michaelis-Menten equation:

$$V_0 = \frac{V_{max} * [S]}{K_m + [S]}$$

Hemagglutinin solid-phase binding assay

A direct solid-phase binding assay using sialylglycopolymers was used as described by Matrosovich and Gambaryan [295]. Briefly, viruses were pelleted by ultracentrifugation (28,000 rpm for 3 hours) through a 20% sucrose cushion and

resuspended in TNE buffer (0.01M Tris, 0.001M EDTA, 0.1 M NaCl, pH 7.2). Purified viruses were normalized to 128 HAU in PBS and incubated overnight at 4°C in fetuin-coated 96-well plates (ThermoFisher Scientific, Waltham, MA). Plates were then washed three times with 0.02% Tween-80 (Sigma-Aldrich, St Louis, MO) in PBS (washing buffer) and blocked with 0.1% desialylated BSA (BSA-NA) in PBS (blocking solution) for 2 hours at room temperature. After blocking, plates were washed three times with washing buffer and 2-fold serial dilution of Neu5Aca2-3Galb1-4GlcNAcb-PAA-biotin (a2,3, 3'SNL, Glycotech, Gaithersburg, MD) or Neu5Aca2-6Galb1-4GlcNAcb-PAA-biotin (a2,6, 6'SLN, Lectinicity Holding, Moscow, Russia) in reaction buffer (0.02% Tween-80, 0.1% BSA-NA, and 2 mM oseltamivir in PBS) were added. Plates were incubated for 1 hour at 4°C. After, plates were washed five times with washing buffer and incubated with a 1:1,000 dilution of HRP-conjugated streptavidin (ThermoFisher Scientific, Waltham, MA) in reaction buffer for 1 hour at 4°C. Finally, plates were washed five times and then incubated with TMB (ThermoFisher Scientific, Waltham, MA) for 10 minutes at room temperature and the reaction was stopped using a stop solution (ThermoFisher Scientific, Waltham, MA). Absorbance was measured at 450 nm using a Synergy HTX Multi-Mode Microplate Reader.

In vivo studies

3-weeks-old healthy cross-bred pigs were obtained from Midwest Research Swine Inc (Gibbon, MN) and housed in animal biosafety level 2 (BSL2) facilities at the University of Georgia. After a 7-day acclimatation period, pigs were bled to confirm the absence of anti-FLUAV antibodies by ELISA (IDEXX, Westbrook, ME), and randomly

distributed into four groups of three pigs each and challenged intranasally and intratracheally with $3x10^6$ $TCID_{50}$/pig of either sOH/04, hVIC/11 or hVIC/11^{A138S} under anesthesia using a cocktail of ketamine (6 mg/kg), xylazine (3 mg/kg), and telazol (6 mg/kg). Pigs were observed daily for clinical signs, and nasal swabs were collected at 0, 2, and 5 days post-infection (dpi). At 2 dpi, a new set of 3 pigs was introduced in the same housing as the inoculated pigs and nasal swabs were collected at 0, 3, and 6 dpc. At 5 dpi/6 dpc, pigs were anesthetized and humanely euthanized by an intravenous pentobarbital overdose (Euthasol, 200 mg/kg), and a new set of contacts was introduced. Upper, middle, and lower trachea, lung lobes (right cranial, left cranial, right caudal, left caudal, and accessory), and bronchoalveolar lavage fluid (BALF) samples were collected post-mortem and stored at -80°C for virus titration and gene expression analysis. All pigs were determined to be negative for Porcine circovirus type 2 (PCV2), Porcine reproductive and respiratory syndrome virus (PRRSV), and Mycoplasma hyopneumoniae by qPCR (Table 3.1) of BALF samples.

Tissue preparation for FLUAV titration and nasal swab virus titration

Lung sections were homogenized using the Tissue Lizer II (Qiagen, Gaithersburg, MD) by adding 1 mL of PBS to each tube containing the sample and a Tungsten carbide 3 mm bead (Qiagen, Gaithersburg, MD) and then homogenizing for 10 minutes at 30 Hz. RNA from tissue and nasal swab samples was then extracted using the MagMax-96 AI/ND viral RNA isolation kit. Tissue samples were then normalized to 1 mg total RNA in 20 mL of nuclease-free water while RNA extracted from nasal swabs was used directly in the RT-qPCR reaction. The one-step RT-qPCR was performed using the Quantabio

qScript XLT one-Step RT-qPCR ToughMix kit as described above and FLUAV $TCID_{50}$ equivalent per mg of total RNA titers ($TCID_{50}$eq/mg total RNA) in tissue sections was calculated according to a standard curve of an exact match of virus stock of known titer.

Tissue immunofluorescence and histopathology

Lung sections were collected in 10% neutral-buffered formalin, paraffin-embedded. For immunofluorescence detection of FLUAV and sialic acid receptors, paraffin-embedded sections were deparaffinized as previously described Zaqout, Becker [296] with minor modifications. Briefly, tissue slides were deparaffinized and rehydrated for subsequent heat-induced antigen retrieval in citrate buffer (10 mM sodium citrate, pH 6.0) for 40 minutes. Rehydrated samples were then permeabilized for 10 minutes with 0.3% TritonX-100 and blocked for 1 hour with 5% bovine serum albumin in PBS. FLUAV was detected using a primary anti-Multi-Hemagglutinin (H3N2) polyclonal antibody (eEnzyme, Gaithersburg, MD) followed by a secondary Alexa 647-conjugated anti-rabbit antibody in a 1:1,000 dilution in PBS containing 0.5 μg/mL 4',6-diamine-2-phenylindole (DAPI, Sigma-Aldrich, St Louis, MO) for 1 hour each. Finally, tissues were washed 5 times with PBS and mounted on glass slides with mounting medium (Vector Laboratories, Newark, CA). Sialic acid receptors were detected by incubation of previously blocked samples with fluorescein-conjugated *Sambucus nigra* agglutinin (SNA) and biotin-conjugated *Maackia amurensis* agglutinin (MAL II) lectins (Vector Laboratories, Newark, CA) in a 1:250 dilution in PBS for 30 minutes followed by a 30-minute incubation with Alexa 594-conjugated streptavidin for MAL II detection (ThermoFisher Scientific, Waltham, MA). Samples were then permeabilized and

incubated with 0.5 µg/mL DAPI for 15 minutes. Slides were imaged using a Nikon A1R confocal microscope (Nikon, Melville, NY).

A duplicate 3.5 µm section was processed for routine histopathology with hematoxylin and eosin staining (HE). Microscopic lesions were evaluated by a veterinary pathologist blind to treatment groups.

Gene expression analysis

To assess the expression level of different cytokines, interferon-induced genes, and pattern recognition receptors, RNA from tissue and BALF samples was extracted using the MagMax-96 RNA isolation kit (ThermoFisher Scientific, Waltham, MA) and samples were normalized to 1 mg RNA/reaction. Contaminant genomic DNA was eliminated by treatment with the RQ1 RNase-free DNase (Promega, Madison, WI). DNA-free RNA was reverse transcribed using the M-MLV reverse transcriptase (Promega, Madison, WI) and oligo(dT) primers according to the manufacturer's instructions (ThermoFisher Scientific, Waltham, MA). The resulting cDNA was used for gene expression analysis by qPCR using the PowerUp SYBR Green Master Mix (ThermoFisher Scientific, Waltham, MA) in 10 mL reactions with the primers listed in Table 3.1. Gene expression was calculated using the 2^{-DDCt} formula and normalizing to the expression of the reference gene ribosomal protein L19 (RPL-19).

Lung sections and BALF single-cell suspension

To collect Alveolar macrophages (AMs), lungs were rinsed twice with 50 mL of PBS-EDTA (ThermoFisher Scientific, Waltham, MA). Lung sections were collected

using 0.8 cm biopsy punches (Integra Miltex, Princeton, NJ) and immediately placed in RPMI-1640 supplemented with 10% newborn calf serum (ThermoFisher Scientific, Waltham, MA), 2mM L-glutamine (Sigma-Aldrich, St Louis, MO), and 1% antibiotic/antimycotic (Sigma-Aldrich, St Louis, MO). Lung sections were then placed in nonculture-treated petri dishes, washed twice with PBS-EDTA, minced, and incubated for 2 hours in RPMI containing 1% antibiotic/antimycotic, 2mM L-glutamine, 2mg/mL collagenase D (Sigma-Aldrich, St Louis, MO), and 0.1 mg/mL DNase I (Sigma-Aldrich, St Louis, MO). The digestion reaction was stopped by adding 1 volume of RPMI supplemented with 10% newborn calf serum. Cells from lung sections and BALF were then passed through 70 mm cell strainers and pelleted at 300x g for 5 minutes at 4°C. Cells were resuspended in PBS-EDTA, and red blood cells were lysed with ACK lysis buffer (ThermoFisher Scientific, Waltham, MA). Following red blood cell lysis, single-cell suspensions were centrifuged at 300x g for 5 minutes at 4°C, resuspended in PBS-EDTA, and passed through 40 mm cell strainers. Cells were then counted and $1x10^6$ cells were used for flow cytometry analysis. The remaining cells were pelleted, resuspended in newborn calf serum containing 10% dimethyl sulfoxide (Sigma-Aldrich, St Louis, MO), and kept in liquid nitrogen for further analysis.

Flow cytometry analysis

Single-cell suspensions were processed for flow cytometry as previously described by Maisonnasse, Boguyon [63] with minor modifications. Briefly, Fc cell surface receptors were blocked by incubating cells with PBS-EDTA containing 5% porcine serum (ThermoFisher Scientific, Waltham, MA) and 5% horse serum

(ThermoFisher Scientific, Waltham, MA) for 30 minutes on ice. Afterward, cells were incubated for 30 minutes on ice with the following antibodies in a 1:200 dilution: Alexa 647-conjugated anti-pig SLA class II DR clone 2E9/13 (Bio-Rad, Hercules, CA), RPE-conjugated anti-pig Monocyte/Granulocyte clone 74-22-15 (Bio-Rad, Hercules, CA), and Alexa 488-conjugated anti-human CD163 clone EDHu-1 (Bio-Rad, Hercules, CA). For FLUAV detection in BALF samples, cells were incubated with the aforementioned antibodies in addition to an anti-Multi-Hemagglutinin (H3N2) polyclonal antibody in a 1:500 dilution followed by a 1-hour incubation with a PE-Alexa 610-conjugated anti-rabbit secondary antibody at a 1:500 dilution (ThermoFisher Scientific, Waltham, MA). For live/dead cell discrimination, samples were treated with LIVE/DEAD Fixable Violet Dead Cell Stain Kit (ThermoFisher Scientific, Waltham, MA) according to the manufacturer's instructions. Finally, cells were fixed for 15 minutes with 37% formaldehyde (Sigma-Aldrich, St Louis, MO) and analyzed using a NovoCyte Quanteon flow cytometer system (Agilent, Santa Clara, CA). Data analysis was performed using FlowJo version 10.8.2 (FlowJo, Ashland, OR).

Apoptosis determination by flow cytometry

3D4/21 cells were infected as previously described by [73]. Briefly, cells were seeded at a density of $8x10^4$ cells/cm^2 and were incubated at 37°C under 5% CO_2 until an 80% confluency was reached. Cells were infected with each virus at 1 MOI for 1 hour at 37°C using infection media without TPCK-treated trypsin. After infection, cells were washed three times with PBS and fresh infection media containing 250 ng/mL TPCK-treated trypsin was added. Cells were incubated at 37°C and at 12 hpi were stained using

the LIVE/DEAD Fixable Violet Dead Cell Stain Kit and the Annexin V Ready Flow Conjugates for Apoptosis Detection kit (ThermoFisher Scientific, Waltham, MA) according to manufacturer's instructions. Samples were fixed using 4% formaldehyde and analyzed as described above.

Results

The A138S mutation modulates HA thermal stability, receptor-binding properties of hVIC/11^{A138S}, and NA activity.

Previous *in vitro* experiments using differentiated primary swine tracheal cells showed a fitness advantage associated with the A138S change of the HA [27, 297]. We analyzed the amino acids present at HA's position 138 in 5,706 unique swine H3N2 sequences available on GISAID (Fig 3.1A). Before the spillover of the 2010.1 human-origin lineage into pigs, 80.3% of swine H3N2 isolates showed alanine (Ala; A138) in position 138 while serine (Ser; S138) was present in less than 15% of swine HA sequences (Fig 3.1A, left panel). However, after 2010, S138 showed a dramatic increase in detection frequency being present in 54.1% of swine isolates and, as of 2022, 96% of deposited sequences showed S138. Conversely, human H3N2 viruses showed a strong preference for A138 (Fig 3.1A, right panel), and as of 2022, 98% of deposited sequences on GISAID showed A138, thus suggesting a potential advantage of the A138S mutation in the HA of swine H3N2 viruses. When we looked at the frequency in a pre-2010.1 lineage (1990.4 lineage) and the 2010.1 lineage (S3.1 Fig)., we found that S138 was present in the 1990.4 lineage with a low frequency (10-20%) until 2019, when S138 was quickly fixed across the entire lineage. Similarly, early 2010.1 sequences showed mainly

A138. However, S138 became fixed earlier (2017) compared to the 1990.4 lineage and showed a 100% frequency in 2022 and 2023.

To assess the impact of this amino acid change, using reverse genetics, we constructed three isogenic viruses carrying the TRIG backbone and the HA and NA genes were replaced for those from the human strain A/Victoria/361/2011 (hVIC/11), an hVIC/11 HA segment carrying the A138S mutation (hVIC/11^{A138S}) and from the swine-adapted virus A/turkey/Ohio/313053/2004 (sOH/04). In terms of morphology, all viruses showed a spherical-like shape with an average diameter of 120 nm (Fig 3.1B), demonstrating that the A138S did not visibly alter the particle morphology. Further, viral plaque analysis showed no differences at either 37 or 39°C for sOH/04 and hVIC/11^{A138S} (Fig 3.1C and 1D), contrasting hVIC/11, which showed increased plaque sizes at 39°C. No significant differences were observed in virus replication in Madin Darby Canine Kidney (MDCK) cells among the 3 viruses evaluated at either 37 or 39°C (S3.2 Fig).

To better understand the impact of the A138S mutation on the HA protein, we analyzed the thermal stability of the viruses (Fig 3.2A). The hVIC/11 showed reduced HA titers at lower temperatures when compared to sOH/04 and hVIC/11^{A138S}, with a half-inactivation temperature (T_{50}) of 57.4$\pm$0.2°C. The swine-adapted sOH/04 and hVIC/11^{A138S} virus had a T_{50} of 58.6$\pm$0.1°C, and 58.7$\pm$0.3°C, respectively. We also analyzed the binding properties of the viruses using a high molecular weight sialylglycopolymer-based assay validated using mammalian- and avian-adapted viruses (S3.3 Fig) [268, 298]. There were no differences between hVIC/11 and hVIC/11^{A138S} for α2,3 receptor binding (3'SLN, Fig 3.2B), while the swine-adapted sOH/04 virus had a higher affinity for 3'SLN. Noteworthy, hVIC/11^{A138S} exhibited an increased binding

affinity to α2,6 receptors (6'SLN, Fig 3.2C) compared to hVIC/11, reaching similar levels as sOH/04.

Evaluation of NA sialidase activity using a MUNANA-based assay and by normalizing each virus to 10^4 plaque-forming units (PFU, Fig 3.2D) under MUNANA-saturated conditions (100 mM), showed that hVIC/11^{A138S} had the highest NA activity with a conversion rate of 0.189 mM/min, which was significantly higher than hVIC/11 (0.110 mM/min) and sOH/04 (0.032 mM/min). Results suggested that the A138S mutation in the HA protein influences NA enzymatic activity. We validated the assay's specificity by oseltamivir inhibition (S3.4 Fig). These results were further confirmed by determining the NA kinetic parameters normalizing based only on NA activity. When the viruses were incubated with variable concentrations of MUNANA (Fig 3.2E), sOH/04 had the lowest V_{max} and K_M (0.408 mM/min and 39.25 mM respectively) whereas hVIC/11^{A138S} had the highest activity (V_{max}= 0.665 mM/min, K_M= 88.78 mM). The hVIC/11 showed an intermediate phenotype (V_{max}= 0.491 mM/min, K_M= 58.4 mM). Taken together, these results demonstrate that the A138S modulates the thermostability of the HA protein, increases affinity for α2,6-type receptors and affects NA activity.

HA A138S improves transmission in pigs and infection of the lower respiratory tract.

To evaluate the effect of the A138S mutation on transmission *in vivo*, 3-week-old pigs were inoculated with $3x10^6$ $TCID_{50}$/pig of hVIC/11, hVIC/11^{A183S} or the swine-adapted sOH/04 (seeders, 3 pigs/virus, S3.5 Fig). Two days post-infection (dpi), 3 naïve pigs were introduced as contacts in each cage (contact 1), and the infection progressed for 3 more days. At 5 dpi seeders were humanely euthanized, and 3 new naïve pigs were

introduced (contact 2). This cycle was repeated for a total of 4 contacts with contacts introduced at 3dpc each time. Tissues and BALF were collected from seeder pigs at 5dpi. In addition, nasal swabs were collected at 0 and 2dpi/3dpc from seeders and contact pigs.

FLUAV infection was evaluated by RT-qPCR from nasal swabs at 2dpi/3dpc (Table 3.2). sOH/04 was detected in all inoculated and contact animals throughout the study. Similarly, the hVIC/11^{A138S} virus was also detected among all contacts, contrasting with the hVIC/11 virus that was only detected in the seeders and contact 1 pigs, confirming the role of the A138S mutation in improving the transmissibility of hVIC/11.

Assessment of viral loads throughout the respiratory tract was performed by collecting different anatomical sections of the upper, middle, and lower trachea, right cranial lobe, left cranial lobe, right caudal lobe, left caudal lobe, and the accessory lobe from seeder pigs at 5 dpi (Fig 3.3A). vRNA was detected in all the collected tissues of all pigs in the sOH/04-infected group. Meanwhile, vRNA was detected in most tissues from the hVIC/11^{A138S}-infected pigs with mean titers of 10^4 $TCID_{50}$eq/mg total RNA, except in the right caudal and the accessory lobe in which titers dropped to 10^1 $TCID_{50}$eq/mg total RNA. Titers in the left caudal lobe showed that 1 out of 3 pigs had virus in this lobe. Additionally, 2 out of 3 pigs showed lower titers in the right cranial lobe compared to sOH/04. Distinctively, vRNA loads in hVIC/11-infected pigs were only observed in the upper and middle trachea in 2 out of 3 seeder pigs with a mean titer of 10^1 $TCID_{50}$eq/mg total RNA. Viral infection was also confirmed by immunofluorescence (Fig 3.3B). Similar to viral RNA titrations, immunofluorescent imaging showed that the A138S mutation resulted in virus infection of the lower respiratory tract of pigs at 5 dpi. Conclusively, the results suggest the hVIC/11 containing the A138S mutation displayed

an intermediate phenotype between the swine-adapted sOH/04 virus and the human hVIC/11 virus.

Histopathological analysis revealed that the sOH/04 group exhibited moderate-severe necrotizing bronchiolitis with concurrent suppurative bronchitis, bronchiolitis, culminating into bronchiolitis obliterans (Fig 3.4). Moderate to severe microscopic lesions were present in the caudal lung lobe sections although, in these, they were principally centered on the airways. Only, mild-moderate lymphohistiocytic tracheitis with mild multifocal epithelial degeneration and necrosis was observed in this sOH/04 group. The hVIC/11 group tracheas also presented mild-moderate lesions with only one section having moderate epithelial necrosis and suppurative inflammation of the submucosal glands. Lungs in this group had mild or mild-moderate suppurative bronchitis and bronchiolitis, contrasting the severe bronchiolitis observed in the sOH/04 group. The hVIC/11^{A138S} group had similar pulmonary and tracheal lesions to the hVIC/11 group. Concurrent catarrhal to suppurative bronchitis and bronchiolitis were accompanied by mild local epithelial degeneration, deciliation and sloughing into the lumen. Evidence suggests that the A138S mutation does not increase the tissue damage compared to the hVIC/11 virus.

To further understand the differences in FLUAV tropism, sialic acid receptor distribution in the respiratory tract of pigs was evaluated by staining a2,3 and a2,6 receptors using lectins (S3.6 Fig). Among multiple pigs, a2,6 receptors were predominant in the trachea, while a2,3 abundance increased in lower respiratory tract. a2,3 and a2,6 receptors were similarly distributed in all the pulmonary lobes which is in agreement with

previous reports [299]. Taken together, evidence suggest that differences observed here may not be because of differences in receptor distribution.

Viruses induced a distinct pattern of innate immune responses in vivo.

To assess the expression of specific pro-inflammatory cytokines, interferon-induced genes, and pattern recognition receptors, RNA from each anatomical section of the lungs was extracted, gene expression was assessed by RT-qPCR, and fold induction was calculated by normalizing expression to the negative control group. In the right cranial lobe (Fig 3.5A, S3.7 Fig), sOH/04 induced the expression of numerous analyzed genes, being statistically significant TLR-7, Mx2, and IL-18. In contrast, hVIC/11^{A138S} showed a similar expression pattern as hVIC/11, which was characterized by a strong TNF-a and TLR-7 expression. In the left cranial lobe (Fig 3.5B, S3.8 Fig), there was a significant amount of IFN-g repression within the sOH/04 and hVIC/11^{A138S}-infected pigs, contrasting with hVIC/11-infected pigs where IFN-g was nor repressed. However, hVIC/11^{A138S}-infected pigs displayed increased expression of IL-6 and IFN-b. For the right caudal lobe (Fig 3.5C, S3.9 Fig), sOH/04 significantly increased the expression of both IL-6 and IL-8, while hVIC/11 and hVIC/11^{A138S} induced a high level of TLR7 transcription. Individually, hVIC/11^{A138S} led to high expression of IFN-g and Mx2, while hVIC/11 induced a strong IFN-b expression when compared to hVIC/11^{A138S}, although the virus was not detected in this lobe at 5dpi (Fig 3.3). Expression patterns observed in the left caudal lobe differed (Fig 3.5D, S3.10 Fig), with all viruses strongly repressing IFN-b but most other genes did not exhibit major changes. Exceptions were seen for IFN-g, which was slightly overexpressed by hVIC/11^{A138S} compared to hVIC/11; and IL-8 and

TNF-a, which were slightly overexpressed by hVIC/11, however, these differences were not statistically significant. Lastly, sOH/04 induced the expression of almost all the PRRs analyzed in the accessory lobe (Fig 3.5E, S3.11 Fig). Meanwhile, hVIC/11 and hVIC/11^{A138S} overexpressed IL-6. In summary, our results showed that each virus induced a unique expression pattern in each lung lobe.

Viruses induce a differential recruitment of immune cells to the lungs upon infection.

To further characterize the host-immune response post-FLUAV infection of seeder pigs, cell populations that infiltrated in the different lung sections at 5 dpi were examined using flow cytometry and staining simultaneously for SLA class II DR (MHC II), CD163, and CD172a (Fig 3.6). This previously reported strategy enabled the detection of 5 different immune cell populations based on their CD163 content and CD172a presence gated on MHCII^{high}CD163^{pos} cells (antigen-presenting cells, APC) (Fig 3.6A) [63]. These populations are CD172a^{neg}CD163^{neg} (type 1 conventional dendritic cells, cDC1), CD172a^{pos}CD163^{neg} (type 2 conventional dendritic cells, cDC2), CD172a^{pos}CD163^{low} (monocyte-derived dendritic cells, moDC), CD172a^{pos}CD163^{int} (monocyte-derived macrophages, moMf), and CD172a^{pos}CD163^{high} (PAMs in BALF or interstitial PAMs in lung tissues, PiAMs). No changes were detected in the abundance of APC (MHCII^{high}CD163^{pos}) in the right cranial lobe (Fig 3.6B, S3.12A Fig). However, the amount of PiAM (CD172a^{pos}CD163^{high}) was lower in sOH/04-infected pigs (36.9%) than the mock controls (46.9%). No significant differences between the infected groups and the mock control were observed in the remaining cell populations. Further, no differences

were observed between groups in the left cranial lobe (Fig 3.6C, S3.12B Fig) and the right caudal lobe (Fig 3.6D, S3.12C Fig). A significant decrease of the PiAMs population was observed in the left caudal lobe in sOH/04-infected pigs (31.1%) compared to the mock group (53.6%) (Fig 63.E, S3.12D Fig). Similarly, we detected an increase in the cDC2 ($CD172a^{pos}CD163^{neg}$) population in the sOH/04-infected pigs (11.8%) compared to the mock (1.87%) in this lobe. No differences were observed between the mock and the other infected groups (hVIC/11 and hVIC/11^{A138S}) in this lobe. In the accessory lobe (Fig 3.6F, S3.12E Fig), sOH/04-infected pigs displayed a significant decrease in the number of APC cells (10.3%) compared to the mock (23.3%). No differences in this lobe were observed between the mock- (50.16%), hVIC/11- (58.93%), and hVIC/11^{A138S}-infected pigs (45.36%) for the PiAMs population, contrasting with sOH/04 -infected pigs (26.9%). Taken together, these results suggest that FLUAV infection with a well-adapted virus such as sOH/04 distinctively disrupts the PiAMs population in different sections of the lungs.

The A138S mutation increases affinity for alveolar macrophages and enhances apoptosis induction.

Since sOH/04-infected pigs showed a decreased number of PiAMs, we next evaluated the effects of FLUAV infection on PAMs in BALF. First, differences in the total number of cells in BALF samples (Fig 3.7A) were assessed. Pigs infected with sOH/04 ($4.4x10^7$ cells) displayed elevated cell counts in comparison to the mock ($8.7x10^6$ cells), hVIC/11 ($9.43x10^6$ cells), and hVIC/11^{A138S} ($1.17x10^7$ cells). No differences were observed in the total cell count between the mock, hVIC/11, and hVIC/11^{A138S} groups.

Following the strategy described above (Fig 3.6A), we further characterized the cell populations present in BALF by multi-color flow cytometry. Results showed that PAMs accounted for more than 75% of cells in BALF samples in both mock- and hVIC/11-infected pigs (Fig 3.7B and 7C, S3.12F Fig). Yet, the PAM population accounted for less than 50% in the hVIC/11^{A138S}-infected pigs (44.6%). Similarly, we observed an increase of the MHCII^{low} CD163^{neg}CD172a^{neg} population that increased proportionally with the reduction in PAMs percentage in BALF samples (Fig 3.7B, S3.12F Fig). A more severe reduction was observed for the sOH/04-infected pigs, where the PAMs population was reduced to 9.51% (Fig 3.7B and 7C, S3.12F Fig).

Analysis of the amount of FLUAV- infected PAMs by flow cytometry by looking at the HA content on the cell surface among the MHCII^{high} CD163^{pos} population (Fig 3.8A) revealed that hVIC/11-infected pigs had the smallest % of HA-positive PAMs (23.56%) (Fig 3.8B and E). An increase of HA-positive cells was observed in hVIC/11^{A138S}- and sOH/04-infected pigs (Fig 3.8C and 3.8D, respectively). sOH/04-infected pigs exhibited 60% of PAMs positive for HA, which was statistically higher compared to both hVIC/11 and the mock control (Fig 3.8E). Meanwhile, hVIC/11^{A138S} -infected pigs contained 40.63% of PAMs positive for HA which was statistically higher compared the mock control. Taken together, the A138S mutation showed an intermediate phenotype between the swine-adapted sOH/04 virus and the human hVIC/11 virus.

Next, the ability of the viruses to suppress the expression of key genes driving PAMs proliferation and immune activity was evaluated. Therefore, we looked at GM-CSF and PPARg expression. GM-CSF is the main factor driving monocyte differentiation into PAMs *in vitro* and has been associated with PAM immune activity [79, 300]. PPARg

is a transcription factor stimulated by GM-CSF; therefore, their expression will help to detect if FLUAV interferes with PAMs activity upstream or downstream the GM-CSF signaling. Analysis of GM-CSF expression in BALF samples showed increased expression upon FLUAV infection with all three viruses (Fig 3.8F); however, expression in hVIC/11-infected BALF showed no statistical differences compared to the mock. The expression of this gene was highly stimulated by sOH/04 infection, while hVIC/11^{A138S} displayed an intermediate phenotype. GM-CSF results contrast with PPARg expression (Fig 3.8F), in which no major differences were detected between the mock, hVIC/11-, and hVIC/11^{A138S}-infected pigs; however, PPARg expression was strongly suppressed, with an expression 5 times lower than the mock control, in BALF samples from sOH/04-infected pigs. Overall, these results suggest that the A138S mutation increases FLUAV affinity for PAMs, but it is not enough to repress PPARg expression as observed in sOH/04.

Finally, to confirm the ability of FLUAV to infect and induce death in PAMs, we used a commercial porcine alveolar macrophages cell line (3D4/21). When we looked at the ability of the viruses to induce apoptosis at 12 hpi (Fig 3.8G), we found that hVIC/11 (~7.5%) induced little apoptosis (Live/Dead^{neg}Annexin V^{pos}, Q3) in the cells compared to the mock control (~6%). However, an increased number of Annexin V^{pos} cells were found in the hVIC/11^{A138S} (~18%) and sOH/04 (~22%) infections. When we evaluated the growth kinetics of each virus in 3D4/21 cells (Fig 3.8H), sOH/04 showed the fastest replication, reaching a maximum titer of 10^7 $TCID_{50}$eq/mL at 24 hpi, which was significantly higher than hVIC/11^{A138S} that had a maximum titer of 10^5 $TCID_{50}$eq/mL at 72 hpi. In contrast, hVIC/11 showed an increase in titer at 24 hpi, but then it stopped

replicating. Together, these results suggest that the increased apoptosis may be influenced by the increased replication ability of the swine sOH/04 compared to the human hVIC/11.

Discussion

Understanding the mechanisms driving FLUAV evolution and adaptation to different species is critical for human and animal health. Human-origin FLUAV gene segments have been introduced in swine FLUAV strains, further expanding the genetic diversity of swine FLUAV [301, 302]. Since the introduction of the TRIG constellation in the late 1990s, multiple human-to-swine spillover events have occurred, with increased frequency after the emergence of the pandemic H1N1 in 2009 [242]. Although this has contributed to the reassortment and maintenance of the human-origin internal genes [242, 303], wholly human-origin viruses do not commonly persist in the swine population [303, 304]. Interestingly, multiple HA and NA genes derived from human-seasonal H3N2 viruses have been introduced to the swine population leading to the emergence of distinct phylogenetic clades [271, 305-307]. In this work, we have found that the adaptation of human-origin FLUAV HA to pigs increases affinity for the lower respiratory tract and leads to PAM depletion, possibly by triggering apoptosis, which might be a critical step for adaptation of human viruses to the swine host.

The H3 HA A138S mutation is prevalent in swine HA genes, and this increased significantly after the emergence of the H3 2010.1 lineage. This mutation has been associated with the adaptation of avian-origin H3, H6, and H7 to mammalian receptors [308] and increased infectivity of H3N2 viruses in swine respiratory epithelial cells [297]. However, no previous studies have evaluated the in-depth impact of this amino acid change on the virus adaptation to the swine respiratory tract and subsequent transmission between animals. Previously, we and others showed that the A138S mutation exhibits increased replication and binding to swine tracheal cells [27, 297].

Using a reassortant hVIC/11^{A138S} virus, we detected a small increase in the HA thermostability but observed that this mutation does not affect viral morphology (Fig 3.1) or replication in MDCK cells. Increased HA thermostability suggests the virus retains biological activity at higher temperatures than the original hVIC/11 virus (Fig 3.2).

NA activity of the viruses revealed that the swine-adapted sOH/04 virus exhibited decreased activity, characterized by a reduced V_{max} and K_M compared to both hVIC/11 and hVIC/11^{A138S}. A previous report showed that viruses with low NA activity are not inhibited by swine mucus, suggesting they are potentially transmissible among pigs but not humans [34]. This result contrasts with the activity of the hVIC/11^{A138S} virus that showed increased NA activity compared to sOH/04 and hVIC/11. Nonetheless, K_M for hVIC/11^{A138S} was almost doubled when compared to sOH/04, which means the virus needs two times more substrate to reach V_{max} than sOH/04. Hence, hVIC/11^{A138S} NA seems to have a decreased substrate affinity but enhanced catalytic activity compared to sOH/04 NA. This is especially interesting since the NA gene from both hVIC/11 and hVIC/11^{A138S} is the same, but differed significantly in NA activity, suggesting that mutations in the HA protein might modulate NA activity. Indeed, when we analyzed the HA affinity for α2,6 sialic acid receptors, hVIC/11^{A138S} displayed higher affinity than hVIC/11, with no differences compared to sOH/04 at high concentrations of 6'SLN (Fig 3.2). This could explain an increased NA activity without disrupting the functional balance between HA avidity and NA activity, considering that hVIC/11^{A138S} NA has less affinity for the receptor than sOH/04. However, more experiments beyond the scope of this study are required to confirm this hypothesis.

hVIC/11 showed reduced transmission *in vivo* and was not detected after contact 1 pigs, contrasting with hVIC/11^{A138S} and sOH/04 that efficiently transmitted through 4 subsequent transmission events. Therefore, the data supports our previous results that the A138S mutation increases viral replication and transmissibility in pigs. The A138S mutation exhibited efficient virus replication in most of the seeders' upper and lower respiratory tracts, displaying a pattern similar to sOH/04 and differing from hVIC/11, which failed to infect the lower respiratory tract by 5 dpi. Numerous studies have demonstrated that efficient transmission of FLUAV is associated with enhanced replication in the lungs of ferrets and mice [309-312]. However, a recent study observed that upper respiratory tract infection is critical for onward transmission in the ferret model [313]. Nonetheless, the lack of transmission of hVIC/11, despite active replication in the nose and trachea, consistently with what has been shown previously [244], suggests a potential role of the lower respiratory tract infection of FLUAV in pigs. Since all the viruses possessed the same internal genes (TRIG backbone), the ability of the hVIC/11^{A138S} virus to infect the lower respiratory tract is most likely from a direct effect of this HA amino acid substitution, potentially linked to enhanced entry into swine cells induced by an increased affinity for α2,6 receptors. However, it cannot be discarded that hVIC/11 infected the lower respiratory tract and was cleared faster than sOH/04 and hVIC/11^{A138S}, therefore impeding detection by the time of tissue collection.

Induction of the cellular immune response by FLUAV infection varied among different anatomical sections of the lungs but was not necessarily associated with virus detection in each lung section (Fig 3.3, Fig 3.5). Most of the analyzed cytokines were upregulated in the lungs of sOH/04-infected pigs, although TNF-a was down-regulated in

almost all lobes except the left cranial lobe. Interestingly, TNF-a was not inhibited by hVIC/11^{A138S} in the right cranial, right caudal, and accessory lobe. TNF-a has been demonstrated to exert a potent antiviral activity in the lungs [314]; therefore, lower virus replication in these lung lobes could be due to overexpression of this cytokine. In addition, we detected higher expression of IFN-g in the left caudal and right caudal lobe of hVIC/11^{A138S}-infected pigs compared to sOH/04 coupled with elevated levels of IFN-b in the accessory lobe. These elevated levels of IFN coincided with limited virus replication in similar tissues. Considering that type I and II IFN are potent FLUAV antivirals [315], the results are consistent with the idea that FLUAV viruses need to inhibit expression of host-specific IFN to efficiently replicate in the lungs of a particular host. However, it must be noted that our study design only captures the expression profile at 5 dpi, and changes in the expression of certain genes and the distribution of the viruses in the respiratory tract before the time of collection may affect the outcome at 5 dpi. We must also note that since the number of animals used in this study was small and pigs were inoculated intratracheally and intranasally, we must exercise caution interpreting gene expression profiles of each lobe as the delivery method inherently causes a virus deposition in the lungs that might differ from what is observed in a natural infection.

FLUAV infection of the lungs considerably impacted the cell populations in different lobes. We observed that sOH/04 infection decreased the presence of PiAMs in the right cranial, left caudal, and accessory lobe, but hVIC/11 and hVIC/11^{A138S} did not affect this population. Interestingly, hVIC/11^{A138S} showed reduced infection in some of these lobes, specifically exhibiting a trend for reduced titer in the left caudal lobe when compared to sOH/04 and no virus replication in the accessory lobe as demonstrated by

RT-qPCR and immunofluorescence analysis at 5dpi (Fig 3.3). These results suggest that PiAMs may limit FLUAV replication in addition to IFN and TNF-a; therefore, the adaptation of human viruses may involve the ability to deplete PiAMs. Hence, the role of both PiAMs, which are phenotypically distinct from PAMs [63] in terms of gene expression profiles and morphology, during FLUAV infection deserves further investigation in future studies.

The cell content in BALF samples revealed that sOH/04 infection recruits a large number of cells to the lungs, noted from the ten-fold increase in the total number of cells compared to the mock group (Fig 3.7). The increased infiltration of cells is due to the recruitment of $MHCII^{low}CD163^{neg}$ cells, most likely neutrophils, and T cells, as has been previously reported [316-318]. The substantial increase in the percentage of neutrophils in the lungs could be due to the ability of the viruses to induce expression of IL-8, a cytokine known to function as a neutrophil chemoattractant [319, 320]. We also detected that sOH/04 efficiently represses IFN-b expression in most of the lobes, which has been reported to act as a repressor of neutrophil infiltration [321, 322]. Notably, results for $hVIC/11^{A138S}$ contrasted with sOH/04 as it failed to repress IFN-b and did not result in an elevated recruitment of cells. When taken together with IL-8 upregulation, the results suggest that $hVIC/11^{A138S}$ infection leads to the recruitment of neutrophils to the site of infection but at lower levels than sOH/04, as shown by our flow cytometric analysis and represented as an increase of $MHCII^{low}$ $CD163^{neg}$ cells (Fig 3.7B).

The content of PAMs in BALF samples represented about 70% of the total cells in the mock- and hVIC/11-infected groups and was significantly reduced in sOH/04- and $hVIC/11^{A138S}$-infected pigs (Fig 3.7), consistent with previous reports showing the

depletion of AMs after FLUAV infection in mice [323]. The role of AMs during FLUAV infection is still debated; while some reports have shown active replication of FLUAV in these cells, others have demonstrated unproductive viral replication [83]. Nonetheless, previous reports showed little to no cell death after infection with human-adapted H3N2 viruses in human and porcine AMs [71, 83, 324] , while infection of PAMs with swine-adapted viruses resulted in effective infection and cell death [75] [325]. Here, we showed that the number of influenza-positive PAMs increased with the level of adaptation to the swine-host, with sOH/04 showing the highest number of infected cells. Our results suggest, in accordance with others [326], that adaptation to the swine host leads to the increased ability to infect, replicate, and induce apoptosis in PAMs (Fig 3.7). We have previously shown that this mutation increases binding and replication in differentiated swine tracheal cells [27], most likely due to enhanced affinity for α2,6 receptors, which could also explain a higher affinity for PAMs. Here, we showed that infection with a virus that is highly adapted to pigs (sOH/04) resulted in downregulation of PPARg. This receptor acts as a crucial transcription factor that promotes monocytes differentiation into AMs *in vivo* and *in vitro* [79]. Additionally, it has been reported to be an important inflammation modulator by limiting the expression of various pro-inflammatory cytokines [327]. In the context of FLUAV infection, PPARg expression has been shown to reduce tissue damage and death of infected mice [328, 329], and some reports have demonstrated that FLUAV inhibits its expression [328], which has been associated with lung injury in accordance with our histopathology data (Fig 3.4). Interestingly, GM-CSF expression was not repressed, and, considering that PPARg expression is GM-CSF dependent, it is most likely that FLUAV interferes downstream of the GM-CSF signaling.

The JAK/STAT pathway mediates GM-CSF signaling [300], which ultimately leads to STAT5 phosphorylation and translocation into the nucleus, where it mediates transcription of a variety of genes, including PPARg [330]. It is possible that FLUAV disrupts the PAPRg expression by inhibiting the JAK/STAT pathway due to the STAT-dependency in PAPRg expression [113, 331-333]. Here, the increased suppression of PAPRg found in sOH/04-infected pigs is most likely due to the increased number of infected PAMs in these animals. This is supported by our data showing better infection and replication of PAMs by sOH/04 (Fig 3.8). Additionally, Annexin V staining revealed that both hVIC/11^{A138S} and sOH/04 induce apoptosis in infected PAMs. These findings, together with PAPRg repression, could explain why sOH/04 is more efficient at depleting PAMs than hVIC/11^{A138S}. While a relationship between viral fitness and PAMs infection was observed, future studies beyond the scope of the present report are needed to further understand the impact of PAMs depletion on the pigs' innate and adaptative immune responses against FLUAV. Similarly, the effects of PPARg suppression should be further studied to better understand its role in PAMs proliferation and anti-FLUAV activity, which could not be assessed with our experimental design.

Overall, our study indicates that the A138S mutation broadly impacts the virus phenotype, HA thermostability, NA activity, HA receptor affinity, host range, and tissue tropism. Notably, viruses carrying this mutation replicate more efficiently in the lower respiratory tract of pigs, possibly due to an increased a2,6 affinity and increased affinity for PAMs. Infection of pigs with swine-adapted viruses depleted PAMs at 5 dpi most likely by triggering apoptosis in infected cells but it might also disrupt their immune activity and proliferation by repressing the expression of PPARg.

Figure and Tables.

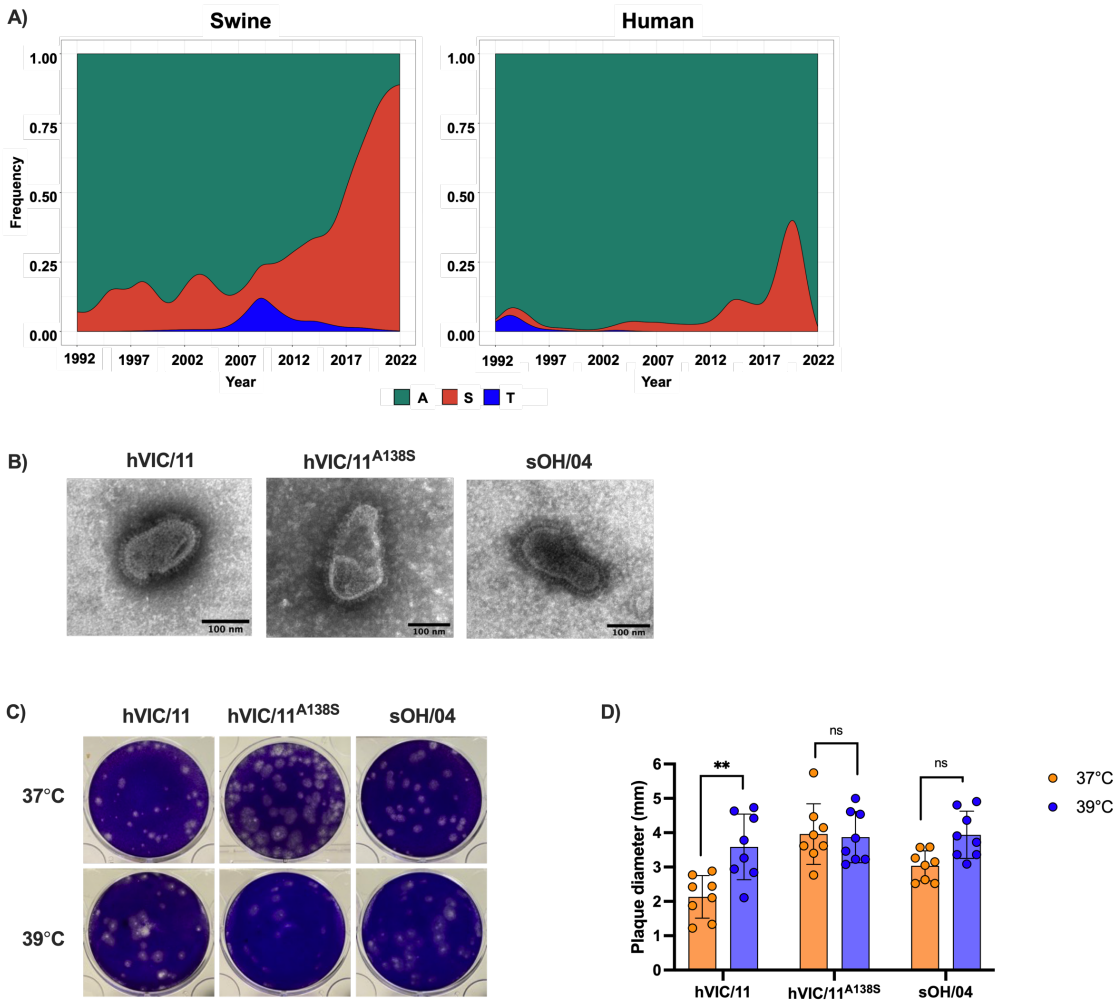

Figure 3.1. In vitro characterization of the hVIC/11^{A138S} virus. (A) Prevalence of the S138 residue in swine and human H3N2 FLUAV isolates reported from 1992 to 2022.

Sequences were obtained from GISAID and aligned using ClustalW. (B) Representative electron microscopy pictures of sOH/04, hVIC/11, and hVIC/11^{A138S}. Scale bar=100 nm (C) Plaque morphology produced by sOH/04, hVIC/11, and hVIC/11^{A138S} in MDCK cells at 37 and 39°C. (D) Plaque sizes produced by the viruses at 37 and 39°C. Two independent experiments were performed in triplicates. Values represent the mean $\pm$ standard error of the mean (SEM). Statistical analysis was performed by two-way ANOVA. **$p<0.005$.

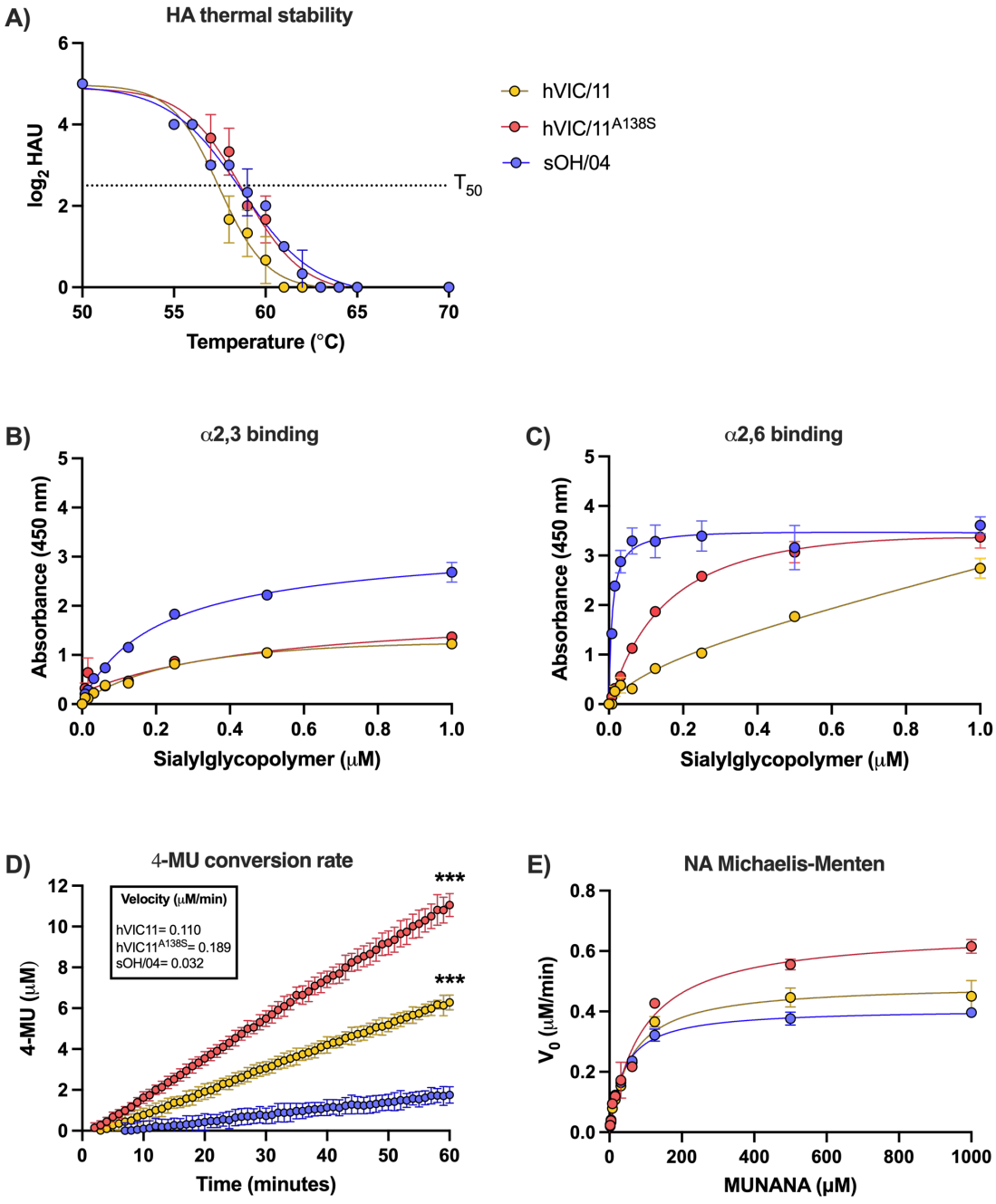
A)
HA thermal stability
log2 HAU
Temperature (°C)
T50
hVIC/11
hVIC/11A138S
sOH/04
B)
α2,3 binding
Absorbance (450 nm)
Sialylglycopolymer (μM)
C)
α2,6 binding
Absorbance (450 nm)
Sialylglycopolymer (μM)
D)
4-MU conversion rate
Velocity (μM/min)
hVIC11= 0.110
hVIC11A138S= 0.189
sOH/04= 0.032
***
***
4-MU (μM)
Time (minutes)
E)
NA Michaelis-Menten
V0 (μM/min)
MUNANA (μM)

Figure 3.2. A138S increases HA thermal stability, binding for α2,6 receptors, and NA activity. (A) Thermal stability of sOH/04 (blue), hVIC/11 (yellow), and hVIC/11^{A138S} (red) was determined by incubating them at different temperatures for 1 hour. Data were fitted to a dose-response-inhibition non-linear fit. Receptor-binding affinity of sOH/04, hVIC/11, and hVIC/11^{A138S} for 3'SLN (B) or 6'SLN (C) was assessed by incubating the viruses with different concentrations of 3'SLN or 6'SLN. (D) NA activity was determined by normalizing the viruses at 10^4 PFU/well in the presence of 100 mM MUNANA. Fluorescence was measured every 60 seconds for 1 hour and data was fitted to a linear regression model. (E) NA activity of the viruses was determined by normalizing based on NA activity. Viruses were incubated at different MUNANA concentrations for 1 hour and kinetic parameters (K_M and V_{max}) were determined by fitting the data to the Michaelis-Menten equation. For all assays, two experiments were performed in triplicates. Values represent the mean $\pm$ SEM. Statistical analysis was performed by two-way ANOVA. ***$p<0.0005$.

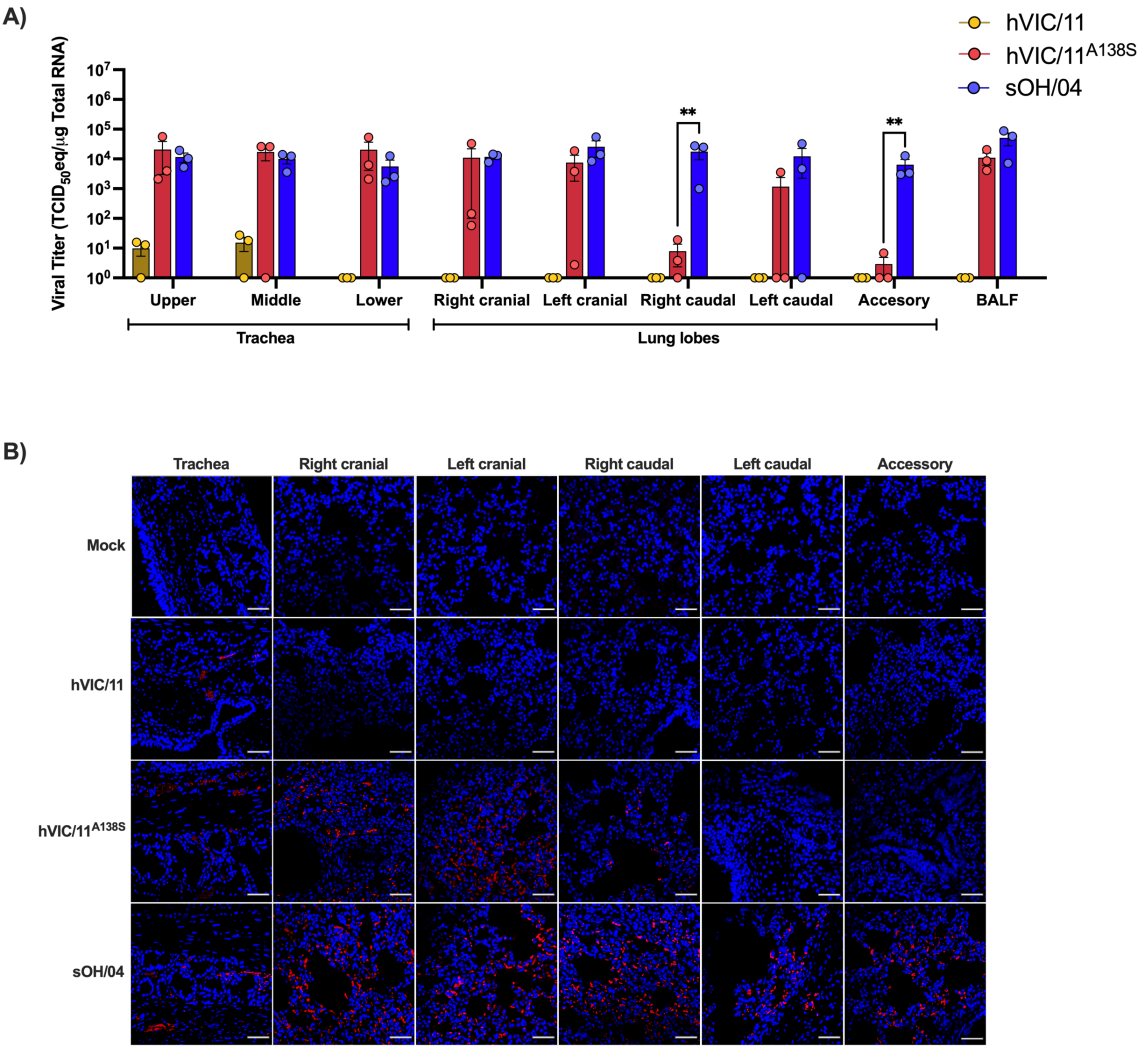
A)
hVIC/11
hVIC/11A138S
sOH/04
Viral Titer (TCID50eq/μg Total RNA)
10^7
10^6
10^5
10^4
10^3
10^2
10^1
10^0
**
**
Upper
Middle
Lower
Right cranial
Left cranial
Right caudal
Left caudal
Accesory
BALF
Trachea
Lung lobes
B)
Trachea
Right cranial
Left cranial
Right caudal
Left caudal
Accessory
Mock
hVIC/11
hVIC/11A138S
sOH/04

Figure 3.3. A138S improves infection of the lower respiratory tract of pigs. (A)Viral titers in different anatomical sections of the lungs of seeder pigs at 5 dpi (n=3) normalized to 1mg total RNA. All statistical analyses were performed by two-way ANOVA. Values represent the mean $\pm$ SEM. *$p<0.05$, **$p<0.005$. (B) Influenza immunofluorescence staining in the respiratory tract of seeder pigs. Hemagglutinin (red) was detected using a polyclonal multi-H3 antibody and cell nuclei (blue) were stained with DAPI. The scale bar represents 50 mm.

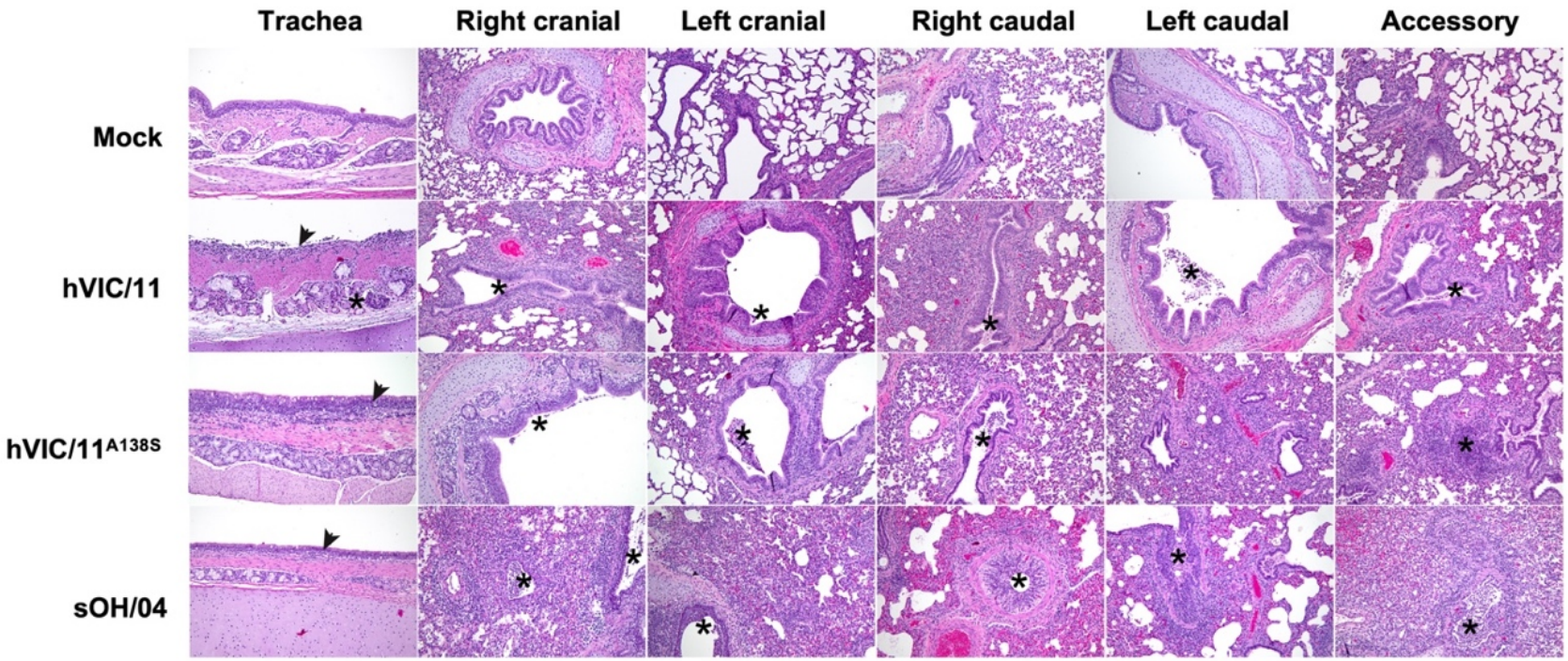
Trachea
Right cranial
Left cranial
Right caudal
Left caudal
Accessory
Mock
hVIC/11
hVIC/11A138S
sOH/04

Figure 3.4. A138S does not affect histopathological findings in tracheas and lung lobes of infected pigs. Tracheas and lungs, 10X, mock group. Tissue sections are within expected normal range. Trachea, 10X, hVIC/11 group: epithelium was diffusely sloughing into the lumen (arrow) and subtended by a mild-moderate suppurative inflammation. Suppurative inflammation reached the submucosal glands (asterisk). Lung, 10X, hVIC/11 group: mild-moderate degree of suppurative bronchitis and bronchiolitis were present, as evidenced by neutrophilic exudate accumulation within the airways (asterisks). Trachea, 10X, hVIC/11^{A138S} group: mild-moderate lymphohistiocytic inflammation expanded the lamina propria and effaced the mucosal epithelium. Lung, 10X, hVIC/11^{A138S} group: mild suppurative and catarrhal bronchitis and bronchiolitis (asterisks) were present with mild lymphohistiocytic cuffing of the airway. Trachea, 10X, sOH/04 group: mild lymphohistiocytic tracheitis (arrow) was present. Lung, 10X, sOH/04 group: marked suppurative inflammation was not only confined to the airways (asterisks), but also extended to the adjacent alveoli.

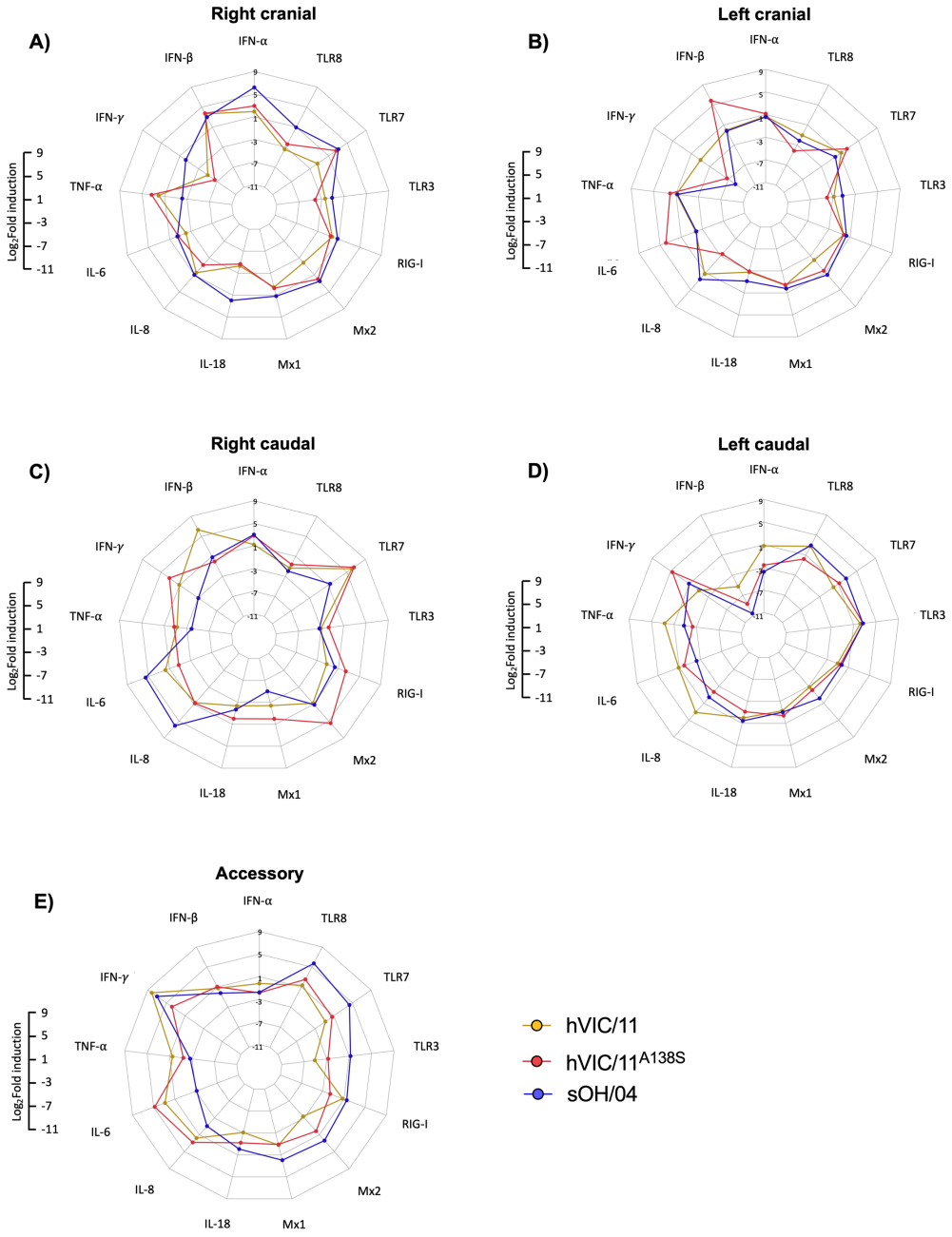
A)
Right cranial
B)
Left cranial
C)
Right caudal
D)
Left caudal
E)
Accessory
IFN-α
TLR8
TLR7
TLR3
RIG-I
Mx2
Mx1
IL-18
IL-8
IL-6
TNF-α
IFN-γ
IFN-β
Log2Fold induction
9
5
1
-3
-7
-11
hVIC/11
hVIC/11A138S
sOH/04

Figure 3.5. Distinct patterns of immune response are triggered by the viruses in different lung anatomical sections of pigs. Relative mRNA levels of pro-inflammatory cytokines, interferon-stimulated genes, and patter-recognition receptors. RNA was normalized to 1mg and gene expression was assessed by qPCR and normalized to RLP-19 expression in the (A) right cranial lobe, (B) left cranial lobe, (C) right caudal lobe, (D) left caudal lobe, and (E) accessory lobe. Values are shown as log_2 fold induction of the mean between the seeder pigs (n=3) of each group at 5dpi. Fold induction of each group was normalized to the non-infected negative control group.

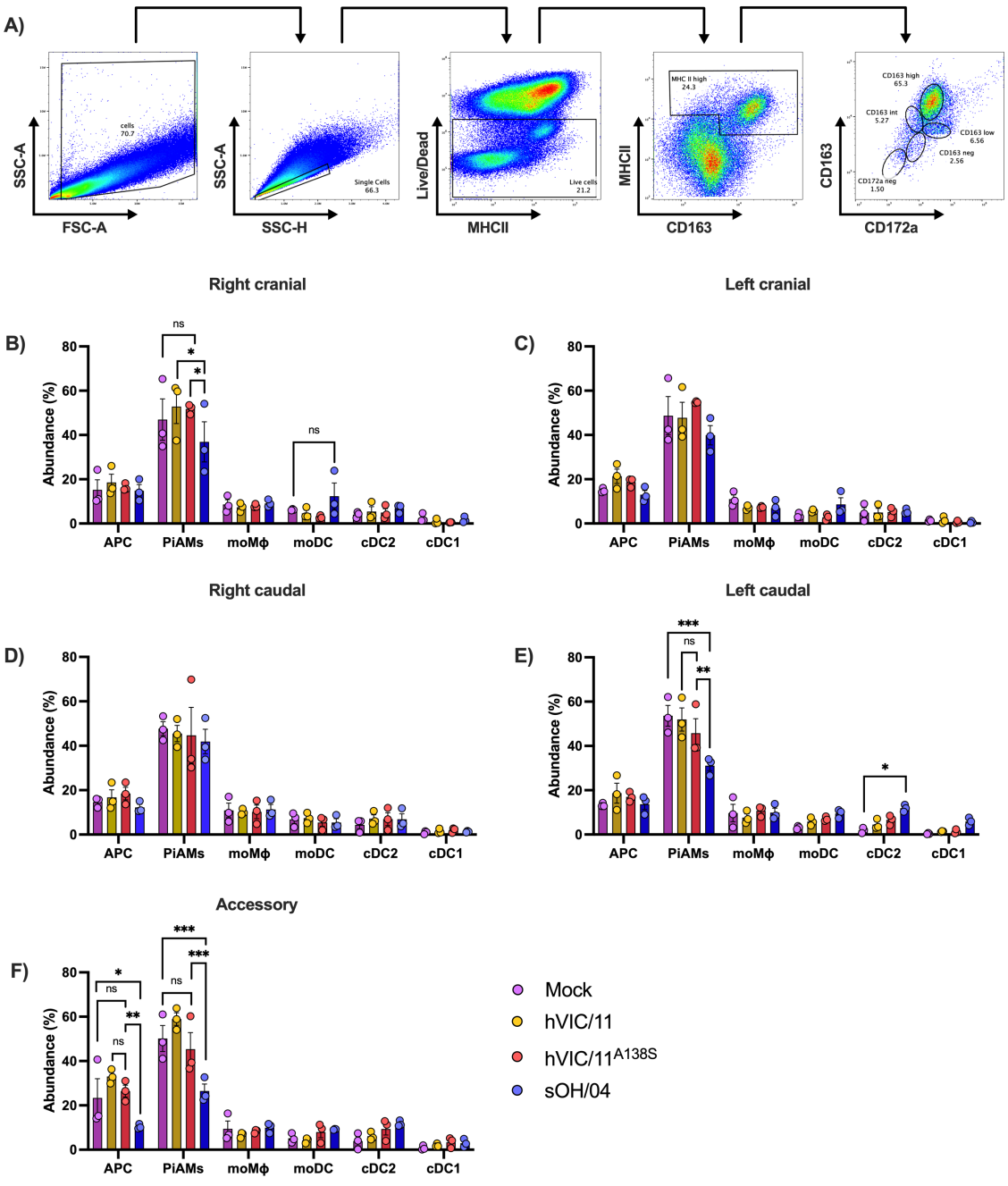
A)
SSC-A
FSC-A
cells
70.7
SSC-A
SSC-H
Single Cells
66.3
Live/Dead
MHCII
Live cells
21.2
MHCII
CD163
MHC II high
24.3
CD163
CD172a
CD163 high
65.3
CD163 int
5.27
CD163 low
6.56
CD163 neg
2.56
CD172a neg
1.50
Right cranial
Left cranial
B)
C)
Abundance (%)
APC
PiAMs
moMϕ
moDC
cDC2
cDC1
Right caudal
Left caudal
D)
E)
Accessory
F)
Mock
hVIC/11
hVIC/11A138S
sOH/04

Figure 3.6. Distinct antigen-presenting cells, macrophages, and dendritic cells abundance induced after infection with influenza viruses in different lung anatomical sections of pigs. (A) Single-cell suspensions were labeled with anti MHCII, CD163, and CD172a antibodies and then analyzed by multi-color flow cytometry. Live cells from singlets were filtered and used to assess MHC II, CD163, and CD172a content. From the $MHCII^{high}$ $CD163^{pos}$ (antigen-presenting cells) population in lung tissue samples, cDC1 cells appear as $CD172a^{neg}CD163^{neg}$, cDC2 are $CD172a^{pos}CD163^{neg}$, moDC are $CD172a^{pos}CD163^{low}$, moMf are $CD172a^{pos}CD163^{int}$, and PiAMs are CD172aposCD163^{high}. Abundance of APC, cDC1, cDC2, moDC, moMf , and PiAMs in the (A) right cranial lobe, (B) left cranial lobe, (C) right caudal lobe, (D) left caudal lobe, and © accessory lobe was quantified among total live cells (APC) or $MHC^{high}CD163^{pos}$ cells (cDC1, cDC2, moDC, moMf , and PiAMs). Values represent the mean $\pm$ SEM for seeder pigs (n=3) in each group. Statistical analysis was performed by two-way ANOVA. *p<0.05, **p<0.005, ***p<0.0005.

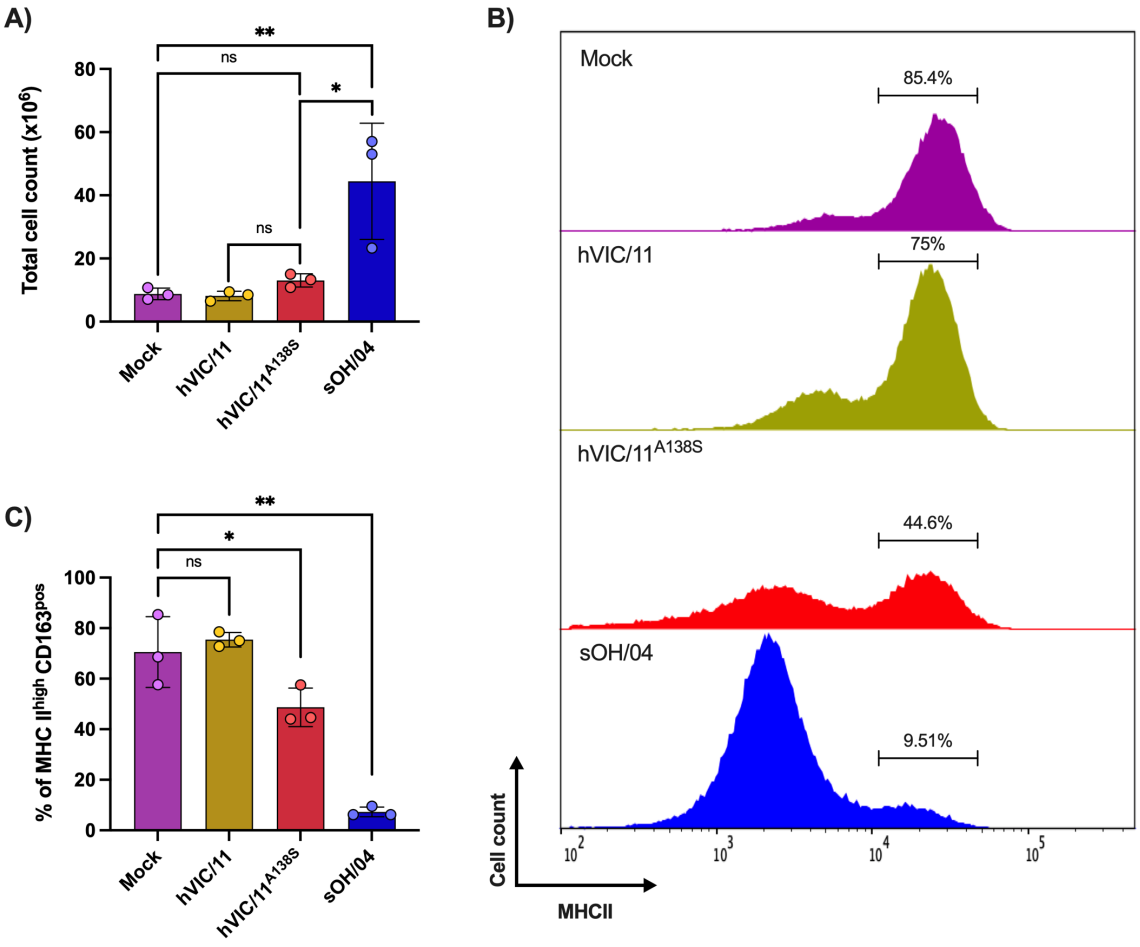
A)
Total cell count (x10^6)
80
60
40
20
0
**
ns
*
ns
Mock
hVIC/11
hVIC/11A138S
sOH/04
B)
Mock
85.4%
hVIC/11
75%
hVIC/11A138S
44.6%
sOH/04
9.51%
Cell count
MHCII
10^2
10^3
10^4
10^5
C)
% of MHC IIhigh CD163pos
100
80
60
40
20
0
**
*
ns
Mock
hVIC/11
hVIC/11A138S
sOH/04

Figure 3.7. hVIC/11^{A138S} infection reduces the abundance of PAMs in BALF. (A) Total cell count in BALF samples from mock, hVIC/11, hVIC/11^{A138S}, and sOH/04-infected pigs. (B) Representative histograms showing PAMs abundance (cell count, MHCII^{high}CD163^{pos}) in BALF samples. BALF samples were analyzed by multi-color flow cytometry and the MHCII content of the populations was quantified among total live cells. (C) Variation of PAMs abundance in mock, sOH/04, hVIC/11, and hVIC/11^{A138S}-infected pigs quantified by flow cytometry. Values represent the mean $\pm$ SEM for seeder pigs (n=3) per group. Statistical analysis was performed by two-way ANOVA. *$p<0.05$, **$p<0.005$.

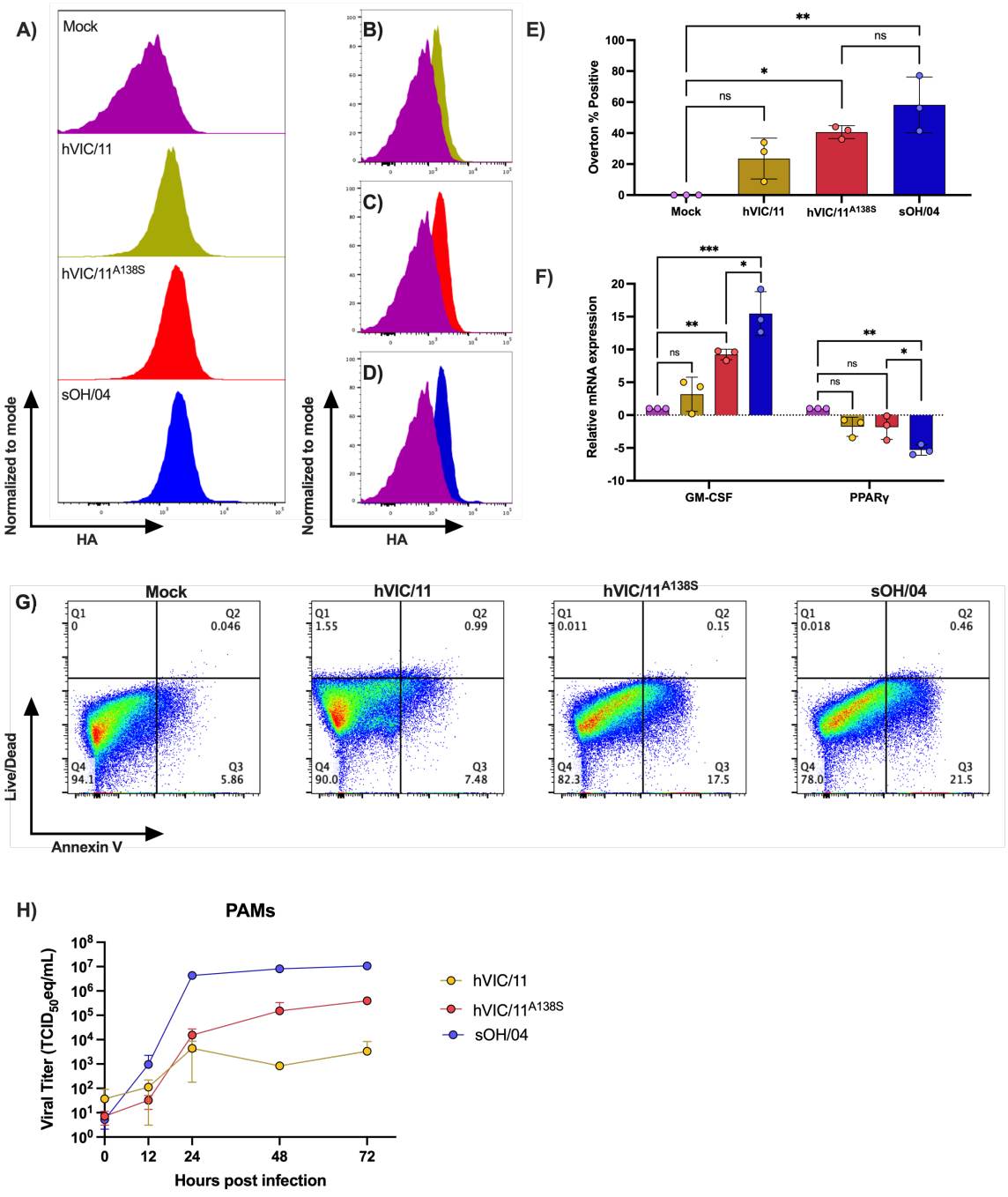
A)
Mock
hVIC/11
hVIC/11A138S
sOH/04
Normalized to mode
HA
B)
C)
D)
Normalized to mode
HA
E)
Overton % Positive
Mock
hVIC/11
hVIC/11A138S
sOH/04
ns
*
**
F)
Relative mRNA expression
GM-CSF
PPARγ
G)
Mock
hVIC/11
hVIC/11A138S
sOH/04
Q1 0
Q2 0.046
Q4 94.1
Q3 5.86
Q1 1.55
Q2 0.99
Q4 90.0
Q3 7.48
Q1 0.011
Q2 0.15
Q4 82.3
Q3 17.5
Q1 0.018
Q2 0.46
Q4 78.0
Q3 21.5
Live/Dead
Annexin V
H)
PAMs
Viral Titer (TCID50eq/mL)
Hours post infection
hVIC/11
hVIC/11A138S
sOH/04

Figure 3.8. FLUAV infection of PAMs affects the expression of GM-CSF but not PPARg expression and promotes apoptosis of alveolar macrophages. (A) PAMs collected from BALF samples of seeders at 5 dpi were stained for HA detection and analyzed by multi-color flow cytometry to detect the amount of $MHCII^{high}CD163^{pos}$ (PAMs) FLUAV -positive cells. Average histograms normalized to mode showing FLUAV -positive PAMs compared to the mock group for (B) hVIC/11, (C) $hVIC/11^{A138S}$, and (D) sOH/04-infected seeder pigs (n=3) per group. From the comparison of FLUAV-positive cells to the mock group, the percentage of FLUAV-positive cells was determined using the Overton % method (E). (F) Relative mRNA levels of GM-CSF and PPARg assessed by qPCR and normalized to RLP-19 expression in BALF samples. Values are shown as log_2 fold induction of the mean between the seeder pigs (n=3) of each group. (G) Flow cytometry analysis of apoptotic cells ($Live/Dead^{neg}Annexin\ V^{pos}$) at 12 hpi. (H) Growth kinetics of sOH/04 (blue), hVIC/11 (yellow), and $hVIC/11^{A138S}$ (red) in 3D4/21 cells at 37°C. Two independent experiments were performed in triplicates each time. Values represent the mean $\pm$ SEM. Statistical analysis was performed by two-way ANOVA. *$p<0.05$, **$p<0.005$, ***$p<0.0005$.

Table 3.1. Primer sequences used for gene expression analysis and pathogens detection from lung tissue and BALF samples.

Primer	Sequence (5'-3')	Reference
RPL-19	F: AACTCCCGTCAGCAGATCC R: AGTACCCTTCCGCTTACCG	Delgado-Ortega, Melo [334]
IL-1b	F: AGAAGAGCCCATCGTCCTTG R: GAGAGCCTTCAGCTCATGTG	
IL-6	F: ATCAGGAGACCTGCTTGATG R: TGGTGGCTTTGTCTGGATTC	
IL-8	F: TCCTGCTTTCTGCAGCTCTC R: GGGTGGAAAGGTGTGGAATG	
IFN-a	F: GGCTCTGGTGCATGAGATGC R: CAGCCAGGATGGAGTCCTCC	
IFN-b	F: ATGTCAGAAGCTCCTGGGACAGTT R: AGGTCATCCATCTGCCCATCAAGT	
TNF-a	F: CCAATGGCAGAGTGGGTATG R: TGAAGAGGACCTGGGAGTAG	
IFN-g	F: GCTCTGGGAAACTGAATGAC R: TCTCTGGCCTTGGAACATAG	
iNOS	F: GAGAGGCAGAGGCTTGAGAC R: TGGAGGAGCTGATGGAGTAG	
Mx1	F: AGTGTCGGCTGTTTACCAAG R: TTCACAAACCCTGGCAACTC	
Mx2	F: CCGACTTCAGTTCAGGATGG R: ACAGGAGACGGTCCGTTTAC	
PKR	F: GACATCCAAAGCAGCTCTCC R: CGCTCTACCTTCTCGCAATC	
RIG-I	F: CGACATTGCTCAGTGCAATC R: TCAGCGTTAGCAGTCAGAAG	
TLR-3	F: CCTGCATTCCAGAAGTTGAG R: TGAGGTGGAGTATTGCAGAG	
TLR-7	F: TCAGCTACAACCAGCTGAAG R: CAGATGTCGCAACTGGAAAG	
TLR-8	F: AGCGCGGGAGGAGTATTGTG R: GCCAGGGCAGCCAACATAAC	
IL-18	F: TCCTTTTCATTAACCAGGGACATC R: GGTCTGAGGTGCATTATCTGAACA	Paulin, Jagannathan [335]
GM-CSF	F: GCAGCATGTGGATGCCATCA R: GCTCCTGGGGGTCAAACATTTC	This work
PPARg	F: TCCAGCATTTCCACTCCACACT R: GAATAAGGCGGGGACACAG	Cui, Chen [336]
PCV2	F: ATAACCCAGCCCTTCTCCTACC R: GGCCTACGTGGTCTACATTTCC	Yang, Habib [337]
PRRSV	F: AAACCAGTCCAGAGGCAAGG R: GCAAACTAA ACTCCACAGTGTAA	Zheng, Chai [338]
Mycoplasma	F: GTCAAAGTCAAAGTCAGCAAAC R: AGCTGTTCAAATGCTTGTCC	Vranckx, Maes [339]

Table 3.2. Virus detection in contact pigs infected with sOH/04, hVIC/11, and hVIC/11^{A138S}. *Number of FLUAV-positive contact pigs determined by RT-qPCR from nasal swab samples at 2dpi/3dpc (C1= contact 1, C2= contact 2, C3= contact 3, C4= contact 4).*

	Virus		
	sOH/04	**hVIC/11**	**hVIC/11^{A138S}**
Seeders	3/3	3/3	3/3
C1	3/3	2/3	3/3
C2	3/3	0/3	3/3
C3	3/3	0/3	3/3
C4	3/3	0/3	3/3

Supplementary material

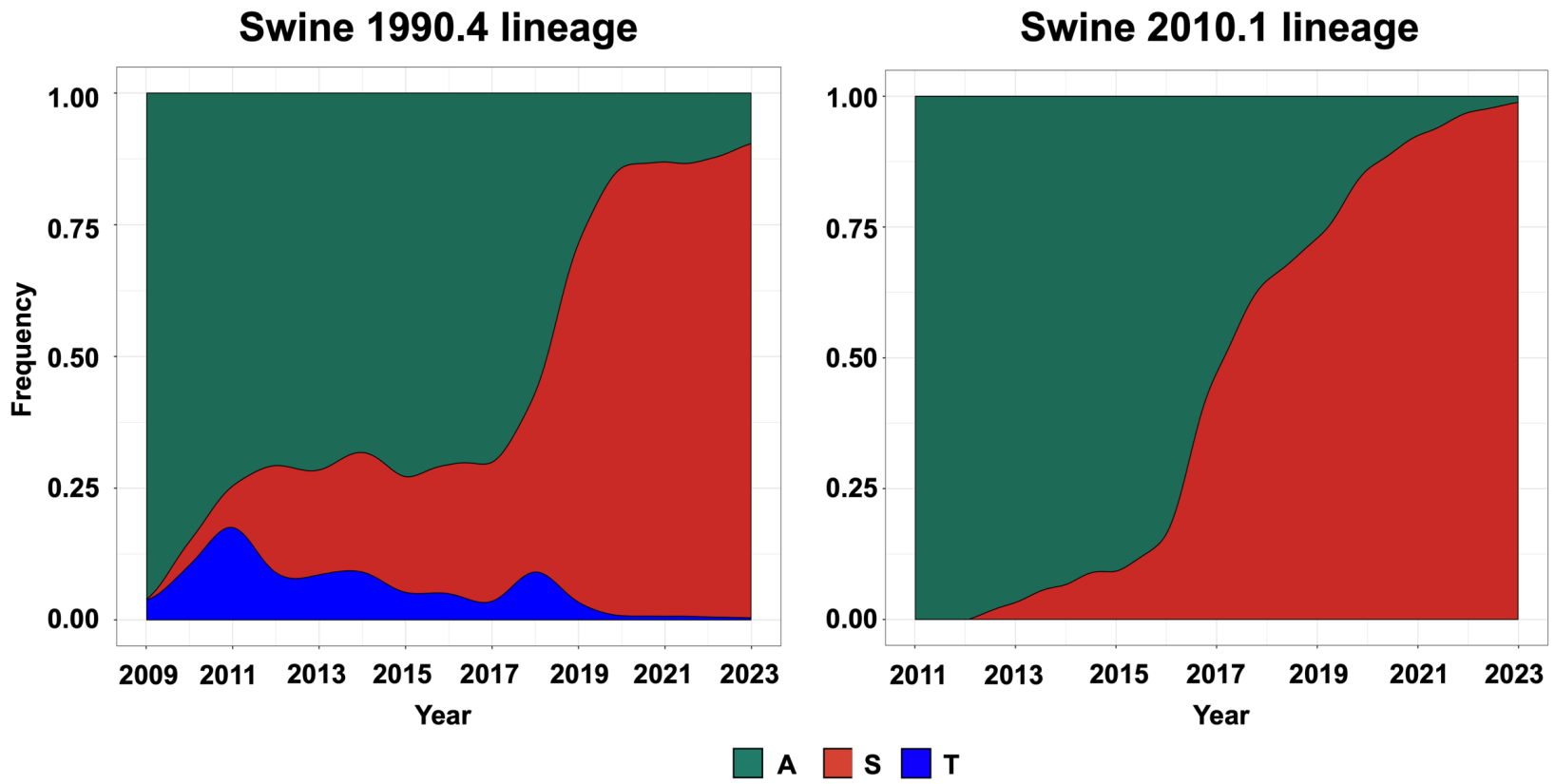

S3.1 Fig. 138S frequency among the swine 1990.4 and the 2010.1 H3 HA lineages. Amino acid frequency at position 138 (H3 numbering) among the 1990.4 and the 2010.1 lineages from isolates reported from 2009 to 2023.

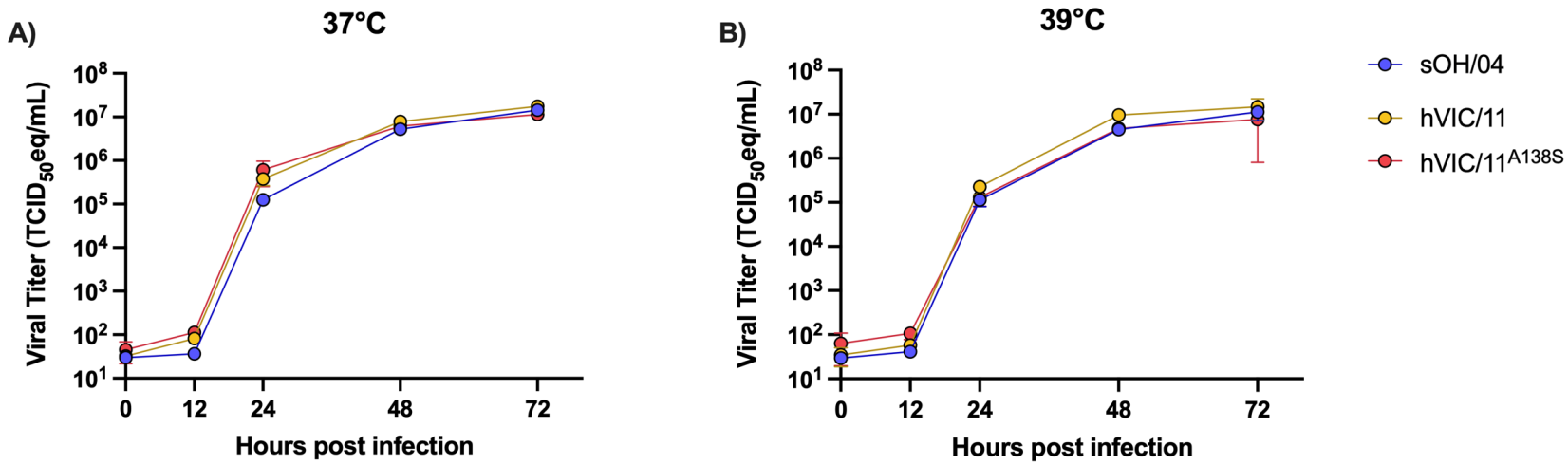

S3.2 Fig. A138S does not confer a replication advantage in MDCK cells. Growth kinetics of sOH/04 (blue), hVIC/11 (yellow), and hVIC/11_A138S (red) in MDCK cells at 37 and 39°C. Experiments were performed two independent times in triplicates each time. Error bars represent the mean ± SEM.

A)

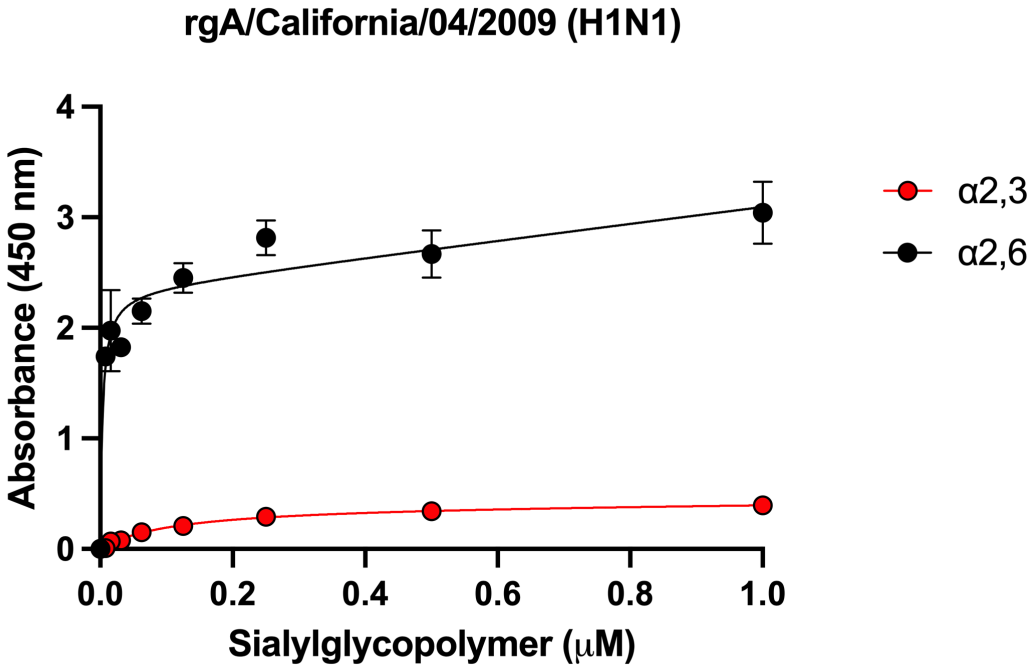
rgA/California/04/2009 (H1N1)
Absorbance (450 nm)
0
1
2
3
4
0.0
0.2
0.4
0.6
0.8
1.0
Sialylglycopolymer (μM)
α2,3
α2,6

B)

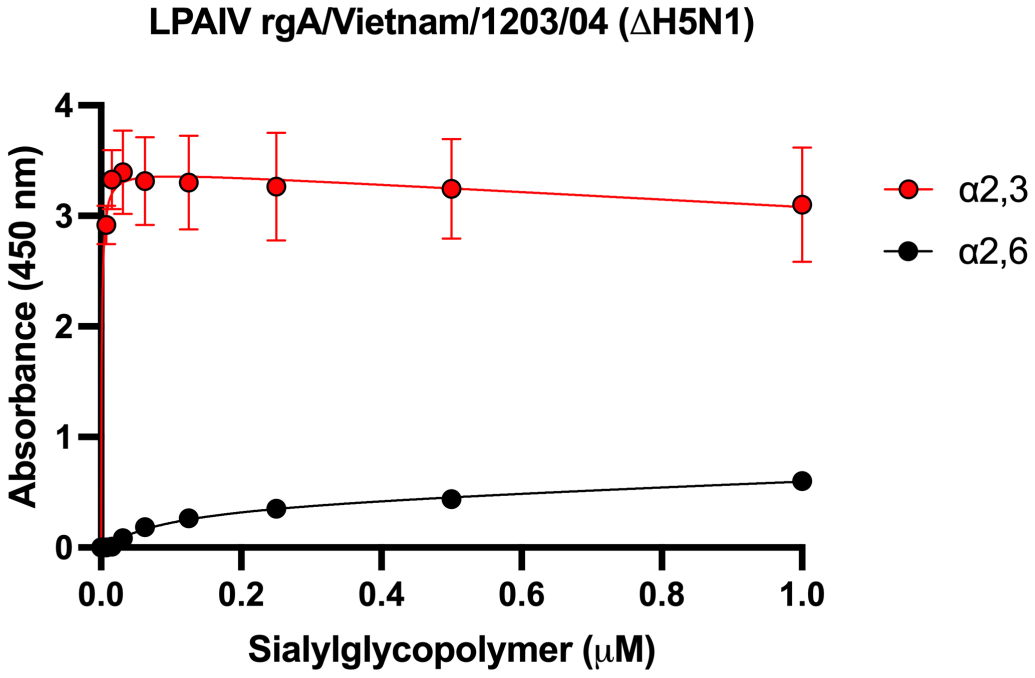
LPAIV rgA/Vietnam/1203/04 (ΔH5N1)
Absorbance (450 nm)
0
1
2
3
4
0.0
0.2
0.4
0.6
0.8
1.0
Sialylglycopolymer (μM)
α2,3
α2,6

S3.3 Fig. Affinity of H1N1 and LPAIV DH5N1 viruses for a2,3 and a2,6 sialylglycopolymers. Solid-phase binding assay curves of control viruses rgA/California/04/2009 (H1N1, A) with high affinity for 6'SLN (black curve) and poor biding to 3'SLN (red curve). LPAIV rgA/Vietnam/1203/04 (DH5N1, B) bound mostly to 3'SLN at low concentrations while poor binding to 6'SLN was detected. Experiments were performed two independent times in triplicates each time. Error bars represent the mean ± SEM.

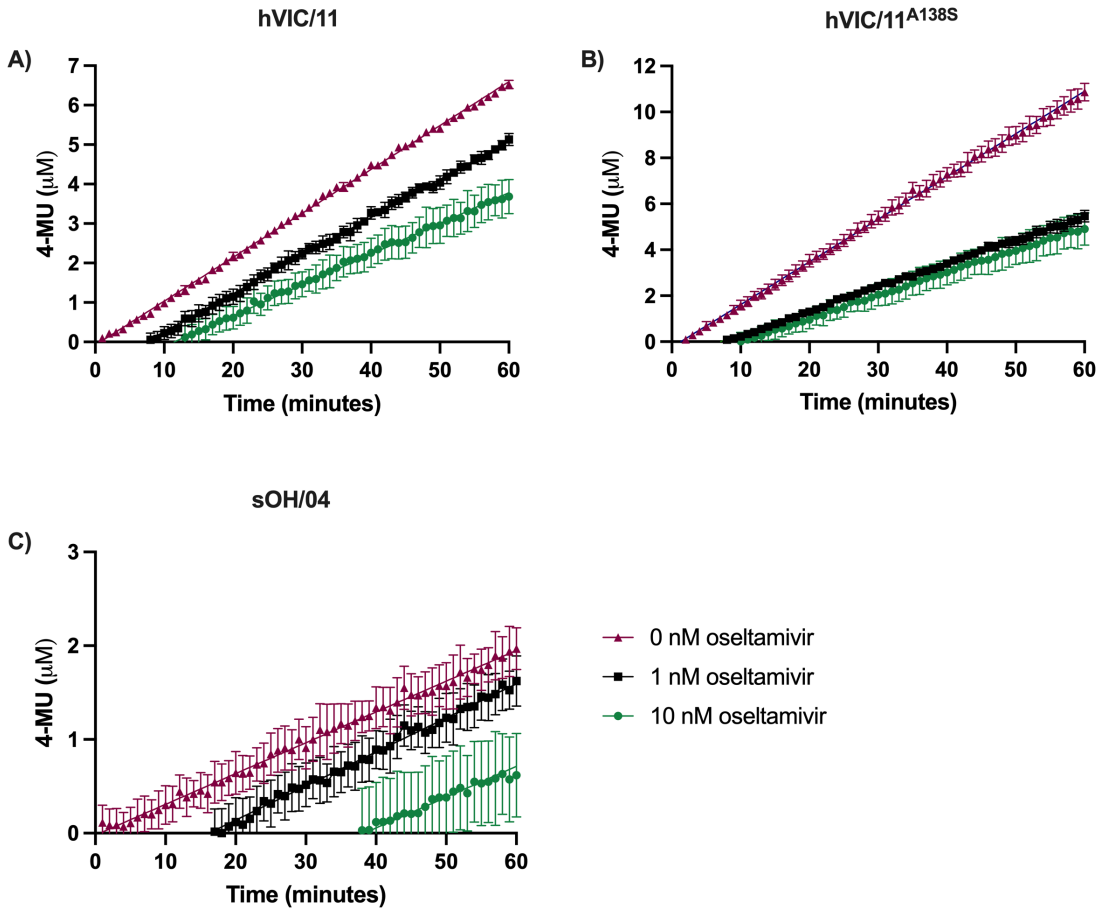

S3.4 Fig. Oseltamivir inhibition of NA. Neuraminidase activity of hVIC/11 (A), hVIC/11^{A138S} (B), and sOH/04 (C) in presence of 0, 1, and 10 nM oseltamivir normalized to 10,000 PFU showing a dose-dependent decrease in NA activity using MUNANA as substrate and supporting the validity of the assay.

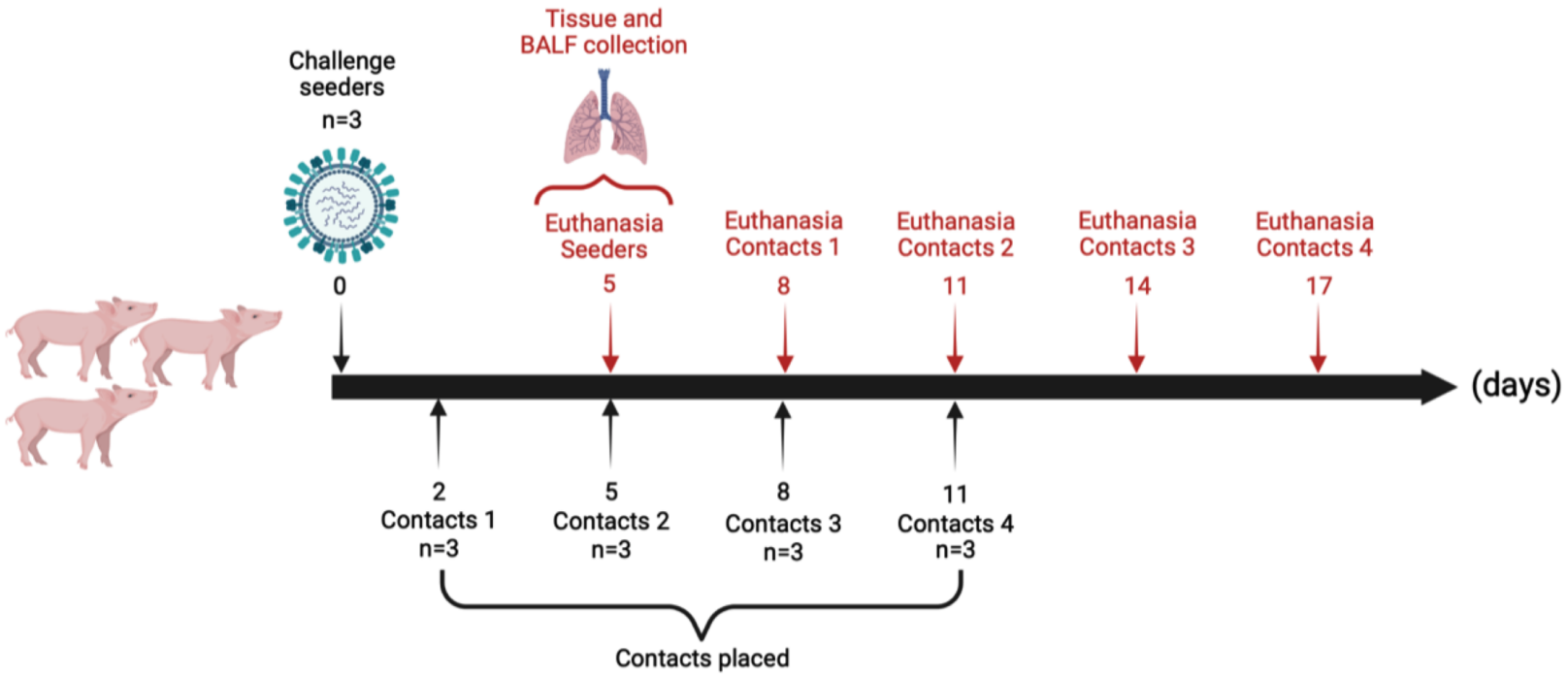

S3.5 Fig. *In vivo* swine study experimental design. Pigs were inoculated with 3 x 10^6 $TCID_{50}$/pig of sOH/04, or hVIC/11, or hVIC/11^{A138S}. At 2 days post-infection (dpi), naïve pigs were placed in contact with inoculated pigs. After 3 days (5dpi), new contacts were introduced after removal of inoculated pigs, and this cycle was repeated for a total of 4 contacts. Pigs were euthanized at 5 dpi/6 days post contact, and bronchoalveolar lavage fluid and lung tissues were collected from seeders pigs. This illustration was created with BioRender.com.

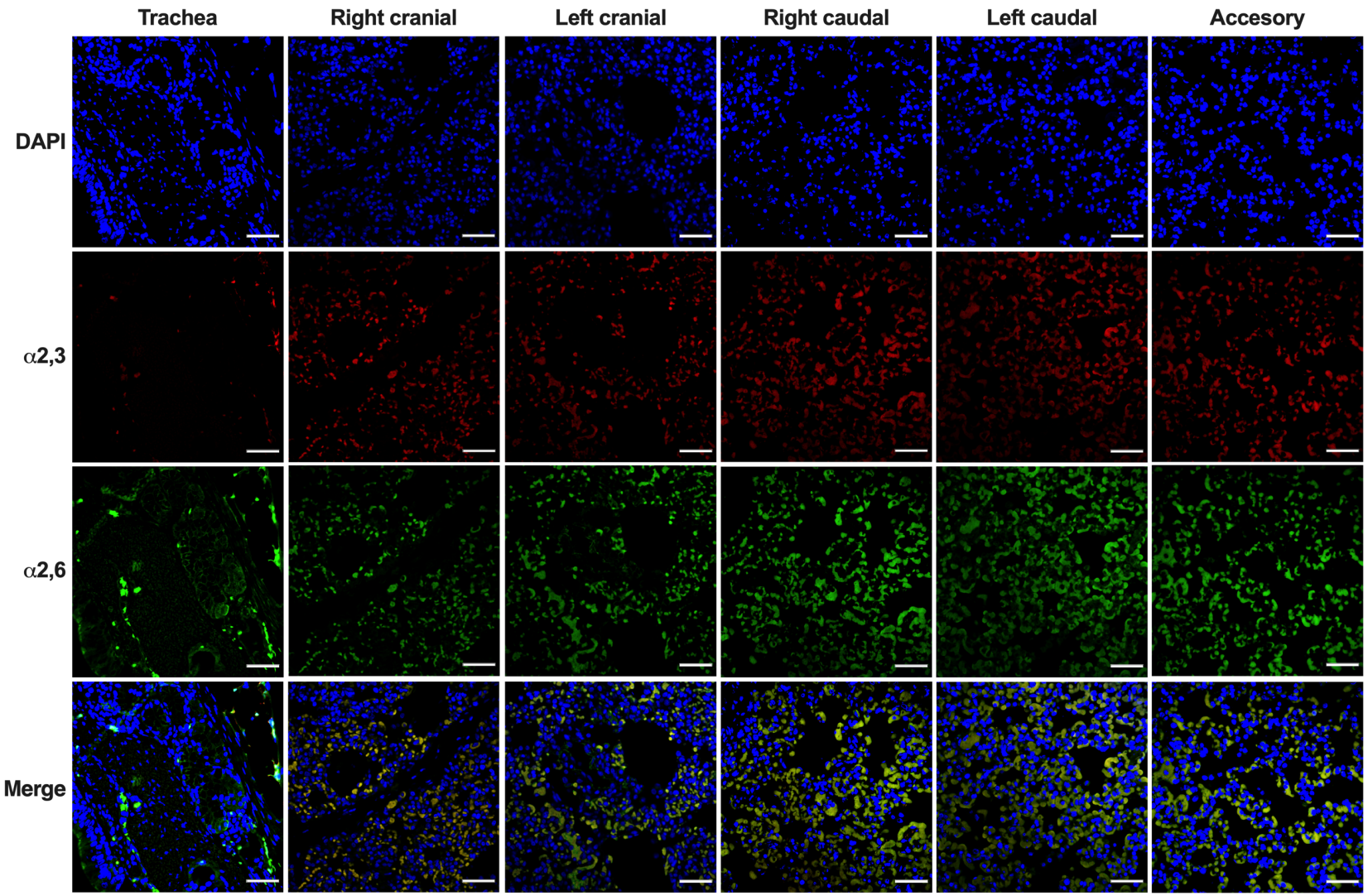
Trachea
Right cranial
Left cranial
Right caudal
Left caudal
Accesory
DAPI
α2,3
α2,6
Merge

S3.6 Fig. a2,3 and a2,6 receptors distribution in the upper and lower respiratory tract of pigs. Representative confocal images showing a2,3 (MAL II, red) and a2,6 (SNA, green) receptors distribution in the upper and lower respiratory tract. a2,6 receptors are predominant in the trachea while in the right cranial, left cranial, right caudal, left caudal, and accessory lobes both receptors are evenly distributed. Cells nuclei was stained with DAPI (blue). The scale bar represents 50 mm.

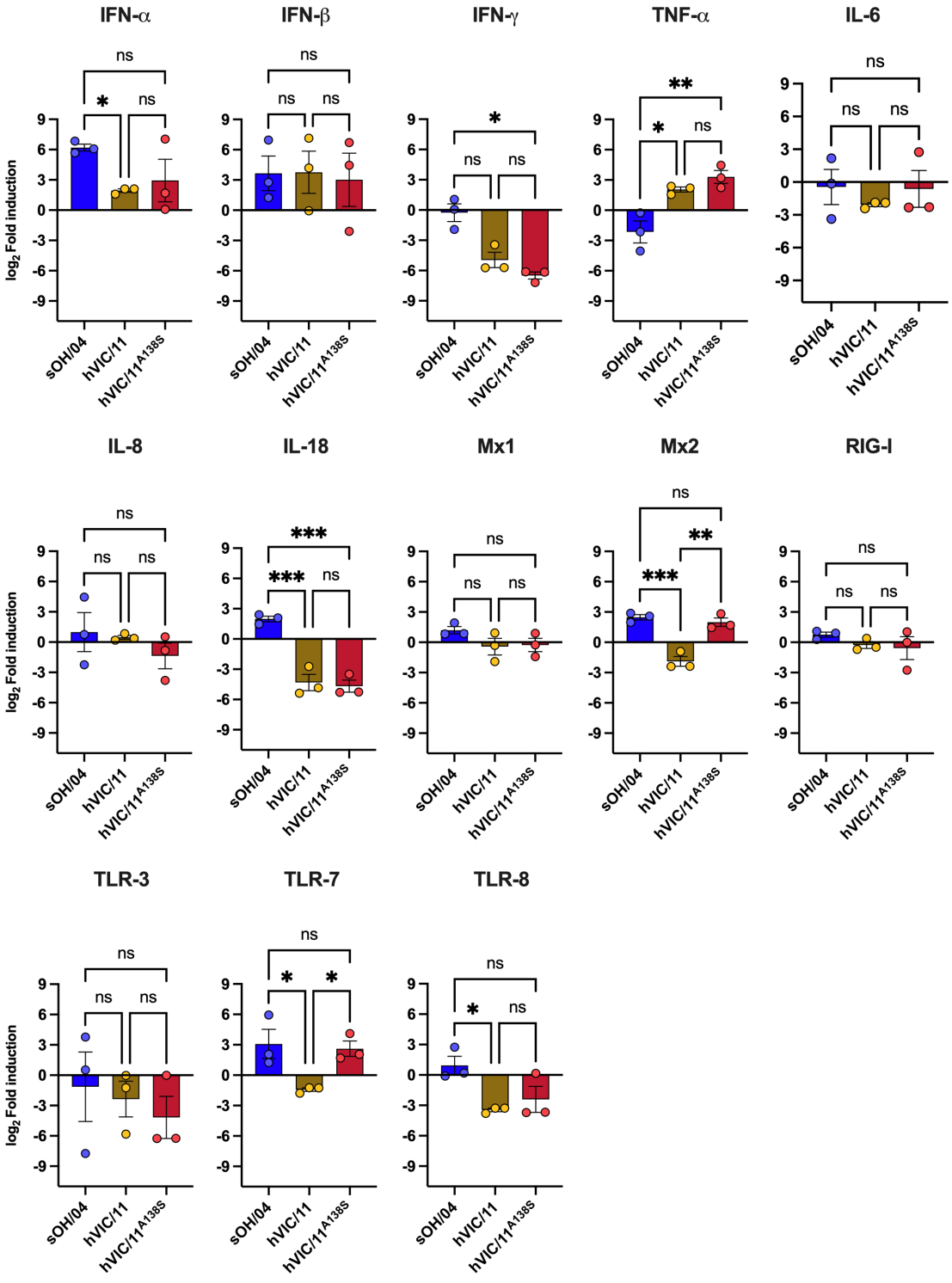
IFN-α
IFN-β
IFN-γ
TNF-α
IL-6
IL-8
IL-18
Mx1
Mx2
RIG-I
TLR-3
TLR-7
TLR-8
log2 Fold induction
sOH/04
hVIC/11
hVIC/11A138S
ns
*
**
***

S3.7 Fig. Relative mRNA levels of pro-inflammatory cytokines, interferon-stimulated genes, and pattern-recognition receptors in the right cranial lobe. RNA was normalized to 1mg and gene expression was assessed by qPCR and normalized to RLP-19 expression in. Values are shown as log_2 fold induction of the mean between the seeder pigs (n=3) of each group at 5dpi. Fold induction of each group was normalized to the non-infected negative control group. Values represent the mean $\pm$ SEM. Statistical analysis was performed by two-way ANOVA. *p<0.05, **p<0.005, ***p<0.0005.

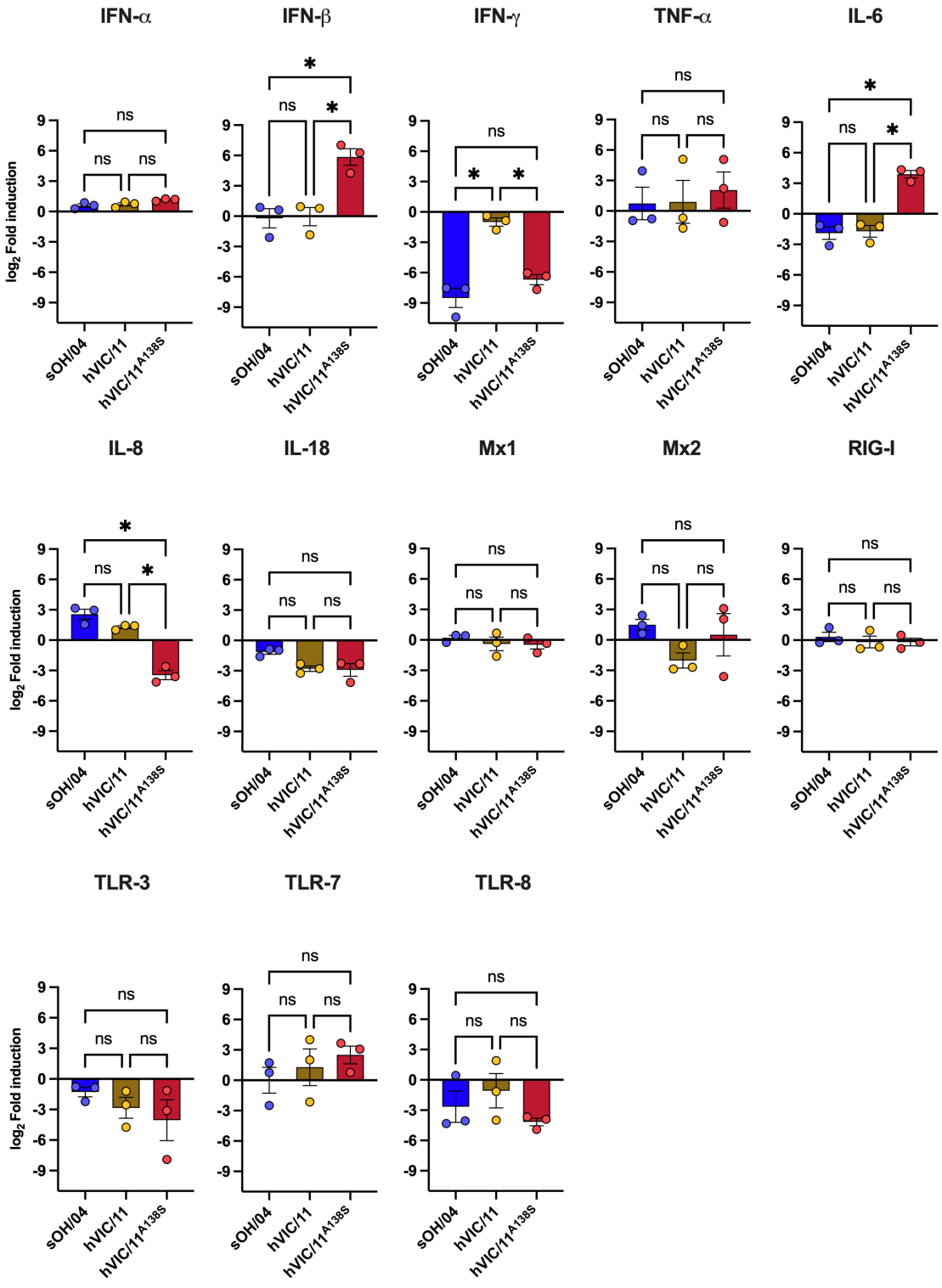
IFN-α
IFN-β
IFN-γ
TNF-α
IL-6
IL-8
IL-18
Mx1
Mx2
RIG-I
TLR-3
TLR-7
TLR-8
log2 Fold induction
ns
*
sOH/04
hVIC/11
hVIC/11A138S

S3.8 Fig. Relative mRNA levels of pro-inflammatory cytokines, interferon-stimulated genes, and pattern-recognition receptors in the left cranial lobe. RNA was normalized to 1mg and gene expression was assessed by qPCR and normalized to RLP-19 expression in. Values are shown as log_2 fold induction of the mean between the seeder pigs (n=3) of each group at 5dpi. Fold induction of each group was normalized to the non-infected negative control group. Values represent the mean $\pm$ SEM. Statistical analysis was performed by two-way ANOVA. *p<0.05, **p<0.005, ***p<0.0005.

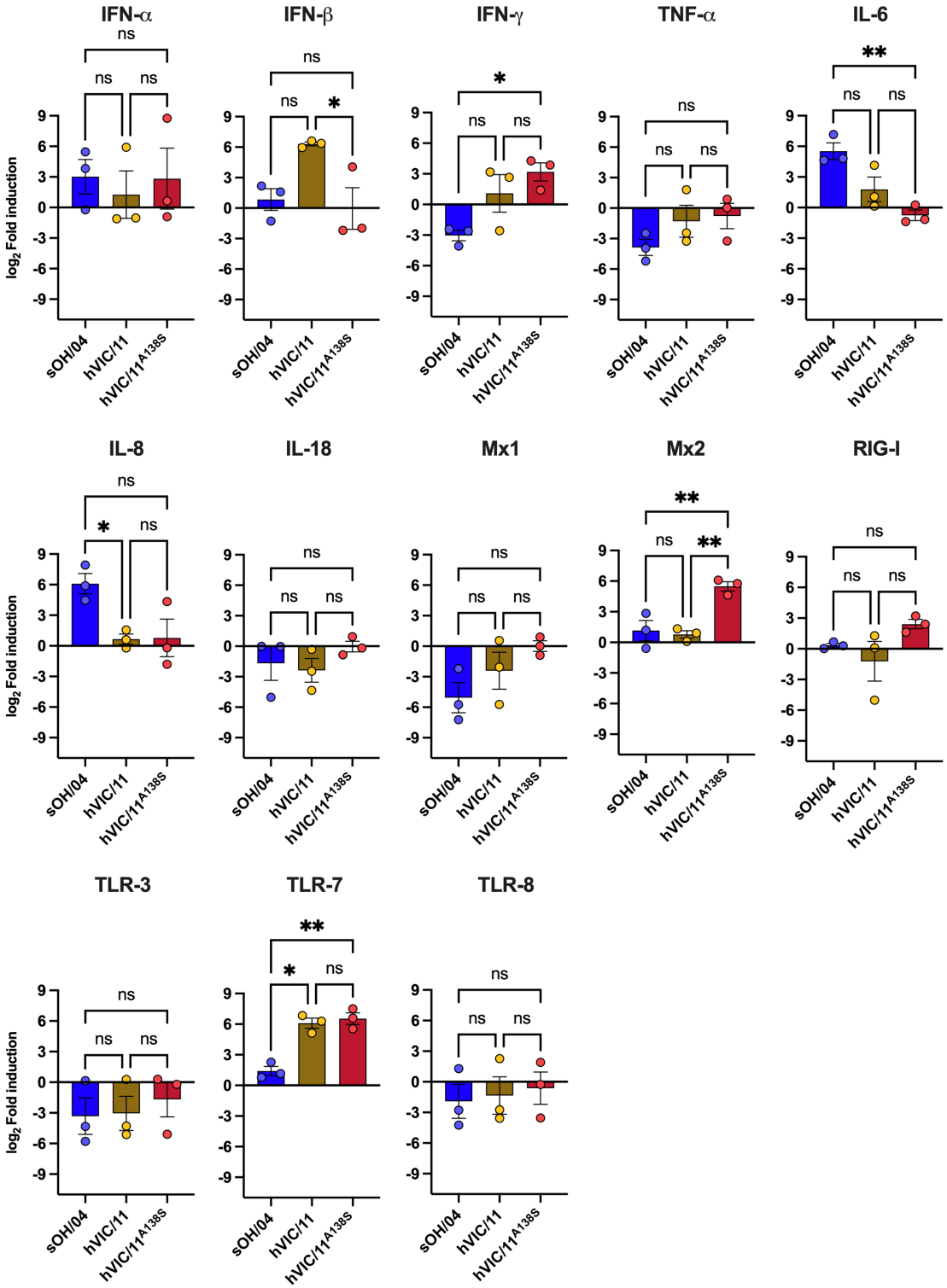
IFN-α
IFN-β
IFN-γ
TNF-α
IL-6
IL-8
IL-18
Mx1
Mx2
RIG-I
TLR-3
TLR-7
TLR-8
log2 Fold induction
ns
*
**
sOH/04
hVIC/11
hVIC/11A138S

S3.9 Fig. Relative mRNA levels of pro-inflammatory cytokines, interferon-stimulated genes, and pattern-recognition receptors in the right caudal lobe. RNA was normalized to 1mg and gene expression was assessed by qPCR and normalized to RLP-19 expression in. Values are shown as log_2 fold induction of the mean between the seeder pigs (n=3) of each group at 5dpi. Fold induction of each group was normalized to the non-infected negative control group. Values represent the mean $\pm$ SEM. Statistical analysis was performed by two-way ANOVA. *p<0.05, **p<0.005, ***p<0.0005.

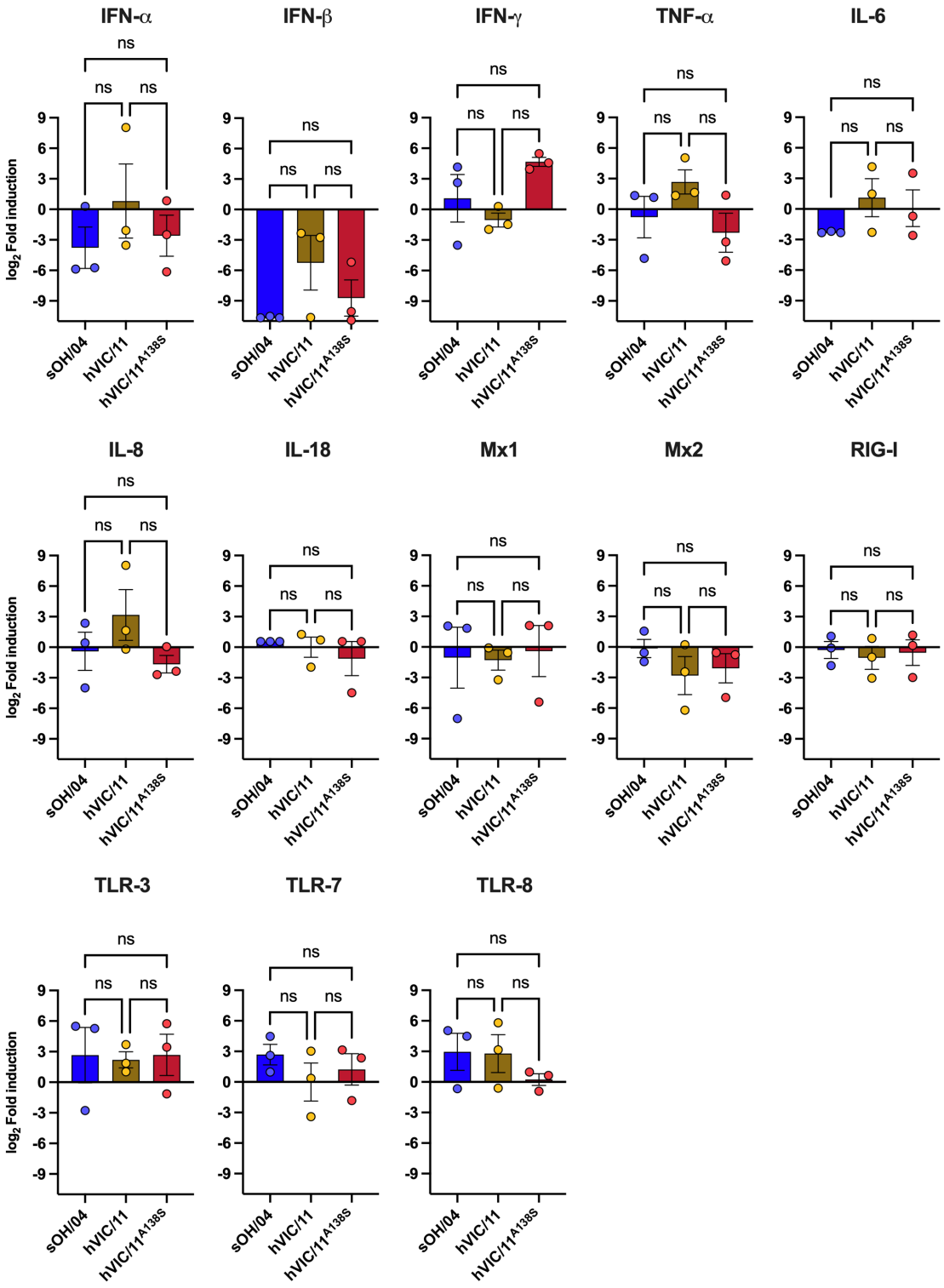
IFN-α
IFN-β
IFN-γ
TNF-α
IL-6
IL-8
IL-18
Mx1
Mx2
RIG-I
TLR-3
TLR-7
TLR-8
log2 Fold induction
ns
9
6
3
0
-3
-6
-9
sOH/04
hVIC/11
hVIC/11A138S

S3.10 Fig. Relative mRNA levels of pro-inflammatory cytokines, interferon-stimulated genes, and pattern-recognition receptors in the left caudal lobe. RNA was normalized to 1mg and gene expression was assessed by qPCR and normalized to RLP-19 expression in. Values are shown as log_2 fold induction of the mean between the seeder pigs (n=3) of each group at 5dpi. Fold induction of each group was normalized to the non-infected negative control group. Values represent the mean $\pm$ SEM. Statistical analysis was performed by two-way ANOVA. *p<0.05, **p<0.005, ***p<0.0005.

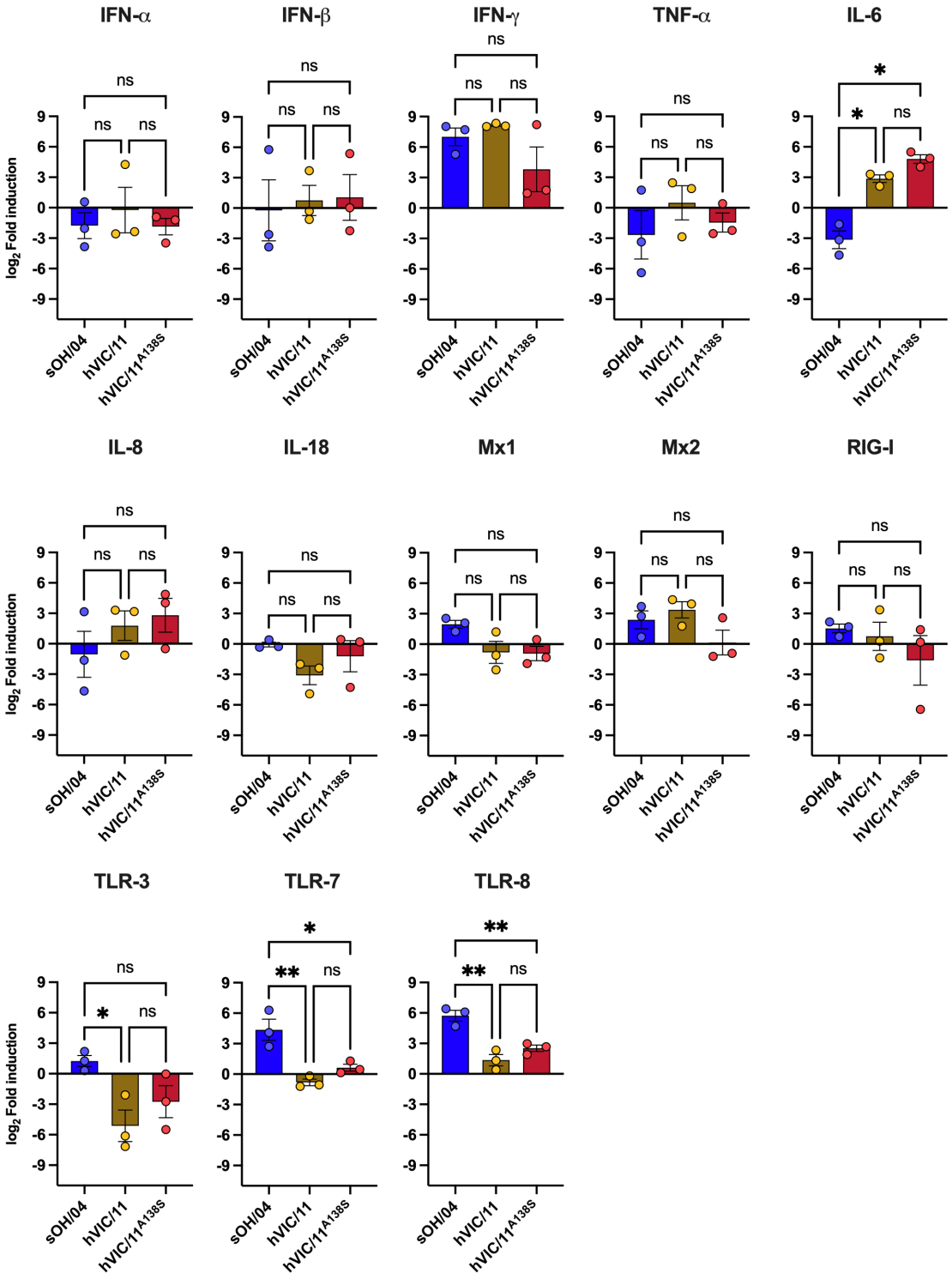
IFN-α
IFN-β
IFN-γ
TNF-α
IL-6
IL-8
IL-18
Mx1
Mx2
RIG-I
TLR-3
TLR-7
TLR-8
log2 Fold induction
sOH/04
hVIC/11
hVIC/11A138S
ns
*
**

S3.11 Fig. Relative mRNA levels of pro-inflammatory cytokines, interferon-stimulated genes, and pattern-recognition receptors in the accessory lobe. RNA was normalized to 1mg and gene expression was assessed by qPCR and normalized to RLP-19 expression in. Values are shown as log_2 fold induction of the mean between the seeder pigs (n=3) of each group at 5dpi. Fold induction of each group was normalized to the non-infected negative control group. Values represent the mean $\pm$ SEM. Statistical analysis was performed by two-way ANOVA. *p<0.05, **p<0.005, ***p<0.0005.

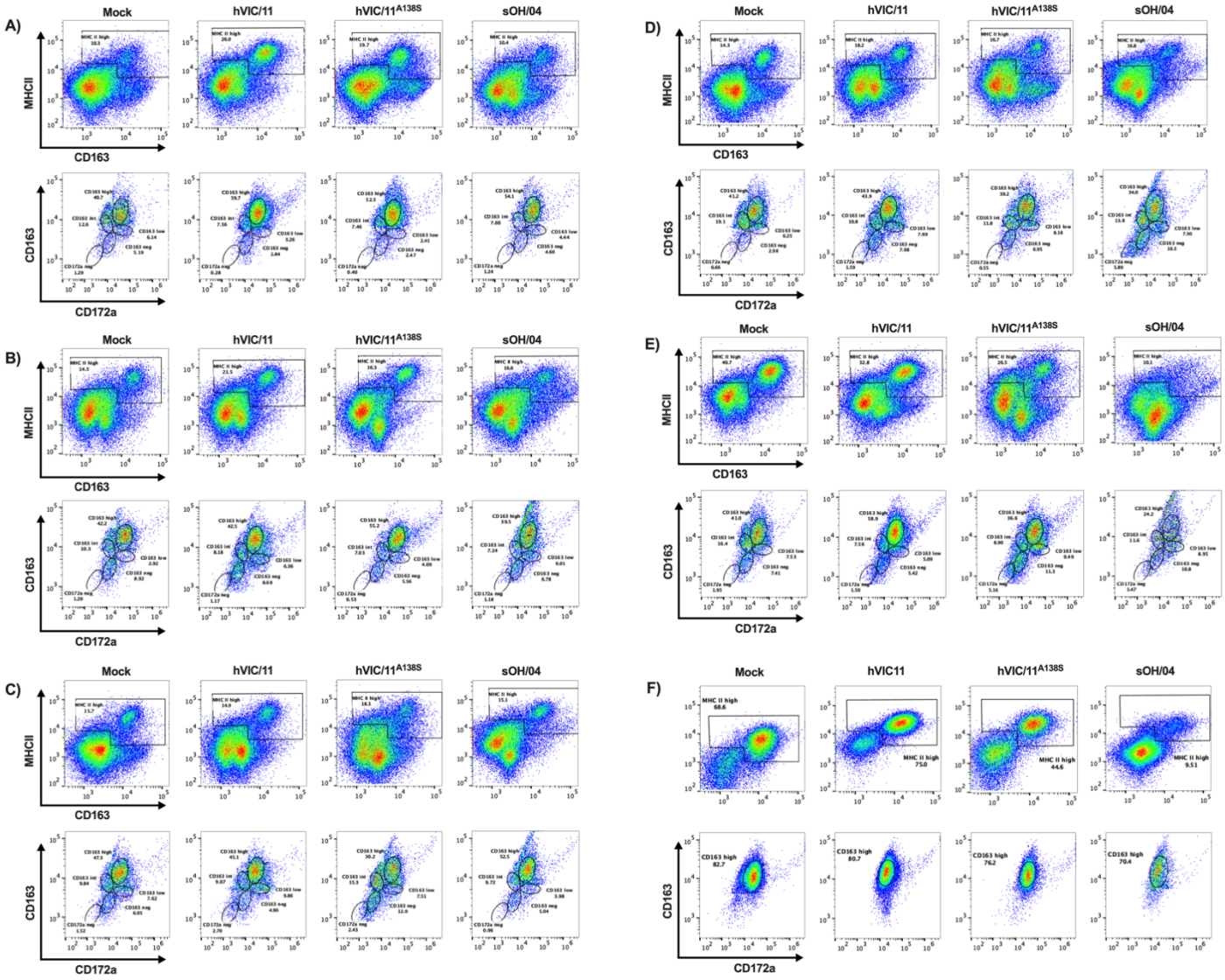
A)
B)
C)
D)
E)
F)
Mock
hVIC/11
hVIC/11A138S
sOH/04
hVIC11
MHCII
CD163
CD172a
MHC II high
CD163 high
CD163 int
CD163 low
CD163 neg
CD172a neg
CD172a high

S3.12 Fig. Flow cytometry analysis of lung and BALF samples. Representative flow cytometry results showing APC (top panels) and cDC1, cDC2, moDC, moMf, and PiAMs (bottom panels) in right cranial (B), left cranial (C), right caudal (D), left caudal (E), and accessory lobes (F) from mock-, hVIC/11-, hVIC/11^{A138S}-, and sOH/04-infected pigs. The gating strategy performed in tissue samples was also used in BALF samples and only one population gated from MHCII^{high} CD163^{pos} cells appeared. This population is composed of PAMs only and characterized as CD172a^{pos}CD163^{high} (G).

Acknowledgments

We thank the University Research Animal Resources personnel at the University of Georgia for assistance with animal care, and the Histology laboratory personnel, College of Veterinary Medicine, University of Georgia, for assistance with histopathology services. This research was supported by Agriculture and Food Research Initiative grant no. 2020-67015-31563/project accession no. 1022827 from the USDA National Institute of Food and Agriculture to DSR. Funding was also provided, in part, by The National Pork Board to DSR under Project #21-085. DSR is also funded by Agriculture and Food Research Initiative grant no. 2022-67015-37205/project accession no. 1028058 from the USDA National Institute of Food and Agriculture. DRP is funded by subcontract 75N93021C00014 Centers for Influenza Research and Response (CEIRR) from the National Institute of Allergy and Infectious Diseases (NIAID) and GRANT12901999, project accession no. 1022658 from the National Institute of Food and Agriculture (NIFA), U.S. Department of Agriculture. DRP receives additional support from the Georgia Research Alliance and the Caswell S. Eidson endowment funds from The University of Georgia. This study was partly supported by resources and technical expertise from the Georgia Advanced Computing Resource Center, a partnership between the University of Georgia's Office of the Vice President for Research and the Office of the Vice President for Information Technology. ALVB and TKA are funded by the USDA-ARS project number 5030-32000-231-000D and the NIAID, National Institutes of Health, Department of Health and Human Services, under Contract No. 75N93021C00015. The funders had no role in study design, data collection and interpretation, or the decision to submit the work for publication.

CHAPTER 4

MODULATION OF HUMAN-TO-SWINE INFLUENZA A VIRUS ADAPTATION BY THE NEURAMINIDASE LOW-AFFINITY CALCIUM-BINDING POCKET

Matias Cardenas, Brittany Seibert, Brianna Cowan, C. Joaquin Caceres, L. Claire Gay, Flavio Cargnin Faccin, Daniel R. Perez, Tavis K. Anderson, Amy L. Baker, and Daniela S. Rajao. (2024). Communications Biology 1230(7). Reprinted here with permission of the publisher.

Abstract

Frequent interspecies transmission of human influenza A viruses (FLUAV) to pigs contrasts with the limited subset that establishes in swine. While hemagglutinin (HA) mutations are recognized for their role in cross-species transmission, the contribution of neuraminidase (NA) remains understudied. In this study, NA's role in FLUAV adaptation was investigated using a swine-adapted H3N2 reassortant virus with human-derived HA and NA segments. Adaptation in pigs resulted in mutations in both HA (A138S) and NA (D113A). The D113A mutation abolished calcium (Ca^{2+}) binding in the low-affinity Ca^{2+}-binding pocket of NA, enhancing enzymatic activity and thermostability under Ca^{2+}-depleted conditions, mirroring swine-origin FLUAV NA behavior. Structural analysis predicts that swine-adapted H3N2 viruses lack Ca^{2+} binding in this pocket. Further, residue 93 in NA (G93 in human, N93 in swine) also influences Ca^{2+} binding and impacts NA activity and thermostability, even when D113 is present. These findings demonstrate that mutations in influenza A virus surface proteins alter evolutionary trajectories following interspecies transmission and reveal distinct mechanisms modulating NA activity during FLUAV adaptation, highlighting the importance of Ca^{2+} binding in the low-affinity calcium-binding pocket.

Introduction

Interspecies transmission of Influenza A viruses (FLUAV) is common; however, sustained transmission within a new host species is rare. This is because the virus must undergo adaptive evolution to replicate, transmit, and become endemic in the new host population. FLUAV have two major surface glycoproteins: hemagglutinin (HA) and neuraminidase (NA). The HA recognizes sialic acids (SAs) on the cell surface and triggers virus entry into the host cells [281, 340]. The NA shows an opposite activity, cleaving SAs to allow the virus to move through the respiratory mucus by preventing binding to decoy receptors and to promote virus release from infected cell [125, 341].

Due to its central role in the infection process, the HA protein is considered the primary driver of adaptation to a new host species. This adaptation often involves the acquisition of mutations in the receptor binding site (RBS) that enhance affinity for host-specific SA conformations [19, 177, 342]. Previous studies have demonstrated that adaptation of FLUAVs isolated from humans to pigs results in amino acid changes in the HA RBS, increasing affinity for swine airway epithelial cells [27] and improving transmission efficiency compared to the original human virus [258]. However, other gene segments also contribute to the adaptation of human-origin FLUAVs to pigs, with the acquisition of a well-adapted internal gene segment constellation seemingly essential [18, 244, 289]. Human FLUAVs introduced to pigs frequently lose their internal gene segments through reassortment, acquiring swine-adapted gene segments from endemic strains [17]. Interestingly, the surface gene segments (HA and NA) often persist in the

swine population, albeit with significant genetic differences from the precursor strains [17, 242], leading to the establishment of new lineages.

The NA protein is a critical factor in FLUAV adaptation across species, as it must maintain a functional balance with HA for successful infection [127]. Adaptive mutations in the HA RBS can disrupt this balance, often prompting compensatory mutations in the NA protein [343]. NA is a homotetrameric enzyme with hydrolase activity, with each monomer consisting of a transmembrane domain, a stalk domain, and a head domain containing the catalytic pocket [181, 205, 344]. While the catalytic pocket is present in each monomer, optimal sialidase activity is only achieved in the tetrameric state [345-347]. Calcium (Ca^{2+}) is an essential cofactor for NA activity, and most NA subtypes possess a high-affinity Ca^{2+}-binding pocket near the active site of each monomer [348-350]. This binding event is thought to induce a conformational change in the catalytic site, facilitating proper SA binding [189, 191]. In addition to the high-affinity site, certain subtypes such as N1 and N2 NAs have a second, low-affinity Ca^{2+}-binding pocket located within the symmetry axis of the tetramer [35, 191]. This second site is believed to contribute to tetramer stability and, indirectly, to NA activity, as NA activity is dependent on the tetrameric form [35, 351, 352]. Notably, the crystal structure of the 2009 pandemic H1N1 virus NA revealed that the virus quickly changed its calcium preference in the symmetry axis after jumping from pigs to humans[35].

Despite these observations, the precise role of the second Ca^{2+}-binding site in the adaptation of FLUAV between species remains poorly understood and requires further investigation. In this study, we investigated the adaptive mechanisms of human-derived FLUAV HA and NA gene segments during transmission in a swine host. Utilizing a

reassortant virus carrying HA and NA segments from the human strain A/Victoria/361/2011 (hVIC/11) in a swine-origin FLUAV backbone. The rapid emergence of an adaptative mutation was observed in HA (A138S, H3 numbering – herein referred to as the hVIC/11-A138S strain) near the RBS that evolved after infection of pigs [27]. Subsequently, and after two serial transmission events *in vivo* in pigs, the emergence and fixation of a novel mutation in the NA, D113A, was observed. *In silico* structural analyses revealed that amino acid 113 in the N2 NA of hVIC/11 interacts with Ca^{2+} in the low-affinity Ca^{2+}-binding pocket, a characteristic typically observed in human H3N2 strains. Remarkably, the D113A mutation abolished Ca^{2+} binding in this pocket, but concurrently enhanced NA thermostability and activity under Ca^{2+}-depleted conditions. However, the A113 variant is uncommon in both human and swine H3N2 strains, and, notably, swine-origin H3N2 FLUAVs harboring this mutation are predicted to be unable to bind Ca^{2+} in the low-affinity pocket. This observation prompted further investigation into the molecular determinants of this differential binding behavior, which revealed an important role of amino acid at position 93 in NA that further influences Ca^{2+} binding in the low-affinity pocket and impacts replication and transmission efficiency in pigs. These findings highlight the intricate molecular determinants of FLUAV adaptation between hosts and underscore the critical role of Ca^{2+} binding in this process.

Materials and Methods

Ethics statement

Animal studies were approved by the Institutional Care and Use Committee (IACUC) at the University of Georgia (protocol A2019 03-031-Y3-A9). Studies were performed under animal biosafety level 2+ (ABSL2+) containment and animals were cared for in accordance with the guidelines set forth in the "Guide for the Care and Use of Agricultural Animals in Research and Teaching (Ag Guide)" (American Dairy Science Association, American Society of Animal Science, and Poultry Science Association, 2020). At the end of the study, animals were euthanized following the American Veterinary Medical Association (AVMA) guidelines. All experiments with mutant viruses were performed under BSL 2+ conditions at University of Georgia (Institutional Biosafety Committee approval number 2020-0035).

Cells and viruses

Madin-Darby canine kidney (MDCK), human lung carcinoma (A549), and porcine kidney (PK15) cells were grown in Dulbecco's Modified Eagles Medium (DMEM, Sigma-Aldrich, St Louis, MO) supplemented with 2mM L-glutamine (Sigma-Aldrich, St Louis, MO), 10% fetal bovine serum (FBS, Sigma-Aldrich, St Louis, MO), and 1% antibiotic/antimycotic (Sigma-Aldrich, St Louis, MO). Cells were cultured at 37°C in a humidified incubator with 5% CO_2.

Human airway epithelial cells (BCi.NS1.1) [353] were kindly provided by Dr. Ronald Crystal (Weill Cornell Medicine, NY, USA) and maintained in PneumaCult-Ex Plus Basal Media (STEMCELL Technologies, Vancouver, Canada) supplemented with

PneumaCult-Ex Plus Supplement (STEMCELL Technologies, Vancouver, Canada), 0.1% hydrocortisone (STEMCELL Technologies, Vancouver, Canada), 1% antibiotic/antimycotic (Sigma-Aldrich, St Louis, MO), and 0.5% gentamycin (Sigma-Aldrich, St Louis, MO). Cells were cultured at 37°C in a humidified incubator with 5% CO_2 and media was replaced every two days. Differentiation of BCi.NS1.1 cells was performed in type IV collagen-coated 12 mm trans well plates (0.4 mm pore size, Corning Inc., NY, USA). Cells were plated at $3x10^5$ cells/well and cultures were maintained at 37°C in a humidified incubator with 5% CO_2 until a 100% confluency was reached. After reaching confluency, cells were differentiated by changing to air-liquid interface (ALI) conditions by removing the apical media and replacing the basal media with PneumaCult ALI Base Media (STEMCELL Technologies, Vancouver, Canada), supplemented with PneumaCult ALI Supplement (STEMCELL Technologies, Vancouver, Canada), 1% PneumaCult ALI Maintenance Supplement (STEMCELL Technologies, Vancouver, Canada), 1% antibiotic/antimycotic (Sigma-Aldrich, St Louis, MO), and 0.5% gentamycin (Sigma-Aldrich, St Louis, MO), 0.2% heparin (STEMCELL Technologies, Vancouver, Canada), and 0.5% hydrocortisone (STEMCELL Technologies, Vancouver, Canada). Cells were maintained at 37°C in a humidified incubator with 8% CO_2 for 5 days and then were cultured at 37°C in a humidified incubator with 5% CO_2 for 16 more days.

Spodoptera frugiperda pupal ovarian tissue (Sf9) cells were maintained in SF-900 II SFM media (ThermoFisher Scientific, Waltham, MA) supplemented with 1% antibiotic/antimycotic (Sigma-Aldrich, St Louis, MO). High Five™ Insect cells (BTI-TN-5B1-4) were cultured in Express Five SFM media (ThermoFisher Scientific,

Waltham, MA) supplemented with 18 mM L-glutamine (ThermoFisher Scientific, Waltham, MA) and 1% antibiotic/antimycotic (Sigma-Aldrich, St Louis, MO). Both insect cell lines were maintained in suspension at 28°C.

FLUAV viruses used in this study (**Table 4.1**) were generated using an eight-plasmid reverse genetics system as previously described [354]. Parental viruses (hVIC/11, sOH/04, and hVIC/11-A138S) were described before[258, 355]. D113A and G93N/N93G mutations were introduced into hVIC/11 or sOH/04 NA by site-directed mutagenesis using the Phusion site-directed mutagenesis kit (ThermoFisher Scientific, Waltham, MA) and the primers listed in **S4.1 Table** according to the manufacturer's instructions and plasmids' sequences were confirmed by whole plasmid sequencing. Viruses were propagated in MDCK cells using Opti-MEM (ThermoFisher Scientific, Waltham, MA) containing 1 mg/ml of tosylsulfonyl phenylalanyl chloromethyl ketone (TPCK)-treated trypsin (Worthington Biochemicals, Lakewood, NJ) at 37°C. Viral titers were determined by $TCID_{50}$ using the Reed and Muench method [293].

In vivo studies

3-weeks-old cross-bred pigs obtained from Midwest Research Swine Inc (Glencoe, MN, USA) and housed in animal biosafety level 2 (ABSL2) facilities at the University of Georgia. Animals were negative for anti-FLUAV NP antibodies by competitive ELISA (IDEXX, Westbrook, ME) and randomly distributed into two groups. Pigs (n=3, seeders) were inoculated intratracheally and intranasally under anesthesia using a cocktail of ketamine (6 mg/kg), xylazine (3 mg/kg), and Telazol (6 mg/kg) with $3x10^6$ $TCID_{50}$ per pig of hVIC/11-A138S or sOH/04. Animals were checked daily for

clinical signs and nasal swabs were collected at 0, 1, 2, 3, and 5 days-post infection (dpi) in 2 mL of brain hart infusion broth (Sigma-Aldrich, St Louis, MO). At 2 dpi, naïve pigs (n=3) were placed as contacts (contact 1, C1) with the directly inoculated animals and were kept together until 5 dpi. At 5 dpi, seeders pigs were sedated using a cocktail of ketamine (3 mg/kg), xylazine (1.5 mg/kg), and Telazol (3 mg/kg) and then humanely euthanized by an intravenous pentobarbital overdose (Euthasol, 390 mg/10 lb). Contact 1 pigs were moved into a clean enclosure after removal of seeder pigs, and additional naïve pigs (n=3) were placed as new contacts (contact 2, C2). This process was repeated for a total of 4 contacts. Nasal swabs from contact pigs were collected at 0, 1, 3, 5, and 6 days-post contact (dpc). At 6 dpc, contact pigs were sedated and humanely euthanized as described above. During necropsies, bronchoalveolar lavage fluid (BALF) and lung tissue were collected from all pigs.

Virus titration from lung tissue, nasal swabs, and BALF samples

Lung samples were homogenized using the Tissue Lizer II (Qiagen, Gaithersburg, MD) and a Tungsten carbide 3 mm bead (Qiagen, Gaithersburg, MD) for 10 min at 30 Hz. Subsequently, RNA from lung tissues, nasal swabs, and BALF samples was extracted using the MagMax-96 AI/ND viral RNA (ThermoFisher Scientific, Waltham, MA) isolation kit according to manufacturer's instructions. RNA from lung tissue was normalized to 1 mg in 20 mL of nuclease-free water while RNA from nasal swabs and BALF samples were used directly for titration. Samples were titrated using the Quantabio qScript XLT One-Step RT-qPCR ToughMix kit (Quantabio, Beverly MA) targeting the M segment **(S4.1 Table)** according to manufacturer's instructions.

Primary swine tracheal epithelial cells isolation

Trachea samples were obtained from three 7-weeks old cross-bred pigs obtained from Midwest Research Swine Inc (Glencoe, MN) and airway epithelial cells were isolated as previously described [356] with minor modifications. Briefly, trachea sections were digested for 12 h at 4°C in DMEM/F12 (Sigma-Aldrich, St Louis, MO) supplemented with 1.5 mg/mL pronase (Sigma-Aldrich, St Louis, MO), and 1% antibiotic/antimycotic (Sigma-Aldrich, St Louis, MO). After overnight incubation, trachea sections were scraped to release individual cells and fibroblasts were discarded by plastic adherence for 4 h [357]. Non-adherent cells were then plated in type I collagen-coated flasks and cultured with BEGM™ Bronchial Epithelial Cell Growth Medium BulletKit™ (Lonza, Bend, OR, USA) at 37°C in a humidified incubator with 5% CO_2. Differentiation was performed by seeding $3x10^5$ cells/well in type I collagen-coated 12 mm transwell plates (0.4 mm pore size, Corning Inc., NY, USA) in BEGM™ media at 37°C in a humidified incubator with 5% CO_2 until a 100% confluency was reached. After reaching confluency, BEGM™ media was removed from the apical and basal compartments and ALI media composed of DMEM/F12 supplemented with 2% NuSerum (Corning Inc., NY, USA), 2mM L-glutamine (Sigma-Aldrich, St Louis, MO), 1% antibiotic/antimycotic (Sigma-Aldrich, St Louis, MO), and 15 ng/mL retinoic acid (Sigma-Aldrich, St Louis, MO) was added to the basal compartment. ALI media was changed every two days and ALI conditions were maintained for 3 weeks prior to use.

Next-generation sequencing

Viral genomic RNA was extracted from nasal swabs collected at 1, 2, and 5 dpi or 1, 3, and 6 dpc and BALF samples using the MagMax-96 AI/ND viral RNA isolation kit (ThermoFisher Scientific, Waltham, MA) according to manufacturer's instructions. After extraction, HA and NA segments were amplified using specific primers **(S4.1 Table)** and the SuperScript III One-Step PCR System (ThermoFisher Scientific, Waltham, MA) according to manufacturer's instructions in duplicates. Duplicate PCR products from both HA and NA PCRs from the same sample were pooled in equal volumes and cleaned with 0.45X Agencourt AMPure XP Magnetic Beads (Beckman Coulter, Brea, CA, USA) according to manufacturer's instructions. Clean PCR product concentration was measured using the Qubit dsDNA HS assay kit (ThermoFisher Scientific, Waltham, MA) on a Qubit 3.0 fluorometer (ThermoFisher Scientific, Waltham, MA) and normalized to 0.2 ng/mL. Sequencing libraries were prepared with the Nextera XT DNA library preparation kit (Illumina, San Diego, CA, USA). Indexed libraries were cleaned with 0.7X Agencourt AMPure XP Magnetic Beads and samples size distribution was analyzed using the Agilent Bioanalyzer 2100 DNA-HS assay (Agilent, Santa Clara, CA, USA). Libraries were then pooled, denatured, and further diluted to 10 pM. Finally, samples were sequenced using a MiSeq Reagent Kit V2, 300 cycles (Illumina, San Diego, CA, USA).

Variant analysis

Analyses of FLUAV variants were performed as previously described [358, 359]. Briefly, sequencing adapters were removed using Cutadapt (version 3.4) and then

mapped back to their respective reference sequence using option *mem* from BWA (version 0.7.17) [360]. Read-pairing errors that may have been introduced by the alignment were corrected using option *fixmate,* and secondary and unmapped reads were removed. The resulting bam file was used by LoFreq [361] following practices outlined in the Genome Analysis Toolkit [362] to identify non-consensus variants. Only variants with a frequency of 0.01 (1%) and coverage equal to or above 100 were used. Synonymous and nonsynonymous mutations were identified using SNPdat (version v1.0.5) [363]. The output from SNPdat was inputted into RStudio (R version 4.1.2) for visualization. Variants with a frequency equal to or above 0.5 (50%) were considered major variants.

Diversity analysis

Nucleotide diversity p was calculated using the pN (nonsynonymous) to pS (synonymous) ratio statistics determined using SNPGenie [364] for estimation of nucleotide diversity from next-generation sequencing. An arbitrary minimal variant frequency of 0.01 was set for p determination.

Amino acid temporal frequency analysis

55,590 human origin and 15,514 swine origin N2 sequences from H3N2 FLUAVS from 1992 to 2022 were obtained from GISAID [365]. Duplicated sequences were discarded, and samples were aligned using Clustal Omega version 1.2.2 [366]. Alignments were exported and amino acid frequency at position 93 and 113 was assessed using Geneious version 2024.0.2.

NA homology model

FLUAV NA sialidase domains were modelled using the SWISS-MODEL server (https://swissmodel.expasy.org/) [367]. hVIC/11 NA model was made using A/Tanzania/205/2010 as template (PDB accession code: 4GZO [188]) while A/Moscow/10/1999 (PDB accession code: 8DWB [368]) was used to generate the sOH/04 NA 3D structure. NA structures were visually inspected using PyMOL 3.0 and model quality was assessed using PROCHECK [369].

Growth kinetics

MDCK, A549, and PK15 cells were seeded in 6 well-plates and incubated at 37°C in a humidified incubator with 5% CO_2 until an 80% confluency before use. Cells were infected at a MOI of 0.01 for 1 h at 37°C. After incubation, cells were washed three times with PBS and supplemented with fresh Opti-MEM containing 1 mg/ml TPCK-treated trypsin. Timepoints were collected at 0, 12, 24, 48, and 72 hpi and viral titers were determined by RT-qPCR. HAE and differentiated swine tracheal cells were infected by adding 200 mL of virus in the respective ALI media into the apical compartment and incubated for 1 h at 37°C. After incubation, cells were washed 5 times with PBS. Timepoints were collected at 0, 12, 24, 48, and 72 hpi by adding 200 mL of PBS onto the cells and incubating them at 37°C for 15 min. Viral titers were determined as described above.

Neuraminidase activity and thermostability

Neuraminidase sialidase activity was evaluated using the whole virus as previously described [294] or purified recombinant NA (rNA). Briefly, viruses were diluted in reaction buffer (32.5 mM 2-(N-morpholino)ethanesulfonic acid -MES-, 2 mM $CaCl_2$ -unless stated otherwise-, pH 6.5) and incubated at 37°C for 30 min. To evaluate purified recombinant proteins, samples were normalized to 50 ng for all of the assays described below. After incubation, 100 mM 2′-(4-Methylumbelliferyl)-α-D-N-acetylneuraminic acid sodium salt hydrate (MUNANA, Sigma-Aldrich, St Louis, MO) was added and reactions were incubated for 60 min at 37°C. Fluorescence was measured every 60 seconds at excitation and emission wavelengths of 360 nm and 460 nm, respectively, using a Synergy HTX Multi-Mode Microplate Reader (Agilent BioTek, Santa Clara, CA).

NA thermostability was assessed by incubating equal amounts of each virus at 33, 37, 40, 43, 46, 49, 52, 55, 58, 61, and 64°C for 10 min. After incubation, viruses' NA sialidase activity was measured as mentioned above. NA relative activity was calculated as percentage of the activity at 33°C. T_{50} values were obtained by adjusting the curves to a non-linear dose-response logarithmic four parameters equation of the form:

$$\boldsymbol{Y = \frac{a + (a - b)}{1 + 10^{((log(T_{50} - X) * H)}}}$$

Where Y is NA activity in percentage, X is the log(temperature), a is the theoretical maximum activity, b is the theoretical minimum activity, and H is the Hill slope.

NA sialidase activity under different concentrations of Ca^{2+} was performed by adding 2, 1.5, 1, 0.5, or 0 mM $CaCl_2$ to the reaction buffer (32.5 mM MES, pH 6.5). Reaction

velocity was measured as described above, and relative NA activity was calculated by comparing the reaction velocity under each condition to the 37°C and 2 mM Ca^{2+} condition.

Enzyme kinetics

rNA samples were diluted in NA reaction buffer and incubated at 37°C for 30 min. Then 4-MU production over time was evaluated under different MUNANA concentrations (1.17, 2.34, 4.68, 9.37, 18.75, 37.5, 75, 150, 300, and 600 mM). Fluorescence was measured every 60 seconds at excitation and emission wavelengths of 360 nm and 460 nm and data was fitted to a simple saturation-kinetics equation (1) and k_{cat} was obtained by rearranging the Michaelis-Menten equation (2) assuming saturated substrate concentrations and a steady-state model:

$$\boldsymbol{v} = \frac{\boldsymbol{v_{max}}*[\boldsymbol{MUNANA}]}{\boldsymbol{K_M}+[\boldsymbol{MUNANA}]} \text{ (1)}$$

$$\boldsymbol{k_{cat}} = \frac{\boldsymbol{v_{max}}}{[\boldsymbol{E_t}]} \text{ (2)}$$

Red blood cells elusion assay

Viruses were normalized at 32 HA units (HAU) in Ca^{2+} -free PBS or PBS supplemented with 2mM Ca^{2+}. Normalized samples were then mixed with 0.5% turkey red blood cells and incubated at 4°C for 1 h. Then, samples were incubated at 37°C and aliquots were collected every 30 min until all HAU were lost. As a control, a duplicate sample supplemented with 1 mM oseltamivir (Sigma-Aldrich, St Louis, MO) was included. Elution due to NA activity was confirmed by incubation at 4°C for 1 h to allow re-agglutination.

NA protein expression and purification

NA ectodomain from hVIC/11 and sOH/04 was cloned into the pFastBac1 transfer vector. The stalk domain was replaced and fused in frame to a GG linker, a thrombin cleavage site, a tetramerization domain from the human vasodilator-stimulated phosphoprotein (VASP), 6x His tag, and a secretion signal as previously described [370]. D113A and G93N/N93G mutations were introduced as described above. Cloned pFastBac1 plasmids were then used to generate the recombinant bacmids by transforming DH10Bac competent cells (ThermoFisher Scientific, Waltham, MA), and insert transposition was confirmed by colony PCR using M13 primers **(S4.1 Table)**. Bacmids were purified by alkaline lysis and used to rescue recombinant baculoviruses in Sf9 cells according to the Bac-to-Bac system manual (ThermoFisher Scientific, Waltham, MA).

NA proteins were produced by infecting High Five cells at an MOI of 10. When cells reached an 80% mortality (~72 hpi), the supernatant was cleared by centrifugation at 3,000 rpm. NA constructs were purified from clarified supernatant by immobilized metal affinity chromatography (IMAC) using the HisPur Ni-NTA Spin purification kit (ThermoFisher Scientific, Waltham, MA) according to the manufacturer's instructions and eluted in elution buffer containing 137 mM NaCl, 2.7 mM KCl, 10 mM Na_2HPO_4, 1.8 mM KH_2PO_4, and 300 mM imidazole. Subsequently, eluted NAs were further purified by size exclusion chromatography using a Superdex-200 (Sigma-Aldrich, St Louis, MO) column with a running buffer composed of 20 mM Tris-HCl, 50 mM NaCl, pH 8.00. NA activity was monitored for each fraction. Finally, purified samples were digested using the Thrombin CleanCleave Kit (Sigma-Aldrich, St Louis, MO) according

to the manufacturer's instructions, and digestion products were passed through a Superdex-200 column.

SDS-PAGE and western blot

Protein concentration was determined using the Pierce BCA Protein Assay kit (ThermoFisher Scientific, Waltham, MA) according to the manufacturer's instructions. 100 ng of either cleaved or non-cleaved NA constructs were boiled for 5 min and resolved by SDS-PAGE using a Mini-Protean TGX Stain-Free Precast Gel (Bio-Rad, Hercules, CA). For total protein imagining, gels were then fixed with 40% ethanol and 10% acetic acid in water for 1 h. Then samples were sensitized for 1 minute with 0.02% $Na_2S_2O_3$ and incubated for 20 min with staining solution (0.1% $AgNO_3$ and 0.02% formaldehyde in water). Finally, gels were developed by incubating them in 3% $NaCO_3$ and 0.05% formaldehyde in water. Gels used for western blot were transferred to a TransBlot Turbo Mini Nitrocellulose membrane and blocked for 2 h in blocking buffer (5% BSA in PBS) at room temperature. After incubation, membranes were washed two times with T-PBS (0.05% Tween-20 in PBS, washing buffer) and incubated for 1 h with an anti-His tag primary antibody (Sigma-Aldrich, St Louis, MO). Membranes were then washed three times (5 min each) and incubated for 1 h with a secondary HRP-conjugated anti-mouse antibody in a 1:1,000 dilution in T-PBS. Finally, membranes were washed 5 times and then developed with the SuperSignal West Femto Maximun Sensibility Substrate kit (ThermoFisher Scientific, Waltham, MA). Membranes were imaged using a ChemiDoc MP Imaging System (Bio-Rad, Hercules, CA).

Plaque assay

MDCK cells were seeded at a density of 10^5 cells/cm^2 and incubated at 37°C in a humidified incubator with 5% CO_2 in Opti-MEM (Life Technologies, Carlsbad, CA, USA) until a 100% confluency before use. The day of infection, culture media was discarded, cells were washed three times with Ca^{2+} -free DMEM (ThermoFisher Scientific, Waltham, MA), and were infected using 10-fold serial dilution of each virus in Ca^{2+} -free DMEM. After 1 h incubation at 37°C, unbound virus was removed by washing cells three times with Ca^{2+} -free DMEM and then cells were supplemented with DMEM containing 2mM L-glutamine, 0.3% bovine serum albumin (BSA, ThermoFisher Scientific, Waltham, MA), 1% antibiotic/antimycotic, 1 mM sodium pyruvate (ThermoFisher Scientific, Waltham, MA), 0.8% avicel, and variable concentrations of Ca^{2+} chloride (2, 0.5 or 0 mM, Sigma-Aldrich, St Louis, MO). Infections were incubated for 72 h at 37°C. Finally, cells were fixed with 37% formaldehyde (Sigma-Aldrich, St Louis, MO) and stained for 15 min with 0.5% crystal violet in 20% methanol.

Viral particle release

Viral particles release was evaluated as previously described [35]. Briefly, MDCK cells were infected at a multiplicity of infection (MOI) of 0.1 and were incubated at 4°C for 30 min. Unbound virus was removed by washing cells three times with PBS and cells were supplemented with fresh Opti-MEM containing 1 mg/ml TPCK-treated trypsin (Worthington Biochemicals, Lakewood, NJ). At 5 hpi, media was discarded and 3 mL of DMEM containing 2mM L-glutamine, 0.3% BSA, 1% antibiotic/antimycotic, 1 mM sodium pyruvate, 1 mg/ml TPCK-treated trypsin, and variable concentrations of $CaCl_2$

was added. Starting at 6 hpi, 100 mL was collected from each condition every 1 h until 12 hpi, and HA titers were measured using 50 mL of sample and 50 mL 0.5% turkey red blood cells.

Aerosol infection

MDCK and PK15 cells were seeded and incubated as described above until 80% confluence was reached. Viruses were diluted in Ca^{2+} -free DMEM supplemented with 2mM L-glutamine (Sigma-Aldrich, St Louis, MO), 0.3% BSA (Sigma-Aldrich, St Louis, MO), and 1% antibiotic/antimycotic (Sigma-Aldrich, St Louis, MO) and used at an MOI of 0.01. For infections performed with Ca^{2+}, 2 mM $CaCl_2$ was added to the infection media. A total of 6 mL of inoculum was aerosolized using the Aeroneb Lab Neubilizer (Small VMD; Kent Scientific, CT, USA) with an expected particle size of 2.5-4 mm. Aerosol was passed through an exposure chamber at a flow rate of 0.1 mL/min. Cells were exposed for 15 min at room temperature, followed by a 5-min purge. Infections were incubated for 1 h at 37°C and then washed three times with PBS. Finally, Opti-MEM media supplemented with 1 mg/ml TPCK-treated trypsin was added, and time points were collected at 0, 12, 24, 48, and 72 hpi.

Statistical analysis

All statistical analyses were performed using GraphPad Prism 10. All data is presented as the mean ± standard error of the mean of at least three independent

experiments unless stated otherwise in the figure legend. *P* values were obtained by ordinary one-way ANOVA with Tukey's multiple comparison test.

Results

hVIC/11-A138S infects the lower respiratory tract and increases affinity following transmission to contact animals.

To evaluate adaptation to a new host, 3-week-old pigs (seeders) were inoculated intratracheally and intranasally with $3x10^6$ $TCID_{50}$/pig of either hVIC/11-A138S [258] or the control swine-adapted virus sOH/04 [371]. Two days post-inoculation (dpi), three naïve pigs (contact 1, C1) were introduced with the inoculated pigs (seeders, Fig 4.1). At 5 dpi, seeders were euthanized, and three new naïve pigs (contact 2, C2) were introduced to the C1 pigs. This cycle was repeated for a total of four contact groups. Nasal swabs were collected throughout the study, and lung samples and bronchoalveolar lavage fluid (BALF) were collected during necropsies at 5 dpi.

Virus titration of nasal swabs confirmed successful transmission of hVIC/11-A138S among all contacts, peaking at approximately 10^5 $TCID_{50}$eq/mL by 3 dpi (Fig 4.1a). The sOH/04 virus control was also detected in all contacts (Fig 4.1b), albeit at higher titers (approximately 10^6 $TCID_{50}$eq/mL). The hVIC/11-A138S virus infected the trachea of all seeders and contact pigs (Fig 4.1c). Virus titers in the right cranial, left cranial, and right caudal lobes (Fig 4.1d, e, and f) increased significantly by contact 4 (approximately 10^4 $TCID_{50}$eq/mL) compared to the seeder and/or C1 pigs. While no significant differences were observed in the left caudal lobe or BALF samples (Fig 4.1g, 1h), although a trend towards higher titers was noted in contact 4 pigs' BALF samples. Notably, the virus initially failed to infect the accessory lobe of seeders and C1 pigs (Fig 4.1i), with titers below the limit of detection ($<10^1$ $TCID_{50}$eq/mL) but was detected in subsequent contacts from C2 onward (approximately 10^3 $TCID_{50}$eq/mL). These findings suggest that hVIC/11-A138S replication efficiency in the lower respiratory tract increased with each transmission, ultimately infecting all lung lobes by the study's conclusion.

Serial transmission of hVIC/11-A138S in pigs selected for a mutant with a single amino acid mutation in NA.

After sequencing analysis of nasal swabs and BALF samples, only minor variants (present in less than 50% of sequences) were observed in the hVIC/11-A138S HA segment (**Fig 4.2a)**, and none of these variants became fixed or were transmitted. However, a mutation in the NA, D113A, was detected in contact 2 pigs as a major variant (present in more than 50% of sequences) that eventually became prevalent and was transmitted to all contact 3 and 4 pigs **(Fig 4.2b)**. No positive selection was observed in the HA segment **(S4.1a Fig)**, while signs of positive selection were observed for the NA segment in contacts 1 and 2 sequences **(S4.1b Fig)**. After acquisition of the D113A amino acid change, no positive selection was observed in this segment. No major changes were observed in the sOH/04 control virus surface gene segments **(S4.2 Fig).** Using the NA crystal structure information that closely matches the sequence of hVIC/11 NA (A/Tanzania/205/2010, **S4.3 Fig**) revealed that the amino acid at position 113 located within the low-affinity Ca^{2+}-binding pocket of the NA is essential for Ca^{2+} binding **(Fig 4.2c)**. The polar side chain of aspartic acid (D) at this position is predicted to stabilize a water molecule via a hydrogen bond (one per monomer) in the symmetry axis **(Fig 4.2c, top panel)**, facilitating the coordination of a single Ca^{2+} ion. When D113 is mutated to alanine (A), this polar interaction is lost, likely impairing Ca^{2+} binding **(Fig 4.2c, bottom panel)**. Notably, temporal analysis of residue frequency reveals that D113 and A113 were similarly prevalent in swine H3N2 viruses until the early 2000s **(Fig 4.2d)**. However, D113 has since become predominant, reaching 100% frequency by 2022.

The adaptive N2 D113A mutation enhances NA stability under Ca^{2+}- depleted conditions and reduces Ca^{2+} requirements for NA sialidase activity.

Prior research with the N1 NA from the 2009 pandemic H1N1 virus demonstrated that disrupting Ca^{2+} binding in the low-affinity Ca^{2+}-binding pocket impairs virus replication *in vitro* [35]. To investigate this effect in viruses with the N2 NA D113A mutation, two recombinant viruses were produced carrying this mutation, with or without the HA A138S mutation (hVIC/11-A138S/D113A and hVIC/11-D113A, respectively). Replication kinetics of these viruses were evaluated in various human and swine cell lines **(Fig 4.3a)** and compared to hVIC/11-A138S, hVIC/11, and sOH/04 viruses. The N2 NA D113A mutation did not affect virus replication in MDCK, PK15, A549, or differentiated human airway epithelial (HAE) cells **(Fig 4.3a)**. Neither hVIC/11 nor hVIC/11-D113A replicated in differentiated primary swine airway epithelial (SAE) cells, unlike hVIC/11-A138S and hVIC/11-A138S/D113A, confirming the advantage conferred by the HA A138S mutation for replication in swine cells [258].

Disruption of Ca^{2+} binding in the symmetry axis may negatively impact NA stability [35]. To investigate this, the temperature at which 50% of NA activity is lost (T50) was established for NAs containing either D113 or A113 **(Fig 4.3b)** in the absence or in the presence of physiological Ca^{2+} concentration (2 mM). The assay revealed that introducing the D113A mutation decreased the T50 of NA proteins at 2 mM Ca^{2+} (hVIC/11-D113A, 52.03°C; hVIC/11-A138S/D113A, 51.19°C) compared to control viruses with wild-type (WT) NA (hVIC/11, hVIC/11-A138S, and sOH/04), which exhibited T50 values averaging 5°C higher **(Fig 4.3b, left panel; Fig 4.3c)**. In the absence of Ca^{2+}, all T50 values decreased compared to those at 2 mM Ca^{2+} **(Fig 4.3b,**

right panel). Remarkably, viruses carrying D113A**,** particularly hVIC/11-A138S/D113A (T50 44.44°C), showed significantly higher values than the WT hVIC/11 (T50 39.51°C) in the absence of Ca^{2+}, behaving more like the sOH/04 strain (T50 43.40°C) **(Fig 4.3c)**. These findings suggest that disrupting Ca^{2+} binding in the symmetry axis decreases NA thermostability at 2 mM Ca^{2+} but stabilizes the protein in the absence of Ca^{2+}.

The sialidase activity in the absence of Ca^{2+}as a percentage of the activity at 2 mM Ca^{2+} measured at 37°C **(Fig 4.3d, S4.4 Fig)** revealed that mutant viruses containing the A113 mutation (hVIC/11-A138S/D113A and hVIC/11-D113A) maintained high levels of NA activity under Ca^{2+}-depleted conditions similar to sOH/04 (39.14%). These mutants also exhibited enhanced activity compared to hVIC/11, which was nearly inactivated in the absence of Ca^{2+} (3.81%). Notably, the virus with both the A138S mutation in the HA and the D113A mutation in the NA retained the highest levels of sialidase activity in the absence of Ca^{2+}, exceeding 50%.

Ca^{2+} binding within the low-affinity Ca^{2+} binding pocket is influenced by amino acid 93.

Analysis of the predicted hVIC/11 and sOH/04 and NA structures (sOH/04 model derived from homology with A/Moscow/10/1999 (H3N2), (**S4.5 Fig**), suggests that the latter likely does not bind Ca^{2+} in this pocket despite having D113 **(Fig 4.4a)**. This model indicates altered interactions between sOH/04 NA and water molecules within the symmetry axis compared to hVIC/11, disrupting Ca^{2+} coordination. This is attributed to a reduced f angle between G111 and G112 in sOH/04's NA (159.3°) relative to hVIC/11's NA (176.8°), which repositions the D113 side chain **(S4.6a Fig)**. To verify this, the

D113A mutation was introduced into sOH/04 NA (sOH/04-D113A). This did not alter NA activity at varying Ca^{2+} concentrations compared to WT sOH/04 NA **(Fig 4.4b)** nor affected thermal stability at 2 mM or 0 mM Ca^{2+}, further supporting the notion that sOH/04 NA does not bind Ca^{2+} in this pocket **(Fig 4.4c)**. Sequence alignment revealed an important difference at position 93, in which asparagine (N) is present in sOH/04 NA and glycine (G) in hVIC/11 NA **(S4.6b Fig)**. Temporal analysis of human and swine H3N2 NA sequences (1992-2023) showed residue 93 in human isolates shifting from K (lysine) to N to D by the early 2010s, with G becoming prevalent as of 2023 **(S4.6c and d Fig)**. Swine H3N2 viruses initially carried K93, gradually replaced by N93 **(S4.6c Fig, bottom panel)**, which became fixed by the 2010s and has not changed ever since. This change at position 93 appears to affect subsequent residues, potentially explaining the altered f angle between G111 and G112 **(S4.6e Fig).** This is further supported by comparing NA activity of swine- and human-origin H3N2 FLUAVs at different Ca^{2+} concentrations. Human H3N2 FLUAVs have exhibited reduced tolerance to Ca^{2+} depletion since the early 2000s **(S4.7a-i Fig)**, contrasting with swine H3N2 strains, which largely retain high sialidase activity in the absence of Ca^{2+} **(S4.7j-q Fig).** This effect on NA activity seems to be associated with the residue at position 93 **(S4.2 Table)**.

To investigate the influence of residue 93 on NA physiochemical properties, the N93 substitution was introduced into the hVIC/11 NA, generating both hVIC/11-G93N and hVIC/11-A138S/G93N mutants. While the presence of Ca^{2+} led to a slight decrease in T50 compared to the unmodified hVIC/11, the absence of Ca^{2+} revealed a distinct pattern. In this Ca^{2+}-depleted environment, the hVIC/11-G93N mutant exhibited a

significant increase in T50 (47.22°C) compared to both hVIC/11 and hVIC/11-A138S/G93N **(Fig 4.4d and e)**. The impact of residue 93 was not limited to the hVIC/11 NA. The N93G mutation in sOH/04-N93G NA also affected stability, resulting in reduced T50 values under both Ca^{2+}-replete and Ca^{2+}-depleted conditions compared to the sOH/04 control virus. These observations underscore the consistent influence of residue 93 on NA stability, regardless of the specific NA mutant or Ca^{2+} availability. Interestingly, this influence on stability extended to NA activity. The hVIC/11 mutants containing N93 demonstrated a remarkable 6-fold increase in sialidase activity compared to hVIC/11 in the absence of Ca^{2+} (hVIC/11-G93N, 22.14%; hVIC/11-A138S/G93N, 31.02%; hVIC/11, 3.8%; **Fig 4.4f and g**). Conversely, the G93 mutation in sOH/04-N93G led to a reduction in activity compared to the sOH/04 control. These contrasting effects suggest that residue 93 not only modulates stability but also plays a crucial role in fine-tuning NA activity in response to Ca^{2+} availability.

Amino acids 93 and 113 differentially modulate neuraminidase enzymatic parameters.

The impact of amino acids 93 and 113 on NA enzymatic activity was investigated by analyzing substrate affinity and sialic acid hydrolysis velocity. Recombinant NA constructs (rNA) consisting of the NA ectodomain fused to various tags (**Fig 4.5a)** were expressed, purified, and evaluated for purity **(S4.8a Fig)**. Upon cleavage of the introduced domains (**Fig 4.5b**, **S4.8b and c Fig)**, the released NA ectodomain was used to assess reaction velocity using MUNANA. While D113A did not affect the velocity of hVIC/11-D113A rNA, it reduced the reaction velocity in sOH/04-D113A rNA **(Fig 4.5c and d)**. Conversely, introduction of N93 increased the reaction velocity five-fold in

hVIC/11-G93N rNA compared to hVIC/11 rNA (0.017 mM/min and 0.0033 mM/min, respectively), while G93 decreased the velocity of sOH/04-N93G rNA compared to sOH/04 rNA (0.011 mM/min versus 0.036 mM/min, **Fig 4.5d)**. These findings suggest that residues 93 and 113, although not part of the active site, influence NA catalytic properties.

Further analysis of substrate affinity using the Michaelis constant (K_M) revealed that neither G93N nor D113A affected the K_M of hVIC/11-G93N rNA or hVIC/11-D113A rNA compared to hVIC/11 rNA **(Fig 4.5e and f)**. Conversely, both sOH/04-N93G rNA and sOH/04-D113A rNA exhibited increased K_M, indicating reduced substrate affinity compared to sOH/04 rNA. Assessment of maximum velocity (V_{max}) showed that hVIC/11-G93N rNA displayed the highest V_{max} among hVIC/11-derived NAs, while hVIC/11-D113A rNA had a reduced V_{max} compared to hVIC/11 rNA **(Fig 4.5G)**. Similarly, G93 and A113 reduced V_{max} in sOH/04 NA. These results suggest that residue N93 enhances the reaction maximum velocity, whereas A113 decreases V_{max}. Calculation of the turnover number (k_{cat}) further supported these observations **(S4.8d and e Fig, S4.3 Table)**, demonstrating increased k_{cat} in hVIC/11-G93N rNA and decreased k_{cat} in hVIC/11-D113A rNA compared to hVIC/11 rNA. The opposite effect was observed in sOH/04 NA mutants. Additionally, the specificity constant (k_{cat}/K_M) was increased in hVIC/11-G93N rNA and reduced in both hVIC/11-D113A rNA and sOH/04 NA mutants **(S4.8f Fig, S4.3 Table)**. This analysis indicates that N93 modulates catalytic power by affecting interactions after enzyme-substrate complex formation, while A113 decreases the catalytic efficiency noted as a reduced k_{cat}/K_M.

Examination of T50 values linked the increased activity of hVIC/11-G93N rNA to enhanced thermostability, whereas hVIC/11-D113A rNA exhibited reduced T50 under 2 mM Ca^{2+} **(Fig 4.5h and i)**. Similar trends were observed in sOH/04 NA mutants. Notably, both hVIC/11-G93N rNA and hVIC/11-D113A rNA displayed increased stability and activity at 0 mM Ca^{2+} compared to hVIC/11 rNA **(Fig 4.5j, S4.9 Fig)**, whereas sOH/04r-N93G rNA showed reduced activity. The correlation between NA thermostability and activity under Ca^{2+}-depleted conditions was confirmed by a Pearson test **(Fig 4.5k)**. Thus, residues 93 and 113 differentially modulate NA catalytic power by influencing the tetramer stability. Notably, amino acids destabilizing Ca^{2+} binding in the low-affinity Ca^{2+}-binding pocket, prevalent in recent swine H3N2 viruses, enhance NA stability and activity in Ca^{2+}-depleted conditions.

Amino acids 93 and 113 impact the HA/NA balance.

To assess the impact of NA mutations at positions 93 and 113 on the balance between HA and NA activities, a red blood cell elution assay was performed, measuring the time required for a 50% reduction in HA titers under NA activity **(Fig 4.6a-f)**. At 2 mM Ca^{2+}, hVIC/11-A138S exhibited the fastest elution, while mutations at either residue 93 (G to N) or 113 (D to A) increased elution time. Similarly, sOH/04-N93G showed slower elution kinetics. In the absence of Ca^{2+}, hVIC/11 and hVIC/11-A138S displayed a marked increase in elution time, which was reversed by introducing either N93 or A113. Conversely, sOH/04-N93G maintained a slower elution time even without Ca^{2+}. No elution was observed in the presence of oseltamivir, confirming assay functionality. These differences were statistically significant, indicating that residues 93 and 113

modulate viral elution time, reflecting alterations in the HA/NA balance. The observed changes in elution kinetics suggest that these residues influence the functional interplay between HA and NA, highlighting their role in optimizing viral fitness and adaptation.

Disruption of Ca^{2+} binding in the low-affinity site reduces Ca^{2+} dependency for viral replication and aerosol infection.

Given the importance of NA activity in the FLUAV replication cycle, the biological significance of the D113A mutation in hVIC/11-A138S/D113A was assessed through plaque assays under varying Ca^{2+} concentrations **(S4.10 Fig)**. At both 2 mM and 0 mM Ca^{2+}, hVIC/11-D113A and hVIC/11-A138S/D113A produced the largest plaques **(Fig 4.7a)**. sOH/04 plaques were larger than those of hVIC/11. The hVIC/11 strain exhibited strong Ca^{2+} dependency, with plaque size reduced by nearly 60% in the absence of Ca^{2+} compared to the 2 mM condition **(Fig 4.7b)**. Conversely, Ca^{2+} concentration had less impact on hVIC/11-A138S, hVIC/11-D113A, and sOH/04, with plaque size reductions around ≤40%. The hVIC/11-A138S/D113A mutant showed minimal plaque size reduction under 0 mM Ca^{2+}.

Viral particle release, predominantly mediated by NA activity, was also evaluated. The hVIC/11 and hVIC/11-A138S viruses showed decreased release in the absence of Ca^{2+} **(Fig 4.7c)**. In contrast, sOH/04 and hVIC/11-A138S/D113A, particularly the latter, exhibited negligible differences among tested Ca^{2+} concentrations. These findings suggest that impairing Ca^{2+} binding in the symmetry axis reduces optimal Ca^{2+} requirements for growth, likely due to enhanced NA activity under low Ca^{2+} conditions, leading to improved viral release. This effect was particularly pronounced in aerosol infectivity

assessments. The hVIC/11 and hVIC/11-A138S viruses showed delayed kinetics in MDCK cells when aerosolized in Ca^{2+}-free media, reaching lower titers at 72 hpi compared to Ca^{2+}-supplemented media **(Fig 4.7d)**. In contrast, hVIC/11-D113A, hVIC/11-A138S/D113A, and sOH/04 showed no differences under both conditions, indicating that viruses with Ca^{2+}-destabilizing mutations are less sensitive to Ca^{2+} concentrations during aerosolization. This phenomenon was even more evident in swine-origin PK15 cells. While no significant differences were observed among viruses upon direct inoculation **(Fig 4.3a)**, aerosol delivery revealed a striking contrast **(Fig 4.7e)**. The hVIC/11 strain exhibited minimal replication with Ca^{2+}-supplemented media and no detectable titers without Ca^{2+}. However, hVIC/11-D113A and hVIC/11-A138S/D113A replicated similarly under both conditions, although hVIC/11-D113A titers were ultimately lower. These results demonstrate that viruses with reduced Ca^{2+} requirements for replication (hVIC/11-A138S/D113A, hVIC/11-D113A, and sOH/04) exhibit reduced dependency on this ion during aerosol infection, with minimal differences in growth kinetics between Ca^{2+} conditions.

Discussion

The NA protein plays a critical role in FLUAV infection, facilitating viral movement through respiratory mucus and promoting viral release by hydrolyzing sialic acid [126, 372]. NA activity is strongly dependent on Ca^{2+} [373, 374], with some subtypes binding up to two Ca^{2+} ions per monomer plus a central ion in the symmetry axis [375]. However, most NA subtypes, including N2, primarily bind two Ca^{2+} ions in distinct high- and low-affinity binding pockets [181]. The high-affinity pocket is

consistently occupied and essential for NA catalysis, as Ca^{2+} binding repositions the catalytic residues for proper sialic acid binding [189]. Recent studies have revealed that the low-affinity pocket's role in modulating N1 NA activity by stabilizing the tetramer is crucial for optimal function [35, 376]. Findings in this report extend this understanding to N2 FLUAV, demonstrating that the low-affinity pocket also modulates N2 NA catalytic properties, potentially serving as a mechanism for regulating the balance between HA and NA activities, and providing a mechanism to modulate NA enzymatic properties without mutating the catalytic residues.

Leveraging a swine sustained transmission model and a mutant virus with mutation in HA (hVIC/11-A138S) previously detected after transmission of a human strain to pigs [27], a potentially compensatory mutation was identified, D113A, in the N2 NA low-affinity Ca^{2+}-binding pocket. N2 crystal structures of prototypical human strains revealed that residue 113 is the sole amino acid involved in Ca^{2+} binding at this site in this FLUAV subtype. This contrasts with N1 NAs, where residues K111, D113, and particularly Y170 play key roles in Ca^{2+} binding in the symmetry axis [35]. Unlike the 2009 pandemic H1N1 virus, acquisition of D113A by the human-origin N2 NA did not affect viral replication in the cell lines tested. Furthermore, the failure of hVIC/11-D113A to replicate in swine respiratory cells suggests that this mutation alone does not enhance replication in pigs **(Fig 4.3a)**, underscoring the critical role of the HA mutation A138S in adaptation to pigs due to increased affinity for swine cells [33, 377, 378]. These findings argue for a sequential adaptation model for human FLUAVs in pigs: initial acquisition of adaptive HA mutations to facilitate binding to swine cells, followed by NA mutations, such as D113A, to restore HA/NA balance disrupted by the prior HA

changes. This model emphasizes the dynamic interplay between HA and NA in viral adaptation to new hosts, highlighting the importance of compensatory mechanisms in maintaining viral fitness during host transitions.

While the D113A mutation did not affect viral fitness *in vitro* in this study, it did impact NA thermostability, which is closely linked to Ca^{2+} binding [379]. The importance of Ca^{2+} in enhancing N2 activity has been previously established [380]. Notably, the D113A mutation increased N2 thermostability under Ca^{2+}-depleted conditions, accompanied by an increase in its activity. Interestingly, swine-adapted N2 NAs inherently exhibit higher sialidase activity in the absence of Ca^{2+}, contrasting with human viruses. The observation of stronger Ca^{2+} dependency in human-origin N2 aligns with previous reports [35, 380]. The high activity of swine FLUAVs under Ca^{2+}-depleted conditions, despite carrying D113, suggests a lack of Ca^{2+} binding in the low-affinity Ca^{2+}-binding pocket. Modeling of sOH/04 NA confirmed this hypothesis, revealing that Ca^{2+} binding is prevented by repositioning of water molecules in the symmetry axis due to a change in D113 side chain location **(Fig 4.4)**. Further support for this mechanism was provided by the introduction of D113A in sOH/04 NA, which resulted in no changes in thermostability compared to sOH/04 **(Fig 4.4 and 4.5)**, confirming that the virus does not bind Ca^{2+} when either amino acid is present. This suggests that the presence of D113, even without direct Ca^{2+} interaction, contributes to the overall stability of the NA structure, highlighting the complex interplay between amino acid residues and Ca^{2+} binding in modulating NA function.

Residue 93 appears to be under different selective pressures in humans and swine. While K93 and N93 were present in both human and swine FLUAV in the early 1990s,

human isolates rapidly transitioned to D93 and G93, while N93 was retained in swine H3N2 FLUAVs. Protein modeling suggests that the N93 residue destabilizes the interaction of D113 with Ca^{2+}, thereby preventing Ca^{2+} binding. Interestingly, a similar mechanism has been reported for residue 106 in N1 NAs, which also modulates Ca^{2+} binding in the low-affinity Ca^{2+}-binding pocket [35]. This suggests a conserved mechanism between N1 and N2 NAs for modulating Ca^{2+} binding at this site, involving specific residues distant from the pocket itself. The presence of this mechanism across subtypes may be due to the high conservation of the low-affinity Ca^{2+}-binding pocket. Such a mechanism could prevent modifications near the Ca^{2+}-binding pocket that might interfere with tetramer formation, as NA oligomerization is driven by both the head and transmembrane domains [381]. However, further investigation is needed to confirm this hypothesis.

Residues 93 and 113 exert similar effects on Ca^{2+} binding in both human and swine N2 FLUAVs, yet their impact on NA catalytic properties differs. Notably, while D113A minimally affects sOH/04 rNA V_{max}, it reduces hVIC/11 rNA velocity. Conversely, N93 drastically increases reaction velocity within the hVIC/11 rNA. Additionally, sOH/04 rNA displays higher substrate affinity than hVIC/11 rNA, with no difference observed in hVIC/11-G93N rNA, suggesting that that N93 seems to influence steps occurring after the enzyme-substrate complex formation, while A113 decreases the catalytic efficiency of the enzyme. This aligns with previous reports of Ca^{2+} modulating reaction velocity by favoring enzyme-substrate interactions [382, 383], although the mechanism remains unclear. The D113A mutation impacts substrate binding, decreasing affinity regardless of NA backbone, potentially explaining its rarity in natural isolates due

to disruption of HA/NA balance [384, 385]. Previous work has demonstrated that hVIC/11-A138S exhibits higher affinity for α2,6-SA, indirectly enhancing NA activity [258]. Based on this, it was hypothesized that the D113A mutation emerged *in vivo* to compensate for the A138S change in HA and regulate NA activity. Indeed, data revealed a higher elution rate for hVIC/11-A138S compared to hVIC/11 and sOH/04, which was restored to sOH/04-like levels upon introduction of D113A **(Fig 4.6)**. These findings underscore the intricate interplay between HA and NA, whereby mutations in one protein can necessitate compensatory changes in the other to maintain optimal viral fitness. Notably, A113 negatively impacted tetramer stability in the hVIC/11 NA backbone, suggesting that other residues might prevent this effect in sOH/04 NA. These two amino acids thus represent distinct mechanisms for N2 NA modulation of activity during host jumps, explaining the tendency of human viruses to bind Ca^{2+} in the low-affinity Ca^{2+}-binding pocket, while swine H3N2 viruses do not. This suggests a novel role for Ca^{2+} in FLUAV host range, where viral changes may modulate sialidase activity without modifying the conserved catalytic pocket, by influencing Ca^{2+} binding in the low-affinity site. This is supported by previous studies on the 2009 pandemic H1N1 NA crystal structures [35]. Early isolates, upon jumping from pigs to humans carried V106 that destabilized the tetramer at 2 mM Ca^{2+}, but it was quickly replaced by I106 that enhanced N1 NA thermostability and activity under this condition. While that study did not directly link FLUAV host range and Ca^{2+} binding, the order of events aligns with the hypothesis that HA changes are required early in host adaptation, followed by NA activity modification through altered substrate affinity or reaction velocity, depending on specific residues involved in Ca^{2+} binding. However, this process seems to cycle between binding

and not binding calcium in the symmetry axis [35], which could represent a mechanism to compensate for changes in the HA, as the D113A mutation alone cannot grant replication in swine airway cells **(Fig 4.3)**.

Increased NA thermostability conferred by the D113A substitution reduced the Ca^{2+} requirement for optimal virus replication to levels comparable to sOH/04. This is likely due to enhanced NA activity under low Ca^{2+} conditions, leading to more efficient virus release from infected cells [35]. The increased stability of A113-containing mutants also resulted in more efficient aerosol infection of MDCK cells when the inoculum was aerosolized in the absence of Ca^{2+}, similar to sOH/04. This effect was even more pronounced in PK15 cells, with limited to no replication observed for hVIC/11 and hVIC/11-D113A. Notably, hVIC/11-A138S/D113A demonstrated similar replication kinetics to sOH/04 across all tested conditions. These findings suggest that the absence of Ca^{2+} in the symmetry axis enhances aerosol infection under Ca^{2+}-depleted conditions, potentially reflecting differences in mucus composition between human and swine, which could select for viruses with distinct aerosol stability. This could explain why hVIC/11 fails to transmit in pigs [258] and only replicates in the upper respiratory tract of swine (»37°C) but not in the lungs [27, 258] (»39°C) as the NA of hVIC/11 is almost inactivated in absence of calcium at 39°C **(Fig 4.3, 4.4, and 4.5)**. However, further investigation is needed to confirm this hypothesis.

Overall, this study demonstrates distinct Ca^{2+} binding profiles in human and swine H3N2 FLUAVs, with swine strains lacking Ca^{2+} binding in the low-affinity pocket. This difference leads to enhanced stability and activity of swine-origin FLUAVs under Ca^{2+}-depleted conditions compared to human-origin FLUAVs, which are almost inactivated

under this condition. Residue 93 modulates Ca^{2+} binding and significantly impacts reaction velocity by affecting steps after SA binding in the NA catalytic pocket. This difference in reaction velocity and Ca^{2+} binding suggests a role of Ca^{2+} in the host range of FLUAV, with those from humans requiring higher Ca^{2+} concentrations for replication while their swine counterparts have reduced Ca^{2+} requirements. A better understanding of the biochemical differences of the upper and lower respiratory tract of humans and pigs is needed to better understand the potential applications of these results into control measures in the field. Nonetheless, the identification of residues N93 and A113 with apparent enhanced fitness in swine could be used in surveillance to detect circulating human H3N2 viruses carrying these swine-adaptative mutations that could potentially jump from humans to pigs. These results provide new insights into the mechanisms utilized by FLUAV to regulate NA activity during host adaptation and the potential effects on the HA/NA balance.

Figures and Tables

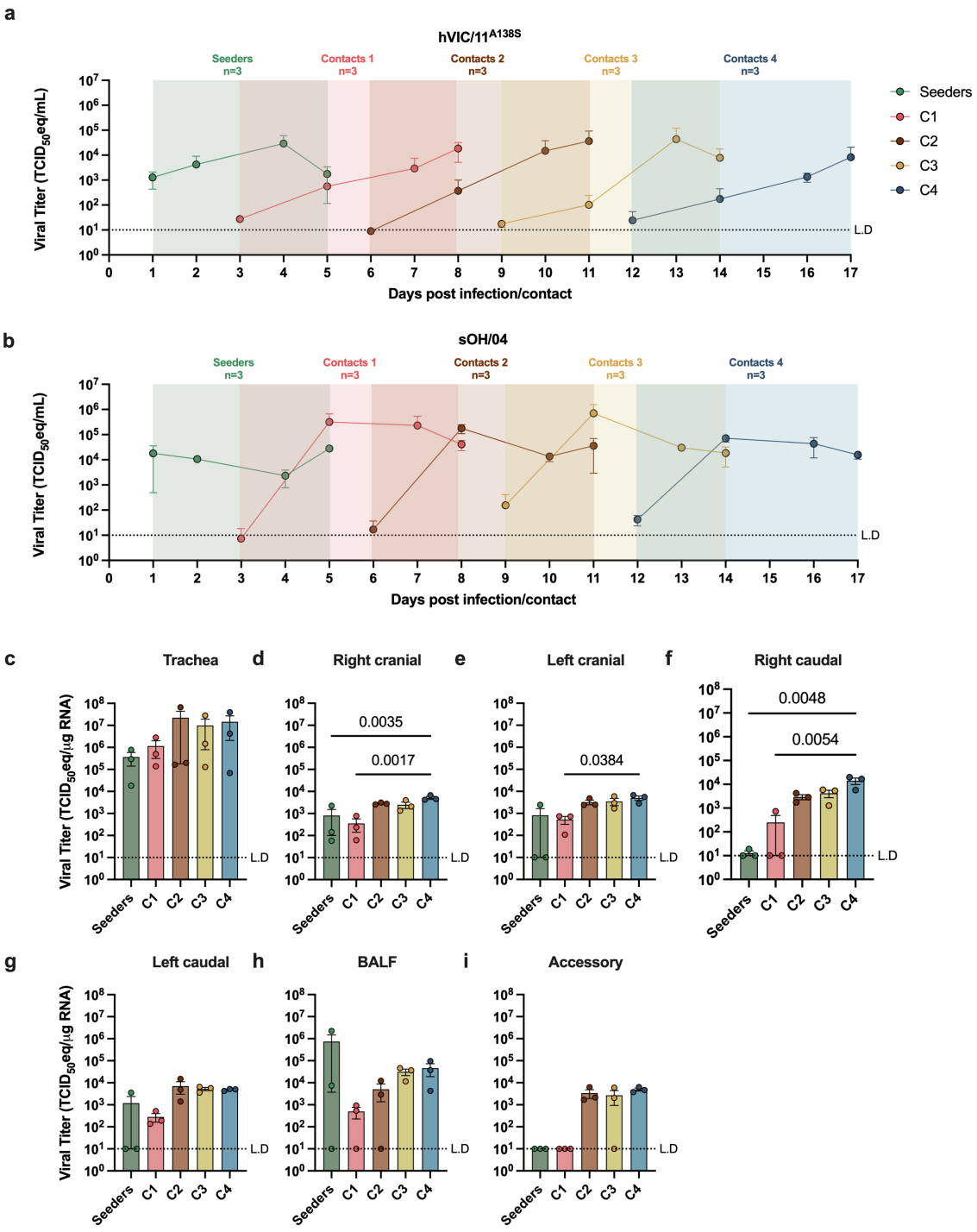
a
hVIC/11A138S
Seeders n=3
Contacts 1 n=3
Contacts 2 n=3
Contacts 3 n=3
Contacts 4 n=3
Seeders
C1
C2
C3
C4
Viral Titer (TCID50eq/mL)
L.D
Days post infection/contact
b
sOH/04
Seeders n=3
Contacts 1 n=3
Contacts 2 n=3
Contacts 3 n=3
Contacts 4 n=3
Viral Titer (TCID50eq/mL)
L.D
Days post infection/contact
c
Trachea
d
Right cranial
0.0035
0.0017
e
Left cranial
0.0384
f
Right caudal
0.0048
0.0054
Viral Titer (TCID50eq/μg RNA)
L.D
Seeders
C1
C2
C3
C4
g
Left caudal
h
BALF
i
Accessory

Figure 4.1. hVIC/11-A138S replicates in pigs' upper and lower respiratory tract with increasing lung involvement by the fourth round of sustained transmission. Pigs were challenged with either sOH/04 or hVIC/11-A138S and nasal swabs were collected. Lung tissue and BALF samples were collected during necropsies at 5 dpi/6 dpc. **(a)** Viral titers in nasal swab samples (n=3 per contact) from pigs challenged with hVIC/11-A138S. **(b)** Viral titers in nasal swab samples (n=3 per contact) from pigs challenged with sOH/04. Viral titers from the trachea **(c)**, right cranial lobe **(d)**, left cranial lobe **(e)**, right caudal lobe **(f)**, left caudal lobe **(g)**, bronchoalveolar lavage fluid (BALF) **(h)**, and the accessory lobe **(i)** from hVIC/11-A138S-infected pigs were determined by RT-qPCR and normalizing all samples to 1mg total RNA. All statistical analyses were performed by two-way ANOVA. Values represent the mean $\pm$ SD.

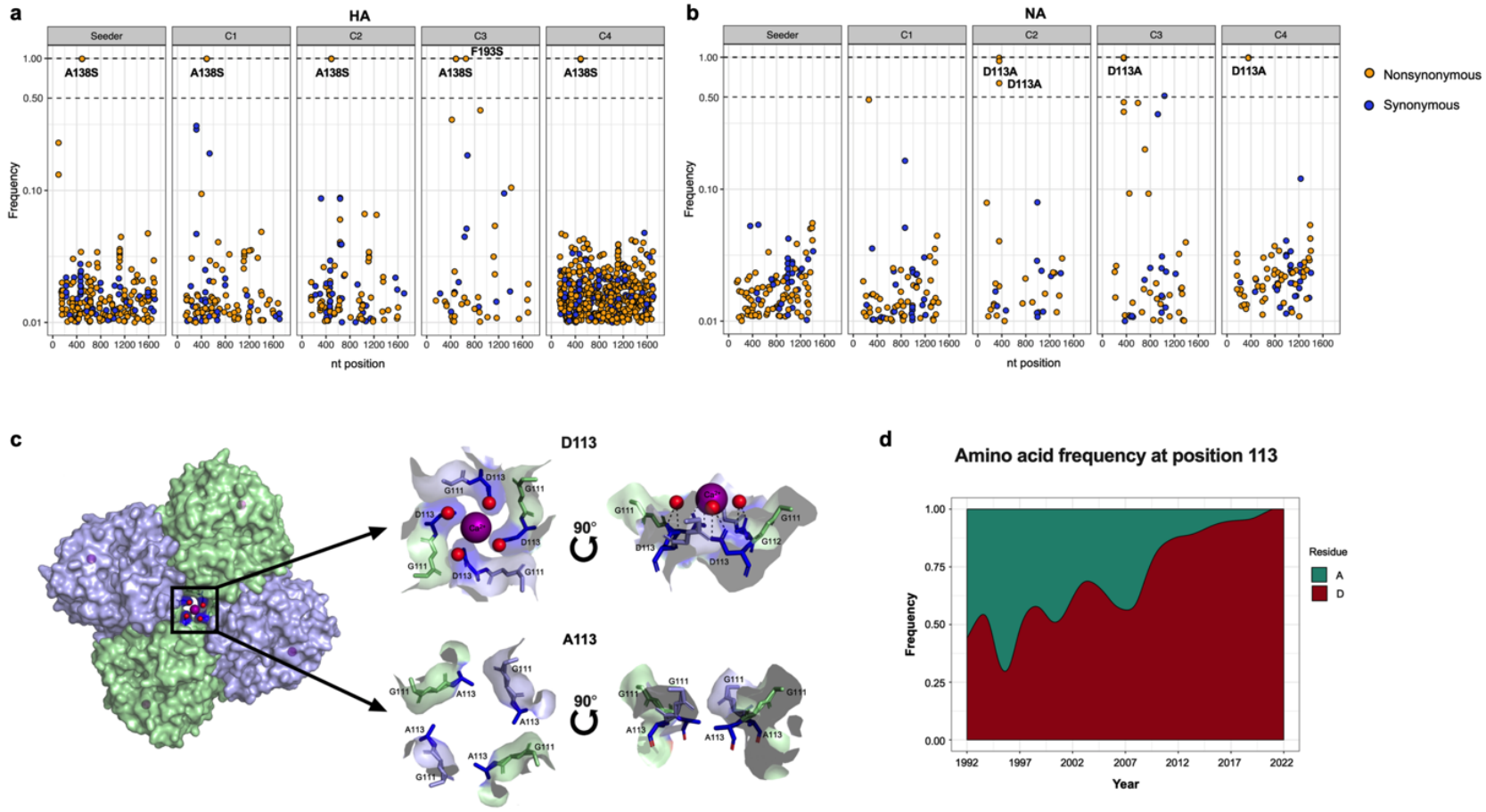
a
HA
Seeder
C1
C2
C3
C4
A138S
F193S
Frequency
nt position
b
NA
D113A
Nonsynonymous
Synonymous
c
D113
A113
90°
d
Amino acid frequency at position 113
Residue
A
D
Year

Figure 4.2. *In vivo* transmission of hVIC/11-A138S selects for a single mutation in the NA segment. Nasal swab samples collected at days 1, 2, and 5 dpi and 1, 3, and 6 dpc were sequenced and viral variants across the HA **(a)** and NA **(b)** segments were identified and their abundance was quantified. Mutations were classified as nonsynonymous (yellow) or synonymous (blue). A minimum threshold for major variants was arbitrarily set at 0.5 and the fixation point at a frequency of 1 (dashed lines). The frequency is expressed in the y axis a log from 0 to 1. The data represents the diversity observed in three pigs per contact. **(c)** hVIC/11 NA tetramer protein model showing the low-affinity Ca^{2+} -binding pocket when D113 and A113 are present. Residue 113 is shown in blue, water molecules in red, and the Ca^{2+} atom in purple. Images were made using PyMOL. **(d)** Frequency of A113 in swine H3N2 isolated reported from 1992 to 2023. Sequences were obtained from GISAID and aligned with Clustal Omega. Alanine (A) is shown in green while aspartic acid (D) is presented in red.

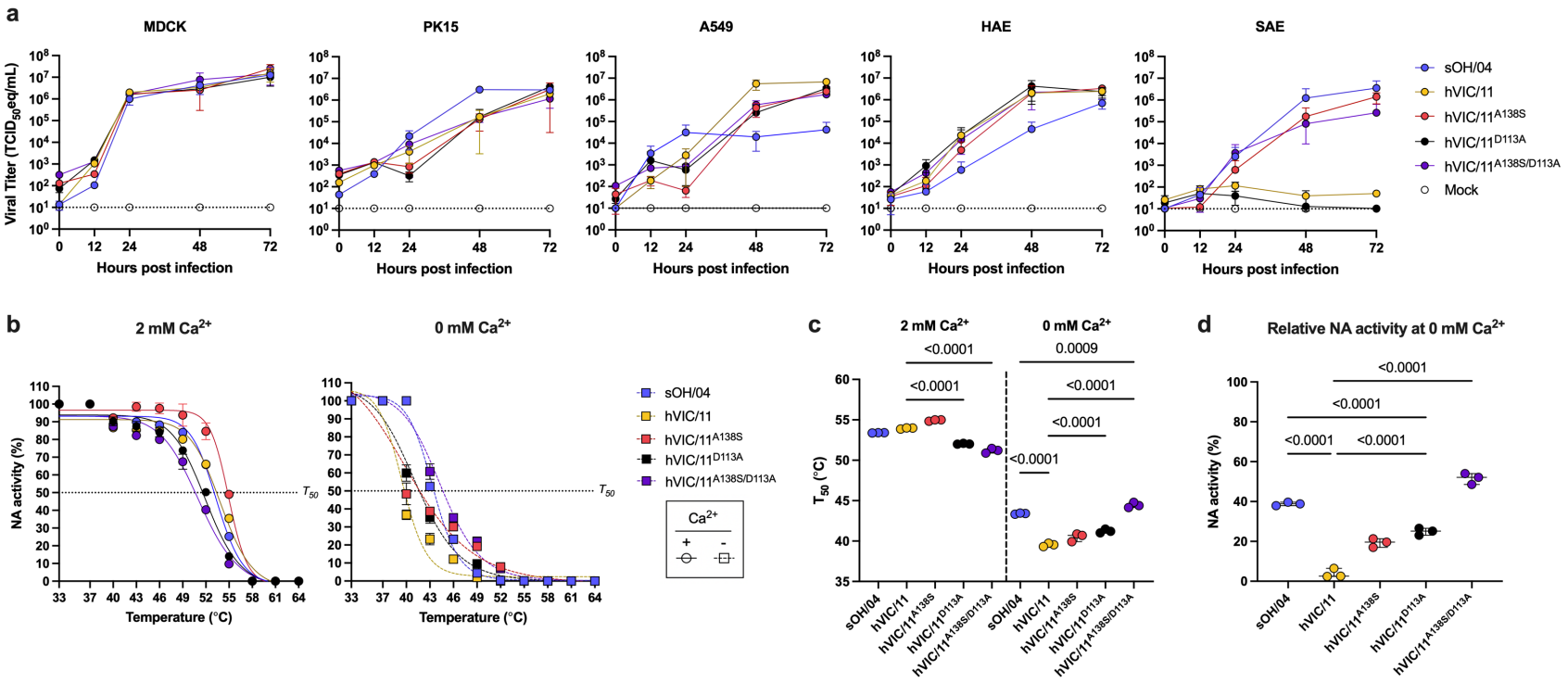
a
MDCK
PK15
A549
HAE
SAE
Viral Titer (TCID50eq/mL)
Hours post infection
sOH/04
hVIC/11
hVIC/11A138S
hVIC/11D113A
hVIC/11A138S/D113A
Mock
b
2 mM Ca2+
0 mM Ca2+
NA activity (%)
Temperature (°C)
T50
Ca2+
+
-
c
2 mM Ca2+
0 mM Ca2+
T50 (°C)
<0.0001
0.0009
d
Relative NA activity at 0 mM Ca2+
NA activity (%)

Figure 4.3. The NA D113A mutation provides no advantage for virus growth in SAE cells but increases NA thermostability and sialidase activity under Ca^{2+} -depleted conditions. (a) Viral growth kinetics of sOH/04 (blue), hVIC/11 (yellow), hVIC/11-A138S(red), hVIC/11-D113A (black), and hVIC/11-A138S/D113A (purple) in MDCK, PK15, A549, HAE, and SAE cells infected at an MOI of 0.01. A mock control (white) is included. Values represent the mean ± SD of three independent experiments. p values were obtained by ordinary one-way ANOVA. **b)** Thermostability of sOH/04 (blue), hVIC/11 (yellow), hVIC/11-A138S(red), hVIC/11-D113A (black), hVIC/11-A138S/D113A (purple) NAs determined in presence (O, solid line) or absence (□, dashed line) of Ca^{2+}. **c)** T50 was obtained by adjusting the data to a dose-response variable slope nonlinear fit and values are shown as the mean of three independent experiments. p values were obtained by ordinary one-way ANOVA. **d)** NA sialidase activity of sOH/04 (blue), hVIC/11 (yellow), hVIC/11-A138S(red), hVIC/11-D113A (black), and hVIC/11-A138S/D113A (purple) at 0 mM Ca^{2+} expressed as a percentage of the reaction velocity compared to 37°C, 2 mM Ca^{2+} (100% NA activity). Values represent the mean ± SD of three independent experiments. p values were obtained by ordinary one-way ANOVA.

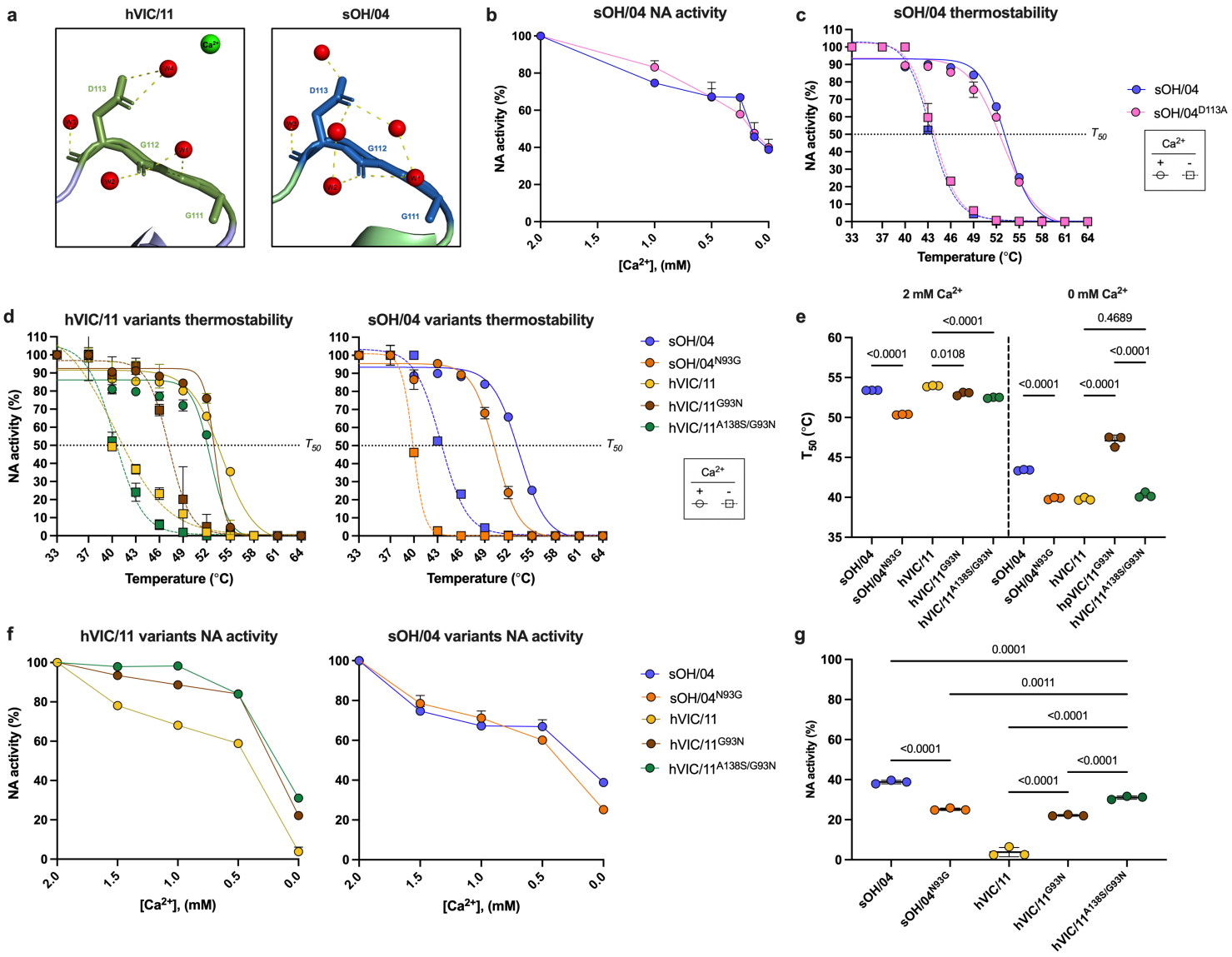
a
hVIC/11
sOH/04
D113
G112
G111
W1
W2
W3
Ca2+
b
sOH/04 NA activity
NA activity (%)
[Ca2+], (mM)
c
sOH/04 thermostability
NA activity (%)
Temperature (°C)
T50
sOH/04
sOH/04D113A
Ca2+
d
hVIC/11 variants thermostability
sOH/04 variants thermostability
NA activity (%)
Temperature (°C)
T50
sOH/04
sOH/04N93G
hVIC/11
hVIC/11G93N
hVIC/11A138S/G93N
Ca2+
e
2 mM Ca2+
0 mM Ca2+
T50 (°C)
<0.0001
0.0108
0.4689
sOH/04
sOH/04N93G
hVIC/11
hVIC/11G93N
hpVIC/11G93N
hVIC/11A138S/G93N
f
hVIC/11 variants NA activity
sOH/04 variants NA activity
NA activity (%)
[Ca2+], (mM)
sOH/04
sOH/04N93G
hVIC/11
hVIC/11G93N
hVIC/11A138S/G93N
g
NA activity (%)
0.0001
0.0011
<0.0001

Figure 4.4. Amino acid 93 modulates Ca^{2+} binding in the low-affinity Ca^{2+} -binding pocket and stabilizes the NA tetramer under Ca^{2+}-depleted conditions. (a) NA protein model showing the interaction of G111, G112, and D113 with water molecules in the symmetry axis of the NA tetramer of hVIC/11 (right panel, green) and sOH/04 (left panel, blue). Water molecules are shown in red, and Ca^{2+} is shown in green. **(b)** sOH/04 (blue) and sOH/04-D113A (pink) NA sialidase activity at different Ca^{2+} concentrations. Values are presented as a percentage of the reaction velocity measured at 37°C and 2 mM Ca^{2+} which was set at 100%. Values represent the mean ± SD of three independent experiments. **(c)** sOH/04 and sOH/04-D113A thermostability assessed at 2 mM Ca^{2+} (O, solid line) or 0 mM Ca^{2+} (□, dashed line). T50 was determined by adjusting the data of three independent experiments to a dose-response variable slope nonlinear fit. **(d)** Left panel: Thermostability of hVIC/11 (yellow), hVIC/11-G93N (brown), and hVIC/11-A138S/G93N (green). Right panel: Thermostability of sOH/04 (blue) and sOH/04-N93G (orange). Thermostability profiles were determined at 2 mM Ca^{2+} (O, solid line) or 0 mM Ca^{2+} (□, dashed line). Values represent the mean ± SD of three independent experiments. **(e)** T50 values were determined by adjusting the data of three independent experiments to a dose-response variable slope nonlinear fit. p values were obtained by ordinary one-way ANOVA. **(f)** Left panel: NA sialidase activity of hVIC/11 (yellow), hVIC/11-G93N (brown), and hVIC/11-A138S/G93N (green) at different Ca^{2+} concentrations. Right panel: NA sialidase activity of sOH/04 (blue) and sOH/04-N93G (orange) at different Ca^{2+} concentrations. Values are expressed as the reaction velocity percentage compared to the velocity at 37°C and 2 mM Ca^{2+} (100% activity). Values represent the mean ± SD of three independent experiments. **(g)** NA activity at 0 mM Ca^{2+} of hVIC/11 and sO/04 NA 93 mutants. p values were obtained by ordinary one-way ANOVA.

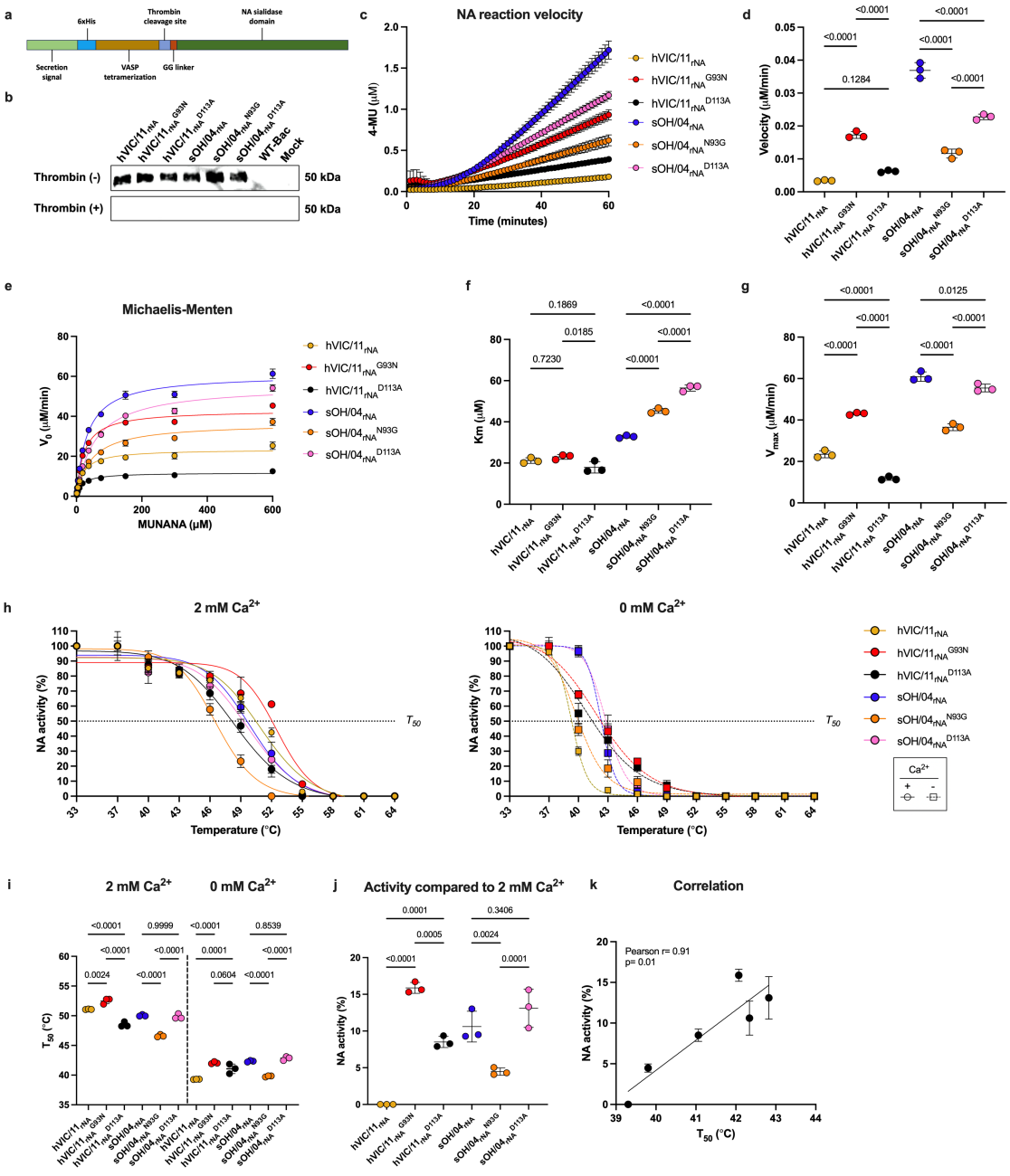
a
6xHis
Thrombin cleavage site
NA sialidase domain
Secretion signal
VASP tetramerization
GG linker
b
Thrombin (-)
Thrombin (+)
50 kDa
50 kDa
WT-Bac
Mock
c
NA reaction velocity
4-MU (µM)
Time (minutes)
d
Velocity (µM/min)
e
Michaelis-Menten
V0 (µM/min)
MUNANA (µM)
f
Km (µM)
g
Vmax (µM/min)
h
2 mM Ca2+
0 mM Ca2+
NA activity (%)
Temperature (°C)
T50
Ca2+
i
2 mM Ca2+
0 mM Ca2+
T50 (°C)
j
Activity compared to 2 mM Ca2+
NA activity (%)
k
Correlation
Pearson r= 0.91
p= 0.01
T50 (°C)

Figure 4.5. Amino acids 93 and 113 distinctly affect NA kinetic parameters and promote NA activity under Ca^{2+}-depleted conditions by stabilizing the NA tetramer. **(a)** Schematic representation of NA constructs expressed in High 5 cells infected with recombinant baculoviruses. **(b)** Western blot of recombinant NAs detected using an anti-His antibody before and after thrombin digestion to release the NA ectodomain. **(c)** NA enzymatic reaction velocity using recombinant proteins from hVIC/11rNA (yellow), hVIC/11-G93N rNA (brown), hVIC/11-D113A rNA (black), sOH/04 rNA (blue), sOH/04-N93G rNA (orange), and sOH/04-D113A rNA (pink). Samples were normalized to 50 ng of protein and velocity was measured as 4-MU production over 60 min. Values represent the mean $\pm$ SD of three independent experiments. **(d)** rNA reaction velocity of hVIC/11 rNA (yellow), hVIC/11-G93N rNA (red), hVIC/11-D113A rNA (black), sOH/04 rNA (blue), sOH/04-N93G rNA (orange), and sOH/04-D113A rNA (pink). p values were obtained by ordinary one-way ANOVA. **(e)** Michaelis-Menten plot of rNA samples normalized to 50 ng of protein and incubated with variable MUNANA concentrations. Data was fitted to the Michaelis-Menten equation, and the K_M **(f)** and V_{max} **(g)** parameters. were obtained. p values were obtained by ordinary one-way ANOVA. **(h)** Thermostability profiles of rNA measured with (2 mM Ca^{2+}, O, solid line) or without (□, dashed line) Ca^{2+}. Values are presented as the mean $\pm$ SD of three independent experiments. **(i)** T50 values were obtained by fitting the data to a dose-response variable slope nonlinear fit. p values were obtained by ordinary one-way ANOVA. **(j)** rNA enzymatic activity at 37°C and 0 mM Ca^{2+}. p values were obtained by ordinary one-way ANOVA. **(k)** Pearson correlation test between rNA activity and T50 at 0 mM Ca^{2+}.

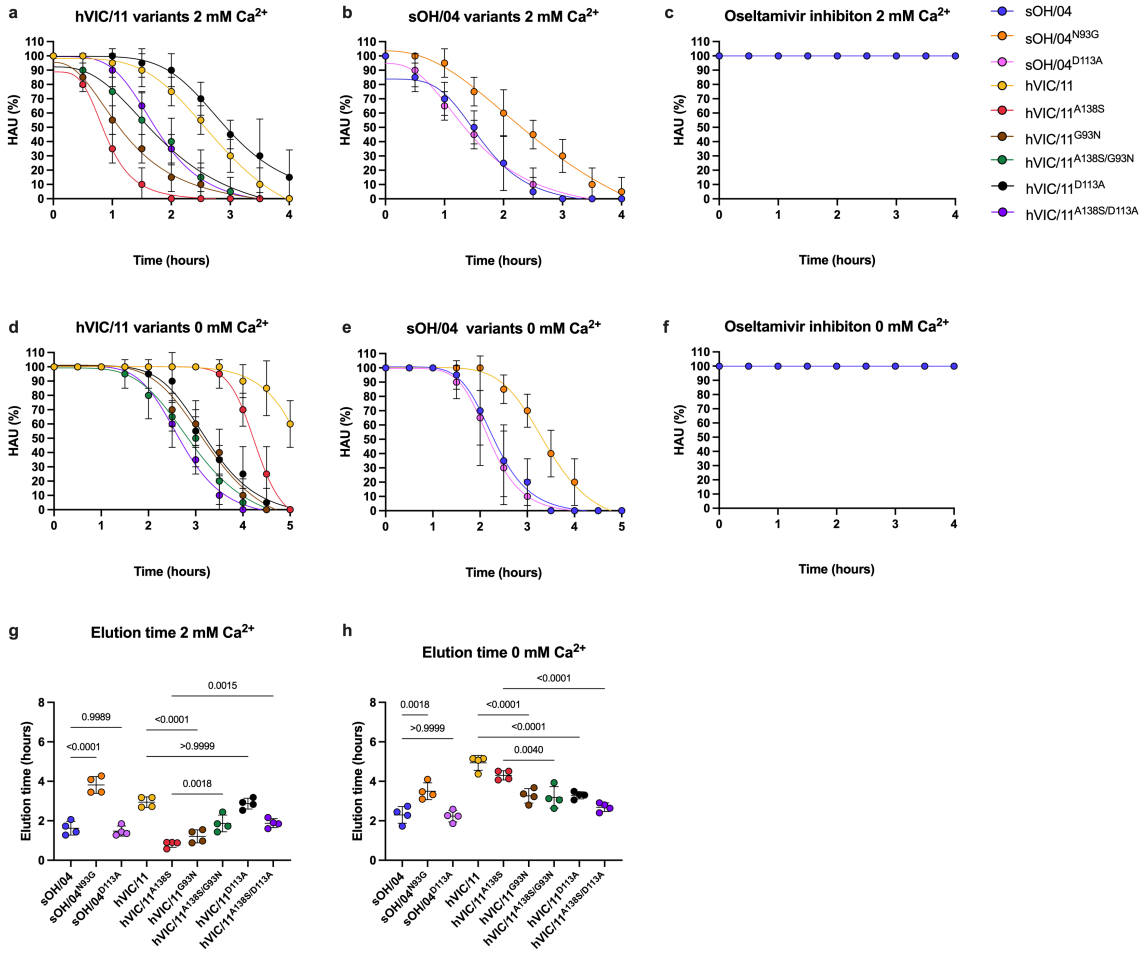
a
hVIC/11 variants 2 mM Ca2+
b
sOH/04 variants 2 mM Ca2+
c
Oseltamivir inhibiton 2 mM Ca2+
sOH/04
sOH/04N93G
sOH/04D113A
hVIC/11
hVIC/11A138S
hVIC/11G93N
hVIC/11A138S/G93N
hVIC/11D113A
hVIC/11A138S/D113A
d
hVIC/11 variants 0 mM Ca2+
e
sOH/04 variants 0 mM Ca2+
f
Oseltamivir inhibiton 0 mM Ca2+
HAU (%)
Time (hours)
g
Elution time 2 mM Ca2+
h
Elution time 0 mM Ca2+
Elution time (hours)
0.9989
<0.0001
<0.0001
>0.9999
0.0015
0.0018
0.0018
>0.9999
<0.0001
<0.0001
<0.0001
0.0040
sOH/04
sOH/04N93G
sOH/04D113A
hVIC/11
hVIC/11A138S
hVIC/11G93N
hVIC/11A138S/G93N
hVIC/11D113A
hVIC/11A138S/D113A

Figure 4.6. Amino acids 93 and 113 affect the HA/NA balance. Viruses were normalized to 32 HAU and incubated at 4°C for 1 h before incubation at 37°C for the indicated time. **(a)** Elution kinetics of hVIC/11 mutants at 2 mM Ca^{2+}. **(b)** Elution kinetics sOH/04 mutants at 2 mM Ca^{2+}. **(c)** Elution kinetics of hVIC/11 and sOH/04 mutants at 2 mM Ca^{2+} and 1 mM oseltamivir. **(d)** Elution kinetics of hVIC/11 mutants at 0 mM Ca^{2+}. **(e)** Elution kinetics sOH/04 mutants at 0 mM Ca^{2+}. **(f)** Elution kinetics of hVIC/11 and sOH/04 mutants at 0 mM Ca^{2+} and 1 mM oseltamivir. **(g)** Elution time of hVIC/11 and sOH/04 mutants at 2 mM Ca^{2+}. **(h)** Elution time of hVIC/11 and sOH/04 mutants at 0 mM Ca^{2+}. Values are presented as the mean ± SD of two independent experiments. p values were determined by one-way ANOVA with Tukey's multiple comparison test.

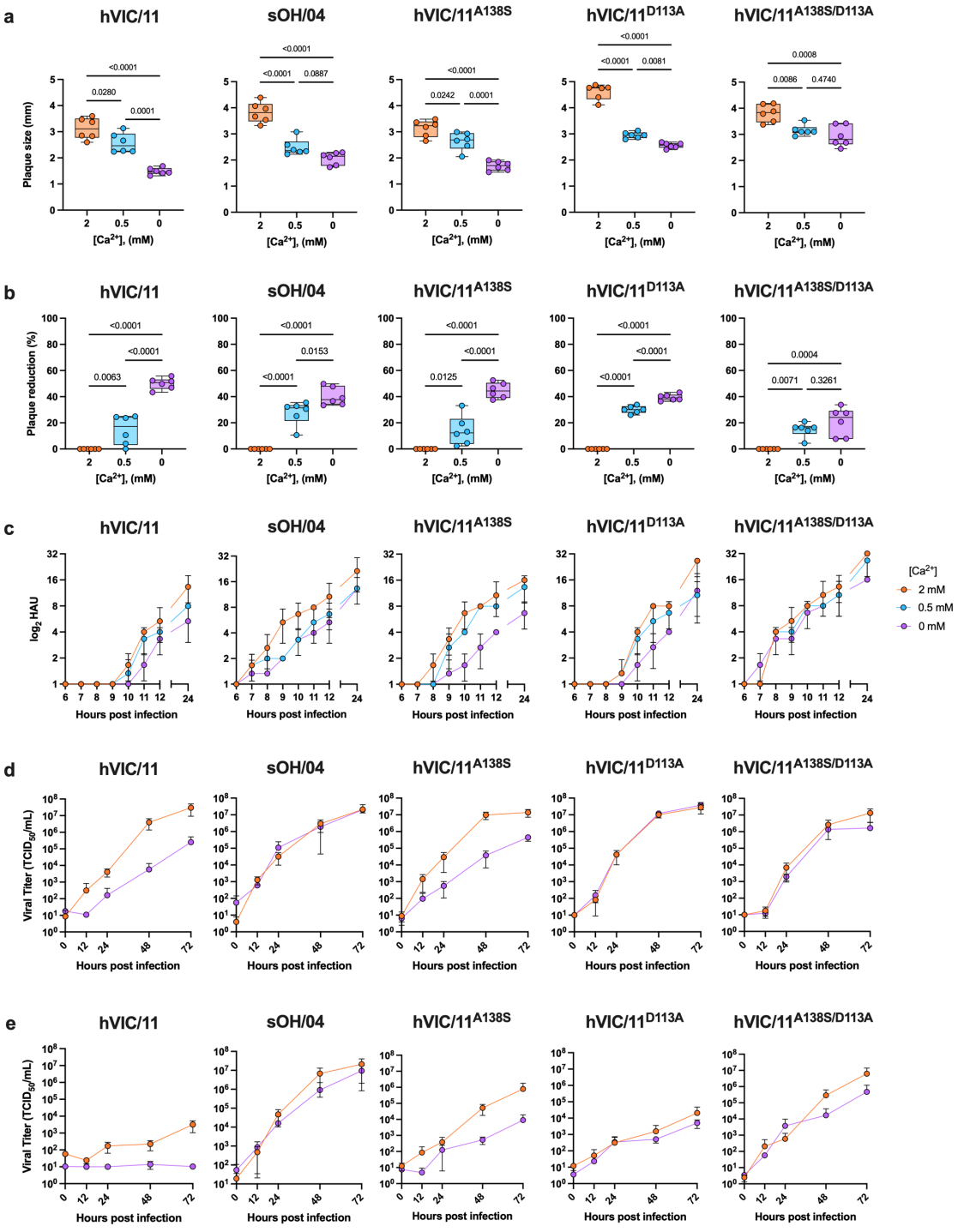
a
hVIC/11
sOH/04
hVIC/11A138S
hVIC/11D113A
hVIC/11A138S/D113A
Plaque size (mm)
<0.0001
0.0280
0.0001
<0.0001
<0.0001
0.0887
<0.0001
0.0242
0.0001
<0.0001
<0.0001
0.0081
0.0008
0.0086
0.4740
[Ca2+], (mM)
b
Plaque reduction (%)
<0.0001
<0.0001
0.0063
<0.0001
0.0153
<0.0001
<0.0001
0.0125
<0.0001
<0.0001
<0.0001
0.0004
0.0071
0.3261
c
log2 HAU
Hours post infection
[Ca2+]
2 mM
0.5 mM
0 mM
d
Viral Titer (TCID50/mL)
e

Figure 4.7. D113A decreases Ca^{2+} requirements for viral replication and enhances aerosol infection under Ca^{2+} -depleted conditions. (a) MDCK cells were infected with 10-fold dilutions of hVIC/11 NA mutants and the control sOH/04 virus in media containing 2 (orange), 0.5 (cyan), or 0 mM Ca^{2+} (purple). At 72 hpi plaque size diameter was measured for each condition. p values were obtained by ordinary one-way ANOVA. **(b)** Effect of Ca^{2+} concentration on plaque size represented as the percentage of the plaque diameter compared to the plaque size at 2 mM Ca^{2+} that was arbitrarily set to 100%. p values were obtained by ordinary one-way ANOVA. **(c)** Viral particle release assay showing the HA units in 50 mL of supernatant of MDCK cells infected with hVIC/11, sOH/04, hVIC/11-A138S, hVIC/11-D113A, and hVIC/11-A138S/D113A. Cells were infected at an MOI of 0.1 and at 5 hpi the media was replaced with fresh media containing the mentioned Ca^{2+} concentrations. Values represent the mean $\pm$ SD of three independent experiments. **(d)** Viral growth kinetics of hVIC/11, sOH/04, hVIC/11-A138S, hVIC/11-D113A, and hVIC/11-A138S/D113A in aerosol infected MDCK cells. Viruses were aerosolized with (orange) or without (purple) Ca^{2+} and viral titers were recorded at 0, 12, 24, 48, and 72 hpi. Values represent the mean $\pm$ SD of three independent experiments. **e)** Viral growth kinetics of hVIC/11, sOH/04, hVIC/11-A138S, hVIC/11-D113A, and hVIC/11-A138S/D113A in aerosol infected PK15 cells. Viruses were aerosolized with (orange) or without (purple) Ca^{2+} and viral titers were recorded at 0, 12, 24, 48, and 72 hpi. Values represent the mean $\pm$ SD of three independent experiments.

Table 4.1. Swine and human H3N2 viruses used in this study*.

Abbreviation	Strain	Surface segments
hVIC/11	rgA/Victoria/361/2011	hVIC/11 HA and NA
hVIC/11-A138S	rgA/Victoria/361/2011-A138	hVIC/11 HA A138S and NA
hVIC/11-D113A	rgA/Victoria/361/2011-D113A	hVIC/11 HA and NA D113A
hVIC/11-G93N	rgA/Victoria/361/2011-G93N	hVIC/11 HA and NA G93N
hVIC/11-A138S/D113A	rgA/Victoria/361/2011-A138S/D113A	hVIC/11 HA A138S and NA D113A
hVIC/11-A138S/G93N	rgA/Victoria/361/2011-A138S/G93N	hVIC/11 HA A138S and NA G93N
sOH/04	rgA/turkey/Ohio/313053/2004	sOH/04 HA and NA
sOH/04-D113A	rgA/turkey/Ohio/313053/2004-D113A	sOH/04 HA and NA D113A
sOH/04-N93G	rgA/turkey/Ohio/313053/2004-N93G	sOH/04 HA and NA N93G
HK/68	A/Hong Kong/1/1968	Wild type virus
VIC/75	A/Victoria/3/1975	Wild type virus
WU/95	A/Wuhan/359/1995	Wild type virus
MO/99	A/Moscow/10/1999	Wild type virus
FU/02	A/Fujian/411/2002	Wild type virus
WY/03	A/Wyoming/3/2003	Wild type virus
BR/07	A/Brisbane/10/2007	Wild type virus
VIC/11	A/Victoria/361/2011	Wild type virus
SW/13	A/Switzerland/2013	Wild type virus
TX/98	A/Swine/Texas/4199-2/1998	Wild type virus
CO/99	A/swine/Colorado/23619/1999	Wild type virus
OH/04	A/turkey/Ohio/313053/2004	Wild type virus
AR/08	A/swine/Argentina/CIP051-82/2008	Wild type virus
IL/11	A/swine/Illinois/A01201606/2011	Wild type virus
NY/11	A/swine/New York/A01104005/2011	Wild type virus
WY/13	A/swine/Wyoming/A01444562/2013	Wild type virus
MN/16	A/swine/Minnesota/A01678475/2016	Wild type virus

*rg backbone derived from sOH/04 triple reassortant FLUAV [371]

Supplementary material

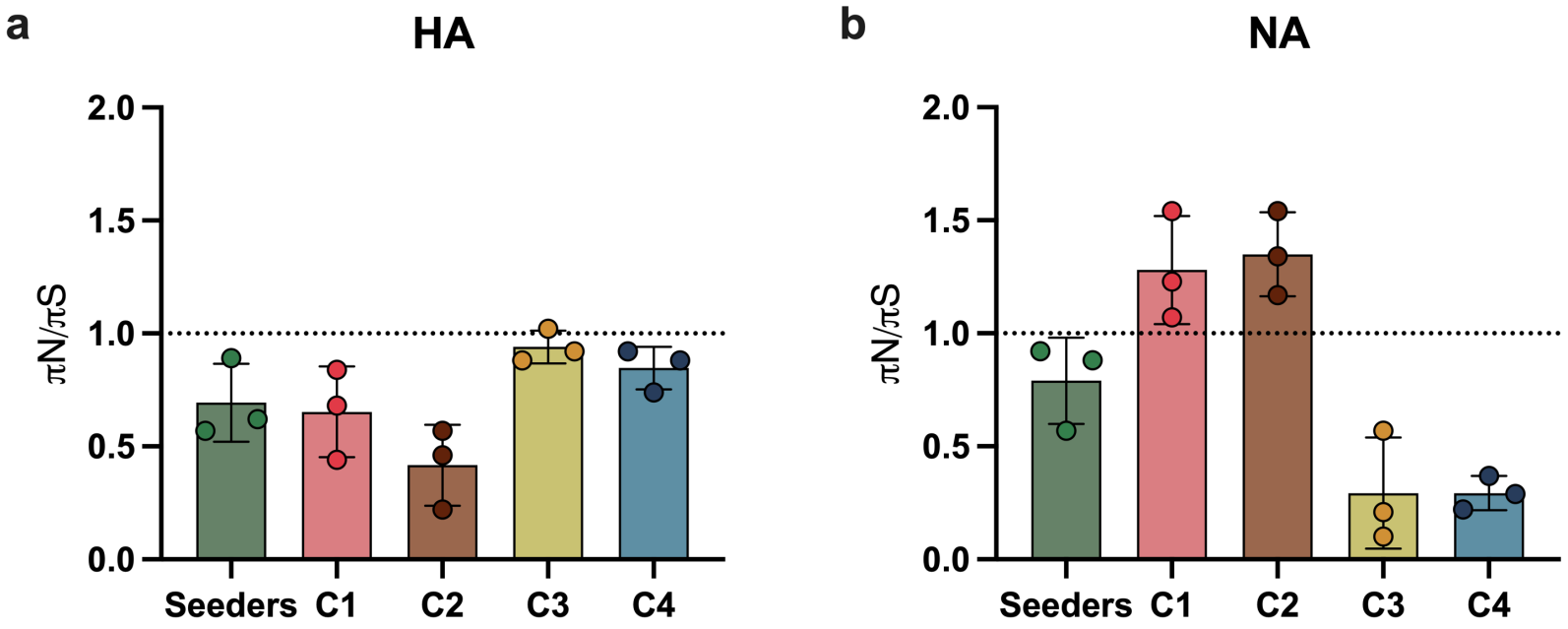

S4.1 Fig. Nucleotide diversity of the NA segment reveals signs of positive selection. Diversity was calculated for both the HA (a) and the NA (b) segments using the pN/pS ration in which values above 1 denote signs of positive selection.

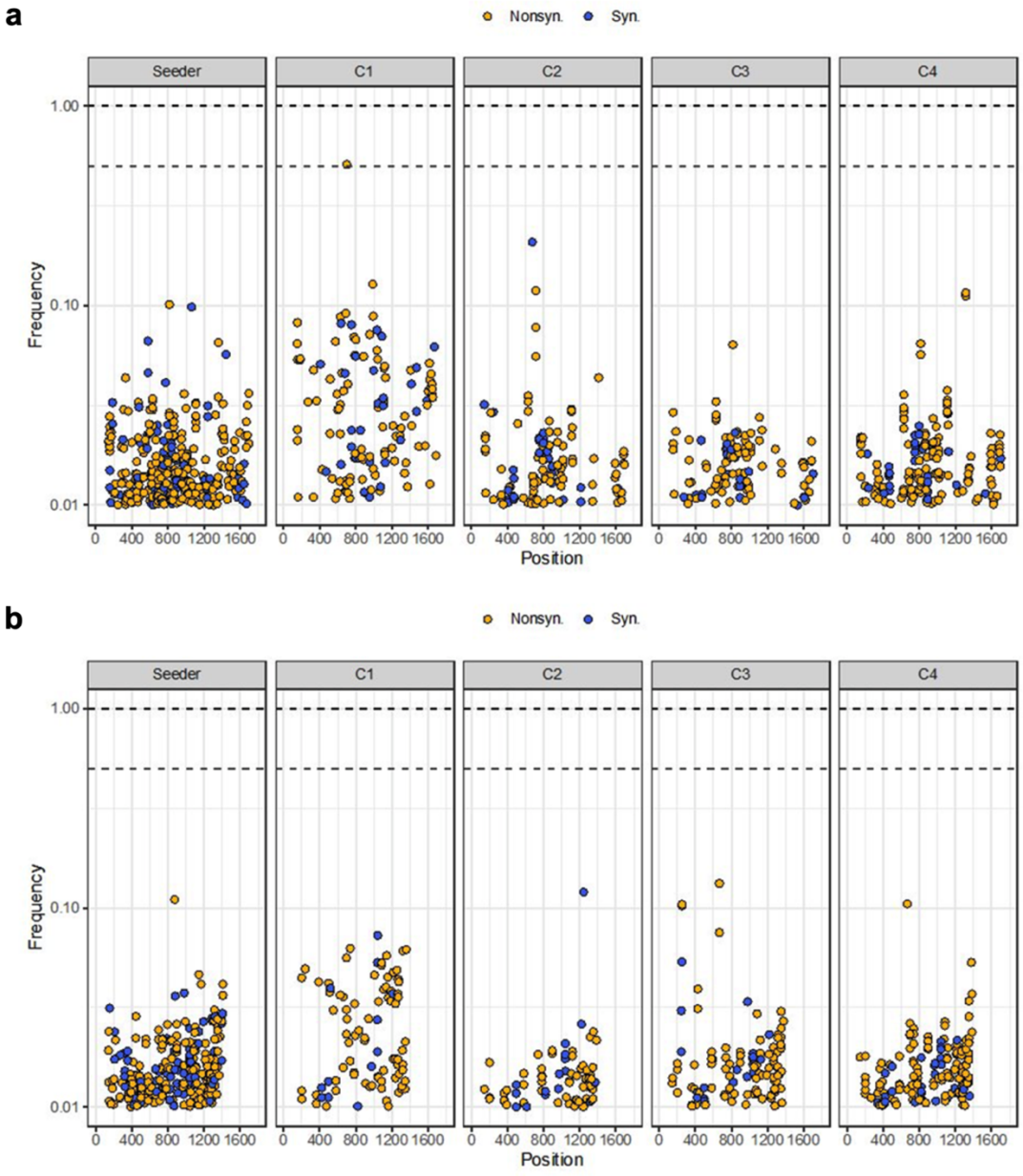
a
Nonsyn.
Syn.
Seeder
C1
C2
C3
C4
1.00
0.10
0.01
Frequency
0
400
800
1200
1600
Position
b
Nonsyn.
Syn.
Seeder
C1
C2
C3
C4
1.00
0.10
0.01
Frequency
0
400
800
1200
1600
Position

S4.2 Fig. Presence of sOH/04 variants in seeders and contact pigs. Nasal swab samples collected at days 1, 2, and 5 dpi and 1, 3, and 6 dpc were sequenced and nucleotide variants were identified in the HA **(a)** and NA **(b)** segments in all seeders and contacts pigs.

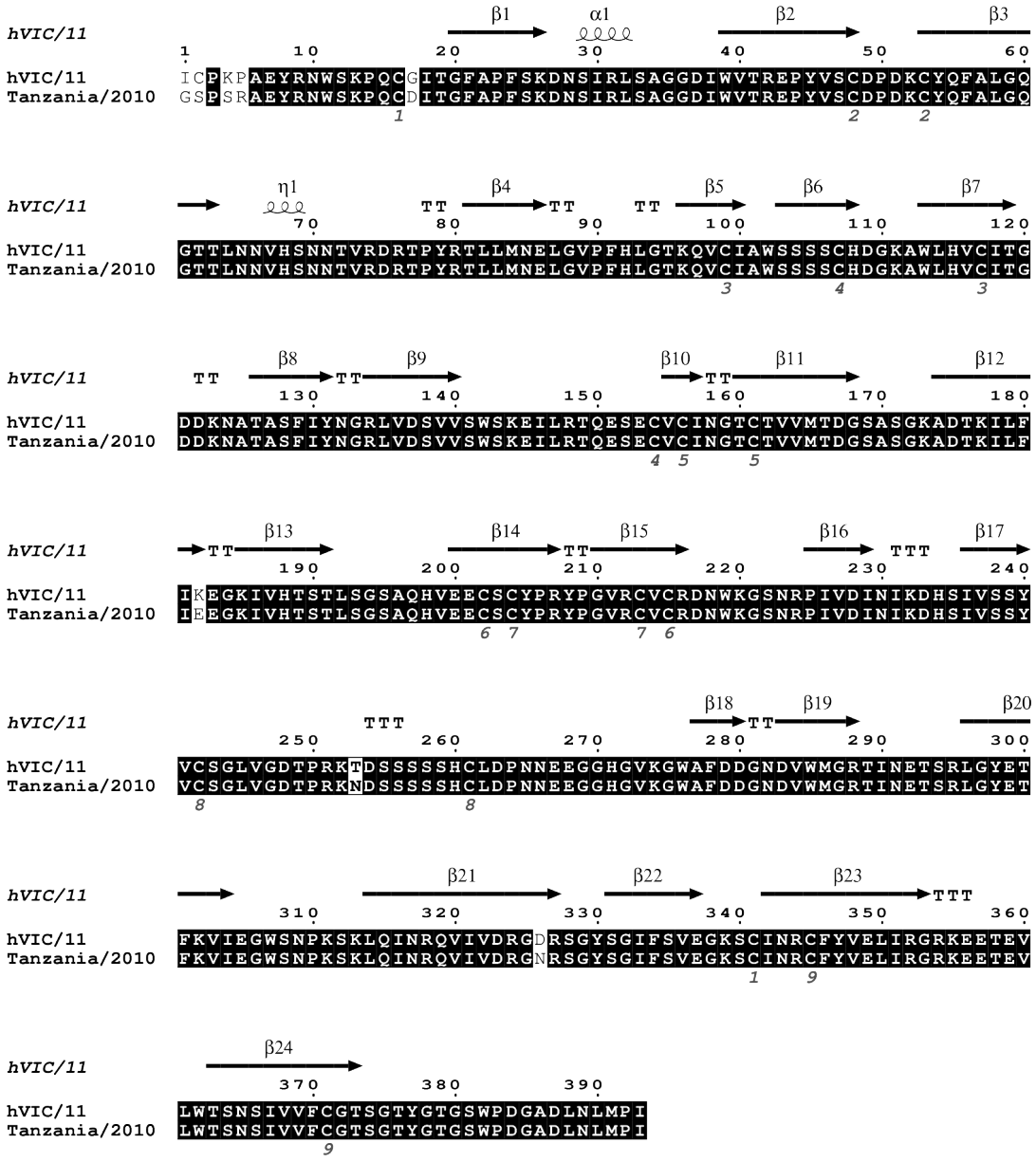

S4.3 Fig. NA sialidase domain alignment between rgA/Victoria/361/2011 and A/Tanzania/205/2010.

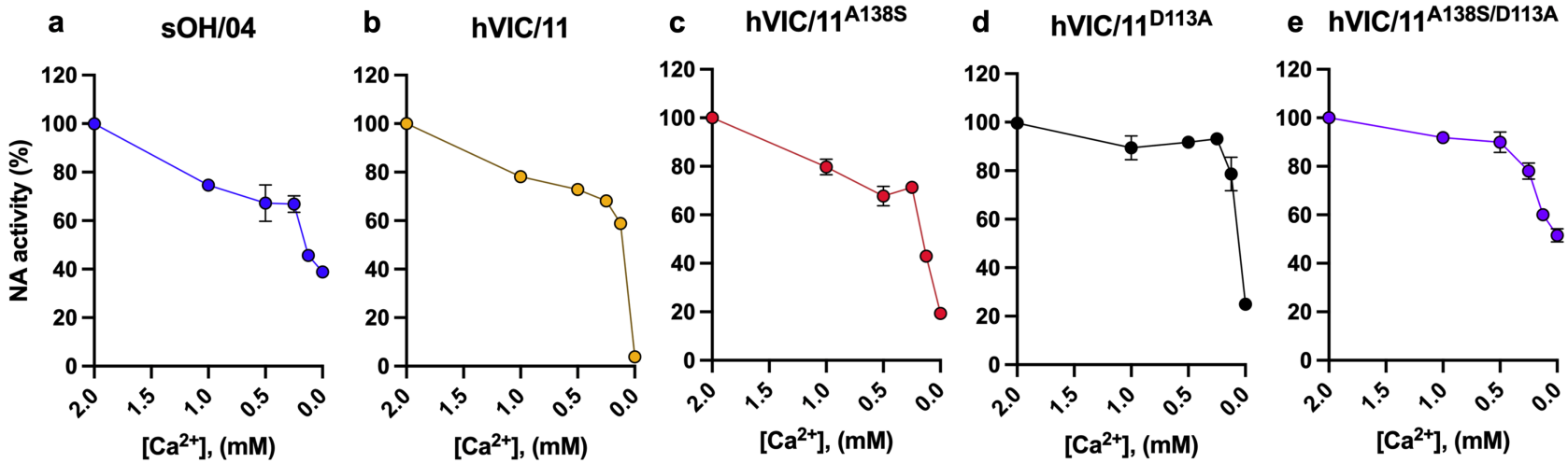

S4.4 Fig. Calcium-dependence of NA activity. NA activity under different calcium concentration of sOH/04 **(a)**, hVIC/11 **(b)**, hVIC/11-A138S **(c)**, hVIC/11-D113A **(d)**, and hVIC/11-A138S/D113A **(e).** Values are presented as the percentage of residual NA activity compared to the reaction velocity of the same virus at 37°C, 2mM Ca^{2+}. Values are shown as the mean ± SD of three independent experiments.

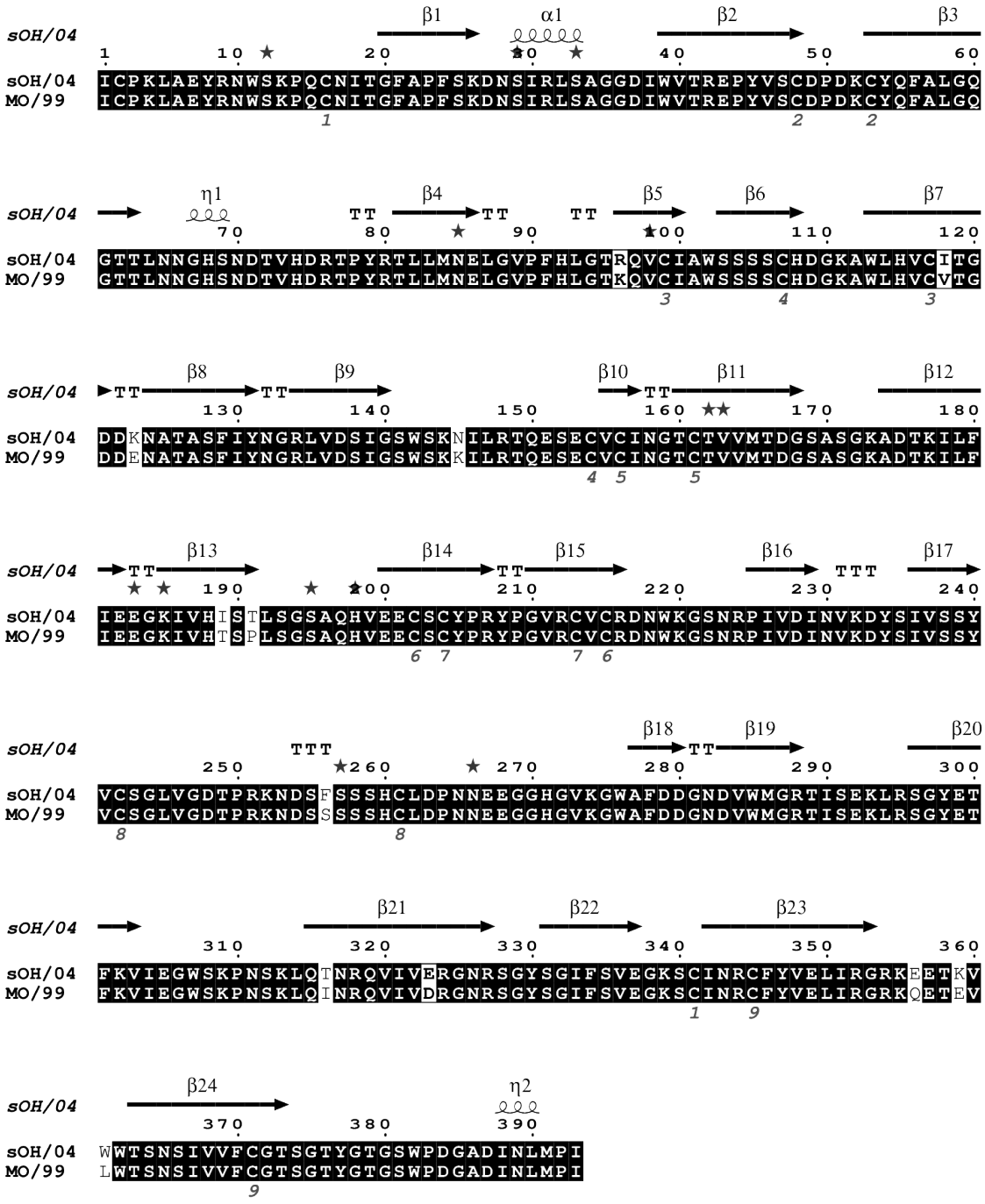

S4.5 Fig. NA sialidase domain alignment between rgA/turkey/Ohio/313053/2004 and A/Moscow/10/1999.

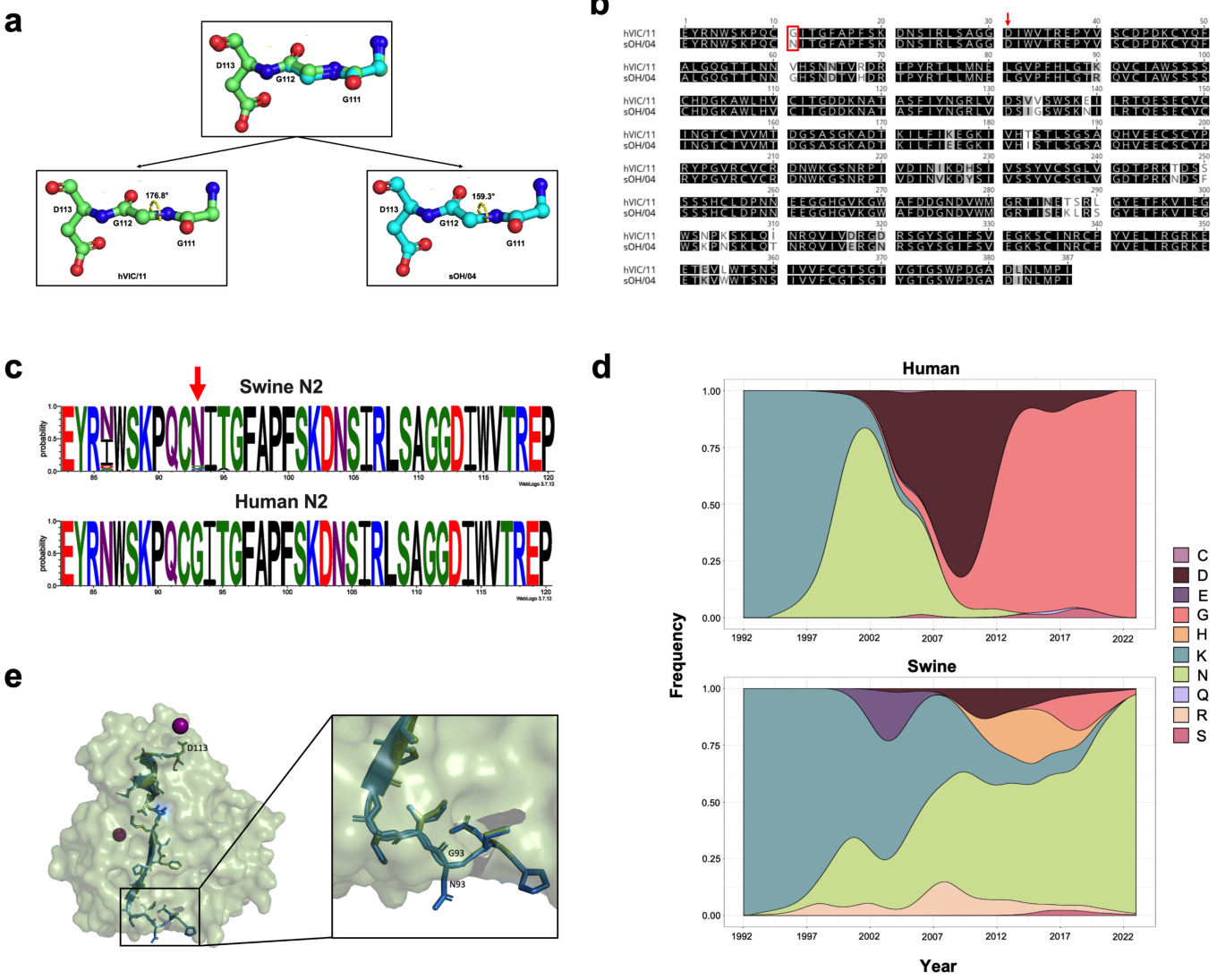
a
D113
G112
G111
176.8°
hVIC/11
159.3°
sOH/04
b
hVIC/11 and sOH/04 NA ectodomain alignment
hVIC/11
sOH/04
c
Swine N2
Human N2
probability
d
Human
Swine
Frequency
Year
C
D
E
G
H
K
N
Q
R
S
e
D113
G93
N93

S4.6 Fig. Role of amino acid 93 in the interaction of NA with calcium. (a) Model showing the f angle between G111 and G112 of hVIC/11 and sOH/04. Image made using PyMOL. **(b)** Sequence alignment between sOH/04 and hVIC/11 NA ectodomain. The red box highlights residue 93 and the red arrow residue 113. **(c)** Sequence logo showing the frequency of amino acids in a portion of N2s ectodomain of 323 swine (top panel) and 11,556 human (bottom panel) H3N2 isolates reported in 2023. Sequences were obtained from GISAID. The red arrow points residue 93. **(d)** Amino acid frequency at position 93 in human (top panel) and swine (bottom panel) H3N2 viruses reported since 1992 to 2023. NA sequences were obtained from GISAID. **(e)** NA monomer model showing N (blue) and G (green) at position 93 and its effect on the reposition of the subsequent residues. Model was made with PyMOL.

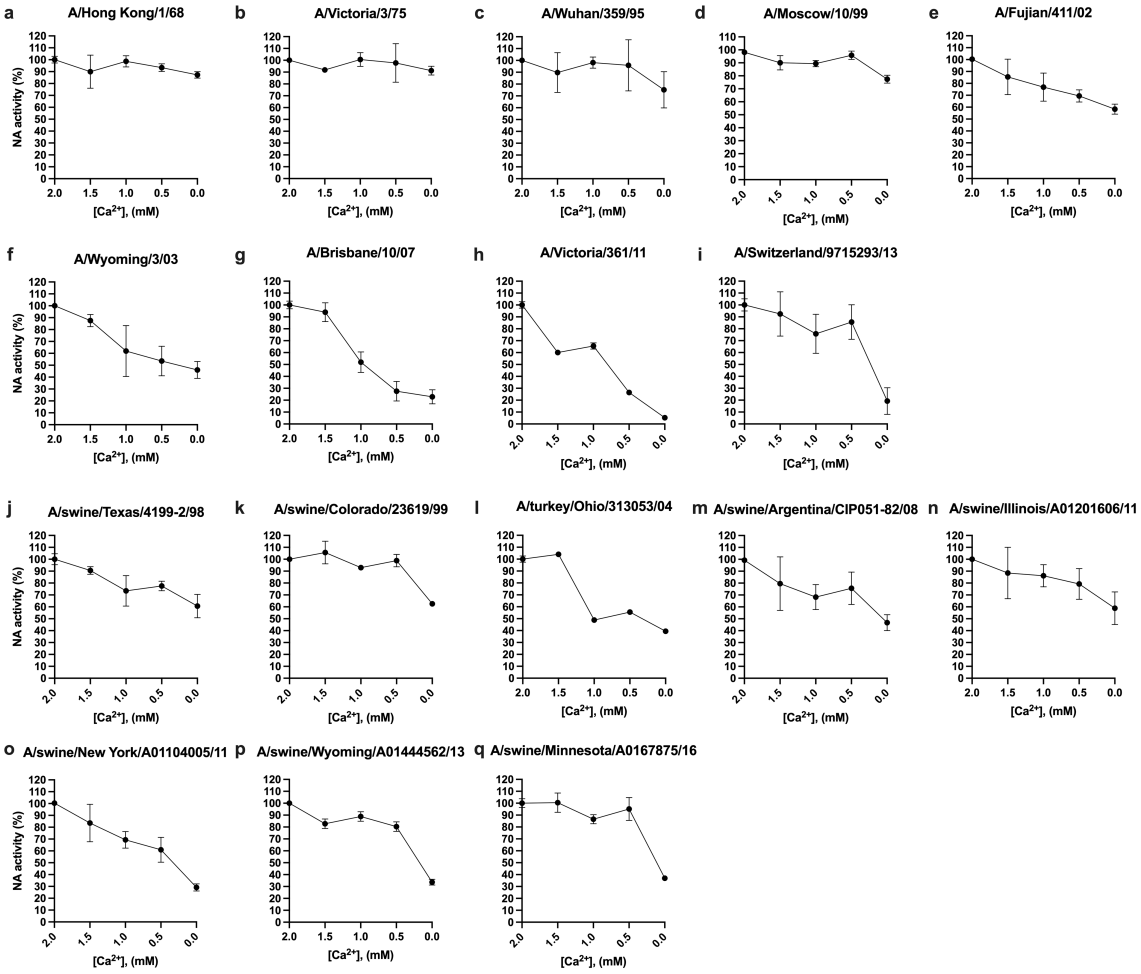
a
A/Hong Kong/1/68
b
A/Victoria/3/75
c
A/Wuhan/359/95
d
A/Moscow/10/99
e
A/Fujian/411/02
f
A/Wyoming/3/03
g
A/Brisbane/10/07
h
A/Victoria/361/11
i
A/Switzerland/9715293/13
j
A/swine/Texas/4199-2/98
k
A/swine/Colorado/23619/99
l
A/turkey/Ohio/313053/04
m
A/swine/Argentina/CIP051-82/08
n
A/swine/Illinois/A01201606/11
o
A/swine/New York/A01104005/11
p
A/swine/Wyoming/A01444562/13
q
A/swine/Minnesota/A0167875/16
NA activity (%)
[Ca2+], (mM)

S4.7 Fig. Comparative analysis of NA sialidase activity in human and swine H3N2 viruses under varying Ca^{2+} concentrations. Human **(a-i)** and swine **(j-q)** viruses from different years were selected and tested for NA activity under different calcium concentrations. Values are presented as the mean ± SD of three independent experiments in which NA activity is expressed as the percentage of the residual reaction velocity compared to the velocity of the same virus at 37°C, 2 mM Ca^{2+}.

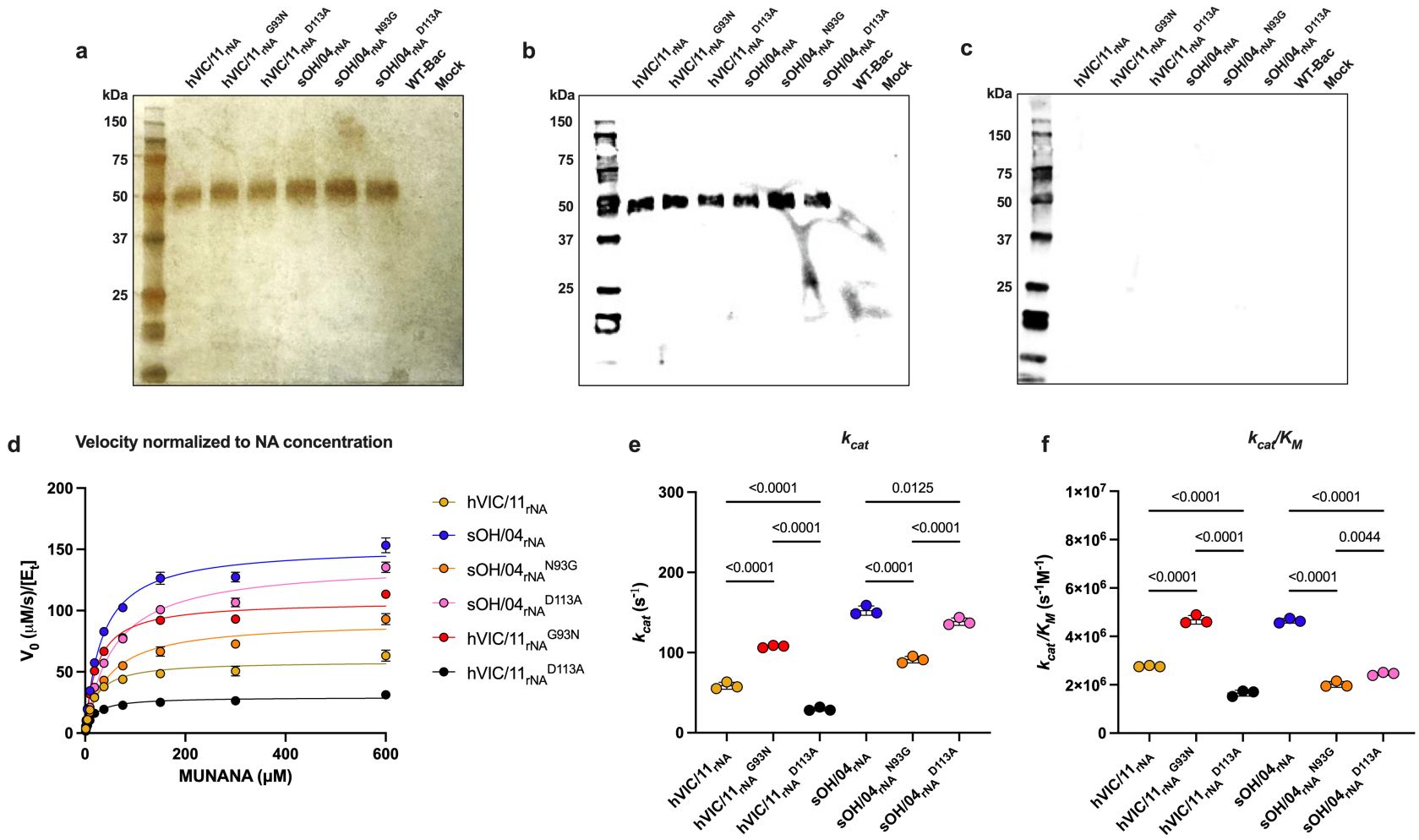
a
b
c
hVIC/11rNA
hVIC/11rNA G93N
hVIC/11rNA D113A
sOH/04rNA
sOH/04rNA N93G
sOH/04rNA D113A
WT-Bac
Mock
kDa
150
75
50
37
25
d
Velocity normalized to NA concentration
V0 (μM/s)/[Et]
MUNANA (μM)
hVIC/11rNA
sOH/04rNA
sOH/04rNA N93G
sOH/04rNA D113A
hVIC/11rNA G93N
hVIC/11rNA D113A
e
kcat
kcat (s-1)
<0.0001
0.0125
f
kcat/KM
kcat/KM (s-1M-1)
0.0044

S4.8 Fig. Recombinant NA expression and determination of enzyme kinetic constants. (a) SDS-PAGE showing the purity of the recombinant NAs after IMAC and size-exclusion chromatography purification, including samples from cells infected with a wild type baculovirus (WT-Bac) and mock infected cells. Full membranes showing western blot of rNAs before **(b)** and after **(c)** thrombin digestion. Samples were incubated with an anti-His antibody. Samples were normalized to 50 ng of protein and the enzymatic reaction velocity was determined as 4-MU production over time. Velocity was normalized to the amount of rNA used in the reaction **(d)** from which k_{cat} **(e)** and k_{cat}/K_M were calculated **(f)**. Values are presented as the mean±SD of three independent experiments. *p* values were determined by one-way ANOVA with Tukey's multiple comparison test.

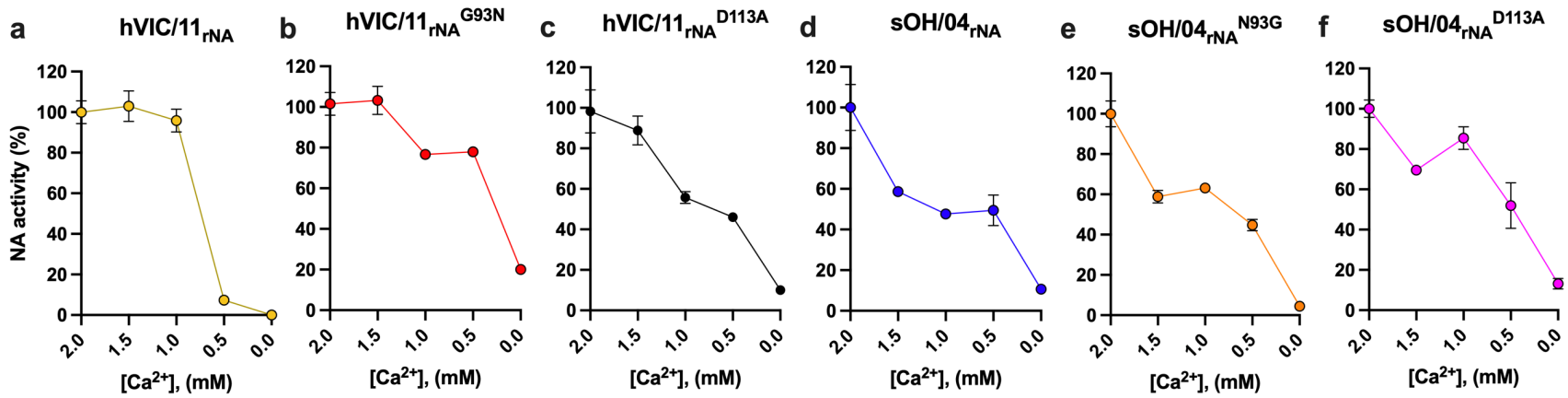

S4.9 Fig. Influence of Ca^{2+} concentration on rNA activity. NA activity of **(a)** hVIC/11 rNA, **(b)** hVIC/11-G93N rNA, **(c)** hVIC/11-D113A rNA, **(d)** sOH/04 rNA, **(e)** sOH/04-N93GrNA, and **(f)** sOH/04-D113A rNA was measured at different calcium concentrations for 60 minutes. NA activity is shown as the percentage of the velocity observed at 37°C and 2mM $Ca^{2+}$of each enzyme. Values are presented as the mean±SD of three independent experiments.

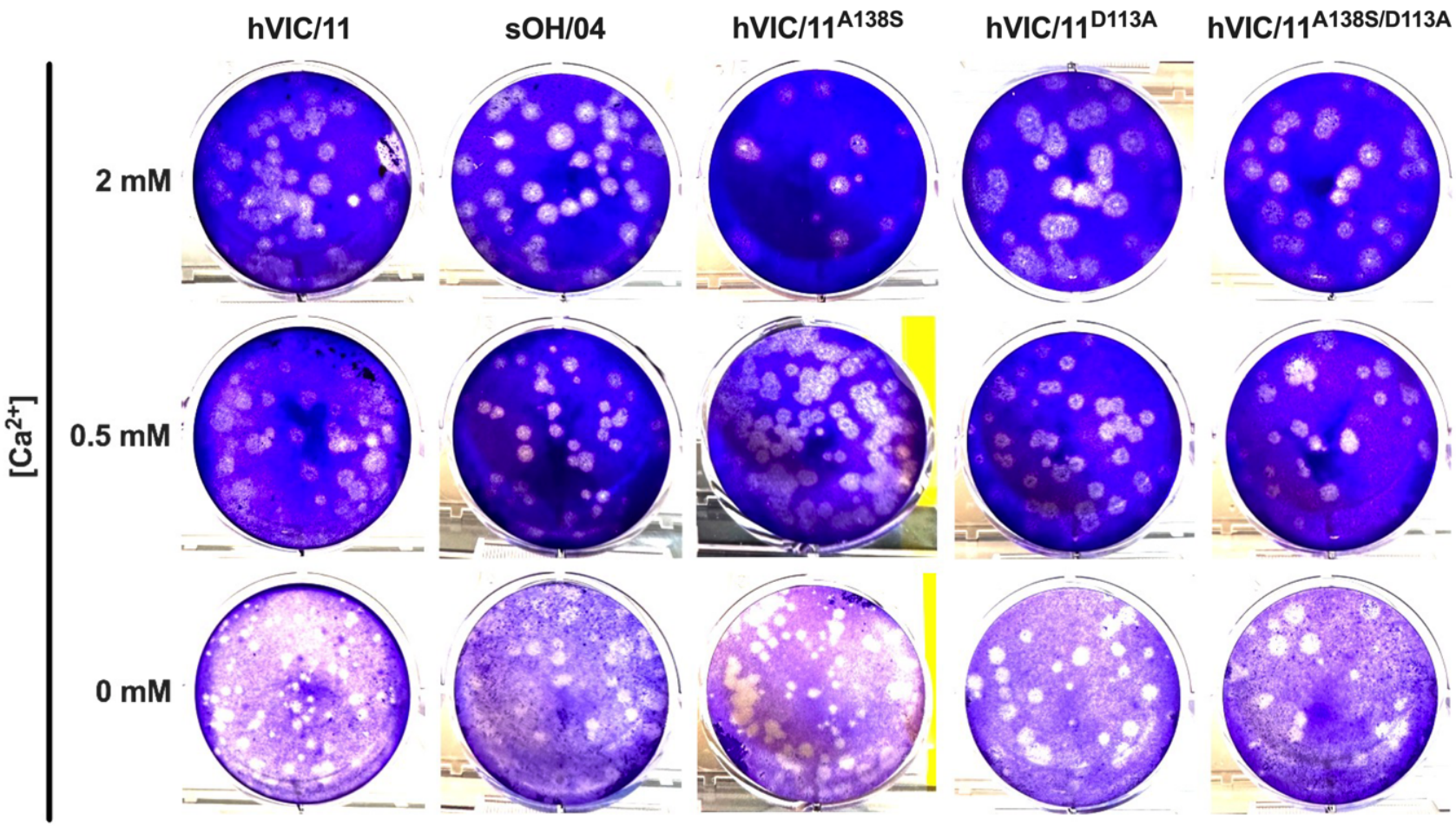
hVIC/11
sOH/04
hVIC/11A138S
hVIC/11D113A
hVIC/11A138S/D113A
[Ca2+]
2 mM
0.5 mM
0 mM

S4.10 Fig. Plaque morphology of hVIC/11 NA variants at different calcium concentrations. Representative pictures of plaques produced by hVIC/11, sOH/04, hVIC/11-A138S, hVIC/11-D113A, and hVIC/11-A138S/D113A. MDCK cells were infected with the mentioned viruses and media was supplemented with 2-, 0.5-, or 0-mM Ca^{+2}.

S4.1 Table. Primers used in this study.

Primer	Sequence (5'-3')
HA_NGS	F: AAAAGCAGGGGATAATTCTATTAACCATGAAGAC R: ATGCACTCAAATGCAAATGTTGCACC
NA_NGS	F1: AGCAAAAGCAGGAGTAAAGATGAATCC F2: CAAGGAGTTTTTTCTAAAATTGCGAAAGC
NA_VIC_G93N_pDP	F: CAAAACCGCAATGTAATATTACAGGATTTGCACC R: ACCAATTTCTGTATTCTGCTGGTTTGGGG
NA_OH04_G93N_pDP	F: AAGCCGCAATGTGGAATTACAGGATTTGC R: GACCAATTTCTGTATTCTGCTAGTTTGGGGC
NA_VSP	F: GGAATTCCATGGAATTTGGATTGTCCTGGATC R: CCCAAGCTTGGGTTATATAGGCATGAGATTGA
NA_VIC_D113A	F: TGGGGCCATCTGGGTGACAAGAG R: CCAGCGGAAAGCCTGATCGAATTG
NA_OH04_D113A	F: TGGGGCCATCTGGGTGACAAGAGAAC R: CCAGCGGAAAGCCGAATCGAATTGTCC
NA_VIC_G93N	F: GCAATGTAACATTACAGGATTTGCACCTTTC R: GGTTTTGACCAATTTCTGTATTCTCCTCCAGATC
NA_OH04_N93G	F: GCAATGTGGAATTACAGGATTTGCACCTTT R: GGCTTTGACCAATTTCTGTATTCTCCTCC
M13	F: CAGGAAACAGCTATGAC R: CAGGAAACAGCTATGAC
M_titration	F: AGATGAGTCTTCTAACCGAGGTC R: TGCAAAGACACTTTCCAGTCTCTG P: GGCCCCCTCAAAGCCGA

S4.2 Table. NA activity at 0 mM $^{Ca2+}$ of different human and swine H3N2 viruses.

Virus	Residue 93	Residue 113	Activity at 0 mM Ca^{2+} [(a)]	Accession no.
HK/68	Q	D	87.2±1.74	HM641198.1
VIC/75	K	D	91.24±3.71	CY113183.1
WU/95	K	D	75.15±15.28	CY112823.1
MO/99	N	D	77.43±3.03	CY121375.1
FU/02	N	D	58.3±4.26	CY112935.1
WY/03	N	D	46.06±7.09	CY116600.1
BR/07	D	D	22.8±5.89	EU199249.1
VIC/11	G	D	5.29±1.38	KJ942682
SW/13	G	D	19.29±11.19	OQ350034.1
TX/98	K	D	60.63±9.78	CY095677.1
CO/99	K	D	62.52±1.42	AF268138.1
OH/04	N	D	39.47±2.03	EU735820.2
AR/08	S	D	46.74±6.69	ADO65973.1
IL/11	K	D	58.89±13.76	CY114841.1
NY/11	N	D	29.14±3.00	JN940424.1
WY/13	N	D	33.66±2.38	KC562196.1
MN/16	N	D	39.94±2.09	KY349114.1

[a] Values presented ± SD.

S4.3 Table. Kinetic constants of recombinant NA proteins. (rNA)

rNA	Amino acid position		K_M [a, b]	V_{max} [a, c]	k_{cat} [a, d]	k_{cat}/K_M [a, e]
	93	113				
hVIC/11	G	D	21.19±1.34	23.46±1.72	58.62±4.31	2.76±0.02
hVIC/11-G93N	N	D	23.01±1.16	43.08±0.58	107.6±1.47	4.68±0.17
hVIC/11-D113A	G	A	17.91±2.78	11.76±0.89	29.39±2.22	1.65±0.12
sOH/04	N	D	32.8±0.67	60.95±2.28	152.3±5.69	4.64±0.09
sOH/04-N93G	G	D	45.32±1.16	36.52±1.64	91.25±4.11	2.01±0.11
sOH/04-D113A	N	A	56.46±1.51	55.46±1.86	138.6±4.65	2.45±0.06

[a] Values presented ± SD. Samples were normalized to 50 ng of protein.

[b] Values presented as mM.

[c] Values presented as mM/min.

[d] Values presented as s^{-1}.

[e] Values presented as $x10^6$ $s^{-1}M^{-1}$.

Acknowledgments

The authors thank the University Research Animal Resources personnel at the University of Georgia for assistance with animal care. We thank Dr. Lucas Ferreri for the development of the pipeline used for variant analysis. This research was supported by Agriculture and Food Research Initiative grant no. 2020-67015-31563/project accession no. 1022827 from the USDA National Institute of Food and Agriculture to DSR. Funding was also provided, in part, by The National Pork Board to DSR under Project #21-085. DSR is also funded by Agriculture and Food Research Initiative grant no. 2022-67015-37205/project accession no. 1028058 from the USDA National Institute of Food and Agriculture. DRP is funded by subcontract 75N93021C00014 Centers for Influenza Research and Response (CEIRR) from the National Institute of Allergy and Infectious Diseases (NIAID) and GRANT12901999, project accession no. 1022658 from the National Institute of Food and Agriculture (NIFA), U.S. Department of Agriculture. DRP receives additional support from the Georgia Research Alliance and the Caswell S. Eidson endowment funds from The University of Georgia. This study was partly supported by resources and technical expertise from the Georgia Advanced Computing Resource Center, a partnership between the University of Georgia's Office of the Vice President for Research and the Office of the Vice President for Information Technology. ALB and TKA are funded by the USDA-ARS project number 5030-32000-231-000D and the NIAID, National Institutes of Health, Department of Health and Human Services, under Contract No. 75N93021C00015. The funders had no role in study design, data collection and interpretation, or the decision to submit the work for publication. Mention of trade names or commercial products in this article is solely for the purpose of

providing specific information and does not imply recommendation or endorsement by the USDA or UGA. USDA is an equal opportunity provider and employer.

CHAPTER 5

EVOLUTION OF A HUMAN H3N2 VIRUS IN PIGS RESTRICTS THE RECEPTOR SPECIFICITY FOR EXTENDED GLYCANS AND ENHANCES RECEPTOR AFFINITY

Matias Cardenas, Pradeep Chopra, Brittany Seibert, Brianna Cowan, C. Joaquin Caceres, Tavis K. Anderson, Amy L. Vincent Baker, Geert-Jan Boons, Daniel R. Perez, and Daniela S. Rajao

To be submitted to Plos Pathogens

Abstract

Interspecies transmission of human influenza A viruses (FLUAV) to swine happens regularly but little is known about the molecular changes required for the virus to establish and transmit within pig populations. Vaccination is a common practice in swine herds, and prior immunity from vaccines or natural infection could alter the susceptibility to and evolution of human-origin viruses in pigs. Here, we studied the evolution of a human-origin H3N2 virus in previously vaccinated pigs using a sustained transmission model. Seeder pigs were vaccinated with a commercial inactivated vaccine and then infected with an antigenically distinct reassortant virus containing human-origin HA/NA paired with internal genes from endemic swine FLUAV lineages. Contact pigs with the same vaccination status were introduced to rooms with the seeder pigs two days later. After 3 days, seeders were removed, and new contacts introduced. This was repeated for a total of 4 contacts. Shortly after infection in the seeders??, sequencing of nasal swabs showed the emergence of mutations in the HA receptor binding site (RBS, V186G and F193Y) and the NA low-affinity calcium-binding pocket (D113A). In contacts 2, the HA1 F193Y mutation became fixed, while the V186G mutation was no longer detected. This amino acid mutation reduced antibody recognition and prevented binding to N-glycolylneuraminic acid (Neu5Gc). Additionally, both V186G and F193Y limited the pool of glycans supporting binding, exhibiting a preference for extended a2,6-linked molecules with at least 3 LacNAc repeats, contrasting with the parental human-adapted virus that recognized glycans with at least 2 LacNAc repeats. However, the restriction observed by the F193Y change was accompanied by increased affinity for a2,6-linked sialic acid. The D113A mutation in the NA appeared to restore the HA/NA

balance in a HA-dependent context, but promoted NA inhibition and was quickly lost. These data suggest that previous non-neutralizing immunity may be associated with adaptation of a human-origin HA to pigs and highlight the role of glycan topology and receptor affinity in the host range of FLUAV.

Introduction

The interspecies transmission of human seasonal influenza A viruses (FLUAV) to pigs occurs relatively frequently and multiple transmission events have contributed to FLUAV diversity in swine [17, 250, 302]. However, the molecular factors associated with virus persistence following human-to-swine spillover events remain unknown [18]. Acquisition of swine-adapted internal genes seems to be an initial critical step [18, 289], as exemplified by reassortment of human H3N2 with endemic swine IAV after introduction to pigs [272, 386]. Following reassortment to acquire swine-adapted genes, mutations near the hemagglutinin (HA) receptor-binding site (RBS) appear to be associated with subsequent transmission between pigs for the establishment of these novel FLUAV to the new swine host [265, 387].

Changes in the HA RBS have been widely shown to affect the host range of FLUAV [388] due to its role in binding to sialic acid (SA)-containing receptors on the host cell and inherent differences in receptor specificity. This specificity is often associated with the linkage to which the terminal SA binds to the sub-terminal galactose in cellular oligosaccharides. Avian viruses mostly bind a2,3-linked sialic acid (a2,3 SA) [24], while mammalian viruses exhibit a preference for a2,6 SA [389]. However, since both humans and pigs express a2,6 SA in the respiratory tract [259, 390], these

differences in specificity are not as clear, and may involve other characteristics of the host cell glycans. Some reports suggest that adaptation to the swine host might select for enhanced affinity for N-Glycolylneuraminic acid (Neu5Gc), which is expressed in most non-human mammals, including pigs [254], but not humans [391]. However, data is contradictory and while some reports have found a preference for Neu5Gc others have reported no difference in Neu5Gc binding between human and swine FLUAV [256, 392-394]. Hence, the role of mutations near the HA RBS on adaptation to swine when human viruses are introduced into pigs remains poorly understood. While the HA binds to receptors on the host cell, the NA displays an opposite activity by cleavage of SA, allowing new virions to be released from the cell [181] Given complementary functions between the HA and NA surface proteins, a balance in activity is important for viral fitness. Hence, changes in the affinity of the HA for certain SA conformations can affect the ability of the virus to produce a successful infection if those mutations disrupt the HA/NA balance [31]. Therefore, changes in the HA are normally accompanied by compensatory mutations in the NA that affect its sialidase activity to restore a functional balance the two glycoproteins [33, 395].

Vaccination is one of the most common and effective strategies to prevent FLUAV infections in swine [275]. Immunization is usually performed with inactivated commercial products and normally induces a strong IgG response against the HA [396] and, to a lesser extent, the NA [397]. Unless the vaccine strain is closely related or matches the circulating virus, it does not prevent infection [398], although it may reduce transmission and clinical disease. However, antibody-mediated immunity creates a selective pressure that may drive the emergence of antigenic variants that drive antigenic

evolution [286]. Prior *in vitro* studies have demonstrated the selection of escape mutations in the presence of immune sera. Further, vaccine-driven antigenic evolution has been shown following immunization of pigs where viruses acquired mutations in the HA RBS and the head domain of the NA [87, 88]. These studies have been conducted using swine vaccines and endemic swine FLUAV, and the impact of host immunity on the evolution of novel human viruses within the swine host is unknown.

In this study, pigs were vaccinated with a commercial vaccine and challenged with a virus containing human-origin HA and NA surface proteins. The challenge virus included a mutation near the HA RBS (A138S, H3 numbering) that we previously showed to allow transmission of the virus in pigs [27, 258]. The human-like virus was serially transmitted between vaccinated contact pigs. After infection, the virus lost the original A138S mutation and acquired new mutations in the HA (V186G and F193Y) and the NA (D113A). The viruses with the 186 and 193 mutations did not display growth differences in MDCK nor differentiated human airway epithelial cells, suggesting that during early stages of adaptation, human viruses could potentially retain the ability to infect humans. However, the HA changes were shown to reduce antibody recognition by vaccine antisera collected from vaccinated pigs 14 days post boost, and to limit the affinity of the virus for extended a2,6-linked glycans. The viruses with V186G and F193Y mutations exhibited higher binding to a2,6-SA compared to the human precursor virus. Overall, our results highlight the importance of glycan topology in the adaptation process of human FLUAV to pigs, suggesting that rather than switching between a2,3-SA and a2,6-SA affinity, viruses increase affinity for specific a2,6-SA to improve replication efficiency in swine.

Materials and Methods

Ethics statement

The animal experiments presented in this study were reviewed and approved by the Institutional Care and Use Committee (IACUC) at the University of Georgia (Protocol #A2019 03-031-Y3-A9). Animals were housed under biosafety level 2 containment and cared for following the guidelines in the Guide for Care and Use of Agricultural Animals in Research and Teaching (American Dairy Science Association®, American Society of Animal Science, and Poultry Science Association, 2020). Water and feed was provided *ad libitum*. Animals were euthanized at the end of the study according to the guidelines provided by the American Veterinary Medical Association (AVMA).

Cells and viruses

Madin-Darby canine kidney (MDCK), and Human Embryonic Kidney 293 (HEK-293) cells were maintained in Dulbecco's Modified Eagles Medium (DMEM, Sigma-Aldrich, St Louis, MO) supplemented with 2mM L-glutamine (Sigma-Aldrich, St Louis, MO), 10% fetal bovine serum (FBS, Sigma-Aldrich, St Louis, MO), and 1% antibiotic/antimycotic (Sigma-Aldrich, St Louis, MO). HEK-293 and MDCK cells expressing A/WSN PB1 (HEK-293-PB1 and MDCK-PB1) were cultured as previously described [399]. HEK-293-PB1 were maintained in the media described above while MDCK-PB1 cells were grown in DMEM supplemented with 2mM L-glutamine (Sigma-Aldrich, St Louis, MO), 10% fetal bovine serum (FBS, Sigma-Aldrich, St Louis, MO), 1% antibiotic/antimycotic (Sigma-Aldrich, St Louis, MO), 0.25 mg/mL Puromycin (ThermoFisher Scientific, Waltham, MA), and 1 mg/mL Geneticin (ThermoFisher

Scientific, Waltham, MA). Cells were incubated at 37°C in a humidified incubator with 5% CO_2.

Human Airway epithelial cells (BCi.NS1.1) were kindly provided by Dr. Ronald Crystal (Weill Cornell Medicine, NY, USA). They were cultured in PneumaCult-Ex Plus Basal Media (STEMCELL Technologies, Vancouver, Canada) supplemented with PneumaCult-Ex Plus Supplement (STEMCELL Technologies, Vancouver, Canada), 0.1% hydrocortisone (STEMCELL Technologies, Vancouver, Canada), 1% antibiotic/antimycotic (Sigma-Aldrich, St Louis, MO), and 0.5% gentamycin (Sigma-Aldrich, St Louis, MO). For differentiation, cells were plated in type IV collagen-coated 12 mm transwell plates (0.4 mm pore size, Corning Inc., NY, USA) at a density of $3x10^5$ cells/well. After reaching 100% confluency, media for the apical compartment was removed and cells were incubated with PneumaCult ALI Base Media (STEMCELL Technologies, Vancouver, Canada), supplemented with PneumaCult ALI Supplement (STEMCELL Technologies, Vancouver, Canada), 1% PneumaCult ALI Maintenance Supplement (STEMCELL Technologies, Vancouver, Canada), 1% antibiotic/antimycotic (Sigma-Aldrich, St Louis, MO), 0.5% gentamycin (Sigma-Aldrich, St Louis, MO), 0.2% heparin (STEMCELL Technologies, Vancouver, Canada), and 0.5% hydrocortisone (STEMCELL Technologies, Vancouver, Canada). After 5 days of incubation at 37°C in a humidified incubator with 8% CO_2, cells were moved to an incubator at 37°C with 5% CO_2 for 16 more days.

Viruses used in this study **(Table 5.1)** were grown in MDCK cells using Opti-MEM (ThermoFisher Scientific, Waltham, MA) containing 1 mg/ml of tosylsulfonyl phenylalanyl chloromethyl ketone (TPCK)-treated trypsin (Worthington Biochemicals,

Lakewood, NJ). For biolayer interferometry experiments, replication-incompetent versions of the viruses described in **Table 5.1** were used. These viruses lacked the PB1 open reading (DPB1), and therefore could only infect and replicate in MDCK- and HEK-293T-PB1 cells. DPB1 viruses were grown in MDCK-PB1 cells using Opti-MEM (ThermoFisher Scientific, Waltham, MA) containing 1 mg/ml of TPCK-treated trypsin (Worthington Biochemicals, Lakewood, NJ), 0.25 mg/mL Puromycin (ThermoFisher Scientific, Waltham, MA), and 1 mg/mL Geneticin (ThermoFisher Scientific, Waltham, MA). Infections were incubated at 37°C for 3 days and viral titers were determined by $TCID_{50}$ using the Reed and Muench method [293].

Animal studies

3-week old cross-bred pigs were obtained from Midwest Research Swine Inc (Glencoe, MN, USA). After a 5-day acclimatation period, animals were confirmed to be seronegative for anti-FLUAV antibodies by competitive ELISA (IDEXX, Westbrook, ME) according to the manufacturer's instructions. Pigs were randomly assigned into four experimental group. Animals in two groups (n=15/group) were immunized intramuscularly using the Zoetis FluSure XP vaccine (Zoetis, Parsippany, NJ) according to the manufacturer's instructions. Animals in two groups were mock vaccinated with PBS. Fourteen days post-vaccination (dpv), primed pigs were boosted using the same vaccine. Fourteen days post-boost (dpb), blood was collected to confirm seroconversion induced by the vaccine. These pigs (seeders) were sedated with ketamine (6 mg/kg, Zoetis, Parsippany, NJ), xylazine (3 mg/kg, Cronus Pharma, Brunswick, NJ), and Telazol (6 mg/kg, Dechra Pharmaceutical, Fort Worth, TX), and challenged intratracheally (2ml)

and intranasally (1ml) with $3x10^6$ $TCID_{50}$/pig of hVIC/11-A138S, a virus carrying the HA and NA segment form A/Victoria/361/2011 in a TRIG backbone and the A138S mutation in the HA [27, 258] . Pigs were checked daily for clinical signs and nasal swabs were collected at 0, 1, 2, 3, and 5 days-post infection (dpi) in 2 mL of brain heart infusion broth (Sigma-Aldrich, St Louis, MO). At 2 dpi, same-vaccination-status pigs (n=3, Contact 1 [C1]) were placed in contact with the directly-inoculated animals (seeders). At 5 dpi, seeders were sedated using a mixture of ketamine (3 mg/kg), xylazine (1.5 mg/kg), and Telazol (3 mg/kg) and then humanely euthanized by an intravenous pentobarbital overdose (Euthasol, 390 mg/10, Virbac, Westlake, TX). C1 pigs were moved to a clean cage and 3 new same-vaccination-status pigs (C2) were put in contact with C1 pigs, and this cycle was repeated for a total of four contacts. Anti-FLUAV antibody levels were measured for very contact the day they were place in contact with infected animals. During necropsies, lungs were rinsed with 50 mL of DMEM to collect the bronchoalveolar lavage fluid (BALF).

Enzyme-linked immune absorbent assay (ELISA)

To quantify antibody levels induced by the Zoetis FluSure XP vaccine, an in-house ELISA was performed: the vaccine contains two H3 components (1990.4.a and 1990.4.b HA clades) along with two H1 components. Briefly, high-binding ELISA plates (ThermoFisher Scientific, Waltham, MA) were coated with 128 HAU of rgA/swine/NY/A01104005/2011 (H3N2, 1990.4.a) diluted in ELISA coating buffer (ThermoFisher Scientific, Waltham, MA). The virus was previously purified by ultracentrifugation using a 20% sucrose cushion at 30,000 rpm. After a 2-hour adsorption,

plates were washed twice with washing buffer (ThermoFisher Scientific, Waltham, MA) and 100 mL of 1:10 diluted serum sample was added and incubated for 1 hour at room temperature. After incubation, plates were washed three times with washing buffer and an HRP-conjugated anti-swine IgG secondary antibody was added (ThermoFisher Scientific, Waltham, MA) in a 1:1000 dilution. The secondary antibody was incubated for one hour, and excess antibody was washed away three times with washing buffer. Finally, 100 mL of 3,3',5,5'-tetramethylbenzidine (TMB, ThermoFisher Scientific, Waltham, MA) was added per well and plates were incubated for 10 minutes in the dark. Reaction was stopped by adding 50 mL of stop solution (ThermoFisher Scientific, Waltham, MA) and absorbance was measured at 450 nm using a Synergy HTX Multi-Mode Microplate Reader (Agilent BioTek, Santa Clara, CA). Samples with an absorbance 3s higher than the mean of mock-vaccinated pigs were considered positive.

Nasal swabs and BALF virus titration

vRNA from nasal swabs and BALF samples was extracted using the MagMax-96 AI/ND viral RNA isolation kit (ThermoFisher Scientific, Waltham, MA) according to the manufacturer's instructions. Purified RNA was used to titrate FLUAV using qRT-PCR using the Quantabio qScript XLT One-Step RT-qPCR ToughMix kit (Quantabio, Beverly MA) targeting the M segment as previously described [258].

Next-generation sequencing (NGS) and data analysis.

Purified RNA was used as template to amplify the HA and NA segments with target-specific primers and using the SuperScript III One-Step PCR System

(ThermoFisher Scientific, Waltham, MA) according to the manufacturer's instructions. Amplification was confirmed by running the PCR products in 1% agarose gels. Replicate HA and NA reactions were then combined and purified using 0.4X Agencourt AMPure XP Magnetic Beads (Beckman Coulter, Brea, CA, USA). DNA concentration was determined using the Qubit dsDNA HS assay kit (ThermoFisher Scientific, Waltham, MA) on a Qubit 3.0 fluorometer (ThermoFisher Scientific, Waltham, MA) and normalized to 0.2 ng/mL. PCR products were fragmented and indexed using the Nextera XT DNA library preparation kit (Illumina, San Diego, CA, USA). Tagmentation was confirmed by running random samples on an Agilent Bioanalyzer 2100 DNA-HS assay (Agilent, Santa Clara, CA, USA). Finally, samples were normalized to 0.2 ng/mL, pooled, denatured, normalized to 10 pM, and sequenced using the MiSeq Reagent Kit V2, 300 cycles (Illumina, San Diego, CA, USA). FLUAV genome was assbmbled and viral varianted were identified as we have previously described [400].

Site-directed mutagenesis and virus rescue

Mutations were introduced in the HA and NA genes of rg-A/Victoria/361/2011 using the Phusion site-directed mutagenesis kit (ThermoFisher Scientific, Waltham, MA) according to the manufacturer's instructions and plasmid sequences were confirmed by whole plasmid sequencing. Recombinant viruses were rescued using an 8-plasmid reverse genetic system using a coculture of HEK-293 and MDCK cells as previously described [401].

To generate replication-incompetent viruses, rescues were performed as described above using a coculture of HEK-293-PB1 and MDCK-PB1 cells without antibiotics. The

pDP plasmid containing the TRIG PB1 gene was replaced with a pHW_PB1packWSN_TdKatushka NLS plasmid which contained the packaging signals of the PB1 segment and the ORF of the TdKatushka fluorescent protein instead of the PB1 coding sequence [402].

In vitro growth kinetics

MDCK cells were seeded in 6-well plates at a density of $3x10^5$ cells/cm^2 in Opti-MEM and incubated at 37°C in a humidified incubator with 5% CO_2 until an 80% confluency before use. Cells were infected at a multiplicity of infection (MOI) of 0.01 for 1 hour at 37°C. After incubation, cells were washed three times with PBS and supplemented with Opti-MEM containing 1 mg/ml TPCK-treated trypsin. Supernatants were collected at 0, 12, 24, 48, and 72 hpi timepoints.

Differentiated HAE cells were infected at an MOI of 0.01 by adding 200 mL of inoculum in the apical compartment. After 1 hour, cells were washed 5 times with PBS and transwells were transferred to a new plate. Cells were maintained in ALI media and no exogenous TPCK-treated trypsin was added. Supernatants were collected at 0, 12, 24, 48, and 72 hpi by adding 200 mL of PBS onto the cells and incubating them at 37°C for 10 minutes.

Viral RNA was extracted, and titers determined by qRT-PCR as described above and data was fit to a $TCID_{50}$ equivalent standard curve of an exact virus match.

Virus neutralization assay

Because hVIC/11-V186G does not agglutinate chicken nor turkey red blood cells (RBC), neutralization titers were determined using a homologous fluorescent virus to rely on mCherry expression in infected cells, similar to luciferase expression as previously described [403]. Briefly, viruses listed in **Table 5.1** were rescued as mentioned above in the isogenic TRIG backbone but carrying the mCherry coding sequence downstream of the NS1 gene [404]. Serum samples were treated with receptor-destroying enzyme (RDE, Denka Seiken, VWR) at 37°C for 18 hours and then RDE was heat-inactivated for 30 minutes at 56°C. Sera was diluted 1:10 and further mixed in a 1:1 ratio with 100 $TCID_{50}$ of each virus for 1 hour at 37°C. Then the mixture was added onto confluent MDCK cells in 96 well-plates. Infections were incubated for 1 hour at 37°C and then cells were washed three times with PBS and overlayed with Opti-MEM supplemented with 1 mg/ml TPCK-treated trypsin. At 48 hours post infection, cell culture media was removed, and cells were lysed using the Pierce IP lysis buffer (ThermoFisher Scientific, Waltham, MA). Supernatant was collected and mCherry fluorescence was measured at excitation and emission wavelengths of 587 nm and 610 nm, respectively, using a Synergy HTX Multi-Mode Microplate Reader (Agilent BioTek, Santa Clara, CA).

Hemagglutinin inhibition assays

Serum samples were treated with RDE as described above. Samples were 2-fold serially diluted in PBS and then 25 mL were mixed with 25 mL of virus containing 4 hemagglutination units (HAU) in V-bottom 96-well plates. Sera/virus mixtures were incubated for 30 minutes at room temperature and after incubation 50 mL of 0.5% turkey

red blood cells were added. Following a 40-minute incubation at room temperature, HI titers were determined and titers below 10 HI were arbitrarily assigned a value of 10.

Glycan array

Array experiments were performed as previously described [405]. Briefly, viruses were diluted to 8 HAU in TSM buffer (20 mM Tris-HCl, 150 mM NaCl, 2 mM $CaCl_2$, and 2 mM $MgCl_2$, pH 7.4). 100 mL of each sample was applied onto the slide and viruses were incubated for 1 hour at room temperature in presence of 200 nM Oseltamivir (Sigma-Aldrich, St Louis, MO). After incubation, slides were washed three times with TSM-wash (TSM-buffer with 0.05% Tween-20) and one time with water. Slides were then incubated with 5 mg/mL of an anti-HA antibody (stem specific antibody, CR8020, Absolute Antibody, Shirley, MA) for one hour. Samples were washed three times as described before, and then incubated with 2 mg/mL of Alexa 647-conjugated secondary antibody. After a 1-hour incubation, slides were washed three times with TSM-wash, one time with water, and air dried. Samples were read using an Innopsys Innoscan 710 microarray scanner and data was processed using the Mapix software version 8.1.0.

Nanoparticle tracking analysis (NTA)

Viral particle concentration of replication-incompetent virus preparations were quantified using a NanoSight NS300 nanoparticle tracker analyzer (Malvern, UK). Briefly, samples were diluted in ultrapure water to 10^8-10^9 particles/mL to fit the linear range of the instrument. Particle concentration was determined by recording 60 second

sample videos, five independent times. Data was then analyzed using the Nanoparticle Tracker analysis 3.0 Software (Malvern, UK).

Biolayer Interferometry (BLI) experiments and HA/NA balance assessment

Replication-incompetent viruses were normalized to 50 pM based on the NTA results and BLI experiments were performed as previously described [406]. Briefly, streptavidin sensors were loaded to saturation for 600 s with 5 mg/mL of either Neu5Acα2-3Galβ1-4GlcNAcβ-PAA-biotin (α2,3, 3'SNL, Glycotech, Gaithersburg, MD) or Neu5Acα2-6Galβ1-4GlcNAcβ-PAA-biotin (α2,6, 6'SNL, Glycotech, Gaithersburg, MD) diluted in reaction buffer (PBS supplemented with 1% BSA, 0.1% Tween-20, and 2 mM $CaCl_2$, pH 6.5). Excess receptor was washed away for 300 s. Virus association was performed for 900 s in presence of 10 mM oseltamivir (Sigma-Aldrich, St Louis, MO) followed by a 300 s dissociation step in presence of oseltamivir. To analyze the HA/NA balance, virus association was performed as described above followed by 3 10 s washes in reaction buffer without oseltamivir. Finally, NA-mediated dissociation was measured for 1,800 s in absence of oseltamivir. All measurements were performed using an Octet RED96e System (ForteBio, Dallas, TX).

Results

Vaccination reduced but did not inhibit hVIC/11-A138S replication *in vivo*.

To evaluate the role of previous immunity on the adaptation of a human-origin virus (hVIC/11-A138S) to pigs, animals were primed and boosted with a heterologous commercial vaccine against swine FLUAV, therefore little protection was expected. Pigs were inoculated (seeders, n=3) with hVIC/11-A138S, followed by four transmission rounds **(Fig 5.1a)**. Vaccinated animals exhibited reduced titers compared to non-vaccinated pigs, with an average of $1x10^4$ $TCID_{50}$eq/mL. Nonetheless, the virus was still transmitted and although differences were not statistically significant, a trend toward higher titers was observed in contact 4 pigs **(Fig 5.1b)**. Titration of viral loads in nasal swabs samples from non-vaccinated animals showed replication and transmission of the virus to all contacts pigs with an average titer of $1x10^5$ $TCID_{50}$eq/mL **(Fig 5.1c)**. This effect was stronger in BALF samples, in which no virus was detected initially, but in contact 4 pigs hVIC/11-A138S was observed in the lungs **(Fig 5.1d)**. Antibody levels were consistent throughout the study and no significant variation was observed between the antibody titers detected at 14 days post-boost and the day the pigs were placed as contacts **(Fig 5.1e)**. These results show that vaccination reduced, but did not prevent, hVIC/11-A138S infection. Replication levels seemed to increase with every contact, noted as higher titers in nasal swabs and BALF samples in later contacts, suggesting that the original hVIC/11-A138S virus may have evolved during the transmission study.

Transmission in vaccinated animals selected for mutation in the HA and NA proteins.

Nasal swabs samples with a Ct value ≥30 were sequenced using next generation sequencing. After analysis of sequences, we detected that the A138S mutation in the HA was lost around 3 dpi in seeders pigs. Two mutations in the HA RBS were detected in contact 1 pigs: V186G and F193Y. Both mutations were transmitted to contact 2 pigs. The V186G appeared to be transient as it was not detected through all the transmission chains. However, the F193Y became fixed and was prevalent in contact 3 and 4 pigs **(S5.1 Table)**. All the amino acid changes detected occurred in the vicinity of the HA RBS, but the majority of the residues did not appear to directly interact with sialic acid **(Fig 5.2a)**. A point mutation in the NA, D113A appeared in contact 1 pigs but reverted to D113 in contact 2 pigs, and no further changes were detected in the NA protein **(S5.2 Table)**.

To characterize the impact of these mutations, we constructed recombinant viruses carrying single (A138S, V186G, or F193Y), double (A138S+V186G, A138S+F193Y, or V186G+F193Y), or three mutations (A138S+V186G+F193Y) in the HA with or without the mutation in the NA (D113A). Replication in MDCK cells revealed no major changes in growth among the variants compared to a swine-adapted control virus (sOH/04) or the precursor virus hVIC/11 **(S5.1 Fig)**. Similarly, introduction of D113A in the NA did not have any impact on replication.

To assess if these mutations would result in fitness loss in humans, the mutant viruses growth kinetics were assessed in differentiated human airway epithelial cells. No changes were observed in the replication kinetics of hVIC/11 **(Fig 5.2b)**, hVIC/11-A138S

(Fig 5.2c), and hVIC/11-V186G **(Fig 5.2d)** even when the NA D113A mutation was also present. The hVIC/11-F193Y showed reduced titers when the D113A amino acid change was also present (**Fig 5.2e).** No changes in replication were observed for the double and triple mutants regardless of the amino acid present at position 113 in the NA **(Fig 5.2f-i)**. sOH/04 was used as control and exhibited replication with a maximum titer of 10^5 $TCID_{50}$eq/mL at 48 hpi **(Fig 5.2j)**. Overall, our data shows that vaccination promoted evolution of hVIC/11-A138S *in vivo,* which resulted in changes in the HA and NA surface proteins. However, these changes did not impact the viruses' ability to infect and replicate in human tracheal cells.

F193Y reduced HA antibody recognition and prevented NA neutralization.

To assess if the mutations affected antigenicity, we evaluated serum samples collected from vaccinated animals against the mutant viruses. The vaccine resulted in low levels of neutralizing antibodies against hVIC/11 (ISD50: <20, **Fig 5.3a)**. Nonetheless, hVIC/11- A138S, showed elevated neutralization levels (ISD50: 405, **Fig 5.3b**). Neutralization titers were significantly reduced for the V186G (ISD50 131.4) and the F193Y (ISD50 49.94) mutants compared to the challenge strain, this last one showing the highest impact in neutralization titers (**Fig 5.3c and d**). These lower titers observed in the single mutants led to lower titers in all combinations of double mutants (**Fig 5.3e-g**) (A138S+V186G: 78.98 ISD50, A138S+F193Y: 73.02 ISD50, and V186G+F193Y: 86.15 ISD50). However, the triple mutant combination hVIC/11-A138S+V186G+F193Y exhibited an increase in ISD50 titers compared to the double mutants (ISD50 of 239.6) but remained lower than the original hVIC/11-A138S **(Fig 5.3h)**. The

A/swine/NY/01104005/2011 H3N2 (NY/11) virus was used as a control as it it from the same genetic clade as the vaccine and is likely to be antigenically similar to the vaccine antigen **(Fig 5.3i)**. This virus exhibited the highest levels of neutralization with an ISD50 of 650. The swine control virus sOH/04 had low levels of neutralizing antibodies (ID50: 24.29, **Fig 5.3j**): this swine virus is from the same lineage as components in the vaccine (1990.4), but isolated more than a decade prior to formulation. Interestingly, introduction of the D113A mutation in the NA had an impact on neutralization titers, but the impact varied with the HA mutations present. For example, introduction of D113A increased neutralization titers in the hVIC/11 virus but reduced titers for the hVIC/11-A138S virus. Notably, hVIC/11-F193, which eventually became fixed, showed increased titers with the D113A change (WT NA: 49.94 ISD560 vs D113A NA: 181.1 ISD50).

To understand the role of the NA amino acid change, we performed a neuraminidase inhibition (NI) assay **(Fig 5.3k, S5.2 Fig)**. This assay revealed that, overall, the D113A only slightly increased the NI titers for mutant viruses except for hVIC/11-F193Y/D113A, which showed an increase compared to hVIC/11-F193Y, although this difference was not statistically significant. As expected, there were no major differences between mutants with or without the D113A NA mutation in hemagglutination inhibition titers **(Fig 5.3l)**, although hVIC/11-F193Y showed significantly higher titers if the D113A mutation was present. The F193Y HA and wild type NA showed a decrease in the HI titers (>40) compared to all mutant viruses, including the originals hVIC/11 and hVIC/11-A138S viruses. Noteworthy, hVIC/11-V186G HI titers could not be determined as the virus did not agglutinate chicken nor turkey red blood cells (RBCs). Together, our results show that F193Y represents an

advantage for hVIC/11 under immune pressure as it decreases the antigenicity of the HA, which led to reduced neutralization.

Acquisition of swine-adaptative mutations reduced the breadth of glycans supporting hVIC/11 binding.

Although amino acid substitutions detected in this study (A138S, V186G, and F193Y) were in close proximity to the HA RBS, modeling onto the previous published hVIC/11 HA crystal structure revealed that none of them directly interacts with sialic acid **(S5.3 Fig)**. Hydrogen bond interactions with sialic acid were only seen with residues R222, N225, Y98, S137, T135, and D190. Due to the proximity of positions 138, 186, and 193 to the RBS pocket, the affinity of the mutant HAs for different SA structures was analyzed using a glycan array system focusing on biologically relevant complex N-glycans exhibiting terminal a2,6 Neu5Ac, a2,3 Neu5Ac, a2,6 Neu5Gc, or a2,3 Neu5Gc.

No binding was observed to a2,3 Neu5Ac nor a2,3 Neu5Gc structures **(S5.4 Fig)**, regardless of the number of N-Acetyllactosamine (LacNAc) repeats. Similarly, none of the viruses showed binding to 2,3 Neu5Gc. The affinity for different a2,6 SA structures was also evaluated **(Fig 5.4).** All mutant viruses retained the ability to bind to a2,6 Neu5Ac **(Fig 5.4 b-i)**, with no preference for single- bi- or tri-antennary structures. The hVIC/11 HA did not bind to structures containing 1 LacNAc repeat, and a minimum of two repeats was necessary for efficient binding **(Fig 5.4b)**. Interestingly, this virus bound to Neu5Gc. Introduction of A138S in the hVIC/11 HA (hVIC/11-A138S) restricted the set of glycans supporting binding as no binding was detected with a2,6 Neu5Ac structures containing less than 3 LacNAc repeats **(Fig 5.4c)**. Additionally, hVIC/11-

A138S, lost the ability to bind any of the Neu5Gc structures tested. hVIC/11-V186G did not show significant binding to any of the structures included in the analysis **(Fig 5.4d)** which correlates with the previous observation that it cannot agglutinate turkey RBCs. hVIC/11-F193Y **(Fig 5.4 e)** exhibited a similar binding pattern as hVIC/11-A138S and no important differences were detected. Combination of two HA mutations (A138S+V186G, A138S+V186G, and V186G+F193Y, **Fig 5.4 f-h**) had no impact on binding as they exhibited similar preference as the single mutants. Lastly, combination of all three mutations (hVIC/11-A138S+V186G+F193) showed an increase of structures supporting binding as this mutant recognized glycans containing as little as one LacNAc repeat (**Fig 5.4i)**. Additionally, hVIC/11-A138S+V186G+F193Y recovered binding to Neu5Gc. Assessment of sOH/04 binding revealed the virus can recognize a large pool of glycans, including single-, bi-, and tri-antennary structures. This virus also bound to Neu5Gc. Taken together, these results suggest that acquisition of mutations in the swine host reduced the pool of glycans supporting hVIC/11 binding, recognizing only a subset of structures with a minimum of three LacNAc repeats and avoiding Neu5Gc recognition.

F193Y enhances affinity for a2,6 Neu5Ac.

Receptor affinity for a2,3 and a2,6 SA was evaluated by biolayer interferometry (BLI). Probes were loaded with either Neu5Acα2-3Galβ1-4GlcNAcβ-PAA-biotin (α2,3, 3'SNL) or Neu5Acα2-6Galβ1-4GlcNAcβ-PAA-biotin (α2,6, 6'SNL). Virus was bound for 900 s in presence of oseltamivir carboxylate (OC) followed by a dissociation step for 300 s in presence of OC. hVIC/11 and all its derived viruses (**Fig 5.5a-h)** presented minimal binding to 3'SNL and the mutants differed in binding affinity to 6'SNL

compared to hVIC/11. sOH/04 exhibited low binding for 3'SLN and a preference for 6'SLN **(Fig 5.5i)**. Notably, all the mutants had increased affinity for 6'SNL compared to hVIC/11, with hVIC/11-A138S and hVIC/11-F193Y showing a three-times higher affinity than hVIC/11 but no differences in binding between them or sOH/04 **(Fig 5.5j)**. The combination of two or more mutations in the HA of hVIC/11 significantly increased affinity for 6'SNL. Nonetheless, this enhanced binding did not directly translate into increased binding strength, as hVIC/11 and hVIC/11-A138S+V186G had increased elution rates compared to sOH/04, hVIC/11-V186G, hVIC/11-F193Y, and hVIC/11-A138S+V186G+F193Y **(Fig 5.5k)**. None of the mutants showed viral particle release by the end of the experiment, suggesting an increased affinity for 6'SNL compared to hVIC/11 that resembled the swine-adapted sOH/04. Taken together, these results demonstrate that introduction of mutations into a human seasonal H3 HA that emerged in the animal study increase binding affinity to a2,6-type SA, with some mutations (V186G and F193Y) also leading to reduced elution rates, suggesting an increased strength of the interaction with the receptor.

D113A in the NA minimally impacts the HA/NA balance when F193Y is present in the HA.

We have previously shown that the D113A mutation in the NA serves as a compensatory mutation to restore the HA/NA balance by modulating NA activity when the A138S amino acid change is present in the HA (Chapter 4). In this study, the D113A mutation was only detected as a major variant in contact 1 pigs. To understand if the loss of the D113A mutation was due to a disturbed HA/NA balance with other HA mutants,

we used BLI to assess the elution of the viruses from the sensor in presence of NA activity. The hVIC/11 showed fast elution times regardless of the NA present **(Fig 5.5a),** and this was different from the sOH/04 that took 804 s to elute 50% of total virus bound **(Fig 5.6b, S5.3 Table)**. The hVIC/11-A138S **(Fig 5.5c)** had increased elution times when carrying a WT NA compared to hVIC/11, and the elution time was increased upon introduction of the D113A mutation, resembling sOH/04. Introduction of D113A with a hVIC/11-V186G HA increased the elution rate **(Fig 5.6d)**, although to a lesser extent compared to hVIC/11-A138S. The hVIC/11-F193Y exhibited little change in the self-elution rate observed with or without the D113A amino acid change **(Fig 5.6e)**. The elution rate displayed when a WT NA was present (688 s) was close to sOH/04 and increased compared to hVIC/11 and hVIC/11-A138S carrying a WT NA. The impact of the D113A mutation in the NA became less evident when two or more mutations were present together in the HA **(Fig 6f-i),** and this was similar to the association rate results described above. The hVIC/11-A138S+V186G+F193Y HA showed the slowest self-elution rate out of all the mutants, which was further increased after introduction of D113A in the NA, suggesting that combination of all three mutations enhances affinity for 6'SNL. Taken together, these results show that D113A generally increases the self-elution rate of the viruses, but its impact on the HA/NA balance decreases when the viruses carry an HA that has a high affinity for SA.

Discussion

Influenza infection is a contributing factor to the porcine respiratory disease complex, causing important economic loses in the swine industry [407]. Vaccination is the main strategy used to control FLUAV infection, and all of the current vaccines approved in the United Stated are inactivated or vectored products [84]. These vaccines lead to a strong antibody response against the FLUAV surface proteins HA and NA that limits infection but does not prevent it [284], which imposes a selective pressure that may result in mutations emerging that reduce antibody recognition [87, 88, 396]. Evasion of the host immune response may also have the indirect impact of driving the evolution of novel strains to become more fit in a new host. However, despite the relatively frequent spillover of human FLUAV into vaccinated herds, the role of prior immunity to endemic swine viruses on the evolution of human-origin FLUAV within pigs is unknown.

Mutations in the HA RBS have been identified as critical for adaptation of avian viruses to pigs [408], normally enhancing or completely switching affinity from a2,3 SA to a2,6 SA [409, 410]. However, it is unclear why human-seasonal viruses bind less efficiently and replicate poorly in pigs when both hosts exhibit a2,6 SA in the respiratory tract [25] [27]. Using our previously established *in vivo* transmission system in pigs [27, 258], we evaluated the role of prior immunity on the evolution of a human H3N2 virus to pigs. Vaccination induced an antibody response against FLUAV but did not prevent hVIC/11-A138S infection and subsequent transmission, highlighting that cross-reactive vaccination immunity may not always prevent human-to-swine spillover events. Sequencing of nasal swabs samples revealed that after infection the S138 reverted back to A138 while V186G and F193Y amino acid changes evolved. These mutations may have

emerged as a consequence of cross-reactive neutralization titers observed associated with the S138 mutation. From these, Y193 was the only mutation that was maintained throughout 4 separate transmission events; the V186G mutation was not detected after the first transmission event (contact 1). These mutations have been previously shown to enhance binding to swine cells [27], to similar levels as A138S, suggesting they result in a replication advantage for a human-origin virus in pigs. Since F193Y exhibited the lowest HI and microneutralization titers, its selection was likely due to its capacity to escape the antibody response while also showing high replication efficiency in the swine host. F193 is located in the antigenic site B of the HA [27] and changes at this position have been previously shown to promote immune escape [411], highlighting that immune escape is a necessary evolution step during adaptation to a new host under immune pressure [412]. An increase in viral titers was detected with every subsequent transmission, reaching the highest titer in contact 4 pigs when lung replication was detected, suggesting that the F193Y mutation that was selected in place of A138S also promoted improved replication in the swine lower respiratory tract.

Neuraminidase inhibition (NI) titers were considerably lower than HI titers, suggesting that the immune response mounted by the commercial vaccine that we used mainly targeted the HA protein. Nonetheless, D113A was shown to increase NI titers in most of the viruses we tested, regardless of the mutations we introduced in the HA1. The 113 residue in the NA is located in the symmetry axis of the tetramer and can modulate tetramer stability [35]. Therefore, changes in this pocket could destabilize the tetramer, indirectly affecting NI cross-reactivity. Our data also showed that the D113A also

increased HI titers, suggesting that antibody binding in this pocket could potentially sterically interfere with the HA protein as has been previously described [413].

Receptor specificity is one of the main factors limiting FLUAV interspecies transmission, and while this has been widely studied at the avian-mammalian interface [200, 389, 414], little is known about glycan specificity of human versus swine viruses. Neu5Gc has been proposed as a candidate glycan modulating adaptation of human viruses to pigs [254]. However, our data suggests that Neu5Gc may not be relevant in this process as the human seasonal H3N2 hVIC/11, a virus that fails to transmit in pigs, is able to bind it, but introduction of mutations such as A138S, which has been previously demonstrated as a determinant of transmissibility in swine [258], abolishes this interaction. Pigs exhibit higher levels of a2,3 SA in the lower respiratory tract than humans, which makes them more susceptible to avian FLUAV infection [25]. Nonetheless, a2,3 SA (or dual receptor) recognition does not seem to play a major role during the adaptation process of human seasonal viruses to swine since none of the variants bound to any of the a2,3 glycans tested in the glycan array nor exhibit significant binding to 3'SLN in the BLI experiments. In recent years glycan topology has been pointed as a determinant for FLUAV evolution and adaptation [28], and human H3N2 viruses have evolved to recognize branched, extended glycan structures [415]. We found that hVIC/11 bound to glycans containing a minimum of 2 LacNAc repeats: the mutant viruses we tested lacked the ability to bind any structure shorter than 3 LacNAc repeats. This suggests that during adaptation, the human-origin FLUAV reduced the pool of glycan supporting binding, being restricted to extended structures. However, the reduction of receptors supporting binding was accompanied by an increase in binding

affinity for a2,6 SA, likely compensatory step that reduces non-productive HA-SA interactions.

The HA and NA proteins exhibit complementary functions and a functional balance between HA avidity and NA activity must be achieved to produce a successful infection and transmission. While HA binds SA to promote entry, NA cleaves SA to prevent binding to decoy receptors through the respiratory mucus and allow virion progeny release [205, 416]. Utilizing biolayer interferometry, we measured the HA/NA balance defined as the time it takes the virus to self-elute from a sialilated surface [32]. We found that hVIC/11 had the shortest elution time, regardless of the NA tested, most likely due to the poor binding exhibited to either 3'SLN and 6'SLN. Introduction of mutations in the hVIC/11 HA RBS greatly increased binding affinity for 6'SLN. This was evident for the hVIC/11-A138S, the original inoculum virus that we previously showed had a disrupted HA/NA balance (Chapter 4). Here we demonstrated that acquiring D113A mutation in the NA restored the balance to similar levels as the swine FLUAV control. However, in the transmission chains, the D113A substitution was lost as soon as the A138S reverted. Our NI data suggests that A113 is more strongly inhibited by vaccine-induced antibodies than D113, suggesting A113 may not have been transmitted due to evolution to escape the immune response coupled with evolution to maintain the HA/NA balance with A138. The F193Y mutation exhibited a reduced antibody neutralization and, hence, was able to escape the antibody response, did not seem to require changes in the NA to maintain an HA/NA balance, which ultimately resulted in its selection during transmission in immune pigs [417, 418]. Increasing the number of mutations in the hVIC/11 HA led to increased self-elution times regardless of the amino acid present at

113 NA position, most likely due to the increased affinity observed for 6'SLN, highlighting that stronger HA avidity may not be compensated by single NA changes.

Overall, our results demonstrate that prior immunity derived from a heterologous vaccine influences the evolution of human viruses in the adaptation process to pigs. This selective force results in the transmission of viruses that have mutations that facilitate antibody escape while maintaining a2,6 SA binding. However, some mutations that emerge in the human virus during transmission under this selective pressure reduce the pool of receptors supporting binding, and viruses were restricted to extended glycans with at least 3 LacNAc repeats. This suggests that glycan topology has an important role in the adaptation of human FLUAV in the swine host following human-to-swine transmission events. All the molecular changes we document are constrained as the virus must maintain a functional HA/NA balance to allow infection and transmission. Our work highlights the role of glycan topology and receptor affinity rather than a switch in the receptor binding preference as critical components of the adaptation of human H3N2 viruses to the swine host.

Figures and Tables

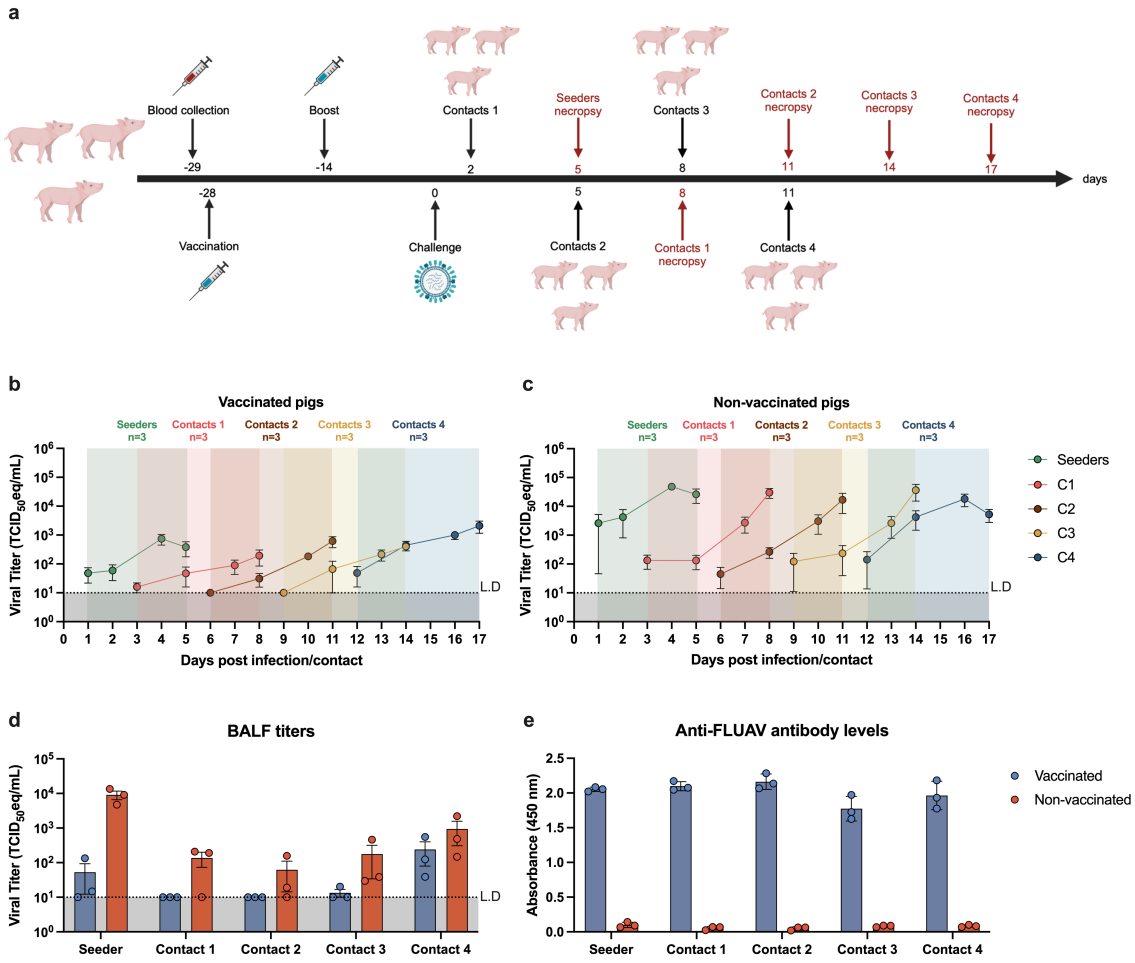

Fig 5.1. Vaccination does not prevent hVIC/11-A138S infection and transmission. a. Animals were immunized in a prime-boost regimen. 14 days post-boost, pigs were challenged with hVIC/11-A138S (seeders). At 5 dpi, seeders pigs were euthanized, and three new pigs within the same vaccine status (vaccinated or not) were introduced as contacts (C1). This process was repeated for a total of four rounds of transmission. Nasal swabs were collected from vaccinated **(b)** or non-vaccinated **(c)** during the study and further titrated by RT-qPCR. Similarly, virus present in bronchoalveolar lavage fluid (BALF) was titrated by RT-qPCR **(d).** Anti-FLUAV antibody levels were measured for all vaccinated and non-vaccinated pigs at 14 days post-boost and the day they were placed as contacts by ELISA. Samples are presented as the mean of three pigs $\pm$ SEM.

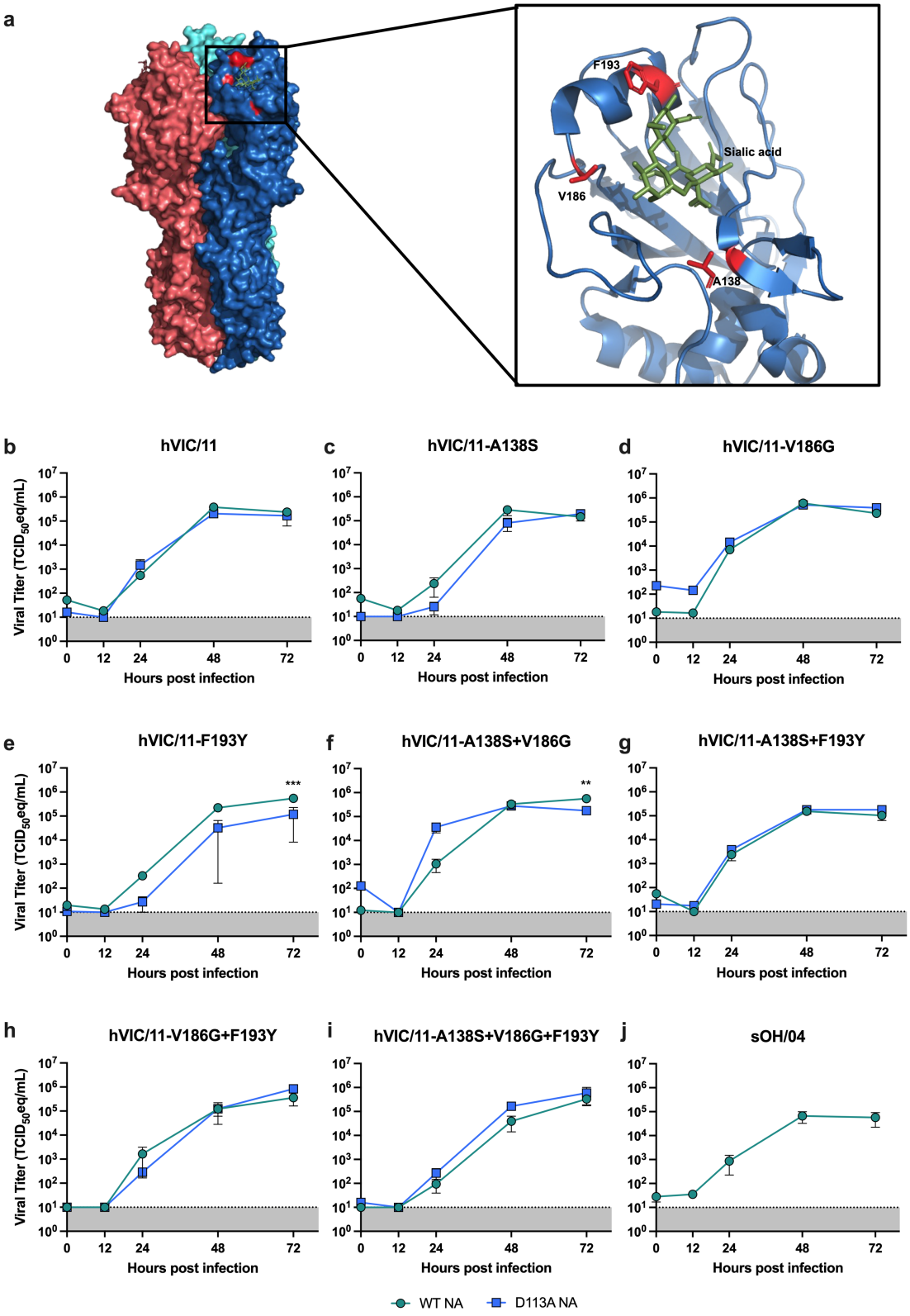
a
F193
Sialic acid
V186
A138
b
hVIC/11
c
hVIC/11-A138S
d
hVIC/11-V186G
e
hVIC/11-F193Y
f
hVIC/11-A138S+V186G
g
hVIC/11-A138S+F193Y
h
hVIC/11-V186G+F193Y
i
hVIC/11-A138S+V186G+F193Y
j
sOH/04
Viral Titer (TCID50eq/mL)
Hours post infection
***
**
WT NA
D113A NA

Fig 5.2. Mutations acquired in the hVIC/11 HA do not affect replication in HAE cells. a. hVIC/11 trimer highlighting in blue the receptor binding site and in red residues 138, 186, and 193. Parental hVIC/11 and mutant viruses carrying A138S, V186G, and F193Y mutations in all possible combinations were rescued by reverse genetics and replication was assessed in differentiated HAE cells **(b-i)**. Replication of viruses carrying either a WT hVIC/11 NA (green) or a hVIC/11 D113A-NA (blue) in addition to the aforementioned HA amino acid changes was also assessed. The swine adapted sOH/04 virus was used as a control (j). Cells were infected at an MOI of 0.01 and supernatant was collected at 0, 12-, 24-, 48-, and 72-hours post-infection. Viral titers were determined by RT-qPCR. Data is presented as the mean of three independent experiments $\pm$ SEM.

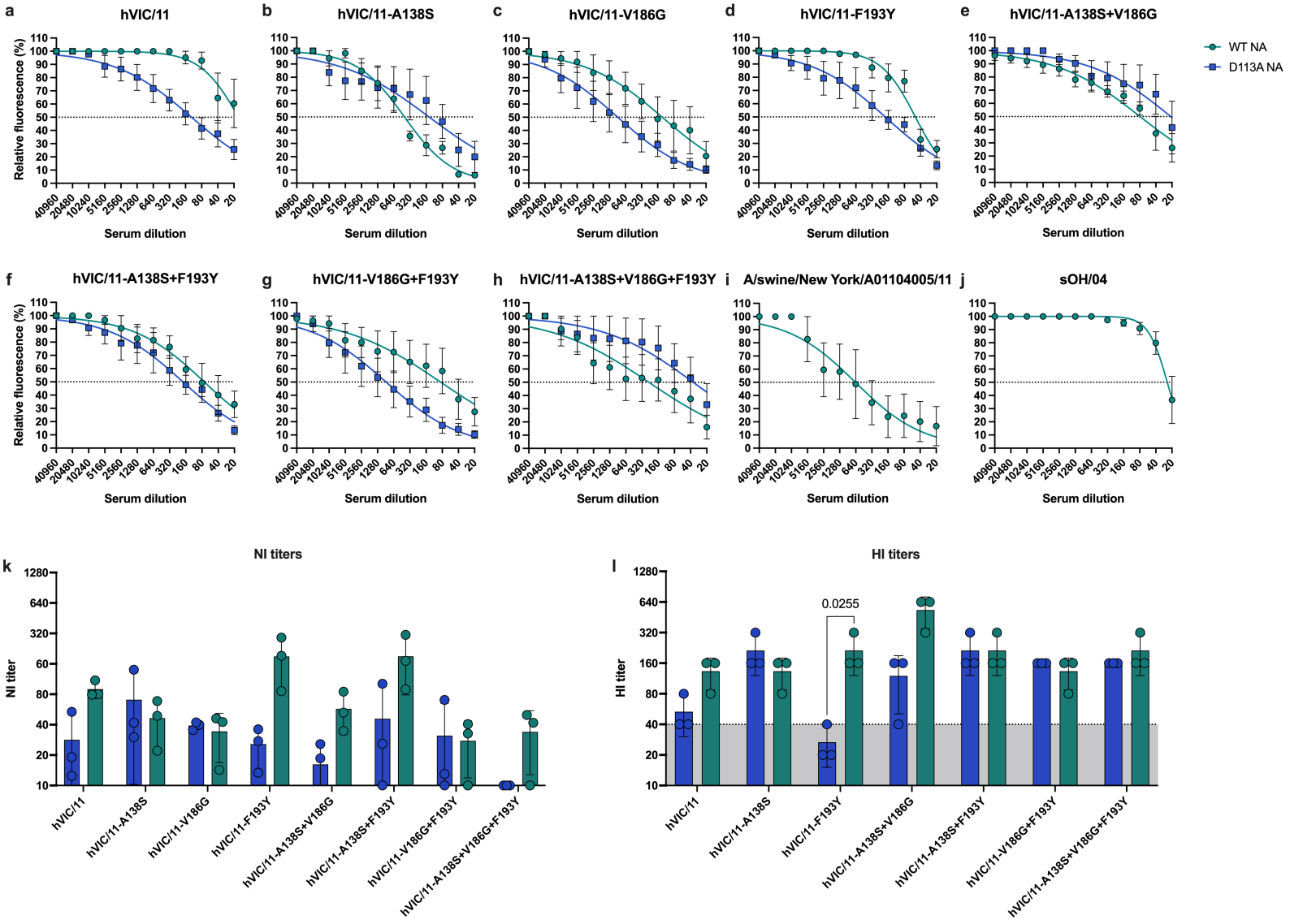
a
hVIC/11
b
hVIC/11-A138S
c
hVIC/11-V186G
d
hVIC/11-F193Y
e
hVIC/11-A138S+V186G
WT NA
D113A NA
Relative fluorescence (%)
Serum dilution
f
hVIC/11-A138S+F193Y
g
hVIC/11-V186G+F193Y
h
hVIC/11-A138S+V186G+F193Y
i
A/swine/New York/A01104005/11
j
sOH/04
k
NI titers
NI titer
l
HI titers
HI titer
0.0255
hVIC/11
hVIC/11-A138S
hVIC/11-V186G
hVIC/11-F193Y
hVIC/11-A138S+V186G
hVIC/11-A138S+F193Y
hVIC/11-V186G+F193Y
hVIC/11-A138S+V186G+F193Y

Fig 5.3. F193Y strongly reduced HA recognition by sera antibodies. Serum samples collected 14 days post boost were analyzed for the antibody response. Microneutralization assays against all hVIC/11 HA and NA variants **(a-h)**, A/swine/New York/A0110405/11 **(i)** representing an antigenically similar vaccine control, and sOH/04 **(j)** were performed by incubating 100 $TCID_{50}$ of each virus with different sera dilutions. Inhibitory titers are shown as the inhibitory sera solution 50 (ISD50). Dotted line represents the 50% inhibition. **k.** The presence of anti-NA antibodies was assessed by evaluating NA activity using MUNANA at different sera dilutions. Neuraminidase inhibition titers (NI) are shown as the sera dilution in which 50% of NA activity was lost compared to the no serum control. **l.** Hemagglutination inhibition (HI) titers were determined except for hVIC/11-V186G. Dotted line represents an HI titer of 40. Data is shown as the mean of three independent experiments $\pm$ SD.

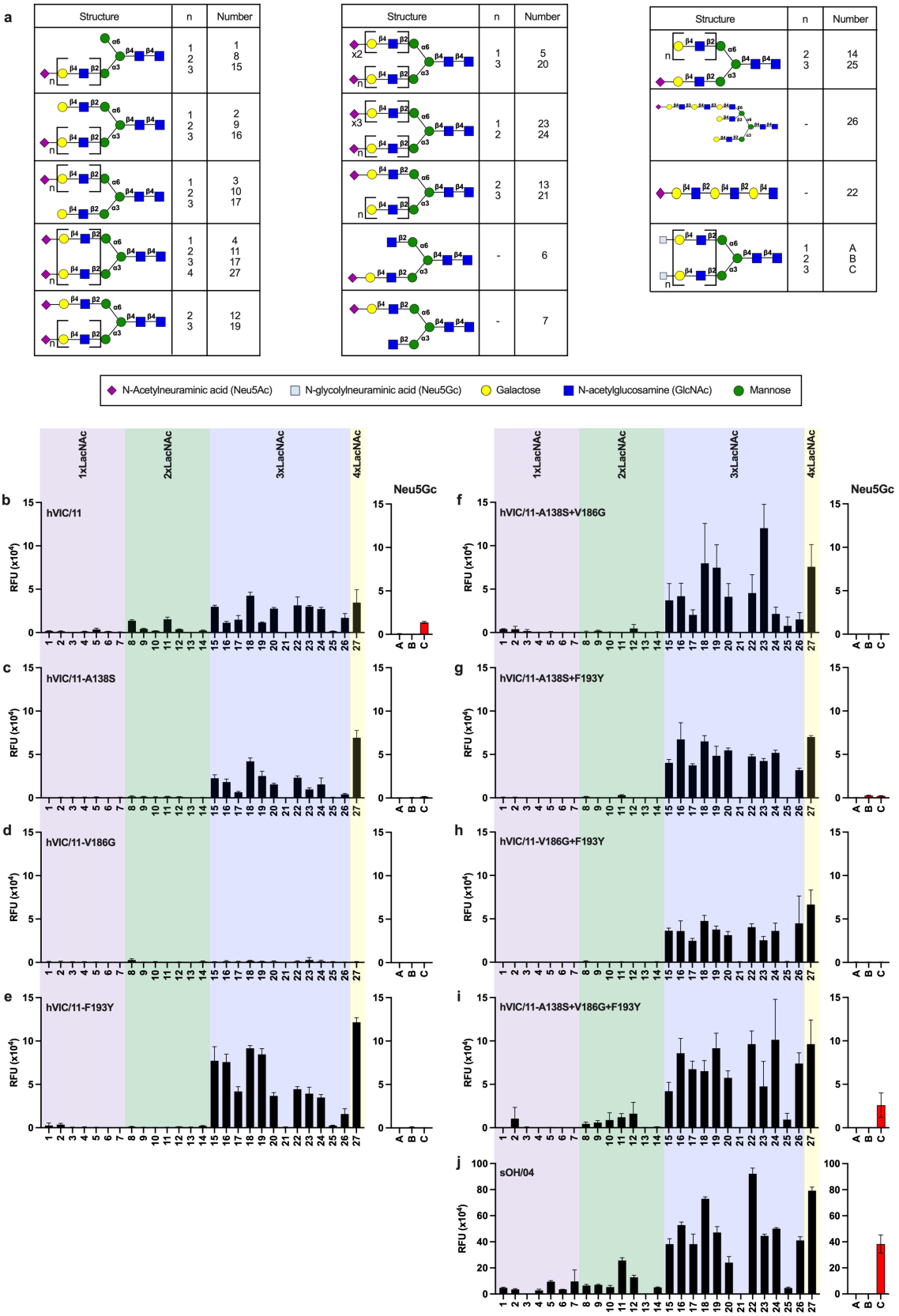
a
Structure
n
Number
1 2 3
1 8 15
1 2 3
2 9 16
1 2 3
3 10 17
1 2 3 4
4 11 17 27
2 3
12 19
x2
1 3
5 20
x3
1 2
23 24
2 3
13 21
-
6
-
7
2 3
14 25
-
26
-
22
1 2 3
A B C
N-Acetylneuraminic acid (Neu5Ac)
N-glycolylneuraminic acid (Neu5Gc)
Galactose
N-acetylglucosamine (GlcNAc)
Mannose
1xLacNAc
2xLacNAc
3xLacNAc
4xLacNAc
Neu5Gc
b
hVIC/11
c
hVIC/11-A138S
d
hVIC/11-V186G
e
hVIC/11-F193Y
f
hVIC/11-A138S+V186G
g
hVIC/11-A138S+F193Y
h
hVIC/11-V186G+F193Y
i
hVIC/11-A138S+V186G+F193Y
j
sOH/04
RFU (x10⁴)

Fig 5.4. Swine-adaptative mutation limit the pool of a2,6 glycans supporting FLUAV binding. a. Structure of glycans assessed on the array. Mutant viruses (b-i) binding preference for different a2,6 glycans was assessed by glycan array. Viruses were normalized to 8 HAU and binding was performed for 1 hour at room temperature. Bound virus was detected using an anti-H3 stalk specific antibody. sOH/04 was used as a swine-adapted virus control (j). Binding to a2,6 Neu5Gc is shown in a separate panel (structures A, B, and C). Data is shown as relative fluorescent units (RFU) $\pm$ SD.

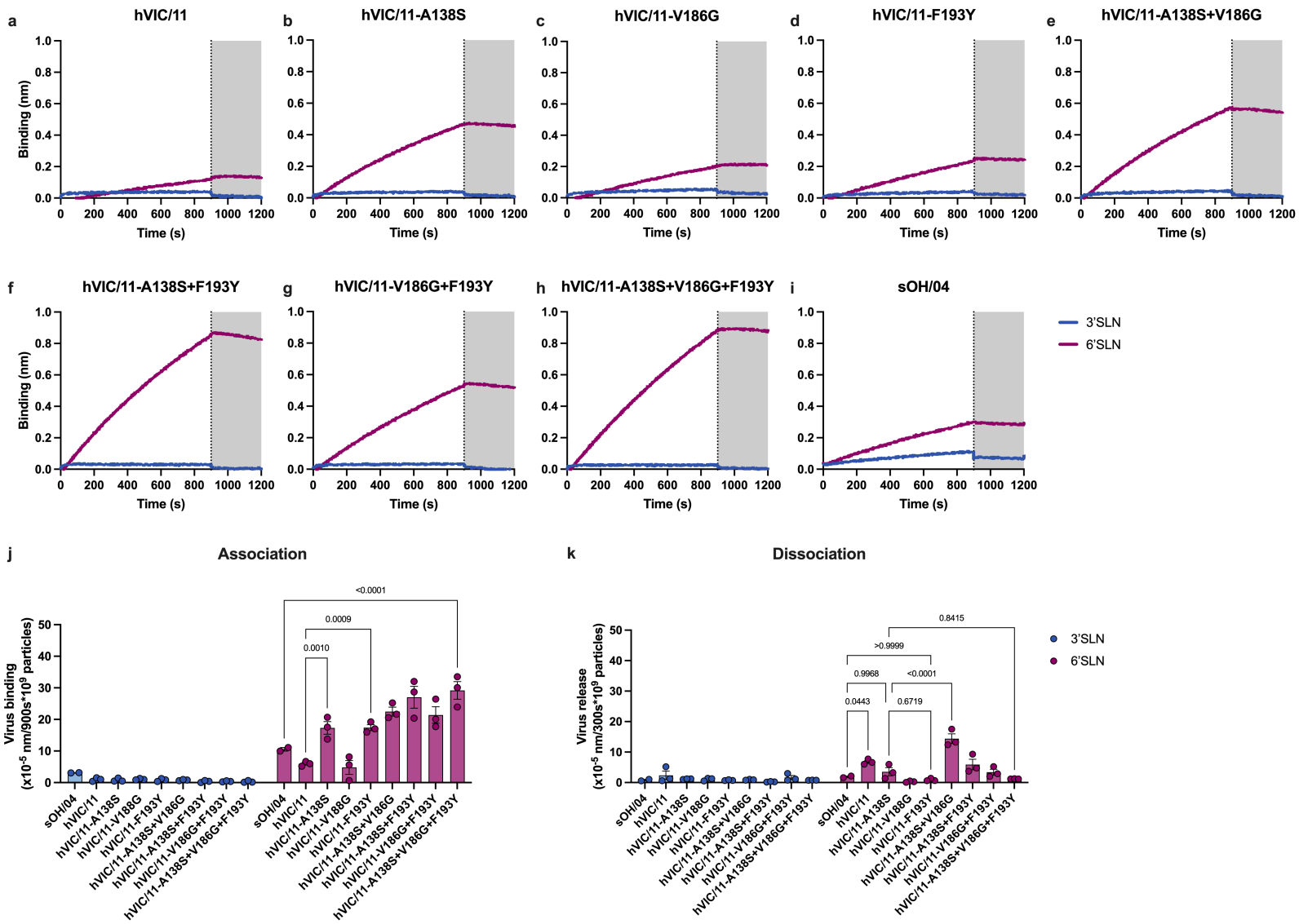
a
hVIC/11
b
hVIC/11-A138S
c
hVIC/11-V186G
d
hVIC/11-F193Y
e
hVIC/11-A138S+V186G
f
hVIC/11-A138S+F193Y
g
hVIC/11-V186G+F193Y
h
hVIC/11-A138S+V186G+F193Y
i
sOH/04
Binding (nm)
Time (s)
3'SLN
6'SLN
j
Association
Virus binding (x10^-5 nm/900s*10^9 particles)
<0.0001
0.0009
0.0010
k
Dissociation
Virus release (x10^-5 nm/300s*10^9 particles)
0.8415
>0.9999
0.9968
<0.0001
0.0443
0.6719
sOH/04
hVIC/11
hVIC/11-A138S
hVIC/11-V188G
hVIC/11-F193Y
hVIC/11-A138S+V186G
hVIC/11-A138S+F193Y
hVIC/11-V186G+F193Y
hVIC/11-A138S+V186G+F193Y

Fig 5.5.HA mutations enhance a2,6 SA binding. Binding affinity for 3'SLN (blue) and 6'SLN (purple) was determined by BLI. Sensors were loaded with each polymer for 600 s. Excess polymer was washed away and binding of 50 nM hVIC/11 **(a),** hVIC/11 HA variants **(b-h**), and the control sOH/04 **(i)** was performed for 900 s in presence of oseltamivir carboxylate. Virus elution in presence of oseltamivir was performed for 300 s. Dotted line represent the dissociation step. Association **(j)** and dissociation **(k)** rate constants were calculated by determining the slope of each curve and normalized to the 10^9 viral particles. Data is presented as the mean of three independent experiments $\pm$ SEM.

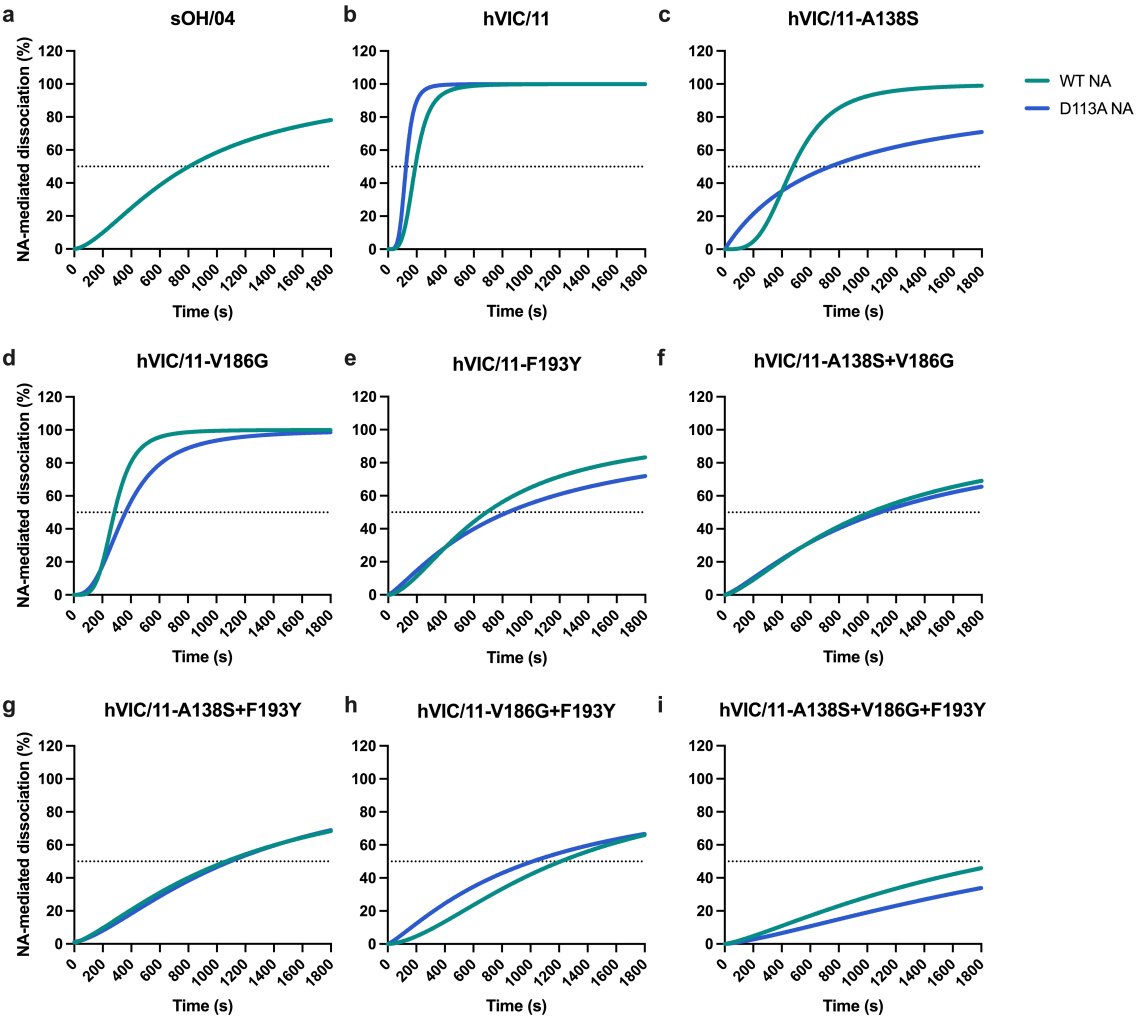
a
sOH/04
b
hVIC/11
c
hVIC/11-A138S
d
hVIC/11-V186G
e
hVIC/11-F193Y
f
hVIC/11-A138S+V186G
g
hVIC/11-A138S+F193Y
h
hVIC/11-V186G+F193Y
i
hVIC/11-A138S+V186G+F193Y
NA-mediated dissociation (%)
Time (s)
WT NA
D113A NA

Fig 5.6. F193Y does not require NA changes to maintain the HA/NA balance. HA/NA balance of viruses carrying an hVIC/11 WT NA (green) or a D113A NA (blue) was evaluated by BLI. 50 nM of hVIC/11 **(a)**, hVIC/11 variants **(b-h),** and sOH/04 **(i)** were bound to sensors previously loaded with 6'SLN for 900 s in presence of oseltamivir. Excess virus was washed away for 10 s in PBS containing oseltamivir, followed by oseltamivir removal by washing three times in PBS for 10 s each wash. NA-mediated virus dissociation was measured for 1,800 s. Elution time in the presence of NA activity was determined by fitting the data to a nonlinear four parameter variable slope equation and was defined as the time in which 50% of the virus was released from the sensor. Data is presented as the mean of three independent experiments $\pm$ SEM.

Table 5.1 Viruses used in this study*.

Abbreviation	Strain	Surface segments
hVIC/11	rgA/Victoria/361/2011	hVIC/11 HA and NA
hVIC/11-A138S	rgA/Victoria/361/2011-A138	hVIC/11 HA A138S and NA
hVIC/11-V186G	rgA/Victoria/361/2011-V186G	hVIC/11 HA V186G and NA
hVIC/11-F193Y	rgA/Victoria/361/2011-F193Y	hVIC/11 HA F193Y and NA
hVIC/11-A138S+V186G	rgA/Victoria/361/2011-A138S+V186G	hVIC/11 HA A138S+V186G and NA
hVIC/11-A138S+F193Y	rgA/Victoria/361/2011-A138S+F193Y	hVIC/11 HA A138S+F193Y and NA
hVIC/11-A138S+V186G +F193Y	rgA/Victoria/361/2011-A138S+V186G+F193Y	hVIC/11 HA A138S+V186G+F193Y and NA
hVIC/11-D113A	rgA/Victoria/361/2011-D113A	hVIC/11 HA and NA D113A
hVIC/11-A138S/D113A	rgA/Victoria/361/2011-A138/D113A	hVIC/11 HA A138S and NA D113A
hVIC/11-V186G	rgA/Victoria/361/2011-V186G	hVIC/11 HA V186G and NA D113A
hVIC/11-F193Y	rgA/Victoria/361/2011-F193Y/D113A	hVIC/11 HA F193Y and NA D113A
hVIC/11-A138S+V186G	rgA/Victoria/361/2011-A138S+V186G/D113A	hVIC/11 HA A138S+V186G and NA D113A
hVIC/11-A138S+F193Y/ D113A	rgA/Victoria/361/2011-A138S+F193Y/D113A	hVIC/11 HA A138S+F193Y and NA D113A
hVIC/11-A138S+V186G +F193Y/D113A	rgA/Victoria/361/2011-A138S+V186G+F193Y/D113A	hVIC/11 HA A138S+V186G+F193Y and NA D113A
sOH/04	rgA/turkey/Ohio/313053/2004	sOH/04 HA and NA
NY/11	rgA/swine/New York/A01104005/2011	NY/11 HA and NA

*All viruses were isogenic rescued in a TRIG backbone.

Supplementary material

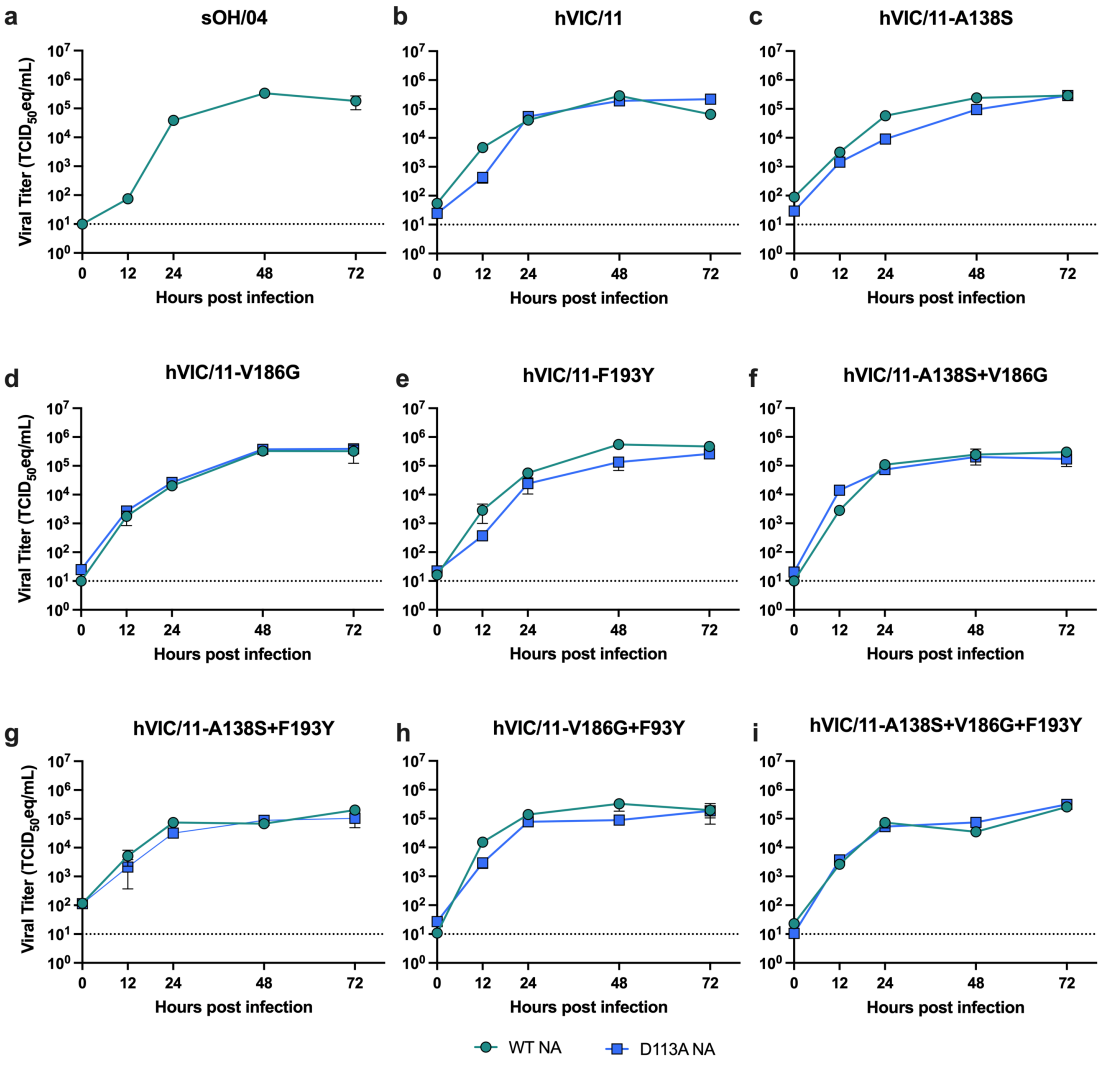

S5.1 Fig. Introduction of swine-adaptative mutations in the hVIC/11 HA does not affect replication in MDCK cells. MDCK cells were infected at an MOI of 0.01 and supernatant aliquots were collected at 0, 12, 24, 48, and 72 hours post infection. Viral titers were determined by RT-qPCR. Dashed line represents the limit of detection. Data is presented as the mean of three independent experiments ± SEM.

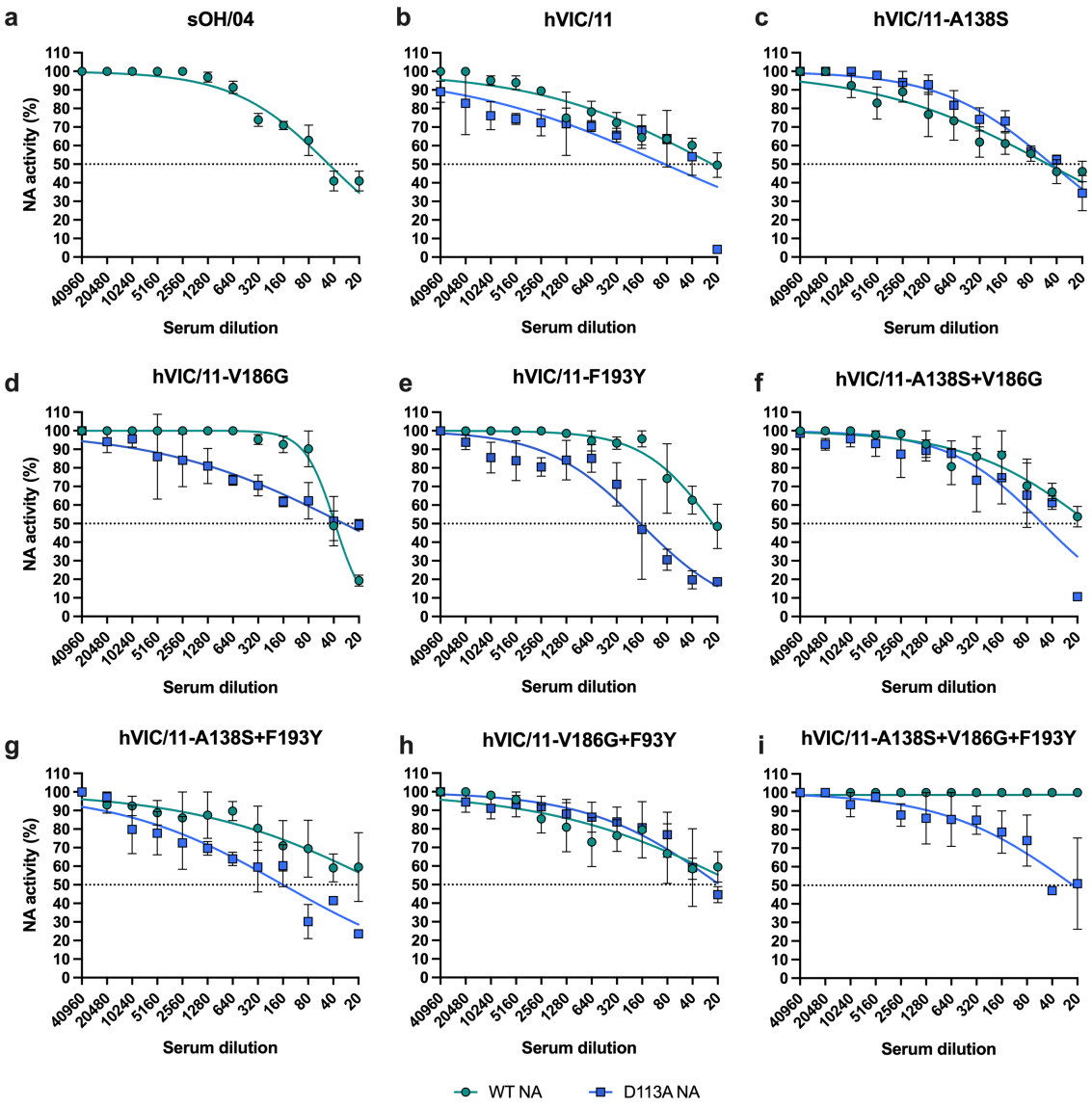

S5.2 Fig. NI titers are modulated by changes in both HA and NA. The presence of anti-NA antibodies in sera samples collected at 14 days post boost was assessed by evaluating NA activity using MUNANA at different sera dilutions. Neuraminidase inhibition titers (NI). Data was adjusted to a non-linear regression and the 50% inhibition was calculated compared to the NA activity observed in the no serum control. Data is presented as the mean of three independent experiments ± SEM.

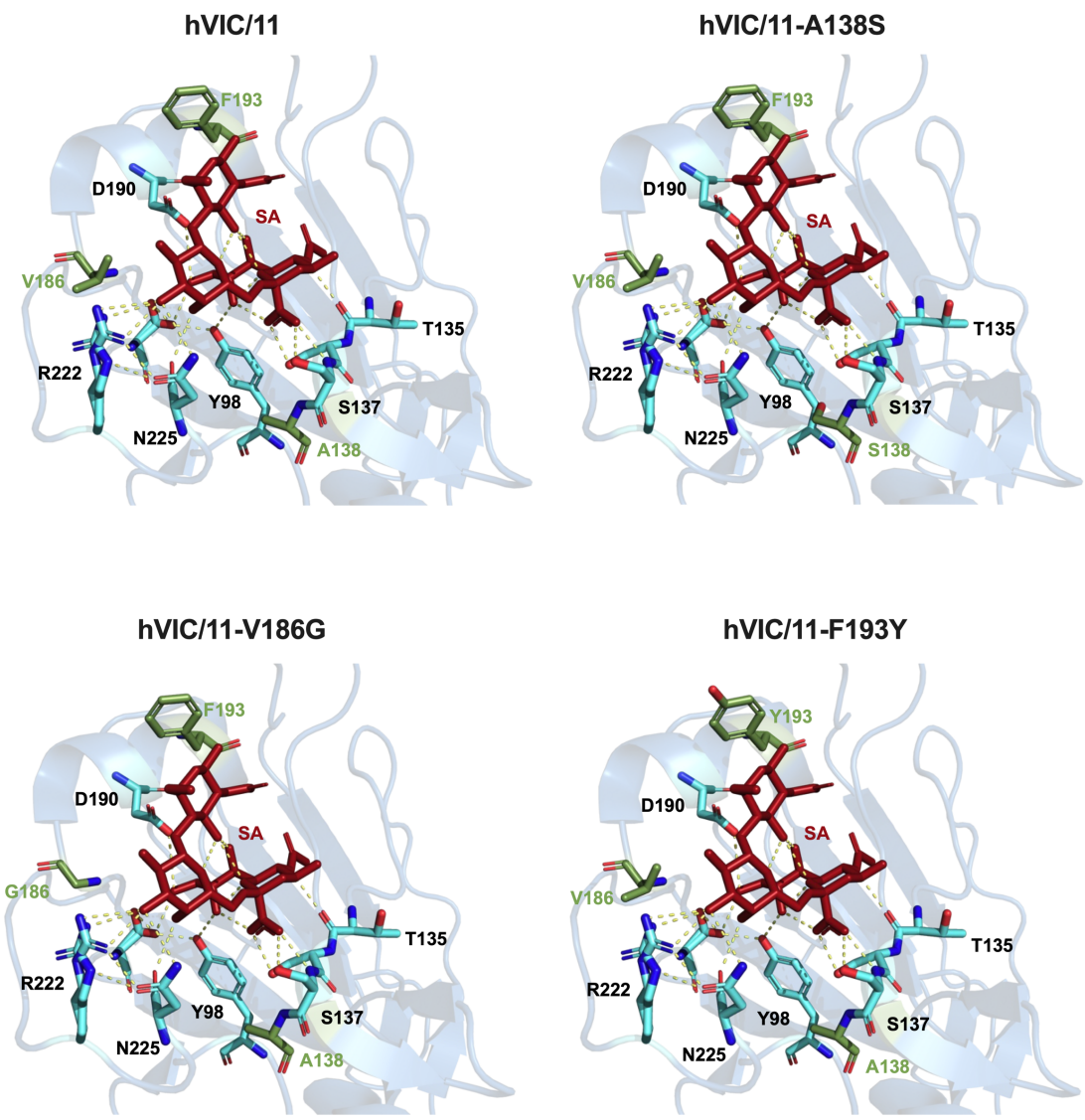

S5.3 Fig. Residues 138, 186, and 193 do not interact directly with sialic acid. Cartoon representation of the hVIC/11 HA RBS showing residues 138, 186, and 193 in green and amino aicds directly interacting with sialic acid in light blue. Model made using PyMOL.

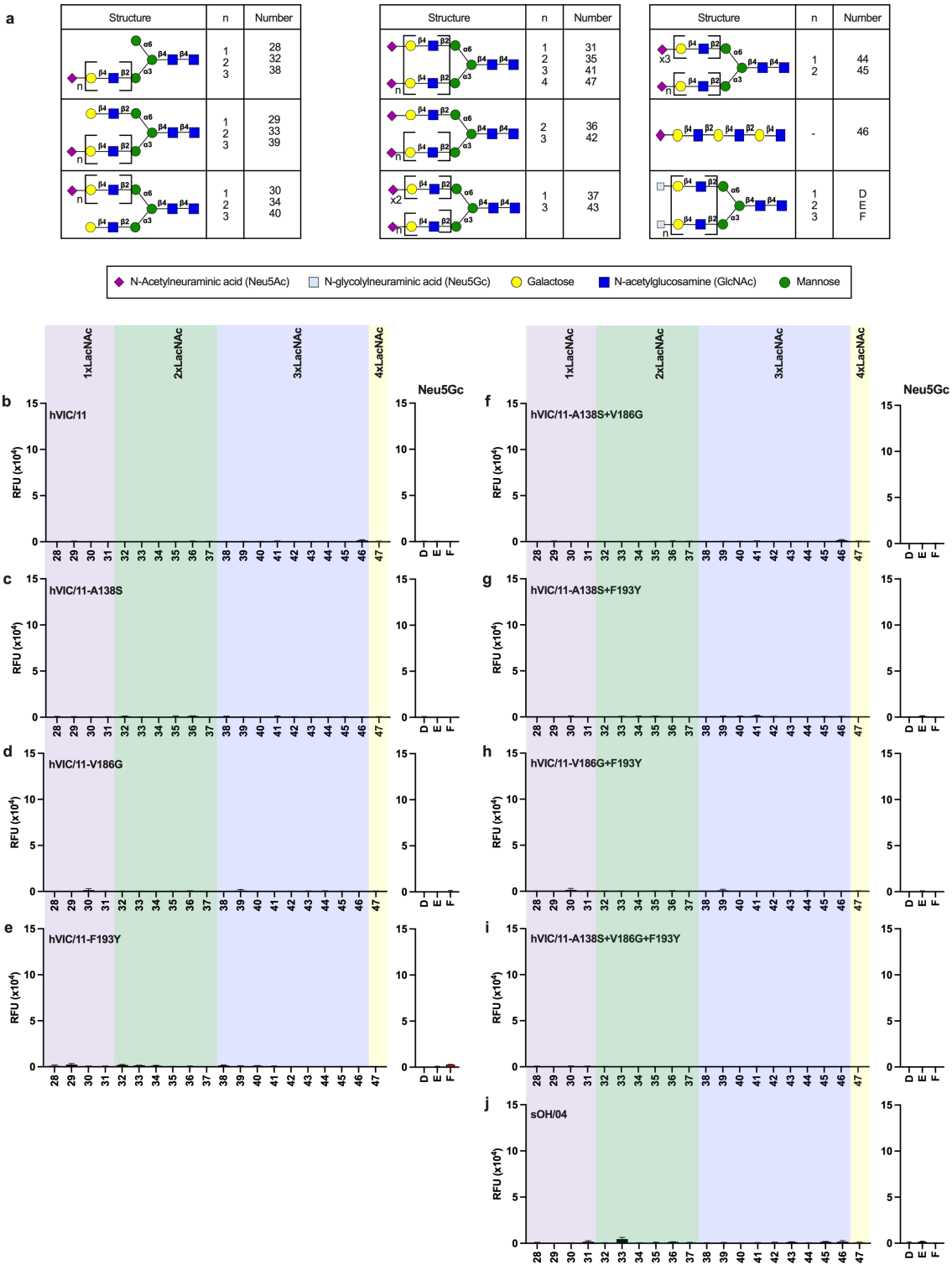
a
Structure
n
Number
1 2 3
28 32 38
1 2 3
29 33 39
1 2 3
30 34 40
1 2 3 4
31 35 41 47
2 3
36 42
1 3
37 43
x3
1 2
44 45
-
46
1 2 3
D E F
x2
N-Acetylneuraminic acid (Neu5Ac)
N-glycolylneuraminic acid (Neu5Gc)
Galactose
N-acetylglucosamine (GlcNAc)
Mannose
1xLacNAc
2xLacNAc
3xLacNAc
4xLacNAc
Neu5Gc
b hVIC/11
c hVIC/11-A138S
d hVIC/11-V186G
e hVIC/11-F193Y
f hVIC/11-A138S+V186G
g hVIC/11-A138S+F193Y
h hVIC/11-V186G+F193Y
i hVIC/11-A138S+V186G+F193Y
j sOH/04
RFU (x10⁴)
0 5 10 15
28 29 30 31 32 33 34 35 36 37 38 39 40 41 42 43 44 45 46 47
D E F

S5.4 Fig. Swine-adaptative mutation do not confer a2,3 binding. a. Structure of glycans assessed on the array. Mutant viruses (b-i) binding preference for different a2,6 glycans was assessed by glycan array. Viruses were normalized to 8 HAU and binding was performed for 1 hour at room temperature. Bound virus was detected using an anti-H3 stalk specific antibody. sOH/04 was used as a swine-adapted virus control (j). Binding to a2,6 Neu5Gc is shown in a separate panel (structures A, B, and C). Data is shown as relative fluorescent units (RFU) $\pm$ SD.

S5.1 Table. HA variants detected in seeders and contacts pigs.

Contact	dpi/dpc	Amino acid change	Frequency (%)
Seeders	1	N/D	N/D
	2	N/D	N/D
	5	S138A	59
Contact 1	1	N/D	N/D
	3	S138A	100
		V186G	77.8
		F193Y	22.3
	6	S138A	100
		V186G	54.8
		F193Y	46.9
Contact 2	1	S138A	100
		F193Y	88.1
	3	S138A	100
		F193Y	87.4
	6	S138A	100
		F193Y	93.1
Contact 3	1	S138A	100
		F193Y	100
	3	S138A	100
		F193Y	100
	6	S138A	100
		F193Y	100
Contact 4	1	S138A	100
		F193Y	100
	3	S138A	100
		F193Y	100
	6	S138A	100
		F193Y	100

N/D= not determined due to no PCR amplification.

S5.2 Table. NA variants detected in seeders and contacts pigs.

Contact	dpi/dpc	Amino acid change	Frequency (%)
Seeders	1	N/D	N/D
	2	N/D	N/D
	5	D113A	58.9
Contacts 1	1	N/D	N/D
	3	N/C	N/C
	6	N/C	N/C
Contacts 2	1	N/C	N/C
	3	N/C	N/C
	6	N/C	N/C
Contacts 3	1	N/C	N/C
	3	N/C	N/C
	6	N/C	N/C
Contacts 4	1	N/C	N/C
	3	N/C	N/C
	6	N/C	N/C

N/D= not determined due to no PCR amplification.

N/C= no changes.

S5.3 Table. Self-elution time of hVIC/11 HA variants. BLI analysis of viruses' self-elution from 6'SLN-coated probes in absence of oseltamivir.

Virus	WT NA		D113A NA	
	Elution (s)	95% CI	Elution (s)	95% CI
sOH//04	804.5	802.7-806.4	-	-
hVIC/11	190.3	188.6-193.9	125.5	123.3-130.8
hVIC/11-A138S	478.0	474.3-481.7	736.3	732.1-738.4
hVIC/11-V186G	285.1	280.3-289.7	362.3	357.8-366.8
hVIC/11-F193Y	688.9	687.5-690.3	836.7	835.3-838.0
hVIC/11-A138S+V186G	1018	1017-1019	1087	1086-1088
hVIC/11-A138S+F193Y	1185	1182-1189	1194	1191-1198
hVIC/11-V186G+F193Y	1211	1209-1212	1014	1014-1015
hVIC/11-A138S+V186G+F193Y	2044	2043-2046	2985	2981-2990

Acknowledgments

The authors thank the University Research Animal Resources personnel at the University of Georgia for assistance with animal care. We thank Dr. Lucas Ferreri for the development of the pipeline used for variant analysis. This research was supported by Agriculture and Food Research Initiative grant no. 2020-67015-31563/project accession no. 1022827 from the USDA National Institute of Food and Agriculture to DSR. Funding was also provided, in part, by The National Pork Board to DSR under Project #21-085. DSR is also funded by Agriculture and Food Research Initiative grant no. 2022-67015-37205/project accession no. 1028058 from the USDA National Institute of Food and Agriculture. DRP is funded by subcontract 75N93021C00014 Centers for Influenza Research and Response (CEIRR) from the National Institute of Allergy and Infectious Diseases (NIAID) and GRANT12901999, project accession no. 1022658 from the National Institute of Food and Agriculture (NIFA), U.S. Department of Agriculture. DRP receives additional support from the Georgia Research Alliance and the Caswell S. Eidson endowment funds from The University of Georgia. This study was partly supported by resources and technical expertise from the Georgia Advanced Computing Resource Center, a partnership between the University of Georgia's Office of the Vice President for Research and the Office of the Vice President for Information Technology. ALB and TKA are funded by the USDA-ARS project number 5030-32000-231-000D and the NIAID, National Institutes of Health, Department of Health and Human Services, under Contract No. 75N93021C00015. The funders had no role in study design, data collection and interpretation, or the decision to submit the work for publication. Mention of trade names or commercial products in this article is solely for the purpose of

providing specific information and does not imply recommendation or endorsement by the USDA or UGA. USDA is an equal opportunity provider and employer.

CHAPTER 6

SUMMARY AND CONLUSIONS

Human-to-swine spillover events are frequent but only a handful of these events have become established in the swine population. Previous studies have pointed that reassortment and acquisition of swine adapted internal genes (PB2, PB1, PA, NP, M, and NS) is critical as human viruses tend to quickly lose their internal genes following introduction to the swine population [246, 263, 264]. Nonetheless, human-origin HA and NA segments are frequently detected in pigs, although normally exhibiting mutations, and differing from the parental genes. The impact of such mutations in the surface genes has been widely understudied. For instance, little is known about the role of swine-adaptative mutations in the HA in human-origin viruses detected in pigs and how they can modify the sialic acid binding preference of the virus. Similarly, the NA protein has been shown to co-evolve with the HA to maintain the HA/NA balance, but little is known about the molecular mechanisms employed by FLUAV to modulate NA activity.

In this project we found that adaptation to the swine host selects for at least one mutation in the HA (A138S), improving infection of the lower respiratory tract compared to the human precursor virus hVIC/11. This effect was linked to a higher affinity for PAMs in the lungs of infected pigs by the A138S amino acid change, which was confirmed *in vitro*. Enhanced infection of PAMs was also linked to increased death of these cells. Therefore, we proposed this enhanced infection serves as a mechanism utilized by FLUAV to deplete PAMs in the lungs and, therefore, enhance infectivity

of the lower respiratory tract. Interestingly, the hVIC/11-A138S virus was unable to infect all the lung lobes analyzed, contrasting with a endemic swine virus sOH/04 and this suggests that more mutations are required to replicate to the full extent of a swine-adapted strain.

In a subsequent experiment, we observed that hVIC/11-A138S was able to infect all the lung lobes after two serial passages *in vivo*. Further characterization showed that the virus only became able to infect the lower respiratory tract upon acquisition of a compensatory mutation in the NA (D113A). This mutation was further mapped to the NA low-affinity calcium-binding pocket. Calcium has been pointed as a critical metal required for efficient NA catalysis as it acts as a cofactor. Previous published work showed that calcium binding in the low-affinity calcium-binding pocket stabilizes the tetramer stability and indirectly enhances NA activity in the pH1N1 NA [35]. Our data further supported this observation and suggest that mutations in the symmetry axis of the NA can differently modulate catalytic properties such as substrate affinity and reaction velocity. These changes can ultimately serve as a mechanism to modify NA activity and restore the HA/NA balance without mutating the catalytic site. This represents a novel mechanism in which the tetramer stability can affect NA activity at different stages of the catalytic reaction solely relying on calcium binding in the low-affinity calcium-binding pocket.

Vaccination has been postulated to increase the mutation rate of FLUAV viruses crossing to a new host [286]. Nonetheless, most studies have overlooked the biological significance of these mutations, especially those in the HA protein and their impact on sialic acid binding. Our study presented demonstrated that vaccination promotes

evolution by selecting escape mutants with reduced antibody recognition, and it concurrently results in mutations that modify the receptor affinity of the virus. These changes seem to increase affinity for a2,6 SA rather than to modify affinity for either a2,3 SA or Neu5Gc. Interestingly, viruses carrying mutations in the HA showed binding to a reduced pool of glycans, being restricted to extended chains with a2,6 terminal SA and at least 3 LacNAc repeats. Moreover, we found that these mutations maintained the HA/NA balance, and the D113A mutation in the NA only arose when this balance was disrupted. These data demonstrated that an intricate mechanism between the HA and NA protein shapes the evolutionary trajectory of the virus, in which changes in the HA induce compensatory changes in the NA protein to restore the balance between HA avidity and NA activity.

Based on the results here presented, future follow up studies should address the following:

1. Although we observed a decrease of alveolar macrophages in BALF samples from pigs infected with sOH/04 and hVIC/11-A138S, little to no impact was seen in interstitial PAMs. Future studies should address this and evaluate the biological differences between PAMs and interstitial PAMs. Additionally, the ability to deplete PAMs in the lungs of infected pigs seem to correlate with the level of adaptation of the virus to pigs. Therefore, the role of PAMs limiting FLUAV infection of the lower respiratory tract should be evaluated in future studies.
2. Our data showed that the NA of swine-adapted H3N2 viruses has a higher tolerance to calcium-depleted conditions compared to human-adapted viruses.

This effect was further demonstrated to be modulated by residues 113 and 93. However, it remains to be elucidated why swine-adapted NAs exhibit sialidase activity in absence of calcium. We hypothesize that this difference could be due to different calcium concentrations in the mucus of swine and humans or a differential calcium release to the cytoplasm upon FLUAV infection. Future studies should evaluate this hypothesis and unveil the biological significance of lower calcium requirements exhibited by swine N2s.

3. Regarding the sialic acid binding profile of viral variants selected in vaccinated pigs, studies assessing the distribution of structures supporting binding of hVIC/11-A138S and hVIC/11-F193Y could provide new insight into the impact of glycan topology on the adaptation process of human H3N2 viruses crossing to pigs. The length of the glycan seems to play an important role and our variants exhibited preference for extended glycans compared to hVIC/11. Detection of this type of glycans throughout the respiratory tract of pigs and humans could reveal molecular differences that allow infection of human viruses in pigs.

REFERENCES

1. Javanian, M., et al., *A brief review of influenza virus infection.* J Med Virol, 2021. **93**(8): p. 4638-4646.
2. Fereidouni, S., et al., *Genetic characterization of a new candidate hemagglutinin subtype of influenza A viruses.* Emerg Microbes Infect, 2023. **12**(2): p. 2225645.
3. Gu, Y., et al., *Role of the Innate Cytokine Storm Induced by the Influenza A Virus.* Viral Immunol, 2019. **32**(6): p. 244-251.
4. Marcelin, G., M.R. Sandbulte, and R.J. Webby, *Contribution of antibody production against neuraminidase to the protection afforded by influenza vaccines.* Rev Med Virol, 2012. **22**(4): p. 267-79.
5. Han, A.X., S.P.J. de Jong, and C.A. Russell, *Co-evolution of immunity and seasonal influenza viruses.* Nat Rev Microbiol, 2023.
6. Skowronski, D.M., et al., *Vaccine effectiveness estimates from an early-season influenza A(H3N2) epidemic, including unique genetic diversity with reassortment, Canada, 2022/23.* Euro Surveill, 2023. **28**(5).
7. Treanor, J., *Influenza vaccine--outmaneuvering antigenic shift and drift.* N Engl J Med, 2004. **350**(3): p. 218-20.
8. Webster, R.G., et al., *Molecular mechanisms of variation in influenza viruses.* Nature, 1982. **296**(5853): p. 115-21.
9. Shiraki, K. and T. Daikoku, *Favipiravir, an anti-influenza drug against life-threatening RNA virus infections.* Pharmacol Ther, 2020. **209**: p. 107512.
10. Joseph, U., et al., *The ecology and adaptive evolution of influenza A interspecies transmission.* Influenza Other Respir Viruses, 2017. **11**(1): p. 74-84.
11. Stallknecht, D.E. and S.M. Shane, *Host range of avian influenza virus in free-living birds.* Vet Res Commun, 1988. **12**(2-3): p. 125-41.
12. Long, J.S., et al., *Host and viral determinants of influenza A virus species specificity.* Nat Rev Microbiol, 2019. **17**(2): p. 67-81.
13. Kida, H., et al., *Potential for transmission of avian influenza viruses to pigs.* J Gen Virol, 1994. **75 (Pt 9)**: p. 2183-8.
14. Ding, F., et al., *Infection and risk factors of human and avian influenza in pigs in south China.* Prev Vet Med, 2021. **190**: p. 105317.
15. Olsen, C.W., et al., *Virologic and serologic surveillance for human, swine and avian influenza virus infections among pigs in the north-central United States.* Arch Virol, 2000. **145**(7): p. 1399-419.
16. Smith, G.J., et al., *Origins and evolutionary genomics of the 2009 swine-origin H1N1 influenza A epidemic.* Nature, 2009. **459**(7250): p. 1122-5.
17. Nelson, M.I., et al., *Introductions and evolution of human-origin seasonal influenza a viruses in multinational swine populations.* J Virol, 2014. **88**(17): p. 10110-9.

18. Rajao, D.S., A.L. Vincent, and D.R. Perez, *Adaptation of Human Influenza Viruses to Swine.* Front Vet Sci, 2018. **5**: p. 347.
19. Shi, Y., et al., *Enabling the 'host jump': structural determinants of receptor-binding specificity in influenza A viruses.* Nat Rev Microbiol, 2014. **12**(12): p. 822-31.
20. Lazniewski, M., et al., *The structural variability of the influenza A hemagglutinin receptor-binding site.* Brief Funct Genomics, 2018. **17**(6): p. 415-427.
21. Giotis, E.S., et al., *Entry of the bat influenza H17N10 virus into mammalian cells is enabled by the MHC class II HLA-DR receptor.* Nat Microbiol, 2019. **4**(12): p. 2035-2038.
22. Karakus, U., et al., *MHC class II proteins mediate cross-species entry of bat influenza viruses.* Nature, 2019. **567**(7746): p. 109-112.
23. Nicholls, J.M., et al., *Evolving complexities of influenza virus and its receptors.* Trends Microbiol, 2008. **16**(4): p. 149-57.
24. Matrosovich, M., et al., *Early alterations of the receptor-binding properties of H1, H2, and H3 avian influenza virus hemagglutinins after their introduction into mammals.* J Virol, 2000. **74**(18): p. 8502-12.
25. Nelli, R.K., et al., *Comparative distribution of human and avian type sialic acid influenza receptors in the pig.* BMC Vet Res, 2010. **6**: p. 4.
26. Griffin, E.F. and S.M. Tompkins, *Fitness Determinants of Influenza A Viruses.* Viruses, 2023. **15**(9).
27. Mo, J.S., et al., *Transmission of Human Influenza A Virus in Pigs Selects for Adaptive Mutations on the HA Gene.* J Virol, 2022. **96**(22): p. e0148022.
28. Chandrasekaran, A., et al., *Glycan topology determines human adaptation of avian H5N1 virus hemagglutinin.* Nat Biotechnol, 2008. **26**(1): p. 107-13.
29. Stevens, J., et al., *Glycan microarray analysis of the hemagglutinins from modern and pandemic influenza viruses reveals different receptor specificities.* J Mol Biol, 2006. **355**(5): p. 1143-55.
30. Shtyrya, Y.A., L.V. Mochalova, and N.V. Bovin, *Influenza virus neuraminidase: structure and function.* Acta Naturae, 2009. **1**(2): p. 26-32.
31. Gaymard, A., et al., *Functional balance between neuraminidase and haemagglutinin in influenza viruses.* Clin Microbiol Infect, 2016. **22**(12): p. 975-983.
32. Guo, H., et al., *Kinetic analysis of the influenza A virus HA/NA balance reveals contribution of NA to virus-receptor binding and NA-dependent rolling on receptor-containing surfaces.* PLoS Pathog, 2018. **14**(8): p. e1007233.
33. Xu, R., et al., *Functional balance of the hemagglutinin and neuraminidase activities accompanies the emergence of the 2009 H1N1 influenza pandemic.* J Virol, 2012. **86**(17): p. 9221-32.
34. Zanin, M., et al., *Pandemic Swine H1N1 Influenza Viruses with Almost Undetectable Neuraminidase Activity Are Not Transmitted via Aerosols in Ferrets and Are Inhibited by Human Mucus but Not Swine Mucus.* J Virol, 2015. **89**(11): p. 5935-48.

35. Wang, H., et al., *Structural restrictions for influenza neuraminidase activity promote adaptation and diversification.* Nat Microbiol, 2019. **4**(12): p. 2565-2577.
36. Rodriguez-Frandsen, A., R. Alfonso, and A. Nieto, *Influenza virus polymerase: Functions on host range, inhibition of cellular response to infection and pathogenicity.* Virus Res, 2015. **209**: p. 23-38.
37. Stevaert, A. and L. Naesens, *The Influenza Virus Polymerase Complex: An Update on Its Structure, Functions, and Significance for Antiviral Drug Design.* Med Res Rev, 2016. **36**(6): p. 1127-1173.
38. Perales, B. and J. Ortin, *The influenza A virus PB2 polymerase subunit is required for the replication of viral RNA.* J Virol, 1997. **71**(2): p. 1381-5.
39. Fechter, P., et al., *Two aromatic residues in the PB2 subunit of influenza A RNA polymerase are crucial for cap binding.* J Biol Chem, 2003. **278**(22): p. 20381-8.
40. Dias, A., et al., *The cap-snatching endonuclease of influenza virus polymerase resides in the PA subunit.* Nature, 2009. **458**(7240): p. 914-8.
41. Dalton, R.M., et al., *Temperature sensitive influenza A virus genome replication results from low thermal stability of polymerase-cRNA complexes.* Virol J, 2006. **3**: p. 58.
42. Killian, M.L., *Avian Influenza Virus Sample Types, Collection, and Handling.* Methods Mol Biol, 2020. **2123**: p. 113-121.
43. Sorrell, E.M., et al., *A 27-amino-acid deletion in the neuraminidase stalk supports replication of an avian H2N2 influenza A virus in the respiratory tract of chickens.* J Virol, 2010. **84**(22): p. 11831-40.
44. Yamaya, M., et al., *Effects of high temperature on pandemic and seasonal human influenza viral replication and infection-induced damage in primary human tracheal epithelial cell cultures.* Heliyon, 2019. **5**(2): p. e01149.
45. Kirui, J., et al., *Conserved features of the PB2 627 domain impact influenza virus polymerase function and replication.* J Virol, 2014. **88**(11): p. 5977-86.
46. Massin, P., S. van der Werf, and N. Naffakh, *Residue 627 of PB2 is a determinant of cold sensitivity in RNA replication of avian influenza viruses.* J Virol, 2001. **75**(11): p. 5398-404.
47. Sun, H., et al., *PB2 segment promotes high-pathogenicity of H5N1 avian influenza viruses in mice.* Front Microbiol, 2015. **6**: p. 73.
48. Soltanialvar, M., R. Goodarzi, and F. Akbarnejad, *Genetic analysis of polymerase complex (PA, PB1 and PB2) genes of H9N2 avian influenza viruses from Iran (1999 to 2009).* Asian Pac J Trop Biomed, 2012. **2**(11): p. 858-62.
49. Hu, M., et al., *Swine H1N1 Influenza Virus Variants with Enhanced Polymerase Activity and HA Stability Promote Airborne Transmission in Ferrets.* J Virol, 2022. **96**(7): p. e0010022.
50. Mehle, A. and J.A. Doudna, *Adaptive strategies of the influenza virus polymerase for replication in humans.* Proc Natl Acad Sci U S A, 2009. **106**(50): p. 21312-6.
51. Chen, X., et al., *Host Immune Response to Influenza A Virus Infection.* Front Immunol, 2018. **9**: p. 320.
52. Sharrock, J. and J.C. Sun, *Innate immunological memory: from plants to animals.* Curr Opin Immunol, 2020. **62**: p. 69-78.

53. Ichinohe, T., *Respective roles of TLR, RIG-I and NLRP3 in influenza virus infection and immunity: impact on vaccine design.* Expert Rev Vaccines, 2010. **9**(11): p. 1315-24.
54. Chua, S., et al., *A Review and Meta-Analysis of Influenza Interactome Studies.* Front Microbiol, 2022. **13**: p. 869406.
55. Bergmann, M., et al., *Influenza virus NS1 protein counteracts PKR-mediated inhibition of replication.* J Virol, 2000. **74**(13): p. 6203-6.
56. Kochs, G., A. Garcia-Sastre, and L. Martinez-Sobrido, *Multiple anti-interferon actions of the influenza A virus NS1 protein.* J Virol, 2007. **81**(13): p. 7011-21.
57. Zhang, K., et al., *Structural basis for influenza virus NS1 protein block of mRNA nuclear export.* Nat Microbiol, 2019. **4**(10): p. 1671-1679.
58. Monteagudo, P.L., et al., *Differential Modulation of Innate Immune Responses in Human Primary Cells by Influenza A Viruses Carrying Human or Avian Nonstructural Protein 1.* J Virol, 2019. **94**(1).
59. Evseev, D. and K.E. Magor, *Molecular Evolution of the Influenza A Virus Non-structural Protein 1 in Interspecies Transmission and Adaptation.* Front Microbiol, 2021. **12**: p. 693204.
60. Liu, H., et al., *The ESEV PDZ-binding motif of the avian influenza A virus NS1 protein protects infected cells from apoptosis by directly targeting Scribble.* J Virol, 2010. **84**(21): p. 11164-74.
61. Cabeza-Cabrerizo, M., et al., *Recruitment of dendritic cell progenitors to foci of influenza A virus infection sustains immunity.* Sci Immunol, 2021. **6**(65): p. eabi9331.
62. Schneider, C., et al., *Alveolar macrophages are essential for protection from respiratory failure and associated morbidity following influenza virus infection.* PLoS Pathog, 2014. **10**(4): p. e1004053.
63. Maisonnasse, P., et al., *The respiratory DC/macrophage network at steady-state and upon influenza infection in the swine biomedical model.* Mucosal Immunol, 2016. **9**(4): p. 835-49.
64. Kumagai, Y., et al., *Alveolar macrophages are the primary interferon-alpha producer in pulmonary infection with RNA viruses.* Immunity, 2007. **27**(2): p. 240-52.
65. Wang, J., et al., *Innate immune response of human alveolar macrophages during influenza A infection.* PLoS One, 2012. **7**(3): p. e29879.
66. Wijburg, O.L., et al., *Alveolar macrophages regulate the induction of primary cytotoxic T-lymphocyte responses during influenza virus infection.* J Virol, 1997. **71**(12): p. 9450-7.
67. He, W., et al., *Alveolar macrophages are critical for broadly-reactive antibody-mediated protection against influenza A virus in mice.* Nat Commun, 2017. **8**(1): p. 846.
68. Kim, H.M., et al., *The severe pathogenicity of alveolar macrophage-depleted ferrets infected with 2009 pandemic H1N1 influenza virus.* Virology, 2013. **444**(1-2): p. 394-403.
69. Tate, M.D., et al., *Critical role of airway macrophages in modulating disease severity during influenza virus infection of mice.* J Virol, 2010. **84**(15): p. 7569-80.

70. Wein, A.N., et al., *IL-36gamma Protects against Severe Influenza Infection by Promoting Lung Alveolar Macrophage Survival and Limiting Viral Replication.* J Immunol, 2018. **201**(2): p. 573-582.
71. van Riel, D., et al., *Highly pathogenic avian influenza virus H5N1 infects alveolar macrophages without virus production or excessive TNF-alpha induction.* PLoS Pathog, 2011. **7**(6): p. e1002099.
72. Yu, W.C., et al., *Viral replication and innate host responses in primary human alveolar epithelial cells and alveolar macrophages infected with influenza H5N1 and H1N1 viruses.* J Virol, 2011. **85**(14): p. 6844-55.
73. Chang, P., et al., *Early apoptosis of porcine alveolar macrophages limits avian influenza virus replication and pro-inflammatory dysregulation.* Sci Rep, 2015. **5**: p. 17999.
74. Perrone, L.A., et al., *H5N1 and 1918 pandemic influenza virus infection results in early and excessive infiltration of macrophages and neutrophils in the lungs of mice.* PLoS Pathog, 2008. **4**(8): p. e1000115.
75. Zhang, J., et al., *The effects of H3N2 swine influenza virus infection on TLRs and RLRs signaling pathways in porcine alveolar macrophages.* Virol J, 2015. **12**: p. 61.
76. Tate, M.D., et al., *Responses of mouse airway epithelial cells and alveolar macrophages to virulent and avirulent strains of influenza A virus.* Viral Immunol, 2011. **24**(2): p. 77-88.
77. Huang, S., et al., *PPAR-gamma in Macrophages Limits Pulmonary Inflammation and Promotes Host Recovery following Respiratory Viral Infection.* J Virol, 2019. **93**(9).
78. Gopalakrishnan, A., et al., *Protection against influenza-induced Acute Lung Injury (ALI) by enhanced induction of M2a macrophages: possible role of PPARgamma/RXR ligands in IL-4-induced M2a macrophage differentiation.* Front Immunol, 2022. **13**: p. 968336.
79. Schneider, C., et al., *Induction of the nuclear receptor PPAR-gamma by the cytokine GM-CSF is critical for the differentiation of fetal monocytes into alveolar macrophages.* Nat Immunol, 2014. **15**(11): p. 1026-37.
80. Ditiatkovski, M., B.H. Toh, and A. Bobik, *GM-CSF deficiency reduces macrophage PPAR-gamma expression and aggravates atherosclerosis in ApoE-deficient mice.* Arterioscler Thromb Vasc Biol, 2006. **26**(10): p. 2337-44.
81. Guilliams, M., et al., *Alveolar macrophages develop from fetal monocytes that differentiate into long-lived cells in the first week of life via GM-CSF.* J Exp Med, 2013. **210**(10): p. 1977-92.
82. Joshi, N., J.M. Walter, and A.V. Misharin, *Alveolar Macrophages.* Cell Immunol, 2018. **330**: p. 86-90.
83. Cline, T.D., D. Beck, and E. Bianchini, *Influenza virus replication in macrophages: balancing protection and pathogenesis.* J Gen Virol, 2017. **98**(10): p. 2401-2412.
84. Ma, W. and J.A. Richt, *Swine influenza vaccines: current status and future perspectives.* Anim Health Res Rev, 2010. **11**(1): p. 81-96.

85. Cox, R.J., K.A. Brokstad, and P. Ogra, *Influenza virus: immunity and vaccination strategies. Comparison of the immune response to inactivated and live, attenuated influenza vaccines.* Scand J Immunol, 2004. **59**(1): p. 1-15.
86. Park, J.K., et al., *Pre-existing immunity to influenza virus hemagglutinin stalk might drive selection for antibody-escape mutant viruses in a human challenge model.* Nat Med, 2020. **26**(8): p. 1240-1246.
87. Lopez-Valinas, A., et al., *Evolution of Swine Influenza Virus H3N2 in Vaccinated and Nonvaccinated Pigs after Previous Natural H1N1 Infection.* Viruses, 2022. **14**(9).
88. Lopez-Valinas, A., et al., *Identification and Characterization of Swine Influenza Virus H1N1 Variants Generated in Vaccinated and Nonvaccinated, Challenged Pigs.* Viruses, 2021. **13**(10).
89. Hause, B.M., et al., *Characterization of a novel influenza virus in cattle and Swine: proposal for a new genus in the Orthomyxoviridae family.* mBio, 2014. **5**(2): p. e00031-14.
90. Matsuzaki, Y., et al., *Clinical features of influenza C virus infection in children.* J Infect Dis, 2006. **193**(9): p. 1229-35.
91. Chen, R. and E.C. Holmes, *The evolutionary dynamics of human influenza B virus.* J Mol Evol, 2008. **66**(6): p. 655-63.
92. Peteranderl, C., S. Herold, and C. Schmoldt, *Human Influenza Virus Infections.* Semin Respir Crit Care Med, 2016. **37**(4): p. 487-500.
93. Salem, E., et al., *Pathogenesis, Host Innate Immune Response, and Aerosol Transmission of Influenza D Virus in Cattle.* J Virol, 2019. **93**(7).
94. Curran, J.M., et al., *Evaluation of avian influenza serologic and virologic diagnostic methods in wild Anseriformes and Charadriiformes.* Avian Dis, 2014. **58**(1): p. 53-9.
95. Russell, C.A., et al., *The global circulation of seasonal influenza A (H3N2) viruses.* Science, 2008. **320**(5874): p. 340-6.
96. Allen, J.D. and T.M. Ross, *H3N2 influenza viruses in humans: Viral mechanisms, evolution, and evaluation.* Hum Vaccin Immunother, 2018. **14**(8): p. 1840-1847.
97. Chon, I., et al., *Detection of influenza A(H3N2) viruses with polymerase acidic subunit substitutions after and prior to baloxavir marboxil treatment during the 2022-2023 influenza season in Japan.* Antiviral Res, 2024. **229**: p. 105956.
98. Kislaya, I., et al., *End of season 2022/2023 quadrivalent influenza vaccine effectiveness in preventing influenza in primary care in Portugal.* Hum Vaccin Immunother, 2023. **19**(3): p. 2263219.
99. Monto, A.S. and K. Fukuda, *Lessons From Influenza Pandemics of the Last 100 Years.* Clin Infect Dis, 2020. **70**(5): p. 951-957.
100. Calder, L.J., et al., *Structural organization of a filamentous influenza A virus.* Proc Natl Acad Sci U S A, 2010. **107**(23): p. 10685-90.
101. Nayak, D.P., et al., *Influenza virus morphogenesis and budding.* Virus Res, 2009. **143**(2): p. 147-61.
102. Badham, M.D. and J.S. Rossman, *Filamentous Influenza Viruses.* Curr Clin Microbiol Rep, 2016. **3**(3): p. 155-161.

103. Seladi-Schulman, J., J. Steel, and A.C. Lowen, *Spherical influenza viruses have a fitness advantage in embryonated eggs, while filament-producing strains are selected in vivo.* J Virol, 2013. **87**(24): p. 13343-53.
104. Elleman, C.J. and W.S. Barclay, *The M1 matrix protein controls the filamentous phenotype of influenza A virus.* Virology, 2004. **321**(1): p. 144-53.
105. Dadonaite, B., et al., *The structure of the influenza A virus genome.* Nat Microbiol, 2019. **4**(11): p. 1781-1789.
106. Fields, S. and G. Winter, *Nucleotide sequences of influenza virus segments 1 and 3 reveal mosaic structure of a small viral RNA segment.* Cell, 1982. **28**(2): p. 303-13.
107. Wandzik, J.M., T. Kouba, and S. Cusack, *Structure and Function of Influenza Polymerase.* Cold Spring Harb Perspect Med, 2021. **11**(9).
108. Fan, H., et al., *Structures of influenza A virus RNA polymerase offer insight into viral genome replication.* Nature, 2019. **573**(7773): p. 287-290.
109. Chauhan, R.P. and M.L. Gordon, *An overview of influenza A virus genes, protein functions, and replication cycle highlighting important updates.* Virus Genes, 2022. **58**(4): p. 255-269.
110. Wise, H.M., et al., *A Complicated Message: Identification of a Novel PB1-Related Protein Translated from Influenza A Virus Segment 2 mRNA.* Journal of Virology, 2009. **83**(16): p. 8021-8031.
111. Tauber, S., et al., *Behaviour of influenza A viruses differentially expressing segment 2 gene products in vitro and in vivo.* J Gen Virol, 2012. **93**(Pt 4): p. 840-849.
112. Guilligay, D., et al., *The structural basis for cap binding by influenza virus polymerase subunit PB2.* Nat Struct Mol Biol, 2008. **15**(5): p. 500-6.
113. Yang, H., et al., *The influenza virus PB2 protein evades antiviral innate immunity by inhibiting JAK1/STAT signalling.* Nat Commun, 2022. **13**(1): p. 6288.
114. Yamayoshi, S., et al., *Identification of a Novel Viral Protein Expressed from the PB2 Segment of Influenza A Virus.* Journal of Virology, 2016. **90**(1): p. 444-456.
115. Pinto, R.M., et al., *Accessory Gene Products of Influenza A Virus.* Cold Spring Harb Perspect Med, 2021. **11**(12).
116. Levene, R.E., S.D. Shrestha, and M.M. Gaglia, *The Influenza A Virus Host Shutoff Factor PA-X Is Rapidly Turned Over in a Strain-Specific Manner.* Journal of Virology, 2021. **95**(8).
117. Ng, A.K., J.H. Wang, and P.C. Shaw, *Structure and sequence analysis of influenza A virus nucleoprotein.* Sci China C Life Sci, 2009. **52**(5): p. 439-49.
118. Hutchinson, E.C. and E. Fodor, *Transport of the influenza virus genome from nucleus to nucleus.* Viruses, 2013. **5**(10): p. 2424-46.
119. Brown, E.G., *Influenza virus genetics.* Biomed Pharmacother, 2000. **54**(4): p. 196-209.
120. Couch, R.B., *An overview of serum antibody responses to influenza virus antigens.* Dev Biol (Basel), 2003. **115**: p. 25-30.
121. Matrosovich, M., G. Herrler, and H.D. Klenk, *Sialic Acid Receptors of Viruses.* Top Curr Chem, 2015. **367**: p. 1-28.
122. Karakus, U., et al., *H19 influenza A virus exhibits species-specific MHC class II receptor usage.* Cell Host Microbe, 2024.

123. Lorieau, J.L., et al., *pH-triggered, activated-state conformations of the influenza hemagglutinin fusion peptide revealed by NMR.* Proc Natl Acad Sci U S A, 2012. **109**(49): p. 19994-9.
124. Eichelberger, M.C. and H. Wan, *Influenza Neuraminidase as a Vaccine Antigen*, in *Influenza Pathogenesis and Control - Volume II*, M.B.A. Oldstone and R.W. Compans, Editors. 2015, Springer International Publishing: Cham. p. 275-299.
125. Ohuchi, M., et al., *Roles of neuraminidase in the initial stage of influenza virus infection.* Microbes Infect, 2006. **8**(5): p. 1287-93.
126. Iseli, A.N., et al., *The neuraminidase activity of influenza A virus determines the strain-specific sensitivity to neutralization by respiratory mucus.* J Virol, 2023. **97**(10): p. e0127123.
127. de Vries, E., et al., *Influenza A Virus Hemagglutinin-Neuraminidase-Receptor Balance: Preserving Virus Motility.* Trends Microbiol, 2020. **28**(1): p. 57-67.
128. Lamb, R.A., C.J. Lai, and P.W. Choppin, *Sequences of mRNAs derived from genome RNA segment 7 of influenza virus: colinear and interrupted mRNAs code for overlapping proteins.* Proc Natl Acad Sci U S A, 1981. **78**(7): p. 4170-4.
129. Ruigrok, R.W., et al., *Membrane interaction of influenza virus M1 protein.* Virology, 2000. **267**(2): p. 289-98.
130. Shimbo, K., et al., *Ion selectivity and activation of the M2 ion channel of influenza virus.* Biophys J, 1996. **70**(3): p. 1335-46.
131. Lamb, R.A. and P.W. Choppin, *Segment 8 of the influenza virus genome is unique in coding for two polypeptides.* Proceedings of the National Academy of Sciences, 1979. **76**(10): p. 4908-4912.
132. Wang, X., et al., *Influenza A virus NS1 protein prevents activation of NF-kappaB and induction of alpha/beta interferon.* J Virol, 2000. **74**(24): p. 11566-73.
133. Fernandez-Sesma, A., et al., *Influenza virus evades innate and adaptive immunity via the NS1 protein.* J Virol, 2006. **80**(13): p. 6295-304.
134. O'Neill, R.E., J. Talon, and P. Palese, *The influenza virus NEP (NS2 protein) mediates the nuclear export of viral ribonucleoproteins.* EMBO J, 1998. **17**(1): p. 288-96.
135. Luo, M., *Influenza virus entry.* Adv Exp Med Biol, 2012. **726**: p. 201-21.
136. Lakadamyali, M., M.J. Rust, and X. Zhuang, *Endocytosis of influenza viruses.* Microbes Infect, 2004. **6**(10): p. 929-36.
137. Sempere Borau, M. and S. Stertz, *Entry of influenza A virus into host cells - recent progress and remaining challenges.* Curr Opin Virol, 2021. **48**: p. 23-29.
138. Eierhoff, T., et al., *The epidermal growth factor receptor (EGFR) promotes uptake of influenza A viruses (IAV) into host cells.* PLoS Pathog, 2010. **6**(9): p. e1001099.
139. Fujioka, Y., et al., *A Sialylated Voltage-Dependent Ca(2+) Channel Binds Hemagglutinin and Mediates Influenza A Virus Entry into Mammalian Cells.* Cell Host Microbe, 2018. **23**(6): p. 809-818 e5.
140. Rossman, J.S., G.P. Leser, and R.A. Lamb, *Filamentous influenza virus enters cells via macropinocytosis.* J Virol, 2012. **86**(20): p. 10950-60.
141. Kaksonen, M. and A. Roux, *Mechanisms of clathrin-mediated endocytosis.* Nat Rev Mol Cell Biol, 2018. **19**(5): p. 313-326.

142. Cardenas, M., et al., *Modulation of infectious Salmon Anaemia virus infection by clathrin-mediated endocytosis and macropinocytosis inhibitors.* Res Vet Sci, 2024. **171**: p. 105223.
143. Kerr, M.C. and R.D. Teasdale, *Defining macropinocytosis.* Traffic, 2009. **10**(4): p. 364-71.
144. Nguyen, P.A., et al., *pH-induced conformational change of the influenza M2 protein C-terminal domain.* Biochemistry, 2008. **47**(38): p. 9934-6.
145. Fontana, J. and A.C. Steven, *At low pH, influenza virus matrix protein M1 undergoes a conformational change prior to dissociating from the membrane.* J Virol, 2013. **87**(10): p. 5621-8.
146. Chang, D.K. and S.F. Cheng, *pH-dependence of intermediate steps of membrane fusion induced by the influenza fusion peptide.* Biochem J, 2006. **396**(3): p. 557-63.
147. Neumann, G., M.R. Castrucci, and Y. Kawaoka, *Nuclear import and export of influenza virus nucleoprotein.* J Virol, 1997. **71**(12): p. 9690-700.
148. Zhu, Z., E. Fodor, and J.R. Keown, *A structural understanding of influenza virus genome replication.* Trends Microbiol, 2023. **31**(3): p. 308-319.
149. Yanguez, E. and A. Nieto, *So similar, yet so different: selective translation of capped and polyadenylated viral mRNAs in the influenza virus infected cell.* Virus Res, 2011. **156**(1-2): p. 1-12.
150. Honda, A., K. Mizumoto, and A. Ishihama, *Two separate sequences of PB2 subunit constitute the RNA cap-binding site of influenza virus RNA polymerase.* Genes Cells, 1999. **4**(8): p. 475-85.
151. Datta, K., et al., *Characterization of PA-N terminal domain of Influenza A polymerase reveals sequence specific RNA cleavage.* Nucleic Acids Res, 2013. **41**(17): p. 8289-99.
152. Reich, S., et al., *Structural insight into cap-snatching and RNA synthesis by influenza polymerase.* Nature, 2014. **516**(7531): p. 361-6.
153. Poon, L.L., et al., *The RNA polymerase of influenza virus, bound to the 5' end of virion RNA, acts in cis to polyadenylate mRNA.* J Virol, 1998. **72**(10): p. 8214-9.
154. Satterly, N., et al., *Influenza virus targets the mRNA export machinery and the nuclear pore complex.* Proc Natl Acad Sci U S A, 2007. **104**(6): p. 1853-8.
155. Meischel, T., et al., *Influenza A virus interactions with macrophages: Lessons from epithelial cells.* Cell Microbiol, 2020. **22**(5): p. e13170.
156. Carter, T. and M. Iqbal, *The Influenza A Virus Replication Cycle: A Comprehensive Review.* Viruses, 2024. **16**(2).
157. Whittaker, G., M. Bui, and A. Helenius, *The role of nuclear import and export in influenza virus infection.* Trends Cell Biol, 1996. **6**(2): p. 67-71.
158. Paterson, D. and E. Fodor, *Emerging roles for the influenza A virus nuclear export protein (NEP).* PLoS Pathog, 2012. **8**(12): p. e1003019.
159. Barman, S. and D.P. Nayak, *Lipid raft disruption by cholesterol depletion enhances influenza A virus budding from MDCK cells.* J Virol, 2007. **81**(22): p. 12169-78.
160. Martyna, A. and J. Rossman, *Alterations of membrane curvature during influenza virus budding.* Biochem Soc Trans, 2014. **42**(5): p. 1425-8.

161. Veit, M. and B. Thaa, *Association of influenza virus proteins with membrane rafts.* Adv Virol, 2011. **2011**: p. 370606.
162. Takeda, M., et al., *Influenza virus hemagglutinin concentrates in lipid raft microdomains for efficient viral fusion.* Proc Natl Acad Sci U S A, 2003. **100**(25): p. 14610-7.
163. Barman, S., et al., *Transport of viral proteins to the apical membranes and interaction of matrix protein with glycoproteins in the assembly of influenza viruses.* Virus Res, 2001. **77**(1): p. 61-9.
164. Petrich, A., et al., *Influenza A M2 recruits M1 to the plasma membrane: A fluorescence fluctuation microscopy study.* Biophys J, 2021. **120**(24): p. 5478-5490.
165. Noton, S.L., et al., *Identification of the domains of the influenza A virus M1 matrix protein required for NP binding, oligomerization and incorporation into virions.* J Gen Virol, 2007. **88**(Pt 8): p. 2280-2290.
166. Li, X., et al., *Packaging signal of influenza A virus.* Virol J, 2021. **18**(1): p. 36.
167. Elkins, M.R., et al., *Cholesterol-binding site of the influenza M2 protein in lipid bilayers from solid-state NMR.* Proc Natl Acad Sci U S A, 2017. **114**(49): p. 12946-12951.
168. Chen, J., et al., *Structure of the hemagglutinin precursor cleavage site, a determinant of influenza pathogenicity and the origin of the labile conformation.* Cell, 1998. **95**(3): p. 409-17.
169. Copeland, C.S., et al., *Assembly of influenza hemagglutinin trimers and its role in intracellular transport.* J Cell Biol, 1986. **103**(4): p. 1179-91.
170. Russell, R.J., et al., *Avian and human receptor binding by hemagglutinins of influenza A viruses.* Glycoconj J, 2006. **23**(1-2): p. 85-92.
171. Lin, T., et al., *The hemagglutinin structure of an avian H1N1 influenza A virus.* Virology, 2009. **392**(1): p. 73-81.
172. Xu, R., et al., *Structural characterization of the hemagglutinin receptor specificity from the 2009 H1N1 influenza pandemic.* J Virol, 2012. **86**(2): p. 982-90.
173. Zhang, W., et al., *Molecular Basis of the Receptor Binding Specificity Switch of the Hemagglutinins from both the 1918 and 2009 Pandemic Influenza A Viruses by a D225G Substitution.* Journal of Virology, 2013. **87**(10): p. 5949-5958.
174. Lee, P.S., et al., *Receptor mimicry by antibody F045-092 facilitates universal binding to the H3 subtype of influenza virus.* Nat Commun, 2014. **5**: p. 3614.
175. Edinger, T.O., M.O. Pohl, and S. Stertz, *Entry of influenza A virus: host factors and antiviral targets.* J Gen Virol, 2014. **95**(Pt 2): p. 263-277.
176. de Vries, E., et al., *Dissection of the influenza A virus endocytic routes reveals macropinocytosis as an alternative entry pathway.* PLoS Pathog, 2011. **7**(3): p. e1001329.
177. Mair, C.M., et al., *Receptor binding and pH stability - how influenza A virus hemagglutinin affects host-specific virus infection.* Biochim Biophys Acta, 2014. **1838**(4): p. 1153-68.
178. Huang, Q., et al., *Protonation and stability of the globular domain of influenza virus hemagglutinin.* Biophys J, 2002. **82**(2): p. 1050-8.

179. Huang, Q., et al., *Early steps of the conformational change of influenza virus hemagglutinin to a fusion active state: stability and energetics of the hemagglutinin.* Biochim Biophys Acta, 2003. **1614**(1): p. 3-13.
180. Winter, S.L. and P. Chlanda, *The Art of Viral Membrane Fusion and Penetration.* Subcell Biochem, 2023. **106**: p. 113-152.
181. McAuley, J.L., et al., *Influenza Virus Neuraminidase Structure and Functions.* Front Microbiol, 2019. **10**: p. 39.
182. von Grafenstein, S., et al., *Interface dynamics explain assembly dependency of influenza neuraminidase catalytic activity.* J Biomol Struct Dyn, 2015. **33**(1): p. 104-20.
183. Meeprasert, A., et al., *Binding pattern of the long acting neuraminidase inhibitor laninamivir towards influenza A subtypes H5N1 and pandemic H1N1.* J Mol Graph Model, 2012. **38**: p. 148-54.
184. Zhu, X., et al., *Crystal structures of two subtype N10 neuraminidase-like proteins from bat influenza A viruses reveal a diverged putative active site.* Proc Natl Acad Sci U S A, 2012. **109**(46): p. 18903-8.
185. García-Sastre, A., *The neuraminidase of bat influenza viruses is not a neuraminidase.* Proceedings of the National Academy of Sciences, 2012. **109**(46): p. 18635-18636.
186. Richard, M., et al., *Impact of influenza A virus neuraminidase mutations on the stability, activity, and sensibility of the neuraminidase to neuraminidase inhibitors.* J Clin Virol, 2008. **41**(1): p. 20-4.
187. Abed, Y., et al., *Role of permissive neuraminidase mutations in influenza A/Brisbane/59/2007-like (H1N1) viruses.* PLoS Pathog, 2011. **7**(12): p. e1002431.
188. Zhu, X., et al., *Influenza virus neuraminidases with reduced enzymatic activity that avidly bind sialic Acid receptors.* J Virol, 2012. **86**(24): p. 13371-83.
189. Smith, B.J., et al., *Structure of a calcium-deficient form of influenza virus neuraminidase: implications for substrate binding.* Acta Crystallogr D Biol Crystallogr, 2006. **62**(Pt 9): p. 947-52.
190. Hanpaibool, C., et al., *Source of oseltamivir resistance due to single E119D and double E119D/H274Y mutations in pdm09H1N1 influenza neuraminidase.* J Comput Aided Mol Des, 2020. **34**(1): p. 27-37.
191. Lawrenz, M., et al., *Impact of calcium on N1 influenza neuraminidase dynamics and binding free energy.* Proteins, 2010. **78**(11): p. 2523-32.
192. Dominiak, P.M., et al., *Combining crystallographic information and an aspherical-atom data bank in the evaluation of the electrostatic interaction energy in an enzyme-substrate complex: influenza neuraminidase inhibition.* Acta Crystallogr D Biol Crystallogr, 2009. **65**(Pt 5): p. 485-99.
193. Gao, J., et al., *Design of the Recombinant Influenza Neuraminidase Antigen Is Crucial for Its Biochemical Properties and Protective Efficacy.* J Virol, 2021. **95**(24): p. e0116021.
194. Matrosovich, M., J. Stech, and H.D. Klenk, *Influenza receptors, polymerase and host range.* Rev Sci Tech, 2009. **28**(1): p. 203-17.
195. Zambon, M.C., *Epidemiology and pathogenesis of influenza.* J Antimicrob Chemother, 1999. **44 Suppl B**: p. 3-9.

196. Cauldwell, A.V., et al., *Viral determinants of influenza A virus host range.* J Gen Virol, 2014. **95**(Pt 6): p. 1193-1210.
197. Franca, M., D.E. Stallknecht, and E.W. Howerth, *Expression and distribution of sialic acid influenza virus receptors in wild birds.* Avian Pathol, 2013. **42**(1): p. 60-71.
198. Suzuki, Y., et al., *Sialic acid species as a determinant of the host range of influenza A viruses.* J Virol, 2000. **74**(24): p. 11825-31.
199. Mayr, J., et al., *Unravelling the Role of O-glycans in Influenza A Virus Infection.* Sci Rep, 2018. **8**(1): p. 16382.
200. Zhao, C. and J. Pu, *Influence of Host Sialic Acid Receptors Structure on the Host Specificity of Influenza Viruses.* Viruses, 2022. **14**(10).
201. Wang, W., et al., *Intermonomer Interactions in Hemagglutinin Subunits HA1 and HA2 Affecting Hemagglutinin Stability and Influenza Virus Infectivity.* J Virol, 2015. **89**(20): p. 10602-11.
202. Shirvani, E., et al., *Contributions of HA1 and HA2 Subunits of Highly Pathogenic Avian Influenza Virus in Induction of Neutralizing Antibodies and Protection in Chickens.* Front Microbiol, 2020. **11**: p. 1085.
203. Russier, M., et al., *Molecular requirements for a pandemic influenza virus: An acid-stable hemagglutinin protein.* Proc Natl Acad Sci U S A, 2016. **113**(6): p. 1636-41.
204. Russell, C.J., M. Hu, and F.A. Okda, *Influenza Hemagglutinin Protein Stability, Activation, and Pandemic Risk.* Trends Microbiol, 2018. **26**(10): p. 841-853.
205. Yang, X., et al., *A beneficiary role for neuraminidase in influenza virus penetration through the respiratory mucus.* PLoS One, 2014. **9**(10): p. e110026.
206. Eccles, R., *Why is temperature sensitivity important for the success of common respiratory viruses?* Reviews in Medical Virology, 2021. **31**(1).
207. Troxell, B., et al., *Poultry body temperature contributes to invasion control through reduced expression of Salmonella pathogenicity island 1 genes in Salmonella enterica serovars Typhimurium and Enteritidis.* Appl Environ Microbiol, 2015. **81**(23): p. 8192-201.
208. Lang, V., et al., *Different incubation temperatures affect viral polymerase activity and yields of low-pathogenic avian influenza viruses in embryonated chicken eggs.* Arch Virol, 2011. **156**(6): p. 987-94.
209. Mirska, B., et al., *In vivo secondary structural analysis of Influenza A virus genomic RNA.* Cell Mol Life Sci, 2023. **80**(5): p. 136.
210. Chursov, A., et al., *Specific temperature-induced perturbations of secondary mRNA structures are associated with the cold-adapted temperature-sensitive phenotype of influenza A virus.* RNA Biol, 2012. **9**(10): p. 1266-74.
211. Botos, I., et al., *The toll-like receptor 3:dsRNA signaling complex.* Biochim Biophys Acta, 2009. **1789**(9-10): p. 667-74.
212. Holzinger, D., et al., *Induction of MxA gene expression by influenza A virus requires type I or type III interferon signaling.* J Virol, 2007. **81**(14): p. 7776-85.
213. Sutejo, R., et al., *Activation of type I and III interferon signalling pathways occurs in lung epithelial cells infected with low pathogenic avian influenza viruses.* PLoS One, 2012. **7**(3): p. e33732.

214. Sareneva, T., et al., *Influenza A virus-induced IFN-alpha/beta and IL-18 synergistically enhance IFN-gamma gene expression in human T cells.* J Immunol, 1998. **160**(12): p. 6032-8.
215. Goraya, M.U., et al., *Web of interferon stimulated antiviral factors to control the influenza A viruses replication.* Microb Pathog, 2020. **139**: p. 103919.
216. Zhao, C., et al., *ISG15 conjugation system targets the viral NS1 protein in influenza A virus-infected cells.* Proc Natl Acad Sci U S A, 2010. **107**(5): p. 2253-8.
217. Zimmermann, P., et al., *The viral nucleoprotein determines Mx sensitivity of influenza A viruses.* J Virol, 2011. **85**(16): p. 8133-40.
218. Haller, O., P. Staeheli, and G. Kochs, *Protective role of interferon-induced Mx GTPases against influenza viruses.* Rev Sci Tech, 2009. **28**(1): p. 219-31.
219. Haller, O. and G. Kochs, *Mx genes: host determinants controlling influenza virus infection and trans-species transmission.* Hum Genet, 2020. **139**(6-7): p. 695-705.
220. Riegger, D., et al., *The nucleoprotein of newly emerged H7N9 influenza A virus harbors a unique motif conferring resistance to antiviral human MxA.* J Virol, 2015. **89**(4): p. 2241-52.
221. Fong, C.H., et al., *Interferon-gamma inhibits influenza A virus cellular attachment by reducing sialic acid cluster size.* iScience, 2022. **25**(4): p. 104037.
222. Nogales, A., et al., *Modulation of Innate Immune Responses by the Influenza A NS1 and PA-X Proteins.* Viruses, 2018. **10**(12).
223. Opitz, B., et al., *IFNbeta induction by influenza A virus is mediated by RIG-I which is regulated by the viral NS1 protein.* Cell Microbiol, 2007. **9**(4): p. 930-8.
224. Chen, Z., Y. Li, and R.M. Krug, *Influenza A virus NS1 protein targets poly(A)-binding protein II of the cellular 3'-end processing machinery.* EMBO J, 1999. **18**(8): p. 2273-83.
225. Noah, D.L., K.Y. Twu, and R.M. Krug, *Cellular antiviral responses against influenza A virus are countered at the posttranscriptional level by the viral NS1A protein via its binding to a cellular protein required for the 3' end processing of cellular pre-mRNAS.* Virology, 2003. **307**(2): p. 386-95.
226. Obenauer, J.C., et al., *Large-scale sequence analysis of avian influenza isolates.* Science, 2006. **311**(5767): p. 1576-80.
227. Tisoncik, J.R., et al., *The NS1 protein of influenza A virus suppresses interferon-regulated activation of antigen-presentation and immune-proteasome pathways.* J Gen Virol, 2011. **92**(Pt 9): p. 2093-2104.
228. Manz, B., M. Schwemmle, and L. Brunotte, *Adaptation of avian influenza A virus polymerase in mammals to overcome the host species barrier.* J Virol, 2013. **87**(13): p. 7200-9.
229. Manz, B., et al., *Adaptive mutations in NEP compensate for defective H5N1 RNA replication in cultured human cells.* Nat Commun, 2012. **3**: p. 802.
230. Brown, I.H., *The epidemiology and evolution of influenza viruses in pigs.* Vet Microbiol, 2000. **74**(1-2): p. 29-46.
231. Yu, H., et al., *Genetic evolution of swine influenza A (H3N2) viruses in China from 1970 to 2006.* J Clin Microbiol, 2008. **46**(3): p. 1067-75.
232. Chambers, T.M., et al., *Influenza viral infection of swine in the United States 1988-1989.* Arch Virol, 1991. **116**(1-4): p. 261-5.

233. Zhou, N.N., et al., *Emergence of H3N2 reassortant influenza A viruses in North American pigs.* Vet Microbiol, 2000. **74**(1-2): p. 47-58.
234. Webby, R.J., et al., *Evolution of swine H3N2 influenza viruses in the United States.* J Virol, 2000. **74**(18): p. 8243-51.
235. Anderson, T.K., et al., *Swine Influenza A Viruses and the Tangled Relationship with Humans.* Cold Spring Harb Perspect Med, 2021. **11**(3).
236. Vincent, A.L., et al., *Swine influenza viruses a North American perspective.* Adv Virus Res, 2008. **72**: p. 127-54.
237. Shu, B., et al., *Genetic analysis and antigenic characterization of swine origin influenza viruses isolated from humans in the United States, 1990-2010.* Virology, 2012. **422**(1): p. 151-60.
238. Shinde, V., et al., *Triple-reassortant swine influenza A (H1) in humans in the United States, 2005-2009.* N Engl J Med, 2009. **360**(25): p. 2616-25.
239. Boëlle, P.Y., et al., *Transmission parameters of the A/H1N1 (2009) influenza virus pandemic: a review.* Influenza and Other Respiratory Viruses, 2011. **5**(5): p. 306-316.
240. Khan, K., et al., *Spread of a novel influenza A (H1N1) virus via global airline transportation.* N Engl J Med, 2009. **361**(2): p. 212-4.
241. Novel Swine-Origin Influenza, A.V.I.T., et al., *Emergence of a novel swine-origin influenza A (H1N1) virus in humans.* N Engl J Med, 2009. **360**(25): p. 2605-15.
242. Nelson, M.I., et al., *Continual Reintroduction of Human Pandemic H1N1 Influenza A Viruses into Swine in the United States, 2009 to 2014.* J Virol, 2015. **89**(12): p. 6218-26.
243. Vijaykrishna, D., et al., *Reassortment of pandemic H1N1/2009 influenza A virus in swine.* Science, 2010. **328**(5985): p. 1529.
244. Rajao, D.S., et al., *Novel Reassortant Human-Like H3N2 and H3N1 Influenza A Viruses Detected in Pigs Are Virulent and Antigenically Distinct from Swine Viruses Endemic to the United States.* J Virol, 2015. **89**(22): p. 11213-22.
245. Powell, J.D., et al., *Characterization of contemporary 2010.1 H3N2 swine influenza A viruses circulating in United States pigs.* Virology, 2021. **553**: p. 94-101.
246. Sharma, A., et al., *Characterization of a 2016-2017 Human Seasonal H3 Influenza A Virus Spillover Now Endemic to U.S. Swine.* mSphere, 2022. **7**(1): p. e0080921.
247. Michael A. Zeller, D.C.d.A.M., Giovana Ciacci Zanella, Carine K. Souza, Tavis K. Anderson, Amy L. Baker & Phillip C. Gauger *Reverse zoonosis of the 2022–2023 human seasonal H3N2 detected in swine.* npj Viruses, 2024. **2**(27).
248. Neumann, G., T. Noda, and Y. Kawaoka, *Emergence and pandemic potential of swine-origin H1N1 influenza virus.* Nature, 2009. **459**(7249): p. 931-9.
249. Freidl, G.S., et al., *Influenza at the animal-human interface: a review of the literature for virological evidence of human infection with swine or avian influenza viruses other than A(H5N1).* Euro Surveill, 2014. **19**(18).
250. Nelson, M.I. and A.L. Vincent, *Reverse zoonosis of influenza to swine: new perspectives on the human-animal interface.* Trends Microbiol, 2015. **23**(3): p. 142-53.

251. Ryt-Hansen, P., et al., *Co-circulation of multiple influenza A reassortants in swine harboring genes from seasonal human and swine influenza viruses.* Elife, 2021. **10**.
252. Wang, G., et al., *Mutations during the adaptation of H7N9 avian influenza virus to mice lungs enhance human-like sialic acid binding activity and virulence in mice.* Vet Microbiol, 2021. **254**: p. 109000.
253. Chou, H.H., et al., *A mutation in human CMP-sialic acid hydroxylase occurred after the Homo-Pan divergence.* Proc Natl Acad Sci U S A, 1998. **95**(20): p. 11751-6.
254. Suzuki, T., et al., *Swine influenza virus strains recognize sialylsugar chains containing the molecular species of sialic acid predominantly present in the swine tracheal epithelium.* FEBS Lett, 1997. **404**(2-3): p. 192-6.
255. Takahashi, T., et al., *Identification of amino acid residues of influenza A virus H3 HA contributing to the recognition of molecular species of sialic acid.* FEBS Lett, 2009. **583**(19): p. 3171-4.
256. Masuda, H., et al., *Substitution of amino acid residue in influenza A virus hemagglutinin affects recognition of sialyl-oligosaccharides containing N-glycolylneuraminic acid.* FEBS Lett, 1999. **464**(1-2): p. 71-4.
257. Broszeit, F., et al., *N-Glycolylneuraminic Acid as a Receptor for Influenza A Viruses.* Cell Rep, 2019. **27**(11): p. 3284-3294 e6.
258. Cardenas, M., et al., *Amino acid 138 in the HA of a H3N2 subtype influenza A virus increases affinity for the lower respiratory tract and alveolar macrophages in pigs.* PLoS Pathog, 2024. **20**(2): p. e1012026.
259. Nicholls, J.M., et al., *Sialic acid receptor detection in the human respiratory tract: evidence for widespread distribution of potential binding sites for human and avian influenza viruses.* Respir Res, 2007. **8**(1): p. 73.
260. Yen, H.L., et al., *Hemagglutinin-neuraminidase balance confers respiratory-droplet transmissibility of the pandemic H1N1 influenza virus in ferrets.* Proc Natl Acad Sci U S A, 2011. **108**(34): p. 14264-9.
261. Moncorge, O., et al., *Investigation of influenza virus polymerase activity in pig cells.* J Virol, 2013. **87**(1): p. 384-94.
262. Neveau, M.N., et al., *Genetic and Antigenic Characterization of an Expanding H3 Influenza A Virus Clade in U.S. Swine Visualized by Nextstrain.* mSphere, 2022. **7**(3): p. e0099421.
263. Thomas, M.N., et al., *Nucleoprotein reassortment enhanced transmissibility of H3 1990.4.a clade influenza A virus in swine.* J Virol, 2024. **98**(3): p. e0170323.
264. Curran, S.J., et al., *Swine influenza A virus isolates containing the pandemic H1N1 origin matrix gene elicit greater disease in the murine model.* Microbiol Spectr, 2024. **12**(3): p. e0338623.
265. Lewis, N.S., et al., *Substitutions near the hemagglutinin receptor-binding site determine the antigenic evolution of influenza A H3N2 viruses in U.S. swine.* J Virol, 2014. **88**(9): p. 4752-63.
266. Abente, E.J., et al., *The Molecular Determinants of Antibody Recognition and Antigenic Drift in the H3 Hemagglutinin of Swine Influenza A Virus.* J Virol, 2016. **90**(18): p. 8266-80.

267. Li, Y., et al., *Single hemagglutinin mutations that alter both antigenicity and receptor binding avidity influence influenza virus antigenic clustering.* J Virol, 2013. **87**(17): p. 9904-10.
268. Santos, J.J.S., et al., *Plasticity of Amino Acid Residue 145 Near the Receptor Binding Site of H3 Swine Influenza A Viruses and Its Impact on Receptor Binding and Antibody Recognition.* J Virol, 2019. **93**(2).
269. Kilbourne, E.D., et al., *Hemagglutinin polymorphism as the basis for low- and high-yield phenotypes of swine influenza virus.* Proc Natl Acad Sci U S A, 1988. **85**(20): p. 7782-5.
270. De Vleeschauwer, A., et al., *Efficient transmission of swine-adapted but not wholly avian influenza viruses among pigs and from pigs to ferrets.* J Infect Dis, 2009. **200**(12): p. 1884-92.
271. Kaplan, B.S., et al., *Evolution and Antigenic Advancement of N2 Neuraminidase of Swine Influenza A Viruses Circulating in the United States following Two Separate Introductions from Human Seasonal Viruses.* J Virol, 2021. **95**(20): p. e0063221.
272. Nelson, M.I., et al., *Evolution of novel reassortant A/H3N2 influenza viruses in North American swine and humans, 2009-2011.* J Virol, 2012. **86**(16): p. 8872-8.
273. Mochalova, L., et al., *Oligosaccharide specificity of influenza H1N1 virus neuraminidases.* Arch Virol, 2007. **152**(11): p. 2047-57.
274. Franca de Barros, J., Jr., et al., *Characterization of sialidase from an influenza A (H3N2) virus strain: kinetic parameters and substrate specificity.* Intervirology, 2003. **46**(4): p. 199-206.
275. Vincent, A.L., et al., *Influenza A virus vaccines for swine.* Vet Microbiol, 2017. **206**: p. 35-44.
276. Van Reeth, K., et al., *Protection against a European H1N2 swine influenza virus in pigs previously infected with H1N1 and/or H3N2 subtypes.* Vaccine, 2003. **21**(13-14): p. 1375-81.
277. Mancera Gracia, J.C., et al., *Influenza A Virus in Swine: Epidemiology, Challenges and Vaccination Strategies.* Front Vet Sci, 2020. **7**: p. 647.
278. Vander Veen, R.L., et al., *Safety, immunogenicity, and efficacy of an alphavirus replicon-based swine influenza virus hemagglutinin vaccine.* Vaccine, 2012. **30**(11): p. 1944-50.
279. Swayne, D.E., *Animal influenza*. 2nd edition. ed. 2016, Ames, Iowa: John Wiley and Sons, Inc.,. 1 online resource.
280. Laursen, N.S. and I.A. Wilson, *Broadly neutralizing antibodies against influenza viruses.* Antiviral Research, 2013. **98**(3): p. 476-483.
281. Skehel, J.J. and D.C. Wiley, *Receptor binding and membrane fusion in virus entry: the influenza hemagglutinin.* Annu Rev Biochem, 2000. **69**: p. 531-69.
282. Knossow, M., et al., *Mechanism of neutralization of influenza virus infectivity by antibodies.* Virology, 2002. **302**(2): p. 294-298.
283. Sylte, M.J. and D.L. Suarez, *Influenza Neuraminidase as a Vaccine Antigen.* Vaccines for Pandemic Influenza, 2009. **333**: p. 227-241.
284. Lorbach, J.N., et al., *Influenza Vaccination of Swine Reduces Public Health Risk at the Swine-Human Interface.* mSphere, 2021. **6**(3): p. e0117020.

285. Souza, C.K., et al., *Swine-to-Ferret Transmission of Antigenically Drifted Contemporary Swine H3N2 Influenza A Virus Is an Indicator of Zoonotic Risk to Humans.* Viruses-Basel, 2023. **15**(2).
286. Murcia, P.R., et al., *Evolution of an Eurasian avian-like influenza virus in naive and vaccinated pigs.* PLoS Pathog, 2012. **8**(5): p. e1002730.
287. Ito, T. and Y. Kawaoka, *Host-range barrier of influenza A viruses.* Vet Microbiol, 2000. **74**(1-2): p. 71-5.
288. Bourret, V., *Avian influenza viruses in pigs: An overview.* Vet J, 2018. **239**: p. 7-14.
289. Rajao, D.S., et al., *Changes in the Hemagglutinin and Internal Gene Segments Were Needed for Human Seasonal H3 Influenza A Virus to Efficiently Infect and Replicate in Swine.* Pathogens, 2022. **11**(9).
290. Neumann, G. and Y. Kawaoka, *Host range restriction and pathogenicity in the context of influenza pandemic.* Emerg Infect Dis, 2006. **12**(6): p. 881-6.
291. Subbarao, E.K., W. London, and B.R. Murphy, *A single amino acid in the PB2 gene of influenza A virus is a determinant of host range.* J Virol, 1993. **67**(4): p. 1761-4.
292. Connor, R.J., et al., *Receptor specificity in human, avian, and equine H2 and H3 influenza virus isolates.* Virology, 1994. **205**(1): p. 17-23.
293. REED, L.J. and H. MUENCH, *A SIMPLE METHOD OF ESTIMATING FIFTY PER CENT ENDPOINTS12.* American Journal of Epidemiology, 1938. **27**(3): p. 493-497.
294. Marathe, B.M., et al., *Determination of neuraminidase kinetic constants using whole influenza virus preparations and correction for spectroscopic interference by a fluorogenic substrate.* PLoS One, 2013. **8**(8): p. e71401.
295. Matrosovich, M.N. and A.S. Gambaryan, *Solid-phase assays of receptor-binding specificity.* Methods Mol Biol, 2012. **865**: p. 71-94.
296. Zaqout, S., L.L. Becker, and A.M. Kaindl, *Immunofluorescence Staining of Paraffin Sections Step by Step.* Front Neuroanat, 2020. **14**: p. 582218.
297. Busch, M.G., et al., *Identification of amino acids in the HA of H3 influenza viruses that determine infectivity levels in primary swine respiratory epithelial cells.* Virus Res, 2008. **133**(2): p. 269-79.
298. Obadan, A.O., et al., *Flexibility In Vitro of Amino Acid 226 in the Receptor-Binding Site of an H9 Subtype Influenza A Virus and Its Effect In Vivo on Virus Replication, Tropism, and Transmission.* J Virol, 2019. **93**(6).
299. Van Poucke, S.G., et al., *Replication of avian, human and swine influenza viruses in porcine respiratory explants and association with sialic acid distribution.* Virol J, 2010. **7**: p. 38.
300. Rodriguez, R.M., et al., *Signal Integration and Transcriptional Regulation of the Inflammatory Response Mediated by the GM-/M-CSF Signaling Axis in Human Monocytes.* Cell Rep, 2019. **29**(4): p. 860-872 e5.
301. Gao, S., et al., *The genomic evolution of H1 influenza A viruses from swine detected in the United States between 2009 and 2016.* J Gen Virol, 2017. **98**(8): p. 2001-2010.
302. Nelson, M.I., et al., *Global transmission of influenza viruses from humans to swine.* J Gen Virol, 2012. **93**(Pt 10): p. 2195-2203.

303. Liang, H., et al., *Expansion of genotypic diversity and establishment of 2009 H1N1 pandemic-origin internal genes in pigs in China.* J Virol, 2014. **88**(18): p. 10864-74.
304. Rajao, D.S., et al., *Reassortment between Swine H3N2 and 2009 Pandemic H1N1 in the United States Resulted in Influenza A Viruses with Diverse Genetic Constellations with Variable Virulence in Pigs.* J Virol, 2017. **91**(4).
305. Ngo, L.T., et al., *Isolation of novel triple-reassortant swine H3N2 influenza viruses possessing the hemagglutinin and neuraminidase genes of a seasonal influenza virus in Vietnam in 2010.* Influenza Other Respir Viruses, 2012. **6**(1): p. 6-10.
306. Karasinski, J., et al., *Detection and identification of bacteria using antibiotic susceptibility and a multi-array electrochemical sensor with pattern recognition.* Biosens Bioelectron, 2007. **22**(11): p. 2643-9.
307. Vijaykrishna, D., et al., *Long-term evolution and transmission dynamics of swine influenza A virus.* Nature, 2011. **473**(7348): p. 519-22.
308. Zhang, Y., et al., *Pandemic threat posed by H3N2 avian influenza virus.* Sci China Life Sci, 2021. **64**(11): p. 1984-1987.
309. Wan, H., et al., *Replication and transmission of H9N2 influenza viruses in ferrets: evaluation of pandemic potential.* PLoS One, 2008. **3**(8): p. e2923.
310. Belser, J.A., et al., *Pathogenesis and transmission of avian influenza A (H7N9) virus in ferrets and mice.* Nature, 2013. **501**(7468): p. 556-9.
311. Pearce, M.B., et al., *Pathogenesis and transmission of swine origin A(H3N2)v influenza viruses in ferrets.* Proc Natl Acad Sci U S A, 2012. **109**(10): p. 3944-9.
312. Pascua, P.N., et al., *Virulence and transmissibility of H1N2 influenza virus in ferrets imply the continuing threat of triple-reassortant swine viruses.* Proc Natl Acad Sci U S A, 2012. **109**(39): p. 15900-5.
313. Xie, C., et al., *A(H1N1)pdm09 Influenza Viruses Replicating in Ferret Upper or Lower Respiratory Tract Differed in Onward Transmission Potential by Air.* J Infect Dis, 2022. **225**(1): p. 65-74.
314. Seo, S.H. and R.G. Webster, *Tumor Necrosis Factor Alpha Exerts Powerful Anti-Influenza Virus Effects in Lung Epithelial Cells.* Journal of Virology, 2002. **76**(3): p. 1071-1076.
315. Svitek, N., et al., *Severe seasonal influenza in ferrets correlates with reduced interferon and increased IL-6 induction.* Virology, 2008. **376**(1): p. 53-9.
316. Khatri, M., et al., *Swine influenza H1N1 virus induces acute inflammatory immune responses in pig lungs: a potential animal model for human H1N1 influenza virus.* J Virol, 2010. **84**(21): p. 11210-8.
317. Barbe, F., K. Atanasova, and K. Van Reeth, *Cytokines and acute phase proteins associated with acute swine influenza infection in pigs.* Vet J, 2011. **187**(1): p. 48-53.
318. Vandoorn, E., et al., *Pathobiology of an NS1-Truncated H3N2 Swine Influenza Virus Strain in Pigs.* J Virol, 2022. **96**(11): p. e0051922.
319. Rot, A., *Neutrophil attractant/activation protein-1 (interleukin-8) induces in vitro neutrophil migration by haptotactic mechanism.* Eur J Immunol, 1993. **23**(1): p. 303-6.

320. Lam, W.Y., et al., *Profiles of cytokine and chemokine gene expression in human pulmonary epithelial cells induced by human and avian influenza viruses.* Virol J, 2010. **7**: p. 344.
321. Veldhuis, W.B., et al., *Interferon-beta blocks infiltration of inflammatory cells and reduces infarct volume after ischemic stroke in the rat.* J Cereb Blood Flow Metab, 2003. **23**(9): p. 1029-39.
322. Cobelens, P.M., et al., *Interferon-beta attenuates lung inflammation following experimental subarachnoid hemorrhage.* Crit Care, 2010. **14**(4): p. R157.
323. Ghoneim, H.E., P.G. Thomas, and J.A. McCullers, *Depletion of alveolar macrophages during influenza infection facilitates bacterial superinfections.* J Immunol, 2013. **191**(3): p. 1250-9.
324. Seo, S.H., R. Webby, and R.G. Webster, *No apoptotic deaths and different levels of inductions of inflammatory cytokines in alveolar macrophages infected with influenza viruses.* Virology, 2004. **329**(2): p. 270-9.
325. Dai, C.H., et al., *The Competitive Endogenous RNA (ceRNA) Regulation in Porcine Alveolar Macrophages (3D4/21) Infected by Swine Influenza Virus (H1N1 and H3N2).* Int J Mol Sci, 2022. **23**(3).
326. Ettensohn, D.B., et al., *Human Alveolar Macrophages May Not Be Susceptible to Direct Infection by a Human Influenza Virus.* J Infect Dis, 2016. **214**(11): p. 1658-1665.
327. Reddy, R.C., *Immunomodulatory role of PPAR-gamma in alveolar macrophages.* J Investig Med, 2008. **56**(2): p. 522-7.
328. Zhang, H., et al., *Influenza virus causes lung immunopathology through down-regulating PPARgamma activity in macrophages.* Front Immunol, 2022. **13**: p. 958801.
329. Huang, S., et al., *Targeting Peroxisome Proliferator-Activated Receptor-Gamma Decreases Host Mortality After Influenza Infection in Obese Mice.* Viral Immunol, 2019. **32**(4): p. 161-169.
330. Wakao, H., et al., *Constitutively active Stat5A and Stat5B promote adipogenesis.* Environ Health Prev Med, 2011. **16**(4): p. 247-52.
331. Uetani, K., et al., *Influenza A virus abrogates IFN-gamma response in respiratory epithelial cells by disruption of the Jak/Stat pathway.* Eur J Immunol, 2008. **38**(6): p. 1559-73.
332. Feng, M., et al., *Inducible Guanylate-Binding Protein 7 Facilitates Influenza A Virus Replication by Suppressing Innate Immunity via NF-kappaB and JAK-STAT Signaling Pathways.* J Virol, 2021. **95**(6).
333. Fleming, S.B., *Viral Inhibition of the IFN-Induced JAK/STAT Signalling Pathway: Development of Live Attenuated Vaccines by Mutation of Viral-Encoded IFN-Antagonists.* Vaccines (Basel), 2016. **4**(3).
334. Delgado-Ortega, M., et al., *Innate immune response to a H3N2 subtype swine influenza virus in newborn porcine trachea cells, alveolar macrophages, and precision-cut lung slices.* Vet Res, 2014. **45**(1): p. 42.
335. Paulin, S.M., et al., *Net replication of Salmonella enterica serovars Typhimurium and Choleraesuis in porcine intestinal mucosa and nodes is associated with their differential virulence.* Infect Immun, 2007. **75**(8): p. 3950-60.

336. Cui, J., et al., *Study on quantitative expression of PPARgamma and ADRP in muscle and its association with intramuscular fat deposition of pig.* Springerplus, 2016. **5**(1): p. 1501.
337. Yang, Z.Z., et al., *Detection of PCV2 DNA by SYBR Green I-based quantitative PCR.* J Zhejiang Univ Sci B, 2007. **8**(3): p. 162-9.
338. Zheng, L.L., et al., *Simultaneous detection of porcine reproductive and respiratory syndrome virus and porcine circovirus 3 by SYBR Green capital I, Ukrainian-based duplex real-time PCR.* Mol Cell Probes, 2020. **49**: p. 101474.
339. Vranckx, K., et al., *Vaccination reduces macrophage infiltration in bronchus-associated lymphoid tissue in pigs infected with a highly virulent Mycoplasma hyopneumoniae strain.* BMC Vet Res, 2012. **8**: p. 24.
340. Pabis, A., R.J. Rawle, and P.M. Kasson, *Influenza hemagglutinin drives viral entry via two sequential intramembrane mechanisms.* Proc Natl Acad Sci U S A, 2020. **117**(13): p. 7200-7207.
341. Cohen, M., et al., *Influenza A penetrates host mucus by cleaving sialic acids with neuraminidase.* Virol J, 2013. **10**: p. 321.
342. Shelton, H., et al., *Mutations in haemagglutinin that affect receptor binding and pH stability increase replication of a PR8 influenza virus with H5 HA in the upper respiratory tract of ferrets and may contribute to transmissibility.* J Gen Virol, 2013. **94**(Pt 6): p. 1220-1229.
343. Mitnaul, L.J., et al., *Balanced hemagglutinin and neuraminidase activities are critical for efficient replication of influenza A virus.* J Virol, 2000. **74**(13): p. 6015-20.
344. Guo, Z., et al., *Neuraminidase Activity Modulates Cellular Coinfection during Influenza A Virus Multicycle Growth.* mBio, 2023. **14**(3): p. e0359122.
345. Colman, P.M., J.N. Varghese, and W.G. Laver, *Structure of the catalytic and antigenic sites in influenza virus neuraminidase.* Nature, 1983. **303**(5912): p. 41-4.
346. Bucher, D.J. and E.D. Kilbourne, *A 2 (N2) neuraminidase of the X-7 influenza virus recombinant: determination of molecular size and subunit composition of the active unit.* J Virol, 1972. **10**(1): p. 60-6.
347. Paterson, R.G. and R.A. Lamb, *Conversion of a class II integral membrane protein into a soluble and efficiently secreted protein: multiple intracellular and extracellular oligomeric and conformational forms.* J Cell Biol, 1990. **110**(4): p. 999-1011.
348. Li, Q., et al., *Structural and functional characterization of neuraminidase-like molecule N10 derived from bat influenza A virus.* Proc Natl Acad Sci U S A, 2012. **109**(46): p. 18897-902.
349. Gong, J., W. Xu, and J. Zhang, *Structure and functions of influenza virus neuraminidase.* Curr Med Chem, 2007. **14**(1): p. 113-22.
350. Colman, P.M., P.A. Hoyne, and M.C. Lawrence, *Sequence and structure alignment of paramyxovirus hemagglutinin-neuraminidase with influenza virus neuraminidase.* J Virol, 1993. **67**(6): p. 2972-80.
351. van der Vries, E., et al., *H1N1 2009 pandemic influenza virus: resistance of the I223R neuraminidase mutant explained by kinetic and structural analysis.* PLoS Pathog, 2012. **8**(9): p. e1002914.

352. Li, Q., et al., *The 2009 pandemic H1N1 neuraminidase N1 lacks the 150-cavity in its active site.* Nat Struct Mol Biol, 2010. **17**(10): p. 1266-8.
353. Walters, M.S., et al., *Generation of a human airway epithelium derived basal cell line with multipotent differentiation capacity.* Respir Res, 2013. **14**(1): p. 135.
354. Hoffmann, E., et al., *A DNA transfection system for generation of influenza A virus from eight plasmids.* Proc Natl Acad Sci U S A, 2000. **97**(11): p. 6108-13.
355. Mo, J.S., et al., *Transmission of Human Influenza A Virus in Pigs Selects for Adaptive Mutations on the HA Gene.* J Virol, 2022: p. e0148022.
356. Meliopoulos, V., et al., *Primary Swine Respiratory Epithelial Cell Lines for the Efficient Isolation and Propagation of Influenza A Viruses.* J Virol, 2020. **94**(24).
357. Wang, H., et al., *Establishment and comparison of air-liquid interface culture systems for primary and immortalized swine tracheal epithelial cells.* BMC Cell Biol, 2018. **19**(1): p. 10.
358. Siegers, J.Y., et al., *Evolution of highly pathogenic H5N1 influenza A virus in the central nervous system of ferrets.* PLoS Pathog, 2023. **19**(3): p. e1011214.
359. Ferreri, L.M., et al., *Intra- and inter-host evolution of H9N2 influenza A virus in Japanese quail.* Virus Evol, 2022. **8**(1): p. veac001.
360. Li, H. and R. Durbin, *Fast and accurate short read alignment with Burrows-Wheeler transform.* Bioinformatics, 2009. **25**(14): p. 1754-60.
361. Wilm, A., et al., *LoFreq: a sequence-quality aware, ultra-sensitive variant caller for uncovering cell-population heterogeneity from high-throughput sequencing datasets.* Nucleic Acids Res, 2012. **40**(22): p. 11189-201.
362. Van der Auwera, G.A., et al., *From FastQ data to high confidence variant calls: the Genome Analysis Toolkit best practices pipeline.* Curr Protoc Bioinformatics, 2013. **43**(1110): p. 11 10 1-11 10 33.
363. Doran, A.G. and C.J. Creevey, *Snpdat: easy and rapid annotation of results from de novo snp discovery projects for model and non-model organisms.* BMC Bioinformatics, 2013. **14**: p. 45.
364. Nelson, C.W., L.H. Moncla, and A.L. Hughes, *SNPGenie: estimating evolutionary parameters to detect natural selection using pooled next-generation sequencing data.* Bioinformatics, 2015. **31**(22): p. 3709-11.
365. Khare, S., et al., *GISAID's Role in Pandemic Response.* China CDC Wkly, 2021. **3**(49): p. 1049-1051.
366. Sievers, F., et al., *Fast, scalable generation of high-quality protein multiple sequence alignments using Clustal Omega.* Mol Syst Biol, 2011. **7**: p. 539.
367. Waterhouse, A., et al., *SWISS-MODEL: homology modelling of protein structures and complexes.* Nucleic Acids Res, 2018. **46**(W1): p. W296-W303.
368. Lei, R., et al., *Mutational fitness landscape of human influenza H3N2 neuraminidase.* Cell Rep, 2023. **42**(10): p. 113356.
369. Laskowski, R.A., et al., *AQUA and PROCHECK-NMR: programs for checking the quality of protein structures solved by NMR.* J Biomol NMR, 1996. **8**(4): p. 477-86.
370. Ellis, D., et al., *Structure-based design of stabilized recombinant influenza neuraminidase tetramers.* Nat Commun, 2022. **13**(1): p. 1825.

371. Pena, L., et al., *Modifications in the polymerase genes of a swine-like triple-reassortant influenza virus to generate live attenuated vaccines against 2009 pandemic H1N1 viruses.* J Virol, 2011. **85**(1): p. 456-69.
372. Sakai, T., et al., *Influenza A virus hemagglutinin and neuraminidase act as novel motile machinery.* Sci Rep, 2017. **7**: p. 45043.
373. Baker, N.J. and S.S. Gandhi, *Effect of Ca++ on the stability of influenza virus neuraminidase.* Arch Virol, 1976. **52**(1-2): p. 7-18.
374. Dimmock, N.J., *Dependence of the activity of an influenza virus neuraminidase upon Ca2+.* J Gen Virol, 1971. **13**(3): p. 481-3.
375. Xu, X., et al., *Structural characterization of the 1918 influenza virus H1N1 neuraminidase.* J Virol, 2008. **82**(21): p. 10493-501.
376. Burmeister, W.P., R.W. Ruigrok, and S. Cusack, *The 2.2 A resolution crystal structure of influenza B neuraminidase and its complex with sialic acid.* EMBO J, 1992. **11**(1): p. 49-56.
377. Youk, S.S., et al., *Mutations in PB1, NP, HA, and NA Contribute to Increased Virus Fitness of H5N2 Highly Pathogenic Avian Influenza Virus Clade 2.3.4.4 in Chickens.* J Virol, 2021. **95**(5).
378. Scheibner, D., et al., *Phenotypic effects of mutations observed in the neuraminidase of human origin H5N1 influenza A viruses.* PLoS Pathog, 2023. **19**(2): p. e1011135.
379. Burmeister, W.P., S. Cusack, and R.W. Ruigrok, *Calcium is needed for the thermostability of influenza B virus neuraminidase.* J Gen Virol, 1994. **75 (Pt 2)**: p. 381-8.
380. Klenow, L., et al., *Influenza virus and pneumococcal neuraminidases enhance catalysis by similar yet distinct sialic acid-binding strategies.* J Biol Chem, 2023. **299**(2): p. 102891.
381. da Silva, D.V., et al., *Assembly of subtype 1 influenza neuraminidase is driven by both the transmembrane and head domains.* J Biol Chem, 2013. **288**(1): p. 644-53.
382. Pegg, M.S. and M. von Itzstein, *Slow-binding inhibition of sialidase from influenza virus.* Biochem Mol Biol Int, 1994. **32**(5): p. 851-8.
383. Buxton, R.C., et al., *Development of a sensitive chemiluminescent neuraminidase assay for the determination of influenza virus susceptibility to zanamivir.* Analytical Biochemistry, 2000. **280**(2): p. 291-300.
384. Shtyrya, Y., et al., *Adjustment of receptor-binding and neuraminidase substrate specificities in avian-human reassortant influenza viruses.* Glycoconj J, 2009. **26**(1): p. 99-109.
385. Kaverin, N.V., et al., *Intergenic HA-NA interactions in influenza A virus: postreassortment substitutions of charged amino acid in the hemagglutinin of different subtypes.* Virus Res, 2000. **66**(2): p. 123-9.
386. Nelson, M.I., et al., *Genomic reassortment of influenza A virus in North American swine, 1998-2011.* J Gen Virol, 2012. **93**(Pt 12): p. 2584-2589.
387. Kida, H., K.F. Shortridge, and R.G. Webster, *Origin of the hemagglutinin gene of H3N2 influenza viruses from pigs in China.* Virology, 1988. **162**(1): p. 160-6.

388. Xiong, X.L., J.W. McCauley, and D.A. Steinhauer, *Receptor Binding Properties of the Influenza Virus Hemagglutinin as a Determinant of Host Range.* Influenza Pathogenesis and Control - Vol I, 2014. **385**: p. 63-91.
389. Stevens, J., et al., *Receptor specificity of influenza A H3N2 viruses isolated in mammalian cells and embryonated chicken eggs.* J Virol, 2010. **84**(16): p. 8287-99.
390. Trebbien, R., L.E. Larsen, and B.M. Viuff, *Distribution of sialic acid receptors and influenza A virus of avian and swine origin in experimentally infected pigs.* Virol J, 2011. **8**: p. 434.
391. Altman, M.O. and P. Gagneux, *Absence of Neu5Gc and Presence of Anti-Neu5Gc Antibodies in Humans-An Evolutionary Perspective.* Front Immunol, 2019. **10**: p. 789.
392. Gambaryan, A.S., et al., *Receptor-binding properties of swine influenza viruses isolated and propagated in MDCK cells.* Virus Res, 2005. **114**(1-2): p. 15-22.
393. Chien, Y.A., et al., *Single Particle Analysis of H3N2 Influenza Entry Differentiates the Impact of the Sialic Acids (Neu5Ac and Neu5Gc) on Virus Binding and Membrane Fusion.* J Virol, 2023. **97**(3): p. e0146322.
394. Bradley, K.C., et al., *Comparison of the receptor binding properties of contemporary swine isolates and early human pandemic H1N1 isolates (Novel 2009 H1N1).* Virology, 2011. **413**(2): p. 169-82.
395. Du, W., et al., *Mutation of the second sialic acid-binding site of influenza A virus neuraminidase drives compensatory mutations in hemagglutinin.* PLoS Pathog, 2020. **16**(8): p. e1008816.
396. Islam, S., et al., *Influenza A haemagglutinin specific IgG responses in children and adults after seasonal trivalent live attenuated influenza vaccination.* Vaccine, 2017. **35**(42): p. 5666-5673.
397. Isakova-Sivak, I., et al., *Influenza vaccine: progress in a vaccine that elicits a broad immune response.* Expert Review of Vaccines, 2021. **20**(9): p. 1097-1112.
398. Van Reeth, K., et al., *Heterologous prime-boost vaccination with H3N2 influenza viruses of swine favors cross-clade antibody responses and protection.* NPJ Vaccines, 2017. **2**.
399. Creanga, A., et al., *A comprehensive influenza reporter virus panel for high-throughput deep profiling of neutralizing antibodies.* Nat Commun, 2021. **12**(1): p. 1722.
400. Cardenas, M., et al., *Modulation of human-to-swine influenza a virus adaptation by the neuraminidase low-affinity calcium-binding pocket.* Commun Biol, 2024. **7**(1): p. 1230.
401. Hoffmann, E., et al., *Eight-plasmid system for rapid generation of influenza virus vaccines.* Vaccine, 2002. **20**(25-26): p. 3165-70.
402. Bloom, J.D., L.I. Gong, and D. Baltimore, *Permissive secondary mutations enable the evolution of influenza oseltamivir resistance.* Science, 2010. **328**(5983): p. 1272-5.
403. Caceres, C.J., et al., *Use of Reverse Genetics for the Generation of Recombinant Influenza Viruses Carrying Nanoluciferase.* Methods Mol Biol, 2024. **2733**: p. 47-74.

404. Nogales, A., S.F. Baker, and L. Martinez-Sobrido, *Replication-competent influenza A viruses expressing a red fluorescent protein.* Virology, 2015. **476**: p. 206-216.
405. Broszeit, F., et al., *Glycan remodeled erythrocytes facilitate antigenic characterization of recent A/H3N2 influenza viruses.* Nat Commun, 2021. **12**(1): p. 5449.
406. de Vries, E., et al., *Quantification of Receptor Association, Dissociation, and NA-Dependent Motility of Influenza A Particles by Biolayer Interferometry.* Methods Mol Biol, 2022. **2556**: p. 123-140.
407. Nakharuthai, C., et al., *Occurrence of swine influenza virus infection in swine with porcine respiratory disease complex.* Southeast Asian J Trop Med Public Health, 2008. **39**(6): p. 1045-53.
408. Mancera Gracia, J.C., et al., *Effect of serial pig passages on the adaptation of an avian H9N2 influenza virus to swine.* PLoS One, 2017. **12**(4): p. e0175267.
409. Yang, W., et al., *Mutations during the Adaptation of H9N2 Avian Influenza Virus to the Respiratory Epithelium of Pigs Enhance Sialic Acid Binding Activity and Virulence in Mice.* J Virol, 2017. **91**(8).
410. Bateman, A.C., et al., *Amino acid 226 in the hemagglutinin of H4N6 influenza virus determines binding affinity for alpha2,6-linked sialic acid and infectivity levels in primary swine and human respiratory epithelial cells.* J Virol, 2008. **82**(16): p. 8204-9.
411. Jorquera, P.A., et al., *Insights into the antigenic advancement of influenza A(H3N2) viruses, 2011-2018.* Sci Rep, 2019. **9**(1): p. 2676.
412. Ferguson, N.M., A.P. Galvani, and R.M. Bush, *Ecological and immunological determinants of influenza evolution.* Nature, 2003. **422**(6930): p. 428-33.
413. Chen, Y.Q., et al., *Hemagglutinin Stalk-Reactive Antibodies Interfere with Influenza Virus Neuraminidase Activity by Steric Hindrance.* J Virol, 2019. **93**(4).
414. Gambaryan, A., et al., *Receptor specificity of influenza viruses from birds and mammals: new data on involvement of the inner fragments of the carbohydrate chain.* Virology, 2005. **334**(2): p. 276-83.
415. Peng, W., et al., *Recent H3N2 Viruses Have Evolved Specificity for Extended, Branched Human-type Receptors, Conferring Potential for Increased Avidity.* Cell Host Microbe, 2017. **21**(1): p. 23-34.
416. Du, R., Q. Cui, and L. Rong, *Competitive Cooperation of Hemagglutinin and Neuraminidase during Influenza A Virus Entry.* Viruses, 2019. **11**(5).
417. Prachanronarong, K.L., et al., *Mutations in Influenza A Virus Neuraminidase and Hemagglutinin Confer Resistance against a Broadly Neutralizing Hemagglutinin Stem Antibody.* J Virol, 2019. **93**(2).
418. Wang, F., et al., *Identification of Hemagglutinin Mutations Caused by Neuraminidase Antibody Pressure.* Microbiol Spectr, 2021. **9**(3): p. e0143921.